



HAL
open science

Characterisation of changes in the overall distribution of precipitation in the Mediterranean region with climate change, in the past and in the future, considering both extreme rainfall and dry-days frequency.

Julie André

► To cite this version:

Julie André. Characterisation of changes in the overall distribution of precipitation in the Mediterranean region with climate change, in the past and in the future, considering both extreme rainfall and dry-days frequency.. Ocean, Atmosphere. Institut Polytechnique de Paris, 2024. English. NNT : 2024IPPAX070 . tel-04829611

HAL Id: tel-04829611

<https://theses.hal.science/tel-04829611v1>

Submitted on 10 Dec 2024

HAL is a multi-disciplinary open access archive for the deposit and dissemination of scientific research documents, whether they are published or not. The documents may come from teaching and research institutions in France or abroad, or from public or private research centers.

L'archive ouverte pluridisciplinaire **HAL**, est destinée au dépôt et à la diffusion de documents scientifiques de niveau recherche, publiés ou non, émanant des établissements d'enseignement et de recherche français ou étrangers, des laboratoires publics ou privés.



INSTITUT
POLYTECHNIQUE
DE PARIS

NNT : 2024IPPAX070

Thèse de doctorat



Characterisation of changes in the overall distribution of precipitation in the Mediterranean region with climate change, in the past and in the future, considering both extreme rainfall and dry-days frequency.

Thèse de doctorat de l'Institut Polytechnique de Paris,
préparée à l'École polytechnique

École doctorale n°626 Institut Polytechnique de Paris (IPParis)
Spécialité de doctorat : Mécanique et Energétique

Thèse présentée et soutenue à Paris, France, le 14 octobre 2024, par

JULIE ANDRÉ

Composition du jury de thèse :

Erika Coppola Professeure au Centre international de physique théorique (ICTP)	Rapporteuse
Paolo Ruti Professeur à EuMetSat	Rapporteur
Jan Polcher Directeur de recherche CNRS, Laboratoire de Météorologie Dynamique (LMD)	Président du jury
Juliette Blanchet Directrice de recherche CNRS, Institut des Géosciences de l'Environnement (IGE)	Examinatrice
Mathieu Vrac Directeur de recherche CNRS, Laboratoire des Sciences du Climat et de l'Environnement (LSCE)	Examineur
Aurélien Ribes Chercheur au Centre National de Recherches Météorologiques (CNRM)	Examineur
Philippe Drobinski Directeur de recherche CNRS, LMD	Directeur de thèse
Fabio d'Andrea Directeur de recherche CNRS, LMD	Co-directeur de thèse
Caroline Muller Chargée de recherche CNRS, Professeure à Institute of Science and Technology Austria (ISTA)	Invitée



Remerciements

J'ai eu la chance de faire une thèse avec un encadrement incroyable : trois personnes pour me guider dans ce projet de thèse sur mesure, ça peut être un peu intimidant au début, mais ça s'est vraiment très bien passé. Un grand merci donc à mon trio d'encadrants !

Merci à Philippe, notre expert sur le cycle de l'eau Méditerranéen ; je trouve toujours impressionnant que tu aies réussi à te dégager du temps régulièrement pour nos points thèse, malgré tes nombreux engagements (enseignant à l'X, directeur du LMD et de Energy4Climate, ...) avec toujours des retours pertinents, des mots encourageants et beaucoup d'énergie ! Merci pour ta vision claire sur mon sujet, et pour avoir su déceler les points originaux dans mes multiples essais-erreurs. Merci pour ton invitation au CDL, ton soutien à ma participation à LMD-Climactions, et à tout ce que j'ai pu faire à côté de la thèse, c'est chouette d'être soutenue !

Merci à Fabio, qui m'a accompagnée au plus près (facile, son bureau était la porte à côté !), chez qui je pouvais toquer à la moindre question — qu'elle soit physique, statistique ou administrative —. Fabio, qui adore imaginer des tests bizarres pour tenter de prouver la significativité statistiques d'une tendance ; qui a inventé une super analogie du nombre de chauves et de la longueur de cheveux des chevelus pour illustrer la fréquence des jours secs et l'intensité jours de pluie ; ou encore qui m'a encouragée à venir à vélo à l'ENS pour contribuer à l'IPSL à vélo. Fabio, tu m'as aidée à relativiser, car tout ce que je pouvais voir comme une épreuve intimidante était, pour toi, quelque chose de fun ;)

Merci enfin à Caroline, ma troisième directrice de thèse (même si officiellement notée comme "invitée" dans mon jury, par limitation du nombre d'encadrants dans le jury...). Caroline, tu m'as marquée dès notre premier entretien, avec ta manière de me mettre en confiance, ta présence très forte et ta bonne humeur entraînante ! Merci pour ton accueil à l'ISTA, c'était super de découvrir ce deuxième labo en Autriche. Caroline, j'ai adoré interagir avec toi, que ce soit pour aligner des équations sur un carnet, pour discuter de convection nuageuse, ou encore d'empreinte carbone des labos, de la place des femmes en recherche, ou encore du fameux "problème à deux corps" dans l'académique... Merci beaucoup d'avoir été toujours à l'écoute, alors même que tu étais souvent à plus de 1000 km de Paris !

Je souhaite aussi remercier les deux membres de mon comité de suivi de thèse, Samuel Somot et Juliette Blanchet, qui non seulement ont été très pertinents dans leurs questions et leurs retours, mais m'ont aussi donné l'opportunité de venir présenter mes résultats dans leur laboratoire respectifs, au CNRM à Toulouse puis à l'IGE à Grenoble. ça a donné lieu dans les deux cas à une semaine riche en interaction scientifique et humaine, merci beaucoup !

Merci à Jan Polcher, que j'ai rencontré à multiples reprises avant et pendant ma thèse, avec des discussions toujours passionnantes sur l'impact du changement climatique sur le cycle de l'eau et l'hydrologie. Merci particulièrement pour ton enthousiasme lorsque j'ai mentionné que j'envisageais un postdoc en hydrologie au Japon : tu as été d'une aide précieuse pour naviguer dans ce nouvel univers, trouver une équipe de recherche dynamique, et même m'aider sur ma proposition de projet pour la bourse JSPS.

Je souhaite remercier bien sûr mon entourage au laboratoire, en commençant déjà par Sophie et Benjamin, mes cobureaux pendant plus de deux ans, qui m'ont permis de me lancer en thèse dans une

ambiance enjouée. Tous les trois, on a pu tester le trajet en train de Paris à Vienne pour visiter Caroline à l'ISTA, on a découvert Vienne en hiver, ainsi que le trajet en bus jusqu'au super campus de l'ISTA, où Caroline nous a toujours chaleureusement accueillis, dans une équipe qui a grossi au fur et à mesure (tout comme le campus, toujours en extension !). Une équipe qui est devenue si grande, que lors de mon dernier passage en juin 2024, lors du resto d'équipe, on a dû fouiller le restaurant pour rajouter des chaises à trois reprises !

Merci à l'équipe du quatrième étage, c'était quelque chose ! Aglaé, Lucile, Fabio et François qui venaient compléter notre bureau pour le "meilleur couloir" du LMD", avec, pour sûr, la plus belle vue, et des plants de tomates à cultiver. Mission arrosage, récolte et dégustation en été ! Merci particulièrement à Aglaé, d'avoir su m'apaiser et me conseiller quand j'avais des doutes ou des questions brûlantes liées à la prise d'un poste IPEF à la fin de thèse : merci pour ton soutien. Merci à tous les permanents que j'ai régulièrement croisés en salle de convivialité, et qui ont fait de ces instants partagés des moments chaleureux : Fabio, Carole, Tjarda, Xavier, Hélène, Gwendal, Lionel, Sabrina, François, Freddy, Guillaume, Christophe, Nicolas, Lila, Gianluca, Mickaël, Luce, Florence, Laurent, ... La liste est trop longue !

Je suis très heureuse de notre belle dynamique de groupe des thésards/postdocs du LMD-ENS, un petit groupe qui s'est construit et enrichi avec l'arrivée des stagiaires (souvent futurs thésards ici) et grâce à vos efforts, que ce soit pour créer ce trombinoscope dynamique, imaginer des moments de travail collectif, et relancer des goûters ! Benjamin, Sophie, Lucile, Pablo, Vinita, Laetitia, Clément, Solange, Yan, Amaury, Nicolas (qui a aussi été stagiaire avec moi, et avec qui j'ai apprécié travailler, tout comme lancer un frisbee !), Myriam, Belen (oui, je sais, tu es "officiellement" côté Géologie, mais dans le cœur au LMD !), Hannah, Julius, ...

Un gros, gros merci à Lucile, avec qui j'ai partagé ces trois années de thèse, merci pour nos discussions de physique, d'encadrement de thèse, de Climactions, de pâte à pain, de théâtre ou de musique, de vélo ou de rando, ou plus récemment de rédaction de manuscrit et d'escalade ! D'ailleurs, c'était bien souvent autour d'un bon thé, voir régulièrement autour d'un goûter... Ah, ces pauses thé vont me manquer !

Un gros merci aussi à Solange qui, grâce à son année de thèse à Göteborg, nous avoir donné l'occasion d'aller jusqu'en Suède en train ! Merci à vous trois, Myriam, Solange et Lucile, d'avoir fait de ce voyage en Suède une magnifique aventure, entre discussions très sérieuses (le voyage low carbone — autant perso que pro, la vision de la recherche, les difficultés d'encadrement en thèse) et moments super funs (visites, rando-glissade, patinage — tenir sur ses deux patins sur un lac glacé, ce n'est pas si simple !) qui étaient rythmés, bien sûr, par nos pauses gustatives (miam les Cinnamon rolls !!).

Merci beaucoup au collectif LMD-Climactions, pour avoir su poser des questions et lancé une belle dynamique, qui donne envie de s'investir ! Un grand merci particulièrement à Antoine Bierjon qui m'a convaincu de donner un peu de mon temps là-dedans, et à Stéphanie Boniface de l'IPSL-Climactions, qui a fait un boulot monstre pour encourager la dynamique dans les différents laboratoires de l'IPSL, avec une énergie positive que j'ai admirée.

Merci à Aude Lemonsu, qui a co-encadré ma mission politique publique avec le CNRM en 2020 avec beaucoup d'énergie et de bienveillance, et qui m'a motivée pendant ma thèse pour qu'on l'écrive, cet article ! Je n'oublie pas non plus Marie-Pierre Lefebvre, qui pendant cette même mission, m'avait accueillie chaleureusement à Météo-France Saint Mandé en pleine troisième vague du COVID, et qui m'a fait découvrir le LMD avant l'heure en me partageant sa propre expérience. Merci Marie-Pierre pour ce plaisir partagé de piqueniquer ensemble de temps en temps.

Enfin, je voulais dire un grand merci à Sylvie Coussot, qui a pris son poste de psychologue pour les doctorants de l'école doctorale IPParis à peu près à mon début de thèse, et qui a été pour moi d'une

grande aide pour me dire, entre autres, que oui, j'avais bien ma place dans cette thèse. Merci beaucoup pour ton investissement pour tous ces doctorants, il y a un gros besoin, et je pense que c'est vraiment utile ce que tu as proposé !

Enfin, en dehors de l'environnement du labo, merci à tous ceux qui m'ont entourée, encouragée et fait rire. Amaury, mon expert Python à domicile, qui, pour m'aider au mieux, à découvert le microcosme des jobs du serveur Spirit avant même de prendre son poste d'ingénieur de recherche. Un grand merci pour tout ton soutien moral, depuis nos discussions sur le fait de baisser la pression que l'on se met soi-même en recherche, jusqu'aux petits plats maison pendant les dernières semaines de rédactions (même avant d'ailleurs !), sans oublier les dessins de Pompompurin qui s'incrument petit à petit, dans mes cahiers et mes scripts python, pour me faire un clin d'œil. . .

Merci à Angelica, tu es une super amie pour moi. Je sais que tu es là quand j'ai un gros coup de mou, ou bien juste une envie d'expo ou de discuter autour d'un resto ;). Un gros merci à mon club d'Ultimate Frisbee, les Phoenix de Montrouge, et particulièrement à l'équipe de compétition féminine guidée par Léna, Élo et A2, pour toute cette énergie positive que vous partagez, et qui m'a aidée à bien m'aérer pendant ces trois ans de thèse !

Et bien sûr, merci à ma famille, Maman, Papa, Camille, Manon et Nico, pour m'avoir soutenue depuis tout ce temps, tout en se moquant régulièrement, mais gentiment, de toutes mes bourdes ;). Merci à mes grands-parents d'avoir voulu prendre le temps de lire mon projet de thèse IPEF sur la Méditerranée — qui est quasiment la seule chose que j'ai écrite tout en français — ça me touche beaucoup que vous ayez voulu comprendre un peu plus ce sur quoi je travaille. Désolée pour vous, mais la suite de ce manuscrit est quasiment tout en anglais. . . Hmm, mais l'anglais scientifique ça ressemble au français, non ;) ?



Résumé

Français

Le changement climatique peut influencer les précipitations moyennes et extrêmes, avec des effets potentiellement impactants pour les sociétés. La région méditerranéenne est particulièrement touchée et est considérée comme un “hot spot” du changement climatique, en termes de température, précipitations et vulnérabilités des sociétés. En Méditerranée, on s’attend dans le futur à un “paradoxe du cycle de l’eau”, c’est-à-dire une diminution des précipitations annuelles moyennes (“assèchement”) tandis que des précipitations très intenses s’intensifient sur sa rive nord. Cependant, ces signaux ne sont pas encore clairs dans les observations. Bien que ces deux aspects de sécheresses et de précipitations extrêmes soient chacun cruciaux en termes d’impacts sur la société et les écosystèmes, et aient été étudiés par deux communautés de recherche, le potentiel lien entre les deux a rarement été exploré. De plus, l’évolution du reste de la distribution des précipitations a été relativement négligée dans la littérature, alors que son étude pourrait aider à obtenir une vision plus large et plus cohérente de la réponse de la région au changement climatique.

Dans ce travail, nous proposons un nouveau cadre théorique pour examiner comment la distribution globale des précipitations évolue dans la région méditerranéenne au cours du passé récent et des projections futures. Nous utilisons des données de précipitations de la réanalyse ERA5 sur la période 1950–2020, et des simulations Euro-CORDEX pour la période 1950–2100, toutes deux à une échelle de temps quotidienne. Nous développons une méthodologie pour étudier les tendances temporelles des quantiles de précipitations et leur signification statistique.

Nous nous concentrons d’abord sur la distribution des jours de pluie (jours avec plus de 1 mm/jour), puis étudions comment le changement de la fréquence des jours secs peut impacter ces changements d’intensité et donner des tendances différentes en distribution annuelle. Pour la distribution des jours de pluie, à la fois les réanalyses ERA5 et les modèles Euro-CORDEX montrent quatre comportements différents. Certaines régions ont une courbe de tendance des quantiles affichant une “forme en U”, avec des quantiles de précipitations décroissants jusqu’à un seuil donné (“quantile d’inversion”) puis des extrêmes qui s’intensifient. Quelques points ont le comportement inverse (hausse des quantiles faibles et médians, mais baisse des quantiles extrêmes). Deux comportements supplémentaires sont souvent observés : des régions où tous les quantiles de précipitations des jours de pluie diminuent, et d’autres où ils augmentent tous.

Nous avons ensuite modélisé la distribution des jours de pluie avec une loi de Weibull simple (deux paramètres), permettant la définition analytique d’un critère pour déduire les régimes de tendance des précipitations basés sur ces deux paramètres. En étudiant la signification statistique des paramètres de Weibull dans la réanalyse ERA5, nous montrons que le comportement en U n’est pas significatif sur le passé, tandis que le comportement en “Tous les quantiles augmentent” en Europe du Nord est significatif.

Dans un second temps, nous revenons à la distribution de l'ensemble des jours de l'année et examinons comment ses tendances peuvent différer de celles de la distribution uniquement des jours de pluie, en raison du changement de la fréquence des jours secs. Nous comparons également le poids relatif de l'occurrence des précipitations et de leur intensité dans les changements de précipitations. Nos résultats montrent qu'en Méditerranée, sur le passé, les changements de précipitations sont dominés par les changements de la fréquence des jours secs plutôt que par les changements d'intensité des jours de pluie.

Nous appliquons enfin la méthodologie développée aux projections futures, en utilisant un sous-ensemble de 15 modèles Euro-CORDEX avec le scénario d'émissions le plus fort, RCP8.5. Nous comparons d'abord les résultats sur la période passée (1950-2020) avec les données ERA5 : le signal CORDEX n'est pas aussi fort que dans cette réanalyse, mais globalement cohérent. Cela valide notre ensemble de modèles sur le passé.

Nous étudions ensuite la période future 2070–2100, où nous trouvons un très bon accord multimodèle sur les comportements des tendances : la plupart des modèles s'accordent sur un régime "Tous les quantiles augmentent" sur l'Europe avec une augmentation de la fréquence des jours de pluie, tandis qu'en Méditerranée les projections sont robustes sur une diminution de la fréquence des jours secs et un signal plus faible d'augmentation de l'intensité des jours de pluie. La Méditerranée est également contrastée en termes de régimes annuels, entre sa rive nord et sa rive sud, ce qui est cohérent avec la littérature sur les différentes tendances projetées des extrêmes de précipitations. En utilisant à nouveau le modèle de Weibull et l'approche analytique, nous montrons que le changement de distribution des précipitations en Méditerranée est largement dominé par l'augmentation forte de la fréquence des jours secs.

Nous analysons enfin l'émergence tout au long du 21ème siècle du signal sur les régimes annuels de précipitations. Nous montrons que ces régimes deviennent de plus en plus robustes à mesure que le siècle progresse, mais que le rythme de cette émergence varie selon les régions, avec quelques décennies d'avance pour l'Europe du Nord par rapport à la Méditerranée, et une décennie d'avance pour la Méditerranée sud par rapport à sa partie nord.

En résumé, cette thèse a développé un cadre méthodologique original pour caractériser l'évolution des distributions de précipitations, qui permet de mettre en lumière l'importance de l'augmentation des jours secs en Méditerranée comparés aux changements d'intensité, que ce soit dans les données historiques ou dans les projections futures.

English

Climate change is known to have consequences on both mean and extreme precipitation, with potentially threatening impacts on societies. The Mediterranean region is particularly affected, being a hotspot of climate change, in terms of temperatures, precipitation, and societies' vulnerabilities. In the Mediterranean, we commonly expect from the existing literature a “water cycle paradox” in the future, i.e. decreasing mean annual precipitation (“drying”) while very heavy precipitation will intensify on its Northern shore. Still, these signals are unclear in observations. Although these two extreme aspects of precipitation (absence of rain - drought, dry spells etc. - and very heavy precipitation) are each crucial in terms of impacts on society and ecosystems, and have been studied by two research communities, the potential link between the two has rarely been looked at. Besides, the evolution of the rest of the precipitation distribution has been quite overlooked in the literature, while its study might help to get a broader and more coherent picture of the evolution of precipitation over the last decades.

In this work, we look at how the whole precipitation distribution changes in the Mediterranean region over the recent past and the future projections. We use precipitation data from ERA5 reanalysis data over 1950–2020, and from Euro-CORDEX simulations over 1950–2100, both at daily timescale. We develop a methodology to study the temporal trends of the precipitation quantiles and their statistical significance.

We first focus on wet-days distribution (days with more than 1 mm/day), then study how the change in dry-days frequency can impact these intensity changes and give the all-days distribution. For the wet-days distribution, both ERA5 reanalysis and Euro-CORDEX models show four different behaviors. Some places have a quantile trend curve displaying a “U-shape”, with decreasing precipitations quantiles up to a given threshold (“inversion quantile”) and then intensifying extremes. A few places have the opposite regime, with an intensification of low to medium quantiles, and a decrease of extremes. Two additional behaviors are widely observed : regions where all wet-days precipitation quantiles decrease, and others where they all increase.

We then model the wet-days distribution with a simple Weibull law (2-parameters), enabling the analytical definition of a criterion to deduce the precipitation trend regimes based on these two parameters. By studying the statistical significance of the Weibull parameters, we show that the “U-shape” behavior is not significant in ERA5 reanalysis, while the “all quantiles intensify” behavior is significant over Northern Europe.

Still in the past period, we then come back to the all-days distribution and look how its trends can differ from the wet-days distribution's, due to the change of the dry-days frequency. We also compare the relative weight of precipitation occurrence and intensity in precipitation changes. Our results show that in the Mediterranean, the changes of precipitation appear dominated by changes in dry-days frequency instead of wet-days intensity change.

We finally apply the developed methodology to future projections, using a subset of 15 Euro-CORDEX models with the strongest emission scenario, RCP8.5. We first compare results on the past periods (1950–2020) with ERA5 data: the CORDEX signal is not as strong as in this reanalysis, but consistent overall. This validates the selected dataset.

We then study the future period 2070–2100, where we find a very good multimodel agreement on the trends behaviors: most models agree about an “all quantiles intensify” regime over Europe together with an increase of the wet-days frequency, while over the Mediterranean the projections are robust on a decrease of the dry-days frequency and a smaller signal of increased wet-days intensity. The Mediterranean is also contrasted in terms of all-days regimes between its north and southern shore, consistent with literature on the different trends in projected extremes. By using again the Weibull model and analytical

approach, we show that the Mediterranean all-days precipitation is widely dominated by the strong increase of the dry-days frequency.

We finally analyze the emergence of the signal on precipitation throughout the 21st century, in all-days regimes. We show that all-days regimes become increasingly robust as the century progresses, but the pace of this emergence varies by region, with a few decades of lead for northern Europe compared to the Mediterranean, and a decade of lead for southern Mediterranean compared to the northern part.

In summary, this thesis develops an original methodological framework to characterize the evolution of precipitation distributions, highlighting the importance of the increase in dry-days frequency in the Mediterranean compared to changes in intensity, whether in historical data or future projections.

Contents

Remerciements	i
Résumé	v
Table of contents	xi
I Introduction	1
Context and general aspects: climate change impacts and precipitation	2
Climate change is happening	2
Climate modelling	4
Main physical aspects of global precipitation changes	6
Specific state of the art: Climate change’s impacts on precipitation in the Mediterranean region	14
A hotspot of climate change, and the paradox of the Mediterranean water cycle	14
A future decrease in mean precipitation	16
Drying of the region	18
Extreme precipitation intensification on the northern basin	20
A remaining gap of knowledge	21
Thesis objectives and outline	22
Thesis outline	23
II Thesis’s results	25
1 Regimes of precipitation distribution change in the past climate - focus on wet-days	27
1.1 Justification of the study	27
1.2 Precipitation data set	28
1.3 Observed regimes for the change of the wet-days distribution	29
1.4 Analytical model for the wet-days precipitation distribution	32
1.4.1 Choice of a distribution model	32
1.4.2 Expression of the four regimes through a Weibull model	32
1.4.3 Analytical expression of the inversion percentile	34
1.4.4 Consequences for the wet-days categories	35
1.5 Conclusion of the chapter	36
Appendix 1.A Influence of the time period	37
Appendix 1.B Comparison of distribution models for ERA5 precipitation	39
Appendix 1.C Weibull parameters values and uncertainties	40
Appendix 1.D Statistical significance test	40
Appendix 1.E Discontinuities in EOBS precipitations	42
2 Regimes of precipitation distribution change in the past climate - impact of the dry-days frequency change	45

2.1	Impact of dry-days frequency change on precipitation annual mean	45
2.2	Influence on all-days quantiles trends of the dry-days frequency	48
2.3	Modified regimes for all-days quantile trends	49
2.4	Conclusion of the chapter	54
	Appendix 2.A Seasonality of the climate change signal on precipitation	55
	Appendix 2.B Separation between all-days regimes and value of the inversion percentile	61
3	Regimes of precipitation distribution change with future global warming	65
3.1	Selection and correction of a multimodel projection datasets	66
3.1.1	Selection of a dataset of climate projections	66
3.1.2	Bias-correction of the models	66
3.1.3	Choices made in the multimodel analysis	68
3.2	Validation of the selected projections on the past period for wet-days and all-days distribution changes	68
3.2.1	Analysis of the wet-days category maps in Euro-CORDEX and comparison with ERA5	69
3.2.2	Analysis of the all-days category maps in Euro-CORDEX and comparison with ERA5	69
3.2.3	Why is there less robust signal in Euro-CORDEX models, for the Mediterranean in the past, in all-days regimes?	73
3.2.4	Comparison of the contributions of the changes in wet-days frequency and intensity	74
3.3	Analysis of the precipitation distribution changes in projections at the end of the 21st century	78
3.3.1	Analysis of the wet-days and all-days precipitation change regimes	78
3.3.2	Comparison of the amplitude of the changes in wet-days frequency and wet-days parameters	82
3.3.3	The Mediterranean precipitation distribution change is dominated by the wet-days frequency change	86
3.3.4	Comparison with literature for Mediterranean projections	86
3.4	Study of the emergence of the distribution change signal throughout the 21st century	89
3.4.1	First metric: proportion of gridpoints per category	89
3.4.2	Second metric: distance between maps of all-days regime	93
3.5	Conclusions	96
	Appendix 3.A Study of the influence of the bias-correction on the results	96
3.A.1	Different effects of bias-correction on wet-days and all-days regimes	96
3.A.2	Reminder: CDF-t and quantile mapping definition	99
3.A.3	Partial explanation of the stronger impact of bias-correction on wet-days regimes	99
III	Conclusions and perspectives	103
	Conclusions	104
	Perspectives	106
	Perspectives in direct line with the thesis	106
	Perspectives toward hydrological impacts	108
	Bibliography	119

IV Other contributions in climate change research	121
How to disseminate the research results on climate change impacts in cities to guide adaptation public policies ? Application to the Paris region (France)	122
Winter climate preconditioning of summer vegetation extremes in the Northern Hemisphere . .	122

Part I

Introduction

Context and general aspects: climate change impacts and precipitation

Climate change is happening

Climate has naturally changed throughout the Quaternary period, i.e. in the last 2.6 million years. For example, the Earth's climate has been following the changes of solar radiative forcing due to the variation of the elliptic orbit of the Earth around the Sun. This, for instance, has been giving regularly spaced glacial-interglacial cycles, which have a period of about 100000 years since the middle Quaternary, with short interglacial periods of about 20000 years. These can be observed in marine and terrestrial paleoclimate records. As a reminder, the difference of averaged global temperatures between glacial and interglacial periods was of “only” -5°C , and had major consequences (for instance, for the last glacial age, the sea level was 100 meters lower than today, and a huge ice cap was covering the whole Scandinavia up to UK and Ireland). The Earth entered its last interglacial period, called the Holocene Epoch, about 12000 years ago, and for the last 6500 years, the long term trend had been a slow cooling. Up to the mid 19th century.

The warming we observe since the preindustrial period in the mid 19th century is totally unprecedented. Between 1850–1900 and 2011–2020, the Earth global temperature is estimated to have warmed by 1.1°C (Intergovernmental Panel On Climate Change (IPCC), 2023), as illustrated on figure 1. As a comparison, the natural warming which occurred at the end of each glacial period took about 5 thousand years, with a maximum warming rate of about $1.5^{\circ}\text{C}/1000$ years. This is about 10 times less than what we observe today, and it highlights how fast and intense the current global warming is.

In 1988, a new organization called the Intergovernmental Panel on Climate Change (IPCC) was established by the United Nations General Assembly, with the mission to provide policymakers with regular scientific assessments on the current scientific state of knowledge about climate change, both concerning its causes and consequences. Since 1988, the IPCC has become worldly known for its work, namely its six successive Assessment Reports (AR), in addition to special reports and technical papers in response to requests from other international organizations. The IPCC work has greatly helped to establish an extremely clear consensus in the scientific community, stating that current climate change is solely due to human activities (illustration on the temperature curve in figure 1). For instance, the Second Assessment, published in 1995, expressed a greater certainty that climate change was largely caused by human activities. In the Fourth Assessment in 2007, the IPCC used words like “unequivocal” to describe the consensus that human activities are the main cause of global warming.

The term of (anthropogenic) climate change in the following, will therefore describe the unequivocal fact that the Earth's climate is warming and changing at a rate that has never registered on Earth history, and that it is due to the rapid increase of the atmospheric concentration of greenhouse gases caused by human activities (transport, energy production, agriculture, deforestation, etc.).

Climate change consequences have already been observed in a number of striking ways. It does not restrict to an atmospheric warming (though regular record-breaking hot temperatures are occurring year after year) but also concerns many other aspects of the Earth components. For example, climate change impacts consists in the surface ocean warming up, in sea level rising (with a current rate of about 4 cm per decades), melting glaciers and sea ice caps, acidification of the oceans, disturbed carbon and nitrogen cycle, disruption of the water cycle, and so on. Note that the effect of climate change on temperature extremes is of much higher amplitude than the effect on precipitation extreme (figure 2), and is also

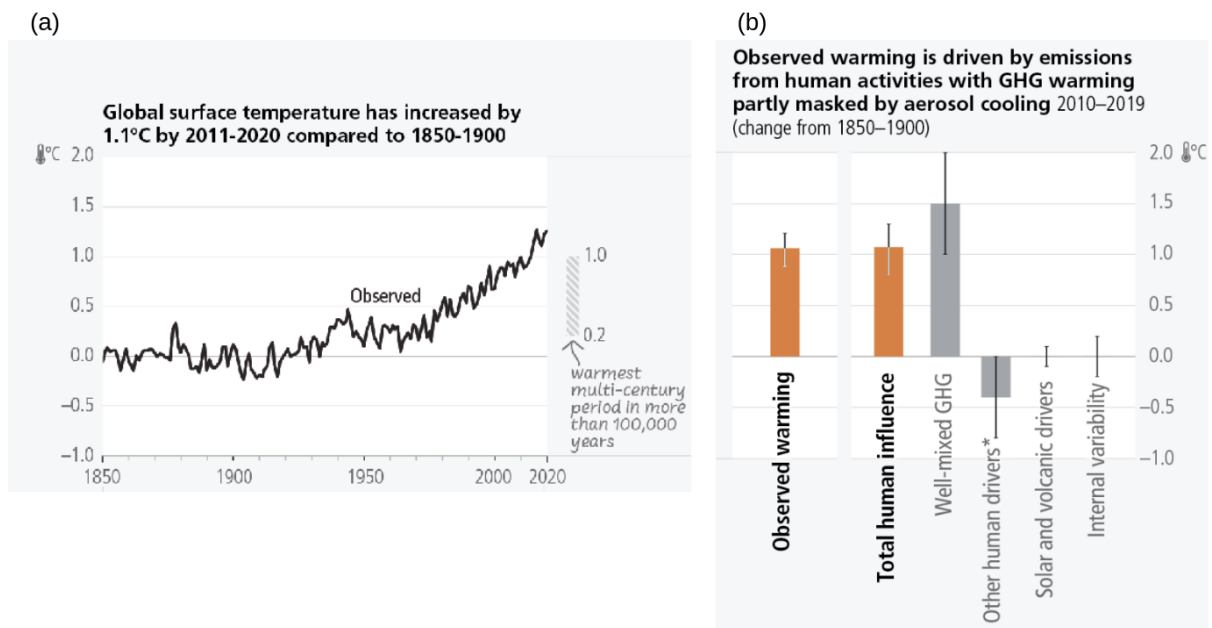


Figure 1: (a) Observed increased of global temperature from 1850 to 2020, and (b) attribution of the current temperature increase to human emissions, far before potential changes due to solar activity and volcanic eruptions, with an offset of cooling aerosols. The subfigures were extracted from Figure 2.1 of the synthesis report of the AR6 (Contribution of Working Groups I & to the Sixth Assessment Report of the Intergovernmental Panel on Climate Change, 2023).

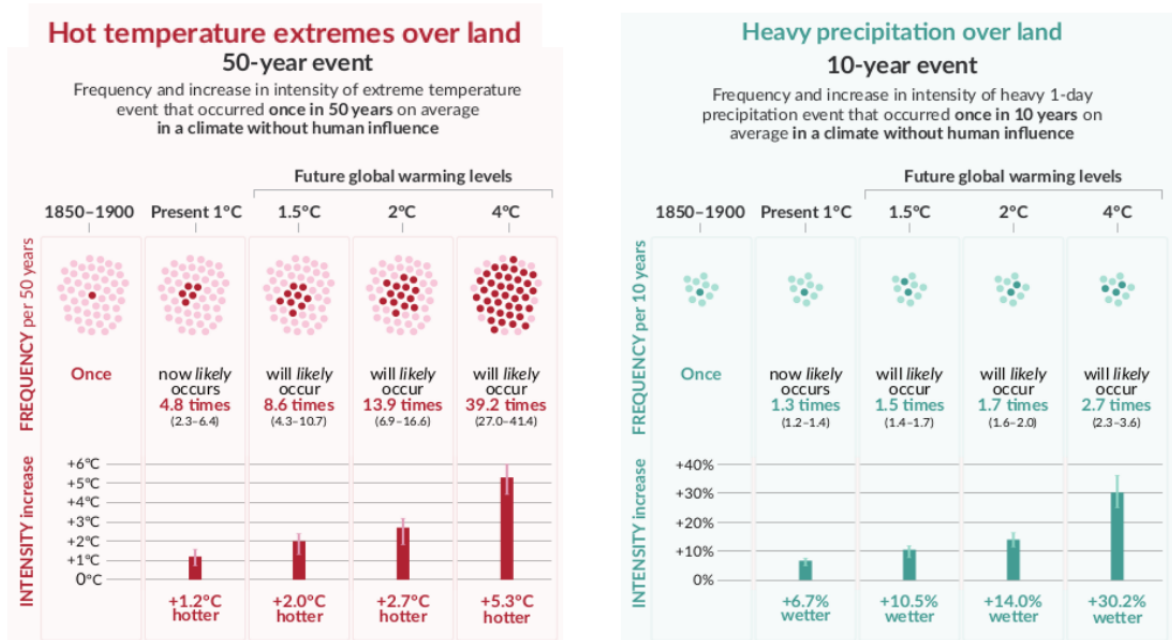


Figure 2: Observed and projected change in terms of (a) extreme temperature (here, a 50-year event) and (b) extreme precipitation (here, a 10-year event), at global warming levels of 1.5°C, 2°C, 3°C, and 4°C relative to 1850–1900. Figure extracted from the summary for policymakers of the IPCC's 6th Assessment Report, Working Group I, Intergovernmental Panel On Climate Change (IPCC), 2023

easier to observe on recent past climate. The precise impacts on the water cycle, in comparison, are more difficult to study.

Climate change also has strong regional variations, with for example a clear land-sea contrast and differences linked to latitudes. They can be due to complex phenomena and feedbacks such as land-atmosphere interactions and changes in the regional or large-scale dynamics. For example, the air above the continents are expected to warm about 1.5 time faster than above the oceans, and the high latitude of Arctic region even faster (about twice as fast) due to an albedo feedback among other mechanisms. Therefore, some regions with particular high projected changes are considered as hotspots of climate change. The Mediterranean region, as we will detail later, is one of those climate change hotspots.

In the next section, we will describe briefly the modeling tools used to model and understand climate change, both at global and regional scale.

Climate modelling

The study of climate change and its impacts on the water cycle greatly relies on our capacity to understand and model the climate system. But what is a climate model? We will describe this tool briefly, both concerning global and regional simulations.

Global models are generally used to derive climate information at global scale, for both past and future climates. These types of models are called General Circulation Models (GCM). In meteorological or climatic modeling, the set of conservation equations for momentum, energy, water and mass, are solved numerically by the model, at each gridpoint, using spatial and temporal discretization. Therefore, the atmosphere domain is divided into meshes, which can be simple latitude longitude meshes as visible in figure 3, or more complex such as icosahedral meshes. In the solving of the equations, a part translates the exchanges between meshes and is explicitly solved by discretizing the partial differential equations on the meshes. This exchange part is identified in blue outline in figure 3.

The nominal horizontal resolution of models is typically 100 to 200 km, and has improved a lot since the first IPCC report, thanks to the huge advances in computational power. The computation time needed for a simulation is proportional to the number of years simulated, but it also increases as the nominal resolution, usually to the power four (since there are three spatial dimensions, plus the temporal one which is usually constrained by the spatial resolution for numerical stability reasons).

Sub-grid phenomena can not be explicitly resolved, and have to be parametrized. Parameterization is a method of replacing, by a simplified description, processes that occur at a too small scale (compared to the model's grid) or which are too complex to be physically represented in a numerical model. In global models, this is the case for the life cycle of convective clouds, the cloud microphysics leading to precipitation, turbulence, surface-atmosphere exchanges such as evaporation, etc.

The effective resolution of a model is around three to five times greater than the grid resolution. This severely limits the model's ability to capture the effects of local forcing (e.g. complex topography and land-surface characteristics) which modulate the climate signal at fine scales. Therefore, to have a more accurate climate information at a regional level, different regionalization methods have been developed in the last few decades, usually divided in either statistical "downscaling" or dynamical "downscaling" methods. Very briefly, statistical downscaling methods estimate a link from the distribution of a large-scale variable (produced by a GCM for example, on the historical period) and the same variable but at a local scale (for example, station based precipitation). It then uses this relation to downscale the future projections of the GCM at a finer scale. On the other hand, dynamical downscaling requires another physically-based model to run, on the domain of interest: a Regional Climate Model.

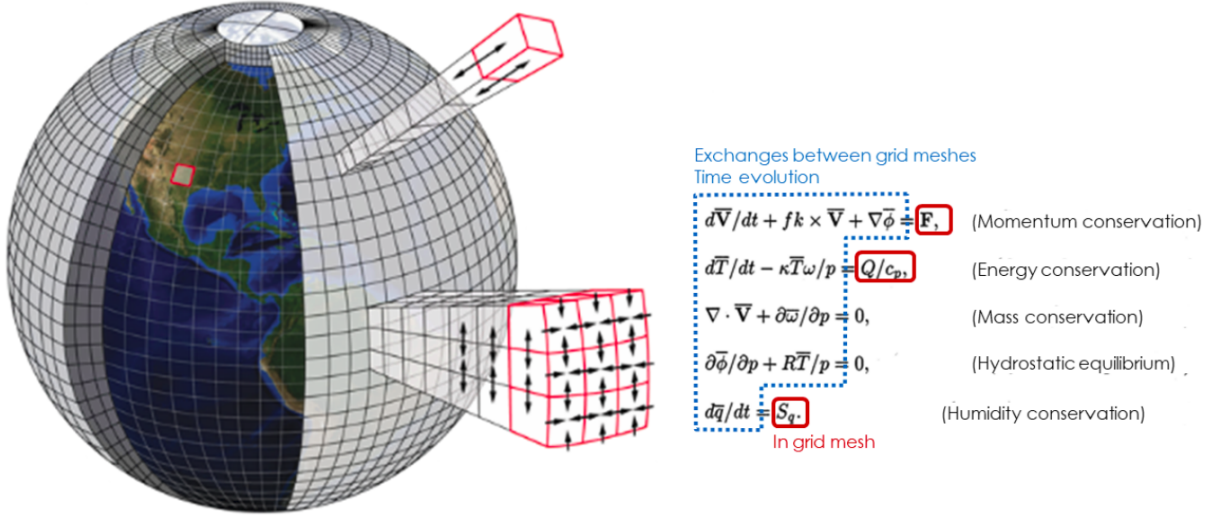


Figure 3: Illustration of a three-dimensional atmospheric mesh used in some climate models, to solve the conservation equations listed on the right side. The part of the equations framed in blue represents the transport of atmospheric variables between meshes, while the part of the equations framed in red correspond to the terms of source or sink in the cell. These terms are called physical parameterization. Source: Drobinski, 2020.

A Regional Climate Model (RCM) is a limited-area model which focuses on the climate of a specific regional domain (for example, Europe), and uses the outputs from a Global Circulation Model at the borders of the domain to get the information of the large-scale atmospheric dynamics. Because they do not cover the whole globe, RCMs can have a higher spatial resolution than GCMs at a lower cost (usually 10 to 30 km for a RCM compared to 100 to 200 km for a GCM). Therefore, RCMs can better represent the land-sea effects, the orography, etc. Regional simulations have been shown to improve the representation of local climate, with for example better intensity and spatial patterns for extreme precipitation.

Outputs from climate models are a very useful tool for understanding the climate, quantifying the effect of a mixture of complex phenomena, of feedbacks mechanisms, etc. But climate models also have many limitations, and some of them impact the representation of precipitation. Climate models have well-known biases, such as the ‘too few, too bright’ representation of clouds, or the “drizzle” issue, i.e. the fact that they produce too often small quantities of rain (Bastin et al., 2019). Extreme precipitation are often underestimated, especially when the spatial resolution of the model is coarser (Khodayar et al., 2016). Besides, the parametrization brings a difficulty in itself, and it has been shown that the choice of the parametrization scheme can greatly impact the resulting precipitation (Cr  tat et al., 2012; Di Luca et al., 2014; Cavicchia et al., 2018).

Because of these limits, an ensemble approach is often used, i.e. studying a given phenomenon in not only one model but an ensemble of models, which have different parametrization schemes, choices of microphysics, etc. This enables to quantify the uncertainties of the modelling. Besides, an ensemble approach also has the advantage to filter out natural variability, by averaging the different models results, and to highlight the signal due to anthropogenic climate change. This is why prior to each of the IPCC assessment reports, there has been a Coupled Model Intercomparison Project (CMIP), which is the analysis of climate projections produced by climatology institutes worldwide (with two institute at the French level, M  t  o-France and Institut Pierre Simon Laplace - IPSL) following a set of guidelines (e.g. temporal period, aerosols or greenhouse gases forcing, availability of the output data, etc.).

An illustration of the multimodel approach of the 6th CMIP is shown in figure 4, where the projected global temperature’s evolution is shown throughout the twenty-first century. On the figure, the five

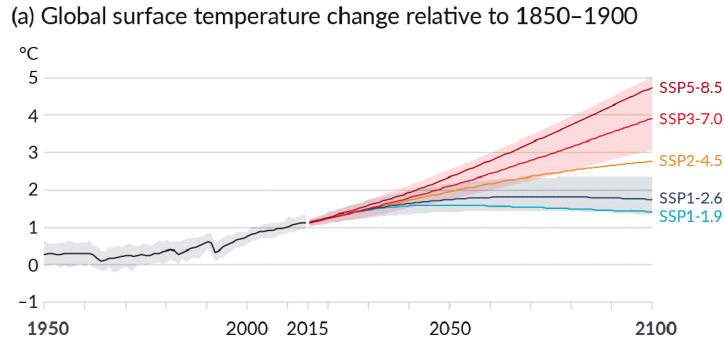


Figure 4: Projected global mean temperature in $^{\circ}\text{C}$, relative to 1850–1900. It is obtained by using a multimodel approach on the simulations done for 6th Coupled Model Intercomparison Project (CMIP6), combined with observational constraints. *Very likely* ranges (colored area) are shown for the scenario SSP1-2.6 and SSP3-7.0. For IPCC, *Very likely* designate an assessed result likelihood of 90–100%. The figure was extracted from the AR6 Summary for Policymakers of Intergovernmental Panel On Climate Change (IPCC), 2023, figure 8(a).

different scenarios for anthropogenic activities used for the 6th Assessment Report are displayed. They are called SSP, for Shared Socio-economic Pathways, and the higher the number associated to the SSP, the higher the greenhouse gases emissions and the resulting global warming.

At the regional level, similar initiatives of models intercomparison have been done, such as the Coordinated Regional Climate Downscaling Experiment (CORDEX), with for example Euro-CORDEX focusing on Europe, MED-CORDEX on the Mediterranean region, CORDEX Africa on Africa, etc.

The present thesis focuses on the climate change’s consequences on regional precipitation, within the Mediterranean region. Before going into the state of the art of the observed and projected changes of diverse precipitation indices within the Mediterranean region, we would like to give some physical sense of how global precipitation is impacted by climate change.

Main physical aspects of global precipitation changes

Precipitation is a paramount part of the water cycle. It designates both rain, snow, hail, or other mix phases such as graupel. Precipitation is created by the condensation of water vapor in a saturated air, forming micrometer droplets, which can merge due to microphysics phenomenon, giving finally birth to large enough drops on which gravity is finally not negligible and make them fall. The precise formation of water droplets and drops is a whole field of microphysics. The conditions favorable to the formation of precipitation is usually an ascendance of moist air, in which the air parcel cools down and finally saturates. How precisely convection favors precipitation and extreme precipitation is also a whole field of research, that we won’t detail further in this introduction. We can still highlight that these conditions are not even across the globe, as can be seen on figure 5. Indeed, due primarily to large scale circulation patterns (caused by the difference of solar heat received between the equator and the poles), there exists a tropical band with high values of annual precipitation, called the Inter-Tropical Convergence Zone, while the subtropical zones have generally very low precipitation, as for example the Sahara desert.

In this section, we will focus on how climate change impacts precipitation at the global scale. We aim to give the reader a rapid overview of the main mechanisms explaining how climate change can impact both total and extreme precipitation. It is usually considered that there is a separation between scales larger than about 4000 km, where the water cycle change is dominated by the thermodynamics and the energy budget, and scales smaller than 4000 km, where the water cycle is dominated by transport of moisture, influenced by both thermodynamic and dynamical aspects (Dagan et al., 2019; Intergovernmental Panel

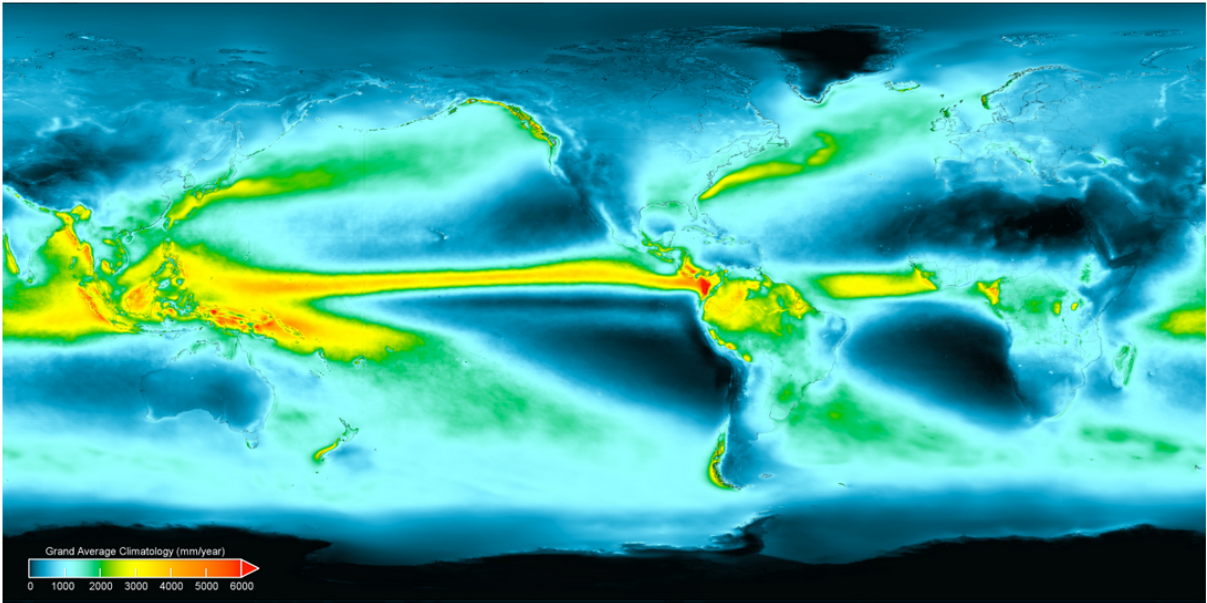


Figure 5: Total annual mean precipitation (mm/year) computed over June 2000–May 2023, using data from the satellite IMERG. This figure highlights the uneven character of total precipitation. Source: [NASA](#)

On Climate Change (IPCC), [2023](#)). We will first detail these thermodynamic aspects, coming from the Clausius-Clapeyron law, and we will then see its consequences on precipitation changes.

Clausius-Clapeyron relationship

The Clausius-Clapeyron law is a thermodynamic relation, which states that the saturation vapor pressure e^* of a parcel of air is a function depending only on the air temperature T , and increases with temperature following a precise rate:

$$\frac{1}{e^*} \frac{de^*}{dT} = \frac{L_v}{R_v T^2} \quad (1)$$

with L_v the specific latent heat of vaporization of water (which we consider as a constant for the range of temperature at stakes) and R_v the gas constant of water vapor, both positive. This rate of change of the saturation vapor pressure ($\alpha = \frac{1}{e^*} \frac{de^*}{dT}$) is equal to $\alpha = 7\%/^\circ\text{C}$ for $T = 0^\circ\text{C}$ and $\alpha = 6\%/^\circ\text{C}$ for $T = 27^\circ\text{C}$, which are within the range of temperature of the lower troposphere. The rate can reach $12\%/^\circ\text{C}$ depending on latitude (O’Gorman & Muller, 2010).

Besides, we can integrate Clausius-Clapeyron between two temperatures, T_0 and T , to get:

$$e^*(T) = e^*(T_0) e^{\frac{L_v}{R_v} \left(\frac{1}{T_0} - \frac{1}{T} \right)}$$

In a case of a warming $T = T_0 + \delta T$ with $\delta T \ll T_0$, we can do a Taylor expansion, $\frac{1}{T_0} - \frac{1}{T} \approx \frac{\delta T}{T_0^2}$, giving:

$$e^*(T) = e^*(T_0) e^{\frac{L_v}{R_v} \frac{\delta T}{T_0^2}}$$

In other words, Clausius-Clapeyron states that the saturation vapor pressure increases quasi-exponentially with warming.

From the saturation water vapor, we can come back to the specific humidity at saturation q_v^* . Specific humidity q_v is defined as the ratio of the density, ρ_v , in kg/m^3 , of water vapor contained in an air parcel to the air parcel total density, ρ : $q_v = \frac{\rho_v}{\rho}$. Since the mass of an air parcel is largely dominated by the mass of the dry air, ρ_d , we can approximate: $q_v \approx \frac{\rho_v}{\rho_d}$. The ideal gas law gives, for respectively the dry air and the water vapor partial pressures:

$$\begin{aligned} e &= \rho_v R_v T \\ p - e &= \rho_d R_d T \end{aligned}$$

with R_d the specific gas constant of dry air, and p the total pressure which, by Dalton’s law, is the sum of the partial pressures of dry air and water vapor. Computing the ratio of the two equations above, and neglecting the water vapor pressure compared to the total pressure, we get:

$$\frac{\rho_v}{\rho_d} = \frac{R_d}{R_v} \frac{e}{p - e} \approx \frac{R_d}{R_v} \frac{e}{p}$$

Thus, the specific humidity is directly linked to the vapor pressure, $q_v \approx \frac{R_d}{R_v} \frac{e}{p}$. Finally, at saturation, we get:

$$q_v^* \approx \frac{R_d}{R_v} \frac{e^*(T)}{p}. \quad (2)$$

Therefore, Clausius-Clapeyron also implies that specific humidity at saturation increases quasi-exponentially with temperature, at the same rate as the saturation vapor pressure.

In other words, air has the capacity to retain more water vapor at higher temperatures, and Clausius-Clapeyron law tells us that this water retention capacity of the atmosphere increases by typically 6–7% per degree Celsius.

Besides, relative humidity RH measures the distance to water vapor saturation, and is defined as: $RH = e/e^*(T)$. It has been observed that the changes of relative humidity are small and negligible

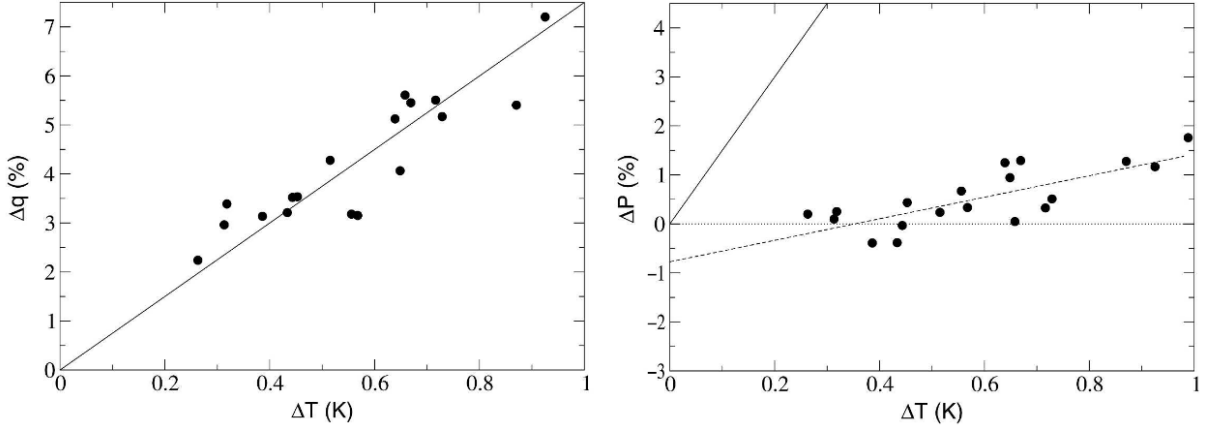


Figure 6: Scatter plot of the percentage change in (left) global mean column-integrated water vapor q and (right) global mean change of precipitation P , with respect to change in surface air temperature, over the twentieth century, as modeled by the 20C3M global simulations from the IPCC fourth Assessment Report. The black line represents the Clausius–Clapeyron rate of about 7.5 %/K, while the dashed line represents the linear fit between ΔP and ΔT , of 2.2 %/K. The figures were extracted from figures 2c and 2d of Held and Soden, 2006.

compared to the changes due to Clausius–Clapeyron (both empirically in global climate simulations and theoretically in last saturation models). Therefore, supposing RH constant, both the water pressure e and the specific humidity q_v should also follow Clausius–Clapeyron rate.

This approximate rate of increase for specific humidity is very well verified in models (Trenberth, 1999; Allen & Ingram, 2002; Held & Soden, 2006; Intergovernmental Panel On Climate Change (IPCC), 2023), and is illustrated in the figure extracted from Held and Soden, 2006, in figure 6. This figure shows that the changes of the global mean column-integrated water vapor (dominated by the lower atmosphere water vapor, thus by specific humidity) of models from the IPCC AR4 show very good agreement with the Clausius–Clapeyron law. It is therefore a very robust change.

This has implications for the response of the global hydrological cycle to climate change. We could expect both total precipitation and extremes to follow Clausius–Clapeyron rate. Yet, as we discuss in the next section, the global averaged total precipitation increases at a slower rate, due to energetic constraints.

Global total precipitation and energetic constraint

It is important to stress that the global total precipitation, which quantifies the strength of the water cycle, does not follow the Clausius–Clapeyron relationship. Instead, total precipitation increases with temperature at a lower rate, of about 2–3 %/°C. Here, we will give the main ideas of how we can get to this estimate.

We can first do a mass balance for the water fluxes, on the atmosphere as a whole. As there is no water exchange with space, and as lateral transports of moisture stay within the atmosphere, the only mass fluxes are the surface ones: a gain due to the evaporation E from the surface and a loss from precipitation P , with P and E both in mm/day. The change of water content of the atmosphere, Q_a , will thus be determined by:

$$\frac{dQ_a}{dt} = E - P. \quad (3)$$

Since the lifetime of water in the atmosphere is very short (typically about 10 days), if we integrate over a longer period, for example a year, the left term vanishes: $\frac{dQ_a}{dt} \approx 0$. Thus, we get that $E = P$, i.e that

total evaporation and total precipitation exactly compensate each other at global scale.

This equivalence between total evaporation and total precipitation is well observed. For example, L'Ecuyer et al., 2015 used satellite observations covering 2000–2009 to assess the water fluxes, which gave $L_v P = 78 \pm 7 \text{ W/m}^2$ for the energetic flux linked to precipitation, and $L_v E = 75 \pm 5 \text{ W/m}^2$ for the evaporative flux (with L_v the latent heat energy of vaporization), thus P and E values have indeed almost identical values in observations.

Let's now write the atmospheric energy budget at the global scale. Let's note Q_{rad} the net energy received by the atmosphere from shortwave and longwave radiation, SHF and LHF the sensible and latent heat flux at the surface, with $LHF = L_v E$. Then, since the latent heat flux is an order of magnitude larger than the sensible heat flux, we get:

$$Q_{rad} = LHF + SHF \approx LHF = L_v E.$$

Since from the global mass budget, we know that evaporation is equal to precipitation, we finally get:

$$Q_{rad} \approx L_v P$$

This balance between the net radiative cooling and the heating produced by water condensation in clouds is called the radiative-convective equilibrium (RCE). The net radiative cooling Q_{rad} is empirically estimated to rise with temperature by about 2–3%/°C, through a set of complex mechanisms (see chapter 8 of Intergovernmental Panel On Climate Change (IPCC), 2023). Therefore, total precipitation and evaporation are expected to increase slowly with warming, by about 2–3%/°C, constrained by this energy budget.

This increase of 2–3%/°C of global total precipitation is well verified in climate models, for example in previous generations of climate simulations (Trenberth, 1999; Allen & Ingram, 2002; Held & Soden, 2006) as illustrated on figure 6, and more recently in the climate simulation from CMIP5 and CMIP6, as illustrated on figure 7.

Faster intensification of extreme precipitation

Extreme precipitation events are events that bring very large quantities of water over a short period of time (of the order of an hour to a day) which may even represent the quantity usually received in one month or sometimes a year. They are usually defined as an event corresponding to high percentile ranks of precipitation occurrence. For instance, the 99.9th percentile corresponds to the amount of daily precipitation exceeded with probability 1/1000, or in average once in 1000 days (thus 1000 days is called the return period). They can also be defined as a block maximum with, for instance, the commonly used maximum daily precipitation over a year. Note that an extreme is dependent on time and space, as it is defined compared to the precipitation distribution of a specific region and on a given period.

Globally, extreme precipitation are expected to increase with climate change. The Clausius-Clapeyron relationship is widely used to quantify the link between warming and the amplitude of extreme precipitation, to first order. The main idea is that an extreme precipitation event occurs when all the moisture contained in the air is precipitated out, thus extreme precipitation is expected to increase with warming following atmospheric water vapor, at the Clausius-Clapeyron rate (Trenberth, 1999; Allen & Ingram, 2002).

More precisely, we can give a scaling for extreme precipitation, showing the contribution of thermodynamics and of other factors, as introduced by Betts and Harshvardhan, 1987 and further developed

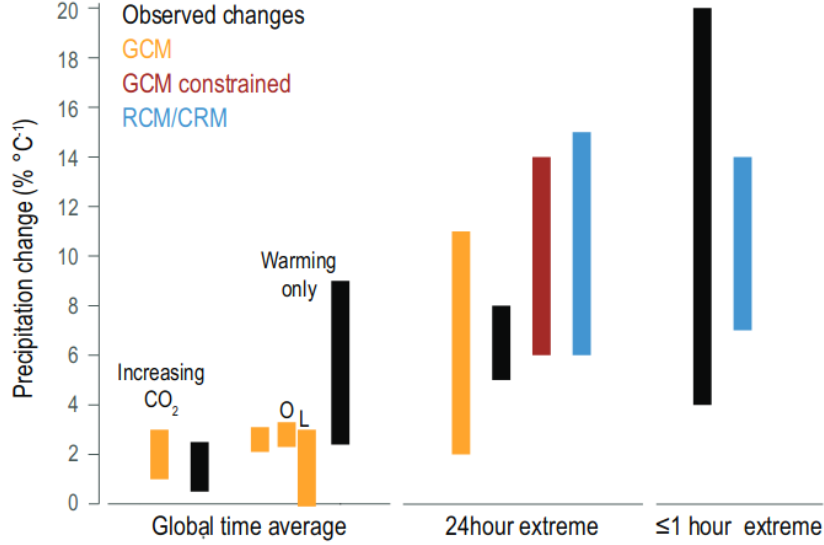


Figure 7: Estimate (5-95% range) of the increase in total precipitation (left), daily (middle) and sub-hourly extremes (right), with global mean surface warming. Daily extreme is defined as either the 99.9th percentile or annual maximum extremes. The data comes either from observations (black bars), global circulation models (GCM, yellow and red bars), or regional climate models and cloud-resolving models (RCM / CRM, blue bars). GCM can decompose the effects in land (L) and ocean (O) components. The figure was extracted from the chapter 8 of the IPCC AR6 report (Intergovernmental Panel On Climate Change (IPCC), 2023).

by O’Gorman and Schneider, 2009; C. J. Muller and O’Gorman, 2011; C. Muller and Takayabu, 2020. It translates the fact that a precipitation event consists of air rising, cooling adiabatically, and when saturation is reached, a certain amount of water vapor condenses as the air parcel continues to rise. The scaling is the following:

$$P_{extr} \sim \epsilon \int_0^H \rho w \frac{dq^*}{dz} dz$$

where P_{extr} is the extreme precipitation, ϵ the precipitation efficiency (fraction of the condensed water vapor which finally reaches the Earth’s surface), H the height of the ascent (typically the tropopause for deep convection), ρ the air density, w the vertical velocity and q^* the saturation specific humidity. If there is no change in vertical velocity, precipitation efficiency nor atmosphere height, then extreme precipitation change would be indeed governed by the saturation specific humidity and thus follow the Clausius–Clapeyron rate. But changes in dynamics, or in microphysics (linked to the efficiency ϵ), can lead to departure from this scaling, for instance due to convective organization (C. Muller & Takayabu, 2020), as confirmed in idealized (Da Silva et al., 2021) and realistic (Bao et al., 2024) storm resolving models.

We can keep in mind that the thermodynamic scaling of extreme precipitation of about 7%/°C is a first order estimation, with which multimodel projections agree quite well, as illustrated on figure 2 for a 10-years extreme precipitation (Held & Soden, 2006), though there can be a large dispersion between models, as seen on figure 7.

Intensification of the water cycle

When we speak of water cycle here, we often refer to the local difference of precipitation P to evaporation E , at a local scale. As mentioned before, at the global scale, the water mass balance forces total evaporation and total precipitation to be equal. Yet, there is not such constraint locally.

Theoretically, we expect from thermodynamics an intensification of the water cycle, defined as an enhancement of the current spatial patterns of $P - E$. A simple scaling was proposed by Held and Soden, 2006. In this article, they considered the water mass balance at a local scale, integrated on the depth of the atmosphere. Then, the divergence of the vertically integrated horizontal moisture fluxes, F , balances the difference of evaporation and precipitation:

$$E - P = \text{div}(F)$$

The authors made the hypothesis that the changes in the moisture flux F was dominated by the change of air moisture, neglecting the changes in dynamics. Therefore, they applied a Clausius Clapeyron scaling for F giving $\delta F = \alpha \delta T F$, with α of about $6\text{--}7\%/^{\circ}\text{C}$ and δT denoting global mean surface temperature change. Therefore, the local water balance equation gives:

$$\frac{\delta(P - E)}{(P - E)} = \alpha \delta T$$

i.e. the patterns of $P - E$ intensify with temperature, following the Clausius-Clapeyron rate.

This intensification of the $P - E$ patterns is often referred to as the “wet get wetter” and “dry get drier” phenomenon. It has been verified particularly well on global ocean observations in Durack et al., 2012 which used surface salinity data as a proxy for the surface fresh water change, on the period 1950–2000. In this article, they proved that the patterns of precipitation minus evaporation over the oceans were enhanced in observations at a rate of $8\%/^{\circ}\text{C}$, therefore following very well the Clausius Clapeyron scaling of Held and Soden, 2006. This mechanisms over the oceans can therefore be described as the “fresh gets fresher, salty gets saltier” phenomenon, and is considered as a *robust evidence* and *high agreement* fact, in the chapter 8 of Intergovernmental Panel On Climate Change (IPCC), 2023.

Nevertheless, this scaling has its limits, since it is based on thermodynamics solely. For example, there is an amplification of this mechanism over the tropical ocean, which is partially due to the upper layer warming faster, enhancing ocean stratification. Besides, the scaling is not adequate on land: usually $P - E > 0$ on lands, as they receive more precipitation than the water lost through evaporation, but Southern Chile and Argentina undergo a decrease in $P - E$ (thus $\delta(P - E)$ and $P - E$ are of opposite signs). Large departures from the thermodynamic scaling can be observed at regional scale on land, due to changes in atmospheric circulation, oceanic moisture supply, or land-surface and vegetation feedbacks. Besides, the change in soil moisture can impact the partitioning between evaporation and runoff, complicating the $P - E$ scaling. What is however robust over land, is an intensification of the very wet and very dry seasons, such that wet spells become wetter and dry spells drier (chapter 8 of Intergovernmental Panel On Climate Change (IPCC), 2023). The IPCC therefore concludes that the $P - E$ response on land is highly region and season dependent.

Uneven changes in precipitation at regional scale

What we presented in this introduction so far is that, when considering global scales, total and extreme precipitation are both expected to increase with warming, with a higher rate for extreme precipitation than total precipitation. But how do these global averages translate regionally?

The key message is that the changes of precipitation are not uniform at all. At regional scales, the changes in local mean and extreme precipitation can indeed vary substantially from their global scale values, due both to dynamical aspects and natural variability (Trenberth, 2011; Fischer et al., 2013; Fischer & Knutti, 2014; Pendergrass & Hartmann, 2014; Pfahl et al., 2017). For instance, contrary to temperature changes which are positive everywhere, there exist some regions such as the Mediterranean,

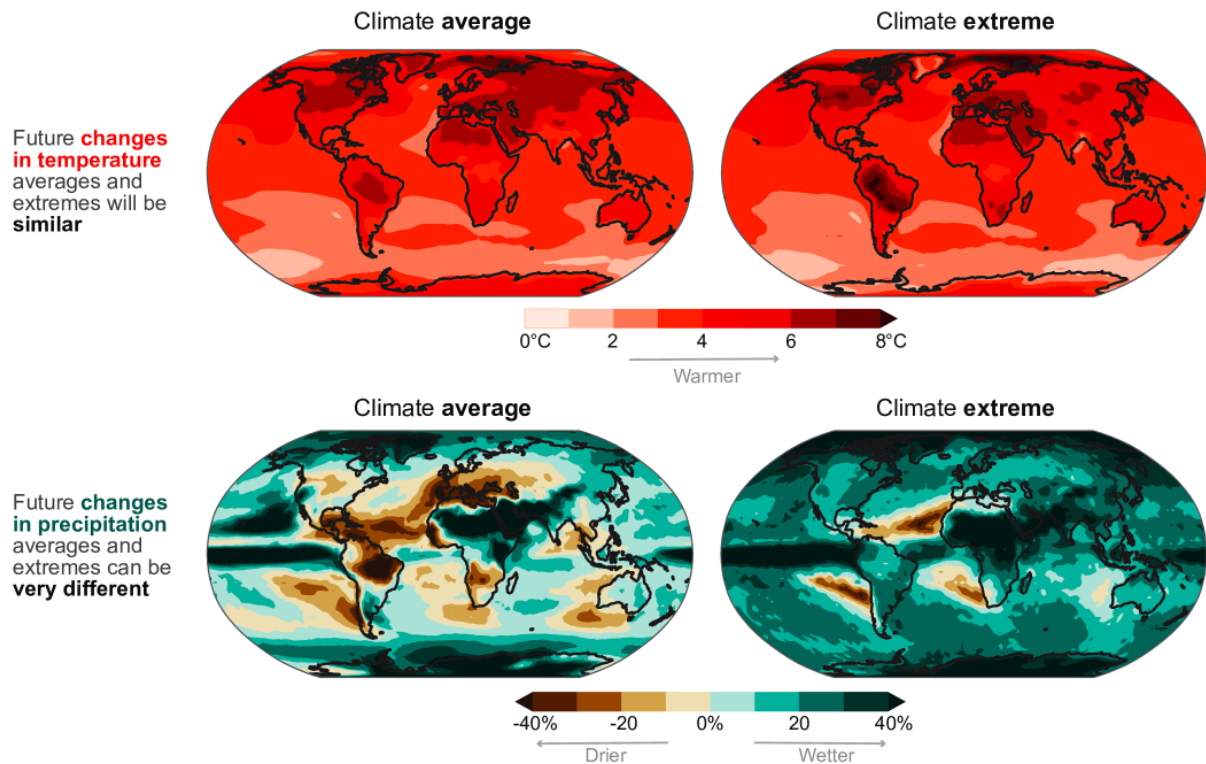


Figure 8: Global maps of future changes in surface temperature (top panels) and precipitation (bottom panels) for long-term average (left) and extreme conditions (right). Extreme temperatures here refer to the hottest day in a year, and extreme precipitation to the largest daily precipitation in a year. Changes are estimated from the Coupled Model Intercomparison Project Phase6 (CMIP6) ensemble median, at global warming levels of 4°C relative to 1850–1900. The figure was extracted from Intergovernmental Panel On Climate Change (IPCC), 2023 (FAQ 11.1, Figure 1).

where averaged precipitation and to a lesser degree the extremes, are projected to decrease, contrary to their globally averaged values. This is well illustrated in figure 8, which displays the maps of projected future changes in mean and extreme precipitation: these two patterns of change are not uniform around the globe, and they differ from one another. The Mediterranean region is also one of the regions with different trends in the mean precipitation compared to extreme precipitation, together with for instance Northern US, Southern Africa, and Southeast-Asia.

We hope we have given the reader an overall view of the different impacts of climate change on the global water cycle and that we provided some evidence that the story can be much different at the regional scale, for the water cycle as for the precipitation. As the Mediterranean region is the focus of the thesis work, we will now describe what the climate change effects on precipitation are within this region.

Specific state of the art: Climate change’s impacts on precipitation in the Mediterranean region

The Mediterranean is the first region worldwide where a local equivalent of the IPCC was created: the Mediterranean Experts on Climate and environmental Change, MedECC, was indeed founded in 2015. It aims to acquire an advanced scientific understanding of the issues related to climate change, in terms of impact on populations, health, energy production, biodiversity, water resources and climate-related risks. The MedECC published its first assessment report in 2020, and a few special reports on some specific topics, such as climate change and coastal risks. Summaries for policymakers have been made available in nine Mediterranean languages on the [MedECC website](#). For French readers, an illustrated summary is also available, aiming at a larger public: [Résumé pour tous par le Collectif Citoyens pour le Climat](#).

In this section, we will describe the state of the art concerning climate change’s impacts on the Mediterranean water cycle, with a focus on the precipitation change. In a nutshell, we’ll see that the Mediterranean is a hotspot of climate change with a paradoxical change of its water cycle, due to a strong drying and a projected intensification of precipitation extremes in the northern part of the region.

A hotspot of climate change, and the paradox of the Mediterranean water cycle

In Giorgi, 2006, the author developed for the first time an indicator of regional sensitivity to climate change based on four terms: the changes in mean and inter-annual variability of temperature and precipitation. The indicator was computed on the 20 climate projections produced for the IPCC fourth assessment report. The Mediterranean region stood out with one of the largest indicators, along with that for northeastern Europe, as visible on figure 9: hence the qualification of the region as “climate change hotspot” (Giorgi, 2006). Multiple studies have since corroborated this qualification of the Mediterranean. In its first report, the MedECC confirmed that the Mediterranean is indeed a climate change hotspot, due to both the projected increase in climate hazards and the high vulnerability of the socioeconomic sectors and natural ecosystems.

In the Mediterranean basin, the average annual temperatures have already risen by 1.5°C compared to pre-industrial times, i.e. 0.4°C higher than the global average change, according to the first MedECC report, Azzopardi et al., 2020. The region is projected to warm up faster than the global average, with an annual temperature increase about 20% higher and a summer temperature increase about 50% higher. The duration and intensity of heatwaves are also on the rise, with a recent absolute record for temperature in France in June 2019 (46°C in the Hérault department), while the August 2003 European heatwave was particularly memorable, both for the strong anomaly it displayed compared to the climatology, and for the high number of deaths it caused in Europe. Note that urban populations, which account for almost three-fourth of the Mediterranean basin’s inhabitants in 2020, are particularly hit by extreme heat, as the urban heat island phenomenon exacerbate heatwaves temperature, especially at night.

The water cycle in the Mediterranean is following a seemingly paradoxical course. On the one hand, water resources are declining overall, with hotter and drier conditions, and more frequent and intense droughts, as explained later on. On the other hand, there is a change in precipitation variability, with an increase in the intensity of intense rainfall events in certain regions around the Mediterranean. This simultaneous decrease in water resources and increase in extreme precipitation is sometimes called a “paradox in the water cycle change” (Brunetti et al., 2000; Alpert et al., 2002; Brunetti, 2004; Zittis et al., 2021). On the contrary, northern western and central Europe are expected to undergo an increase

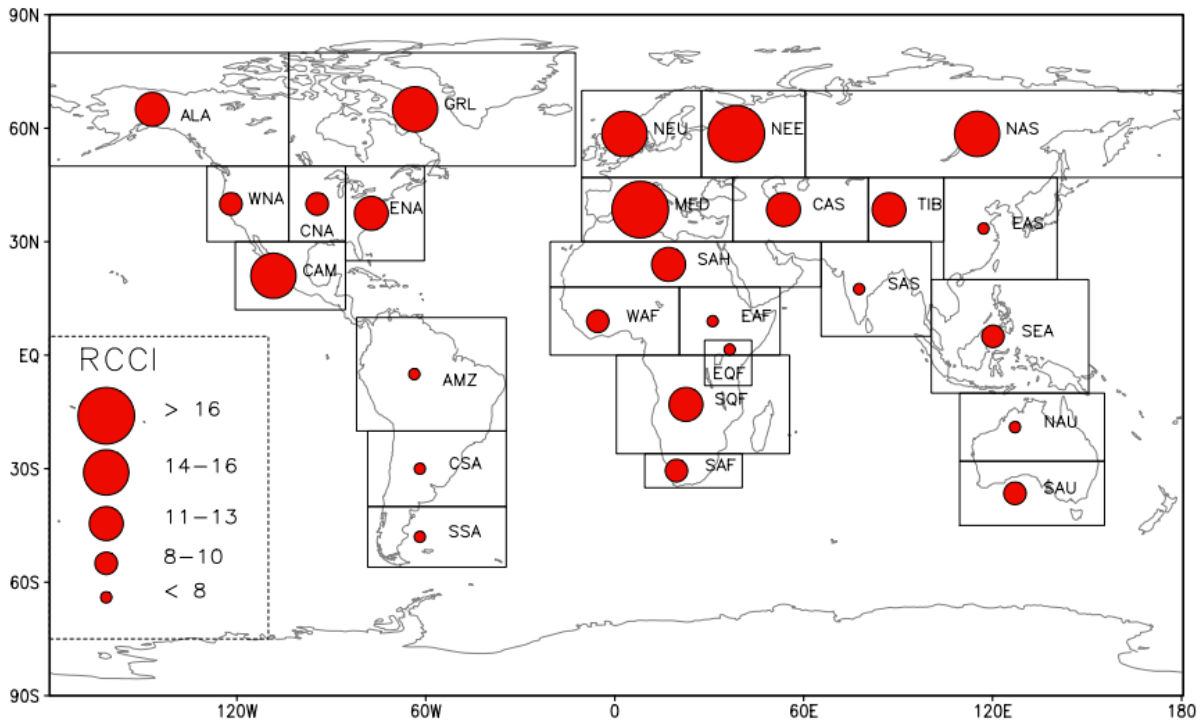


Figure 9: Regional Climate Change Index computed for different continental regions (with the acronym MED for the Mediterranean), by Giorgi, 2006, for 20 global climate projections with three different emission scenari.

of both total precipitation and extreme precipitation (Zittis et al., 2021; Intergovernmental Panel On Climate Change (IPCC), 2023).

This paradoxical change in the Mediterranean can have considerable impacts, for instance on the water resources. There is already a considerable pressure on the Mediterranean water resources, especially on so-called “renewable” water (groundwater which can be recovered in a short period of time on a human scale), in Spain and on the southern Mediterranean coast, particularly in Libya and Egypt (figure 10). In several southern Mediterranean countries, water is drawn from “fossil” sources that are non-renewable. With climate change, the net loss of freshwater observed in the Mediterranean, combined with demographic and socio-economic factors (such as a growing population, urbanization, change of life-style, development of intensive agriculture, etc.) are further reducing groundwater recharge. The region is particularly

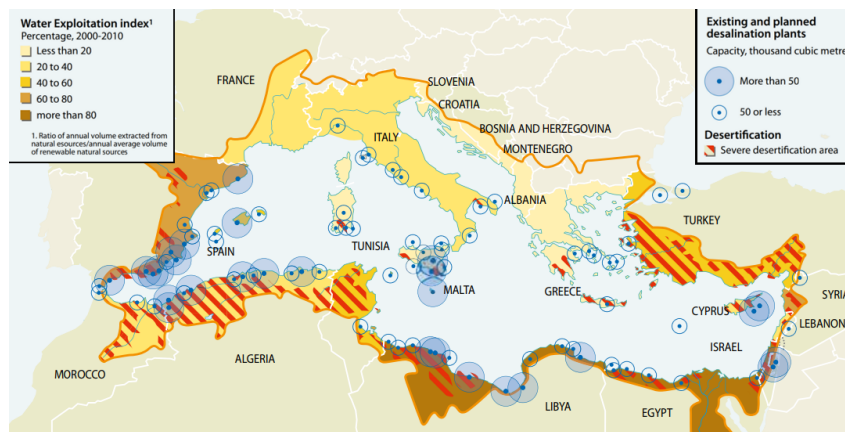


Figure 10: Representation of the level of pressure on water resources in the Mediterranean region, in 2012. Source: UNEP/MAP, 2012

vulnerable to a limited water security as some of its major economic sectors, intensive agriculture and tourism development, are highly dependent on water availability (Sabater & Barceló, 2010). Besides, with a lower quantity of water in rivers or groundwater, pollutants tend to concentrate, impacting the quality of the water resources. Therefore, climate change impacts on the scarcity of freshwater resources increase the risk of conflict in the Mediterranean, for example between countries or between different types of users.

Mediterranean land ecosystems are also impacted by climate change drier conditions. The drying impacts negatively forest ecosystems, with smaller growth rate and health of trees, and an increased wildfire risk in the region. Climate change is also projected to increase soil erosion in semiarid areas (Jiménez Cisneros et al., 2014; on Climate Change (IPCC), 2014b).

In the following subsections, we describe more precisely what are the observed and projected changes for precipitation in the Mediterranean, both mean and extreme.

A future decrease in mean precipitation

The past trends of mean annual precipitation in the Mediterranean are subject to debate, and are unclear when looking at historical observations on long-term periods. A significant decline in mean annual precipitation on both the northern and southern Mediterranean has been found in multiple studies (Tanarhte et al., 2012; Trambly, El Adlouni, et al., 2013; Mariotti et al., 2015; Caloiero et al., 2018; Zittis, 2018; Azzopardi et al., 2020), with for instance Mariotti et al., 2015 finding a significant diminution of about $-0,65$ mm/day/decades on Mediterranean lands, between 1902 and 2005. However, these different trends, derived on time periods of the order of a few decades or on Mediterranean sub-regions, seem actually to be driven mainly by natural variability and not by climate change (Peña-Angulo et al., 2020).

More precisely, in Peña-Angulo et al., 2020, the authors collected daily precipitation time series from 58 stations in Southwestern Europe, which they checked for quality and temporal homogeneity. They combined them with different precipitation rain-gauges based gridded datasets (CRU, EOBS and GPCC) to create a long time series, covering more than 150 years (1850–2018). They performed different trend analyses on this series by varying the time period considered for the trends. This enabled them to show that there is no significant trend in annual rainfall change in observations over a long-term period over Southern Europe. On the other hand, they have shown that over shorter periods (typically 1950–2018) significant trends can be detected. They therefore deduced that these mean precipitation trends are probably due only to natural variability, rather than climate change. Since this article, several publications confirmed this stationary condition in the observations (Lionello & Scarascia, 2018; Vicente-Serrano et al., 2021) and the IPCC concluded in the AR6 that there is no long-term trend of the mean precipitation for the whole Mediterranean region since the pre-industrial era (Intergovernmental Panel On Climate Change (IPCC), 2023).

What is however robust for total precipitation in the past observations is the decrease of winter precipitation, especially since 1950 (Intergovernmental Panel On Climate Change (IPCC), 2023). For instance, Hoerling et al., 2012 found a change of between -5% and -10% , depending on the observation dataset, for the cold season (defined as from November to April) precipitation in the Mediterranean land, over 1971–2005 compared to 1902–1970. Figure 11, extracted from the later paper, shows this decrease tendency but also highlights the large decadal variability of precipitation in the Mediterranean, and the uncertainties due to the observational sources themselves. As the period from September to April concentrates most of the annual total precipitation for the Mediterranean, between $50\text{--}60\%$ for western and northern regions and $70\text{--}90\%$ for southern and eastern regions, this period is essential for replenishing water resources in most of the Mediterranean countries.

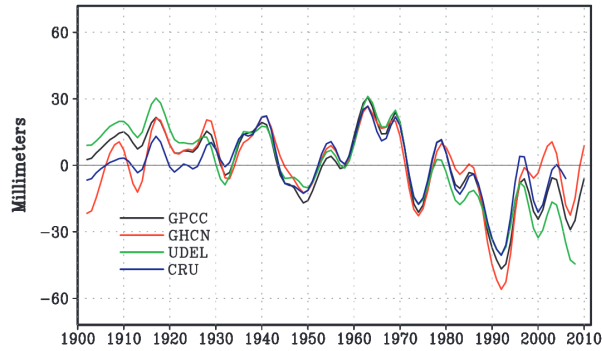


Figure 11: Time series of the Mediterranean region (30° – 45° N, 10° W– 40° E) cold season (November to April) cumulated precipitation over land, for the period 1902–2010, for four different observation datasets: GPCC, GHCN, UDEL, and CRU. Anomalies (in mm) are referenced to the whole period (1902–2010) and are smoothed with a nine-point Gaussian filter. Figure extracted from figure 1(a) of Hoerling et al., 2012

In the future, the signal of a decrease in mean annual precipitation is much clearer and more robust, with an average rate of about -20 mm/ $^{\circ}$ C or -4% /K (Giorgi & Lionello, 2008; Lionello & Scarascia, 2018; Ali et al., 2022). Note that this projected decrease of mean precipitation characterizes the Mediterranean in contrast with the global average of $+2$ – 3% / $^{\circ}$ C, and even with the average behavior of the other regions of the same latitudes (between 30° N and 45° N) where precipitation is projected to increase (see figure 8). Some parts of the Mediterranean will be particularly stricken, such as large parts of the Iberian, the Balkan, and the Anatolian Peninsula, with a reduction larger than 40 mm/ $^{\circ}$ C on an annual basis, i.e. twice as large as the average value for the Mediterranean (Lionello & Scarascia, 2018).

In terms of seasonal analysis, the climate projections show a pronounced decrease in precipitation in the warm season over the whole region, while the decrease in the cold season only concerns southern Mediterranean. For the Northern Mediterranean, the precipitation decrease will be concentrated in summer -with up to a decrease of 20% for a $+2^{\circ}$ C global warming level (Vautard et al., 2014)- while there is no robust trends in winter precipitation, or even positive trends at the very northern border of Mediterranean region (transition to central Europe where precipitation does increase).

The absence of precipitation can also play an important role for the Mediterranean. Despite being a very simple variable, the dry-days frequency and its trends have not been studied in details in the Mediterranean region, especially in observations. Only a few studies point to an observed increase in the dry-days frequency in Italy (Brunetti et al., 2000; Brunetti, 2004), over Southern Europe (Benestad et al., 2019), and in the northern Maghreb (Tramblay, El Adlouni, et al., 2013). Note that the reverse trend is observed in Northern Europe, i.e. a decrease of dry-days frequency. In the future, the global climate projections of CMIP5 studied by Polade et al., 2014 showed that the reduction in the number of wet-days in the southern Mediterranean region would be mainly responsible for the drop in mean winter precipitation. Similarly, Pichelli et al., 2021, which studied the results of kilometer scales projections, showed that the future annual precipitation decrease over the greater Alpine region will be driven by the reduction in the frequency of rainfall events.

Looking for a clearer signal on precipitation on the observations, some studies have turned to the evolution of rain-free periods in the cold season. The term “dry spell” refers to a series of consecutive days with no precipitation, or less than 1 mm/day. As explained earlier, there is a high agreement that globally on lands, dry spells will become drier. In the Mediterranean, various studies have sought to quantify the evolution in dry spells length, their return frequency, etc., based on both available observations (Tramblay, El Adlouni, et al., 2013; Raymond et al., 2016) and simulations (see Raymond et al., 2019 as illustrated

on figure 12), where for example they showed that these rain-free periods will become increasingly long with climate change.

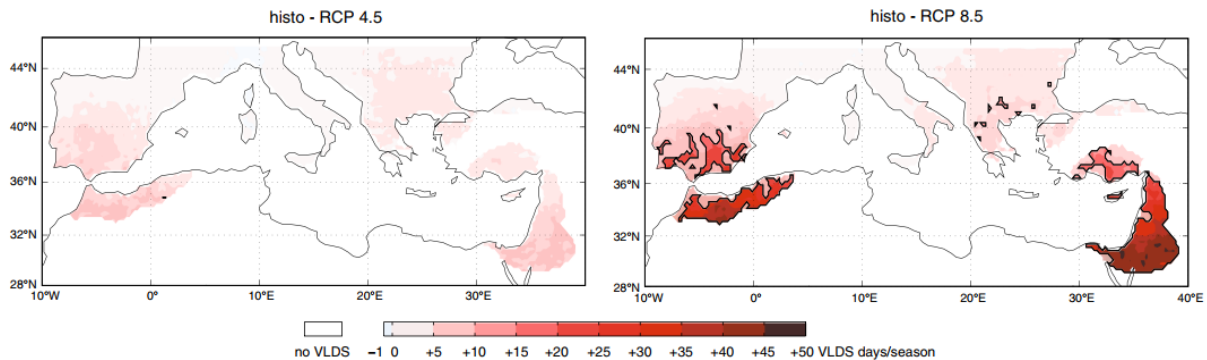


Figure 12: Evolution of very long dry spells (VLDS) in number of additional days per wet season (September to April) in the Mediterranean region, over the period 2066–2100 compared to 1971–2005, according to two emission scenarios, RCP 4.5 (medium emissions) and RCP 8.5 (high emissions). Figure extracted from Raymond et al., 2019.

Drying of the region

Concerning the water cycle, one of the biggest signal of climate change for the Mediterranean is actually a drying of this region. The drying of a region is not only driven by the decrease of the incoming water (precipitation) but also by the outgoing fluxes (evaporation, runoff, etc.).

A warmer climate contributes to an increased atmospheric evaporative demand. This is expected from the Clausius-Clapeyron relation, presented in equation (1), which implies that as the temperature rises, air can contain more moisture before saturation, and that the potential evaporation increases. Thus, if enough moisture is available in the soil, or if vegetation have enough water available to transpire, rising temperatures can lead to an increase of evapotranspiration, drying out the soil. This thermodynamic scaling is quite well verified in observations and models. For example, Tramblay et al., 2018 estimated on CMIP5 models an increase of potential evapotranspiration of about 7% to 14% in Northern Africa, between 1976–2005 and 2066–2095 under the scenario of medium emissions RCP4.5.

Actual evaporation is very difficult to measure, with only a few stations in the region and short time series, while this physical quantity is highly spatially variable and depends on many factors (temperature, wind, solar radiation, soil moisture, vegetation, etc.). Therefore, evaporation is often studied by modeling, either by land-surface models or using empirical formula such as the Penman-Monteith equation.

The Mediterranean is a water-limited region (compared to Northern Europe which is energy-limited) and about 90% of the precipitation received by the Mediterranean region is estimated to be lost through evaporation (Wilcox et al., 2003). Therefore, despite the strong increase in potential evaporation, the actual evaporation doesn't necessarily follow the atmospheric evaporative demand, due to water limitation. In past data, the trends in evapotranspiration are not so clear over the Mediterranean. Some global studies did find a decrease in soil evaporation (Y. Zhang et al., 2016), counterbalanced by an increase in plant transpiration, giving a total increase in evapotranspiration (Miralles et al., 2014; Y. Zhang et al., 2016; Y. Zhang et al., 2019). In future projections, the signal is clearer, with for instance Tramblay and Somot, 2018 showing a projected decrease of actual evapotranspiration by 10% to 25%, in the Maghreb region under the scenario RCP4.5. The authors showed that this decrease seems correlated with the decrease in total precipitation, in this water-limited region.

Soil moisture is one of the most important water resources for agriculture during the summer, and it also plays a role in the moderation of the temperature variability (d’Andrea et al., 2006). Soil moisture is defined as the water contained in unsaturated soil surfaces, in either the first centimeters or the first 2 meters, depending on the definition. Numerous articles noted a sharp decline in soil moisture in the Mediterranean in observations (Sheffield & Wood, 2008; Mariotti et al., 2015). For instance, Sheffield and Wood, 2012 showed that beyond the annual variations, there is a long-term drying trend in the Mediterranean over the course of the 20th century (figure 13).

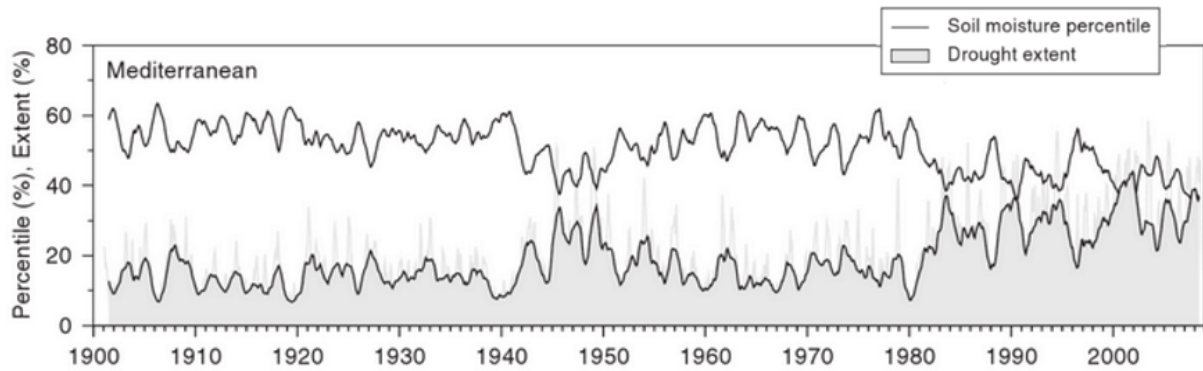


Figure 13: Changes over the 20th century in the surface area of soils considered to be suffering from drought in the Mediterranean region, and in the “soil moisture percentile” index, representing one of the driest soil moisture value (Sheffield & Wood, 2012).

In the future, soil moisture drought areas are expected to increase in the European Mediterranean, by about 15% to 35% for a global warming of 1.5°C and 2°C, depending on the studies. This is consistent with the results of Sousa et al., 2011, which found a clear trend toward drier conditions during the twentieth century for most western and central Mediterranean region. In addition, groundwater recharge and soil water content are projected to decline in Southern Europe and North Africa, especially during summer (on Climate Change (IPCC), 2014a, 2014b). This can lead to longer hydrological droughts, defined as the effects of periods of precipitation deficiency on the surface and groundwater supplies. The MedECC highlighted in its first assessment report that the likelihood of more extreme and frequent meteorological, hydrological and agricultural drought events is likely to increase considerably in the future, with droughts 5 to 10 times more frequent in many Mediterranean regions.

As an aside, the change in large-scale circulation can amplify the drying in some parts of the Mediterranean. Facing the fact that some hotspot regions, such as the Iberian Peninsula, the Arabian Peninsula and the Sahara, will dry out even more than their surrounding regions, Drobinski et al., 2020 proposed an explanation by studying the advection of moisture by the atmosphere over the whole Mediterranean. The paper tracked the trajectories and water content of air parcels: the absolute humidity of the parcel is highest when over the ocean or sea (water saturation), then decreases as it travels over land. The paper observed that in future projections, these hotspot regions find themselves isolated from the oceanic or sea moisture advection, due to a type of cyclonic circulation, a heat low, which will tend to settle more often over these areas. With climate change, the heat low phenomenon is favored, due to an increased temperature gradient between land and ocean. This atmospheric blockage, limiting the supply of moisture and precipitation, should further exacerbate the drying of soils on these hotspot regions. In conclusion, in addition to the regional aridification mentioned above, moisture transport by large-scale atmospheric circulation also plays a major role in the local drying of subregions within the Mediterranean.

Extreme precipitation intensification on the northern basin

Similarly to mean precipitation, significant trends of extreme precipitation over the past are challenging to discern, due to the large variability and the very local characteristic of extreme precipitation. Besides, extreme events are, by definition, rare events, so they are sampled at a low rate in the observations. There is an additional difficulty when assessing the literature of extreme precipitation trends, which comes from the variety of indices used: annual maximal daily precipitation, event more intense than a given threshold (e.g. 20 mm/day, 50 mm/day), precipitation above a given percentile intensity (e.g. the 99th percentile) which can be defined either in all-days distribution or considering wet-days only, and so on.

There is little literature about past extreme precipitation trends in the Southern Mediterranean, where long time series for precipitation are scarce. For the Maghreb region, there seems to be no significant trends, or only a few negative ones (Tramblay, El Adlouni, et al., 2013; Zittis, 2018). Concerning the Eastern Mediterranean — Greece, Anatolian Peninsula, the Levant region — an increase of extreme precipitation was found in most of the domain for extreme precipitation (defined as event larger than 10 mm/day or 20 mm/day, as well as annual daily maximum), with a trend of about -1.3 to -3.5 mm/decades for annual maximum (Mathbout et al., 20a18). This was in contradiction with Zittis, 2018 which found no significant trends over the Levant and the Anatolian Peninsula.

The signal is clearer for the changes in the European Mediterranean, with mainly positive trends (Benestad et al., 2019; Myhre et al., 2019), though some discrepancies subsist. Indeed, in Southern France, several papers found an intensification of extremes for annual maxima, with different rates depending on the domain: +22% in 1961–2015 in Ribes et al., 2019 for the large French Mediterranean, +40% in 2 decades for the Cevennes mountainous region in Blanchet et al., 2018, a trend of +4%/decades in the Cevennes for autumnal maxima in Vautard et al., 2015. Another paper however found no significant trend in Southern France, highlighting the difficulty of having consistent results between studies, even in countries with long time series observations (Tramblay, Neppel, et al., 2013). Besides, the signal is mainly an increase of extremes for Italy, especially for its northern part (Alpert et al., 2002; Brunetti, 2004), as well as in the Balkans (Nastos & Zerefos, 2008; Bocheva et al., 2009; Zittis, 2018). Finally, the Iberian Peninsula is one of the few regions in Northern Mediterranean with decreasing (and robust) trends in extreme precipitations (Benestad et al., 2019; Myhre et al., 2019), except for its northern part where some positive trends were found (Alpert et al., 2002; Bartolomeu et al., 2016).

The IPCC concluded that in the observations, there exists a positive trend of extreme precipitation in the Northern Mediterranean (but with *low confidence*), while the signal is considered as mixed and too uncertain in the Southern Mediterranean (Ali et al., 2022).

In the future, however, the signal becomes increasingly robust with higher levels of global warming. Climate projections predict with *high confidence* that the Mediterranean region will experience more extreme precipitation on the northern shore, while a tendency toward a decrease of extremes is considered in the southern shore but with *low confidence* (Giorgi et al., 2014; Vautard et al., 2014; Drobinski et al., 2018; Myhre et al., 2019; Pichelli et al., 2021; Ali et al., 2022). We therefore expect a North-South dipole of extreme precipitation changes, as illustrated in figure 14 by Tramblay and Somot, 2018. This article also showed that the time of emergence of the extreme precipitation positive trends in the northern Mediterranean was around the year 2000 (i.e. the signal would already have emerged), while for the southern Mediterranean, the emergence would occur only around the years 2050, thus much later. In Pichelli et al., 2021, the analysis of an ensemble of downscaled simulations over the greater Alpine region, using convection-permitting models at 1 km resolution, showed an increase of extreme

precipitation, both at daily and hourly resolution (defined as a precipitation event above the 99th wet-days percentile or the 99.9th wet-hour percentile). Interestingly, they found a rate of increase slower than the Clausius-Clapeyron thermodynamics scaling, for both daily and hourly extremes.

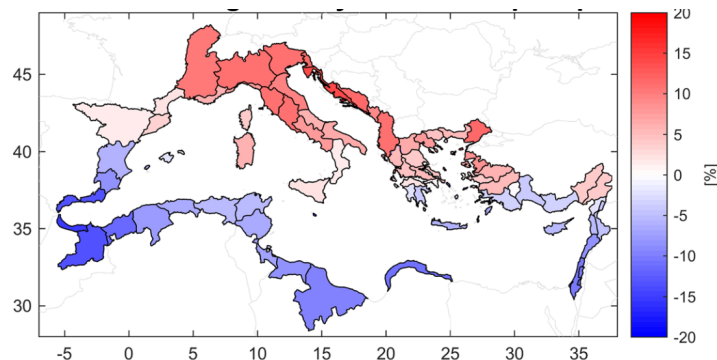


Figure 14: Mean change in 20-year extreme precipitation for 102 Mediterranean basin, on a selection of Euro-CORDEX models, under the high emission scenario RCP8.5. Figure extracted from Tramblay and Somot, 2018.

Concerning the rate of increase for northern Mediterranean extreme precipitation, an original approach was proposed in Drobinski et al., 2018. This article did not study temporal trends of heavy precipitation, but the shape of the heavy precipitation-local temperature relation, in a “stationary” climate. They compared the slope of this curve with the Clausius-Clapeyron thermodynamic scaling ($+7\%/^{\circ}\text{C}$), on rain gauges data in the French Mediterranean. They showed that Clausius-Clapeyron scaling was well verified for low to medium temperature (i.e. winter and spring), while summer precipitation extremes had a sub-Clausius-Clapeyron rate. According to the article, this smaller rate could be due to a drop in precipitation efficiency in summer conditions, because of the very dry environment and insufficient sources of humidity in the French Mediterranean. These results demonstrate the importance of soil aridification and atmosphere-surface interaction in the response of rainfall extremes to climate change in the Mediterranean.

A remaining gap of knowledge

To sum up, numerous studies have been carried out on the evolution of different precipitation indices in the past and future in the Mediterranean, with less literature on the Southern part. They have shown that there is a downward trend in the future for total precipitation over most of the Mediterranean basin, while in the recent past the signal is highly dependent on the region studied and the time period considered, due to high decadal natural variability. Other studies have focused on the changes in the length of dry spells or the decrease of soil moisture, and showed that there is a strong and robust signal of land drying in Med. Yet another branch of the literature has been focusing on the change of extreme rainfall in the Mediterranean, which is not so clear on past observations, while in the future a robust North-South dipole appears, with intensification of extremes for the Northern part of the region and decreasing extremes in the Southern part. These key elements of the Mediterranean water cycle change and their associated uncertainties are summed up in figure 15.

Nevertheless, as we have seen above, the three different aspects of the Mediterranean precipitation changes (dry conditions, total precipitation, extreme precipitation) are mostly dealt with separately and by distinct research communities. However, these aspects are not strictly independent, as was illustrated for example with the sub-Clausius-Clapeyron rates of summer extreme precipitation in Mediterranean France (Drobinski et al., 2018). A comprehensive vision of the evolution of the entire precipitation

Synthesis of observed and projected (1.5°C and 4.0°C global warming levels) changes in climate drivers affecting the Mediterranean region

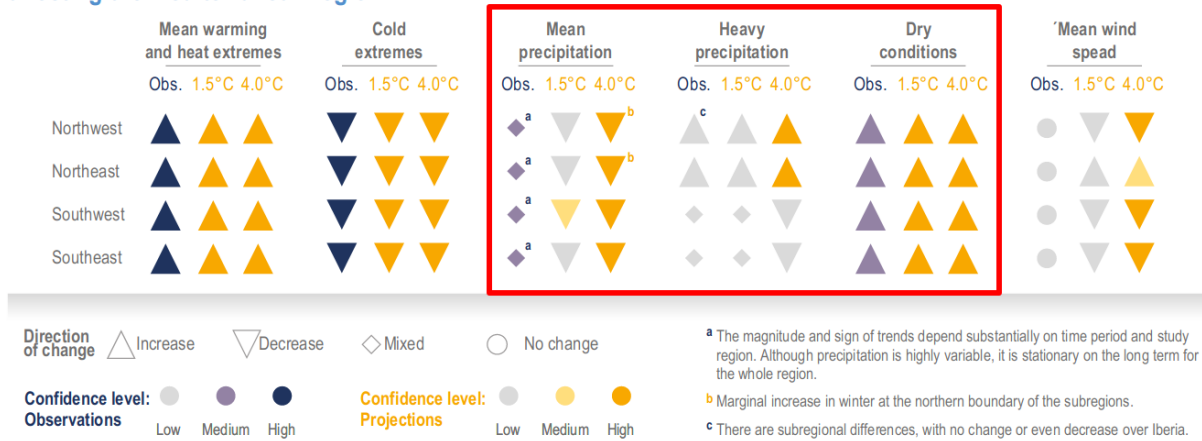


Figure 15: Observed and projected (at global warming levels of 1.5°C and 4°C) direction of change of climate drivers and confidence levels for Mediterranean land sub-regions. Figure extracted from the IPCC AR6, Ali et al., 2022, figure CCP4.3. For this thesis, the three most important variables are the ones which we squared in red: mean precipitation, heavy precipitation and dry conditions.

distribution in the Mediterranean, which would cover both the drying out of the region, the signal on total precipitation and the presumed intensification of extremes, is lacking (besides a few studies as discussed in chapter 1). This is what this thesis aims to bring.

Thesis objectives and outline

As we have seen in this introduction, when it comes to the impact of climate change on the Mediterranean water cycle, one of the main challenges is to understand the changes in the overall precipitation, which in this region can be very different from the global mean. The problem is that the trends detected in the observations show different and sometime contradictory results depending on the subregions, the time periods and the precipitation indices used. It can also differ due to the focus of a study, with some studies looking at all-days precipitation, while others focus on precipitating events; two approaches that we will compare in this thesis. All these aspects make it difficult to compare different observed or projected trend analyses. As a result, it is still difficult to give a clear message to public policy-makers, in order to take appropriate measures to adapt to future risks induced by changes in precipitation (droughts, water resources, etc.).

The present thesis tries to make a step forward a better understanding of the changes of precipitation as a whole, in the Mediterranean region. We aim at characterizing the past and future changes in the whole distribution of daily precipitation in the Mediterranean with climate change, considering both extreme precipitation and dry-days frequency change, by proposing a statistical diagnostic. Although the focus is statistic, the aim is to inform our physical understanding of the Mediterranean region. We build our analysis on daily precipitation, as it is at the intersection of the temporal scales of meteorological droughts (usually studied at annual or monthly scale, or with accumulation of dry-days) and of extreme precipitations (usually studied at daily, hourly or sub-hourly time scales). Note that looking at higher frequency precipitation, e.g. hourly, and their distribution change, would be interesting to better link the extreme events with the clouds' convective life cycle, yet it is out of the scope of this thesis.

Thesis outline

The present thesis is constructed around three main chapters, which progressively build up the statistical framework for studying the whole precipitation distribution change, and apply it to past data and future projections.

The aim of chapter 1 is to characterize the evolution of the entire wet-days precipitation distribution, over the Mediterranean and in the past, in order to gain a coherent view of the change in precipitation intensity. Dry-days were therefore temporarily set aside. To achieve this, the idea was first to classify past trends in Mediterranean for wet-days quantiles into several regimes, as the literature had highlighted the existence of different behaviors within Mediterranean. This was done by grouping wet-days quantiles trend curves of the same shape, to highlight similar behaviors. The aim was then to reduce the information contained in the different regimes to a few simple parameters, to enable a more quantitative analysis of the trends in the different regimes. To do this, we selected from among distribution laws used in the literature, the one that gave the best score on daily precipitation in Mediterranean while having a reduced number of parameters. We were then able to develop a redefinition of the patterns based on this model parameters. Finally, we wanted to study the robustness of the Euro-Mediterranean trend regimes over the past, to see if the observed trends are statistically significant over the past. This was done by means of a statistical test on the trends in the model parameters. This chapter was featured in the first half of André et al., 2024.

The aim of chapter 2 is to extend the methodology developed in chapter 1 to take into account the influence of dry-days frequency changes on the overall precipitation distribution. We began by studying the relative contributions of changes in dry-days compared with those of the wet-days distribution on a case study, the changes in total precipitation. Total precipitation is indeed a much-studied variable in the literature, and several papers have already mentioned the potentially important role of dry-day frequency in certain regions (Pierce, Cayan, Das, Maurer, Miller, Bao, Kanamitsu, Yoshimura, Snyder, Sloan, et al., 2013a; Polade et al., 2014), although this has not been studied in details for the Mediterranean. The idea was then to generalize by analytically studying the effect of the change in dry-days on the trends of the all-days distribution. To do so, we took up the framework proposed by Schär et al., 2016, which compares all-days and wet-days quantile trends, and applied it to a Weibull distribution for wet-days precipitation. Finally, we wanted to assess the importance of changes in dry-days frequency for the overall all-days distribution in the Mediterranean in the past. To do so, we deduced from the above analysis and precipitation data which parts of the Mediterranean all-days distribution are affected by the change in dry-days, and which part are essentially concerned by a change in wet-days intensity. This made it possible to see whether the all-days change categories differ from the wet-days ones due to the occurrence aspect. This chapter was featured in the second half of André et al., 2024.

The aim of chapter 3 is to apply the methodology developed in this thesis, to study the regimes of precipitation distribution change with future global warming. As it is known that the climate signal on precipitation is much stronger in climate projections than in observations and reanalyses, we expect a clearer signal in the Mediterranean region. The idea was first to choose a representative selection of Euro-Cordex projections and validate them over the past period. Indeed, it is necessary to check whether the models are consistent with our previous results for the past, in order to give them confidence in future trends. Next, the aim was to study future wet and all-days regimes as well as their multimodel robustness by applying our framework to projections to the end of the 21st century. To this end, we applied our classification into wet-days and all-days regimes to the selected simulations, and assessed the future relative contributions of the change in dry-days frequency compared with the intensity's, in the Mediterranean region and in Europe. Finally, the idea was to study the temporal emergence of the

all-days distribution change signal during the 21st century. Indeed, the question of when a clear and robust signal on precipitation distribution will emerge is indeed a preoccupation for climate adaptation. We apply two complementary metrics, to assess when the all-days precipitation regimes become robust within the Mediterranean.

The conclusions and perspectives from this work are then given, in part **III**.

Part II

Thesis's results

The following two chapters are essentially the work published in an article to the Journal of Geophysical Research Atmospheres (André et al., 2024). We restructured the article’s content into two chapters, to enhance the two different steps in the developpement of the methodology. In the first chapter, we first focus on the wet-days distribution. In the second chapter, we develop further the previous work to incorporate the effects of dry-days frequency change in the all-days distribution.

Compared to the version of the published article, we also added three supplementary materials: an appendix about the discontinuities found in EOBS precipitation dataset (section 1.E), one about the seasonality of the changes of precipitation distribution (section 2.A), and another about the theoretical separation between the all-days precipitation regimes and their inversion percentile (section 2.B).

The methodology developed and applied to past precipitation in these two chapters will then be used on future projections in chapter 3.

Chapter 1

Regimes of precipitation distribution change in the past climate - focus on wet-days

1.1 Justification of the study

In this chapter, we want to study the whole precipitation distribution over the Mediterranean region. Compared to droughts and extreme precipitation, which have been extensively studied, the research on the whole precipitation distribution is relatively less developed. In the few papers that do study the whole range of the precipitation distribution, two main approaches can be distinguished: non-parametric and parametric studies. Non-parametric studies focus on the changes of frequency of fixed precipitation intensity amounts or on the changes of intensity for fixed percentile ranks or on the change of contribution from given precipitation amounts to the total precipitation (Alpert et al., 2002; Brunetti, 2004; Klingaman et al., 2017; Berthou et al., 2019; Berthou et al., 2020). These methods are interesting, but when one wants to allow diagnostics or interpretation in terms of a few key parameters, parametric studies are needed.

Still, very few parametric studies consider the whole precipitation distribution and do not focus only on extreme precipitation. One of these few studies took a simple exponential law with a single parameter (Benestad et al., 2019) while another study took a gamma law, which was shown to perform quite well for the low to medium precipitation (Ben-Gai et al., 1998; Groisman et al., 1999). A more complex model, tailored for wet-days precipitation, has been recently proposed by Naveau et al., 2016 and gives very good results for both the low precipitation and the extremes (Tencaliec et al., 2020; Rivoire et al., 2022), still with a little more complexity (it has three parameters compared to two for the gamma law or one for the exponential). In this work, we choose the intermediate approach of a Weibull law with two parameters, which, as will be shown below, represents a minimal framework to model wet-days distribution and its quantile trends regimes.

In this work, we propose a framework which describes the change over time of the whole distribution of precipitation: from absence of precipitation to low and moderate precipitation, up to extreme events. We first perform a description of the wet-days trends, quantile by quantile. As underlined by Schär et al., 2016, such a method should consider the change in frequency of non-precipitating days (or “dry-days”). Therefore, we also study how the wet-days quantile trends can be influenced by the change in dry-days frequency. We illustrate this methodological framework on the recent past in Europe and the

Mediterranean. The main question addressed here is the following: how does the whole precipitation distribution change across Europe and the Mediterranean region?

The outline of the chapter is as follows: Section 1.2 presents the data set used, then Section 1.3 presents the different kinds of regimes that can be observed over Europe and the Mediterranean concerning the wet-days quantile trends. Section 1.4 proposes the Weibull law as a wet-days distribution to represent the observed regimes, and analyze them more thoroughly.

1.2 Precipitation data set

We chose to use a single data set in this study to focus on the development of a methodological framework. Yet, we would like to highlight that the methodology we present in this chapter can be applied to any other precipitation data sets.

The choice of the data set was driven by the need for a data covering the whole Euro-Mediterranean region, with spatially and temporally homogeneous precipitation, as well as covering a period of time long enough to help detect small changes in the precipitation distribution out of the natural variability.

We choose not to use EOBS gridded data, although it is considered as the reference of its kind for Europe and covers a long enough period (since 1950) at 0.25° resolution, because it suffers temporal and spatial inconsistencies (Cornes et al., 2018). Indeed, EOBS precipitation data set is based on the spatial interpolation of precipitation gauge data from stations which number and density have changed significantly over time, therefore one is advised not to use it for the analysis of long-term trends. Since most of the over available observational data sets cover either a smaller domain (IBERIA01 in Portugal and Spain (Herrera et al., 2019), or CARPATCLIM covering the Carpathians), a shorter period of time (the IMERG reanalysis product starts in 2000, the FROGS product in the 1970s), or have a coarser temporal or spatial resolution (CRU starts is a monthly data set, while REGEN is daily but at 1°), we turned to ERA5 reanalysis.

We used ERA5 reanalysis, the latest global reanalysis provided by the European Center for Medium-Range Weather Forecasts (Hersbach et al., 2020) at a resolution of 0.25° , on the period 1950-2020. We computed the daily accumulated precipitation from ERA5 hourly variable “total precipitation”, which incorporates both convective and large-scale precipitation. Our domain covers the area between 25°W and 45°E in longitude, and between 25°N and 71°N in latitude, enabling the study of both the Mediterranean and Europe.

ERA5 assimilates observations which constrain properties like large scale moisture convergence, and the model is run at an improved resolution compared to the previous version, ERA-Interim. Thus it has been argued that ERA5 shows reduced uncertainty in its representation of the convective environment (Taszarek, Allen, et al., 2021; Taszarek, Pilguy, et al., 2021) and of heavy precipitation (Chinita et al., 2021). ERA5 reanalysis has been shown to be of very good quality on the pan-European domain, with a wet-days frequency spatial pattern well represented, though it overestimates this frequency, by about 10 to 20% over land, and thus the mean precipitation (Rivoire et al., 2021; Bandhauer et al., 2022). ERA5 wet-days precipitation intensity has been shown to be in very good agreement with the reference European station-based gridded data set EOBS (Cornes et al., 2018) over European lands, especially where EOBS is most trusted, i.e. where its station density is high (especially in Germany, Ireland, Sweden, and Finland).

As our results are derived from ERA5 reanalysis only, we are aware of potential temporal inhomogeneities in the precipitation data: trends might be susceptible to time-dependent biases, for example due

to the change of assimilated observations in the reanalysis. Yet, temporal inhomogeneities in reanalyses have been mainly noticed in region with sparse data, such as Africa and more generally the southern hemisphere (Kistler et al., 2001; Ambrosino & Chandler, 2013), usually due to the addition of satellite data (for example Krueger et al., 2013 on storms, or Shangguan et al., 2019 on ozone data), or to an increase in station density mainly before the 1950s (Pohlmann & Greatbatch, 2006; Ferguson & Villarini, 2012). Therefore, we expect the ERA5 data in Europe and the Mediterranean to be much less prone to temporal inhomogeneities. Besides, we compared trends in precipitation standard deviation in ERA5 and in EOBS gridded data set, and while we noticed strong temporal biases on EOBS - with very strong non-physical differences between neighbor countries - such biases were not visible at all in ERA5 precipitation data.

1.3 Observed regimes for the change of the wet-days distribution

One way to study the changes of distribution of precipitation is to look at the evolution of the cumulative distribution function, or equivalently its inverse function, the quantile curve, on which we will focus in this study. In the following, we designate as trend the absolute change of a given variable between two periods of 31 years, 1950–1980 and 1990–2020. We choose to take periods of three decades to smooth out the natural variability within those periods when taking the mean statistics. The impact of the choice of the dates on our results is negligible (see Section 1.A). To study the evolution of the quantile curve with time, we thus computed the trends between the quantile curves of the two time periods: we thus obtain the curve of the intensity change for each wet-days percentiles.

A precipitation distribution usually has a high probability of the event 0 mm, corresponding to the many dry-days, i.e. days with no to very low precipitation accumulation. In this chapter, we will look at both the change of precipitation occurrence and intensity of precipitation (i.e. wet-days distribution) but also the all-days distribution. For methodological issues, it is indeed handy to set aside the dry-days and fit a model on the wet-days distribution only (which will be done in the next section). We are conscious that a quantile trend defined on a wet-days distribution may be influenced by a change in the frequency of dry-days, f_d , as discussed in detail in Schär et al., 2016: this aspect will be further developed in Section 2.2.

We followed the work from Expert Team on Climate Change Detection and Indices, which recommends the use of 1 mm/day as the threshold for the definition of dry and wet-days. This value enables to better deal with both the issues of under-reporting of small precipitation amounts in observations and the “drizzle problem” of models and reanalyses - which usually have too many days with weak precipitation (Karl et al., 1999; X. Zhang et al., 2011). The frequency of dry-days (days with less than 1 mm/day) is far from being negligible in our domain, and can vary from 20% in northern Europe up to 90% in the Maghreb (and almost 100% in the desert).

We illustrate in Figure 1.1(a) the four main qualitatively different regimes which can be found on the domain, depending on the shape of the wet-days precipitation quantiles trend curve :

- a regime where nearly all quantiles intensify (for ex. in the UK),
- a regime where nearly all quantiles decrease (for ex. in the North of Portugal, although a few of the most extremes may have a slightly positive trend),
- a U-shape regime, consisting in negative trends for low to medium quantiles but positive trends on extremes, with a certain inversion percentile in between (for ex. in the North of Italy),

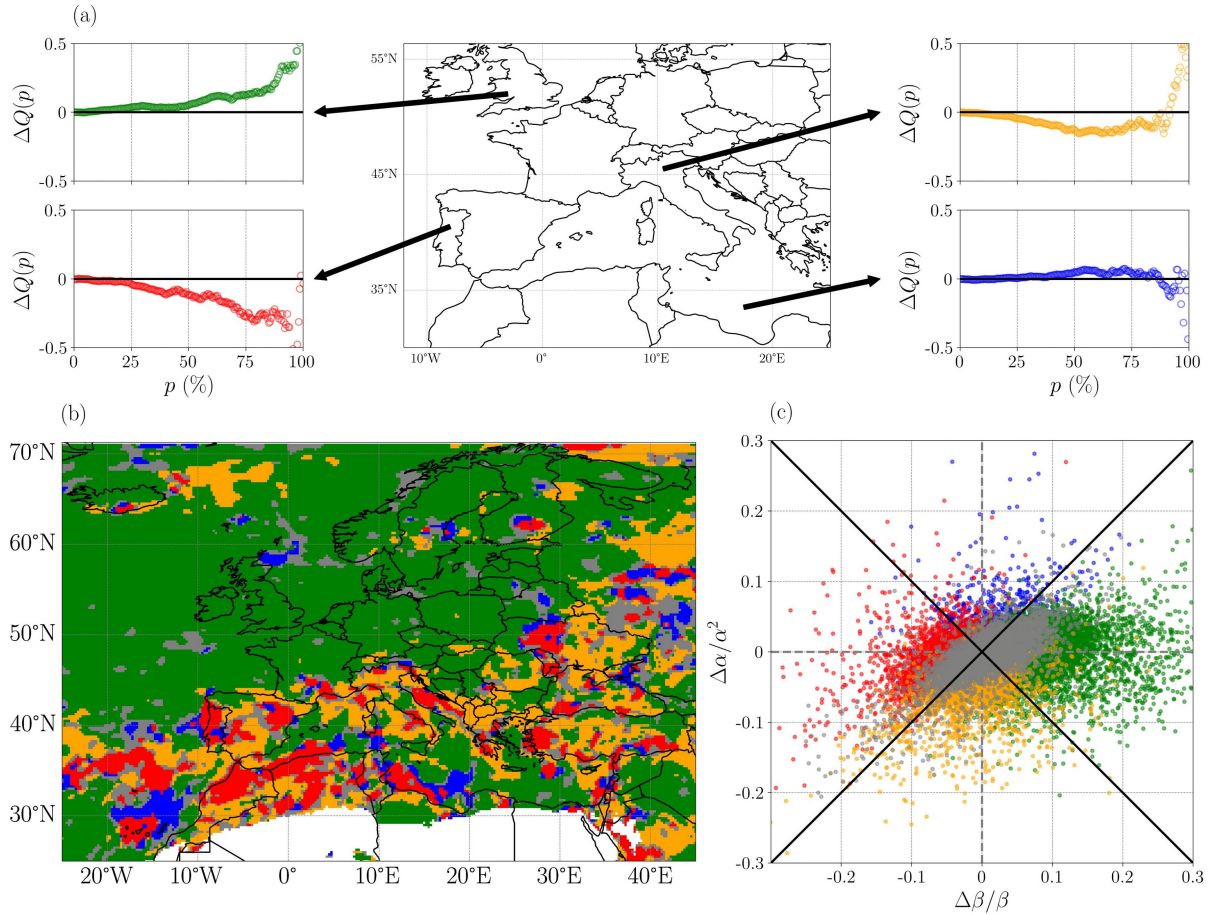


Figure 1.1: (a) Illustration of the four types of behaviors for wet-days quantile trend curve (between 1950–1980 and 1990–2020), at four chosen locations. The quantile trends $\Delta Q(p)$ are plotted in mm/day/decades. (b) Wet-days category map obtained from the classification algorithm, applied on the trends between 1950–1980 and 1990–2020, with a sliding window of nine grid-points. Green corresponds to “nearly all quantiles intensify” category, red to “nearly all quantiles decrease”, orange to “U-shape” and blue to “reversed U-shape”. Gray means the category is unclear. White designates desert location (less than 2% of wet-days). (c) Relative change of Weibull parameters $\left(\frac{\Delta\beta}{\beta}, \frac{\Delta\alpha}{\alpha^2}\right)$ for the wet-days precipitation distribution, plotted for the whole domain. This Weibull model is defined in 1.4. Colors indicate as before the category detected by the classification algorithm. The black thick lines are the theoretic limits between the influence zones of the two Weibull parameters.

- a reversed U-shape regime, with increasing low to medium percentiles with decreasing extremes (for ex. in the Mediterranean Sea just North of Libyan coast).

Note that by construction, the trend of the 0% wet-days percentile will always be zero, as its intensity is by definition fixed to 1 mm/day.

Note that a regime comparable to this “U-shape”, with a “crossover” or “inversion percentile”, was already mentioned in literature for the Mediterranean region (Boberg et al., 2010; Colin, 2011).

In order to quantitatively distinguish between those regimes of trends, we developed a simple classification algorithm, which takes in input a list of percentiles and associated quantile trends, looks at the shape of the trend curve and assesses in which of the four categories it falls into. It uses the signs of the trends for both low to medium ranks (the “belly” of the curve, for percentiles $p \in [10\%, 60\%]$) as well as for extreme high ranks (the “tail” of the curve, for percentiles $p \in [85\%, 99\%]$). It also uses the slope of the linear regression for percentiles $p \in [60\%, 99\%]$.

More precisely, the algorithm is the following:

1. If the means of the belly is positive, and the tail has a positive mean and slope, then the category is defined as “all quantiles intensify”.
2. If the mean of the belly is negative, but the tail has a positive mean and slope, then the category is defined as “U-shape”.
3. If the mean of the belly is negative and the tail has a negative mean and slope, then the category is defined as “all quantiles decrease”.
4. If the mean of the belly is positive while the tail has a negative mean and slope, then the category is defined as “reversed U-shape”.

Finally, if the curve doesn’t fall into any of these four categories, it is set into the “unknown” category.

This classification algorithm was applied over the whole Mediterranean and European domain, between 1950–1980 and 1990–2020, giving the category map shown in Figure 1.1. Note that this map was obtained by applying the algorithm on a sliding window of nine pixels (which for each grid-point merges together the quantiles trends of its eight neighboring grid-points) to smooth out very local irregularities.

The first thing that becomes manifest on the category map in Figure 1.1(b) is a clear North/South pattern: a large majority of North-West Europe as well as subtropical Atlantic Ocean belongs to the same regime (“all quantiles intensify”), while the Mediterranean region is mainly in the “U-shape” regime (i.e., decreasing low to medium quantiles but increasing extremes) with also a certain amount of “all precipitation quantiles decrease” regime. This is consistent with what one would expect from a Mediterranean type behavior, with both drying and extreme precipitation events intensification. In the southern part of the Mediterranean basin, the “all decrease” regime is more predominant. We remind that the differences between the “all-decrease” and “U-shape” categories are mainly due to their opposite trend signs for very heavy precipitation. We can also observe that for the Mediterranean Sea far from the coasts (about 200 km away), the dominant category is the “all quantiles intensify” one. As for African land equatorward of 30°N, the category map becomes extremely spotty, which could be due to a higher natural variability in the wet-days distribution, mainly due to the very small number of wet-days. Therefore, we won’t look at desert regions, where there is less than 2% of wet-days.

We also note that the map of categories is much spottier within the Mediterranean region than in northern Europe. This spottiness seems to stem primarily from a strong natural variability, which may have prevented a clear long-term climate change pattern from emerging in the distribution of wet-days in the Mediterranean. Indeed, as shown in Section 1.A, the agreement between wet-days category maps computed for different time periods over 1950–2020 is much lower for the Mediterranean than for northern Europe.

Section sum up: Observed regimes for the change of the wet-days distribution

In this section, four types of behavior in terms of wet-days quantile trends were found in ERA5 reanalysis precipitation data. The four regimes are called “all quantiles intensify”, “all quantiles decrease”, “U-shape” and “reversed U-shape”, and are detected by an algorithm based on the form of the quantile trend curve. The “all quantiles intensify” regime is predominant over most of northern and central Europe, signaling an intensification of all quantiles of the wet-days precipitations. In opposition, the Mediterranean region displays a patchwork of regimes, thus does not seem to have yet a signal strong enough to overcome the noise of natural variability. This is a motivation to try to assess more quantitatively the significance of a signal by taking a parametric approach.

1.4 Analytical model for the wet-days precipitation distribution

In order to synthesize the information on each and every quantile trends into a smaller number of parameters, we turn to a parametric approach. We first focus on finding a model for the wet-days distribution. Then in Section 2.2 we will see how all-days quantiles trends can be influenced by the changes of both the wet-days distribution and the dry-days frequency.

1.4.1 Choice of a distribution model

There is no standard model for precipitation’s annual distribution in the literature, but different choices depending on the aim of the study and the data considered. For example, Benestad et al., 2019 used an exponential law for the wet-days precipitation distribution, which worked well on their observational data and gave a good “rule of thumbs” to relate extremes probability or quantile trends to the wet-days mean. However, since this wet-days model has a single parameter (the wet-days mean), it can only represent a shift of all quantiles to higher (resp. lower) intensities if the parameter increase (resp. decrease). Thus this exponential model can not represent the two other quantile trends regimes we observe, the “U-shape” and “reversed U-shape”, which have opposite trends for low and high percentiles. We need at least two parameters in the wet-days distribution in order to represent the four regimes presented in 1.3.

We compared different models with two or three parameters, among some usually-used models for precipitation distribution (Gamma, Weibull, Lognormal, Pearson, etc.) on ERA5 precipitation data, using the maximum likelihood estimation method and two goodness-of-fit estimators (Kolmogorov-Smirnov and Cramer von Mises). See Section 1.B for more details. From this comparison of the different models fitted on ERA5 precipitation data, we showed that the best model was the 3-parameters so-called Naveau distribution (Naveau et al., 2016) seconded by the 2-parameters Weibull distribution. For this study, we preferred to work with the Weibull distribution, as its two parameters are in theory already sufficient to describe the four quantiles regimes, as we show in the following.

1.4.2 Expression of the four regimes through a Weibull model

A Weibull distribution is defined by two parameters: a shape parameter (called α) and a scale parameter (called β). The cumulative distribution function of a Weibull law is expressed as:

$$g(x) = 1 - e^{-(x/\beta)^\alpha}$$

where x is the intensity of precipitation ($x > 1$ mm/day by definition of wet-days), and $g(x) = p \in [0, 1]$ is the probability of having a wet-day with a precipitation inferior or equal to x . Note that p is also the percentile rank corresponding to an event of precipitation intensity x . Note that α and β are both strictly positive, and $\alpha \leq 1$. The scale parameter β can be thought of as representative of the distribution median and has a unit of mm/day, while the shape parameter α is linked to the precipitation variance (though it is dimensionless). For a given percentile p , the quantile intensity $Q(p)$ in mm/day is obtained as the inverse of the cumulative distribution function:

$$Q(p) = x = \beta \left[\ln \left(\frac{1}{1-p} \right) \right]^{1/\alpha} \quad (1.1)$$

In Equation (1.1) it becomes clear that β is also the intensity of the quantile of rank $p = 1 - e^{-1} \approx 0.63$, giving $\beta \approx Q(63\%)$. We can thus think of the scale parameter β as (quite close to) the wet-days

precipitation median. We finally note that when $\alpha \rightarrow 1$, the Weibull model simplifies to an exponential distribution, giving the same expressions as in Benestad et al., 2019, with the parameter β becoming the wet-days mean. The values of the Weibull parameters for ERA5 precipitation data are provided in Section 1.C, as well as their trends and the fit uncertainties.

Quantile trend curves like the ones shown in Figure 1.1 can be expressed analytically as $\Delta Q(p)$, Δ denoting the change between two periods of time (denoted by the subscripts 1 and 2):

$$\Delta Q(p) = Q_2(p) - Q_1(p) = \beta_2 \left[\ln \left(\frac{1}{1-p} \right) \right]^{1/\alpha_2} - \beta_1 \left[\ln \left(\frac{1}{1-p} \right) \right]^{1/\alpha_1} \quad (1.2)$$

This expression is simple and depends on only four parameters: $(\alpha_1, \beta_1, \alpha_2, \beta_2)$, or equivalently $(\alpha_1, \beta_1, \Delta\alpha, \Delta\beta)$.

We observed (not shown here) that a change in the scale parameter β , keeping α fixed, gives the category “all precipitation quantiles intensify” for $\Delta\beta > 0$ and “all precipitation quantiles decrease” for $\Delta\beta < 0$. In opposition, a change in the shape parameter α while keeping β fixed gives either a U-shape for $\Delta\alpha < 0$ and a reversed U-shape category for $\Delta\alpha > 0$. Note that when β is fixed, then the percentile of inversion is also fixed, at a precise rank, $p_{inv} = 1 - e^{-1} \approx 63\%$.

When both parameters change at the same time, their two effects will add up, with a weight depending on the relative change of α and β . Considering small relative changes, i.e. $\frac{\Delta\alpha}{\alpha} \ll 1$ and $\frac{\Delta\beta}{\beta} \ll 1$, the quantile trends for a Weibull law can be written, at the first order, as:

$$\forall p \in (0, 1), \Delta Q(p) \approx \frac{\partial Q}{\partial \alpha}(p) \Delta\alpha + \frac{\partial Q}{\partial \beta}(p) \Delta\beta \quad (1.3)$$

with the following expressions for the partial derivatives:

$$\begin{aligned} \frac{\partial Q}{\partial \alpha}(p) &= -\frac{\beta}{\alpha^2} \ln \left(\ln \frac{1}{1-p} \right) \left(\ln \frac{1}{1-p} \right)^{1/\alpha} \\ \frac{\partial Q}{\partial \beta}(p) &= \left(\ln \frac{1}{1-p} \right)^{1/\alpha} \end{aligned}$$

The sensitivity of the trend curve to the two parameters α and β can be expressed as a simple ratio:

$$\left| \frac{\frac{\partial Q}{\partial \alpha}(p) \Delta\alpha}{\frac{\partial Q}{\partial \beta}(p) \Delta\beta} \right| = \frac{\beta}{\alpha^2} \left| \frac{\Delta\alpha}{\Delta\beta} \right| \left| \ln \left(\ln \frac{1}{1-p} \right) \right| \quad (1.4)$$

The change in α dominates the trend curve if it dominates the trends of at least the low percentiles and the tail. When plotting the logarithmic function $p \rightarrow |\ln(\ln \frac{1}{1-p})|$ on $p \in [0, 1]$, we can show that this term is of order unity (except in the very near vicinity of the extremes percentiles 0 and 1 and of the inversion percentile $p = 1 - e^{-1}$). Thus, we will take the approximation that the logarithmic term is of order unity on the ranks that are of interest for distinguishing between the four different regimes. Finally, we come to the following result: the change in α dominates over β in the quantile trend curve when:

$$\left| \frac{\Delta\alpha}{\alpha^2} \right| \gg \left| \frac{\Delta\beta}{\beta} \right| \quad (1.5)$$

This means that knowing which of the changes of α or β dominates the trend curve boils down to comparing their normalized changes.

Therefore, in the space $\left(\frac{\Delta\beta}{\beta}, \frac{\Delta\alpha}{\alpha^2} \right)$, the two diagonals $\left(\left| \frac{\Delta\beta}{\beta} \right| = \left| \frac{\Delta\alpha}{\alpha^2} \right| \right)$ theoretically set the approximate limits between the four precipitation quantile trend regimes. More precisely, we expect:

- a U-shape for $\left| \frac{\Delta\beta}{\beta} \right| \ll \left| \frac{\Delta\alpha}{\alpha^2} \right|$ and $\Delta\alpha < 0$
- a reversed U-shape for $\left| \frac{\Delta\beta}{\beta} \right| \ll \left| \frac{\Delta\alpha}{\alpha^2} \right|$ and $\Delta\alpha > 0$
- all quantiles intensify for $\left| \frac{\Delta\beta}{\beta} \right| \gg \left| \frac{\Delta\alpha}{\alpha^2} \right|$ and $\Delta\beta > 0$
- all quantiles decrease for $\left| \frac{\Delta\beta}{\beta} \right| \gg \left| \frac{\Delta\alpha}{\alpha^2} \right|$ and $\Delta\beta < 0$

Thus, the 2-parameters Weibull model seems a very pertinent representation of the four regimes.

We can validate this theoretical result on ERA5 precipitation data by comparing the theoretical limits from the Weibull model between the four regimes with the classification obtained by the detection algorithm (which doesn't make any assumption about a distribution model). In Figure 1.1(c), we plotted all grid-points of the domain in the normalized Weibull phase space, and colored them by their category as detected by the classification algorithm. The bottom quadrant of the plot is mainly occupied by "U-shape" gridpoints (orange), the left quadrant mainly "all decrease" category (red) and the right one mainly "all quantiles intensify" (green) points.

Note that the inference uncertainties on α and β parameters have little influence on these results. Indeed, the only locations which regimes deduced from Weibull parameters can be impacted by the fit errors are those near the diagonals and the center of the Weibull phase plot, i.e. points which lie at the limits between two categories (see 1.C). Furthermore, these points are at the same geographical locations where both $\Delta\alpha$ and $\Delta\beta$ are small and not significant, therefore where the wet-days regimes are considered as not robust.

1.4.3 Analytical expression of the inversion percentile

When the regime is a "U-shape", the quantile curve has negative trends up to a certain percentile rank, which we will define as the "inversion percentile". After that rank, almost all the following percentiles have a positive trend. We can get an analytical expression for the inversion percentile p_{inv} with the Weibull model, by solving the equations $\Delta Q(p_{inv}) = 0$ for $p_{inv} > 0$. This results in the following expression:

$$p_{inv} = 1 - \exp\left(-\left(\frac{\beta_2}{\beta_1}\right)^{\frac{\alpha_1\alpha_2}{\alpha_2-\alpha_1}}\right) \quad (1.6)$$

Since the changes of α and β are small for precipitation in ERA5 data (about a few percents), we can simplify this expression. Let's write $\Delta\alpha = \alpha_2 - \alpha_1$ and $\alpha = (\alpha_2 + \alpha_1)/2$, and similarly for β , then we have $\frac{\beta_2}{\beta_1} \approx 1 + \frac{\Delta\beta}{\beta}$ and $\frac{\alpha_1\alpha_2}{\alpha_2-\alpha_1} \approx \frac{\alpha^2}{\Delta\alpha}$, and we can simplify the exponent:

$$\ln\left(\frac{\beta_2}{\beta_1}\right)^{\frac{\alpha_1\alpha_2}{\alpha_2-\alpha_1}} = \frac{\alpha_1\alpha_2}{\alpha_2-\alpha_1} \ln\left(\frac{\beta_2}{\beta_1}\right) \approx \frac{\alpha^2}{\Delta\alpha} \ln\left(1 + \frac{\Delta\beta}{\beta}\right) \approx \frac{\alpha^2}{\Delta\alpha} \frac{\Delta\beta}{\beta}$$

where the last approximation is done by taking the development at the first order in $\Delta\beta/\beta$. We finally get this expression for the inversion percentile:

$$p_{inv} \approx 1 - \exp\left(-\exp\left(\frac{\Delta\beta}{\beta} \frac{\alpha^2}{\Delta\alpha}\right)\right) \quad (1.7)$$

Geometrically speaking, this means that at first approximation, the angle in the Weibull parameter space $(X, Y) = \left(\frac{\Delta\beta}{\beta}, \frac{\Delta\alpha}{\alpha^2}\right)$ gives the value for the inversion percentile p_{inv} .

We can also derive a lower and upper limit for the inversion percentile. Indeed, the inversion percentile is properly defined only in the case where the change of α dominates (U-shape or reversed U-shape), i.e. when $|\frac{\Delta\alpha}{\alpha^2} \frac{\beta}{\Delta\beta}| \gg 1$. The limit cases for this to be true would be when the change in α doesn't dominate anymore, i.e. when $\frac{\Delta\alpha}{\alpha^2} \frac{\beta}{\Delta\beta}$ is close to -1 or 1 . Those two cases give the minimal and maximal values of p_{inv} for a U-shape according to the Weibull law are: $p_{0,\min} \approx 1 - e^{-e^{-1}} \approx 30\%$ and $p_{0,\max} \approx 1 - e^{-e^1} \approx 93\%$. These values are consistent with the range of inversion percentile observed on the reanalysis (not shown).

1.4.4 Consequences for the wet-days categories

Since the Weibull distribution enables a description of the four regimes by the relative change of the models' two parameters α and β , we can obtain information on the significance of the regimes from α and β . We assimilate the robustness of the wet-days categories to the statistical significance of Weibull parameters change: a "all quantiles intensify" and "all quantiles decrease" regimes are considered as robust if $\Delta\beta$ is statistically significant. Similarly, the "U-shape" and "reverse U-shape" regimes are considered as robust if $\Delta\alpha$ is statistically significant.

The results of the significant test are shown in figure 2.5 (more details about the test in 1.D). It shows that the Mediterranean region doesn't have a significant signal on wet-days categories, while in most parts of northern Europe, the "All quantiles intensify" regime is statistically significant. This result is consistent with our intuition we had, which was based on the stronger dependence of the Mediterranean regimes with the definition of the two time periods.

Section sum up: Analytical model for the wet-days precipitation distribution

In this section, we have used a Weibull model on the wet-days precipitation distribution to reduce the information of the quantile trend curve to only two parameters and their changes. These parameters are enough to separate between the four observed wet-days regimes, based on the competition of the two parameters' relative changes. From this analytical description, we can also easily deduce some quantities of interest, such as the percentile of inversion for a "U-shape" regime. Finally, the statistical significance of $\Delta\alpha$ and $\Delta\beta$ indicate whether the of the wet-days regimes are considered as robust. We found that the "all quantiles intensify" regime of northern and central Europe is the only statistically robust regime.

1.5 Conclusion of the chapter

In this chapter, we developed a methodology to characterise the change of the whole wet-days distribution, looking at both low, medium and extreme quantiles. Using the ERA5 reanalysis, we studied the evolution of the wet-days precipitation distribution in the recent past, since the 1950s. We showed that it could evolve in four different regimes, defined on the quantiles trends curves: “all precipitation quantiles intensify”, “all precipitation quantiles decrease”, “U-shape” and “reversed U-shape”. The map of the four regimes computed over Europe and the Mediterranean shows a strong contrast between these two regions. While in northern Europe all quantiles are intensifying with a clear and robust signal, the Mediterranean’s regimes are shared between a dominant “U-shape” regime mixed with “all quantiles decrease”, but are overall more spotty due to strong natural variability. This suggests that a climate change signal and its impact on the wet-days precipitation distribution, shift or distortion, have not (or not yet) emerged in the Mediterranean region, contrary to northern Europe.

By modeling the wet-days distribution with a Weibull law, we were able to reduce the information of the quantile trends to just two parameters, a scale and shape parameters, and their changes (representative of the precipitation distribution shift and distortion respectively). We showed that the categorization in four regimes can be estimated directly from the ratio and signs of the relative changes of the two Weibull parameters, as can be done for the percentile of inversion, when it exists. A statistical significance test on the change of the Weibull parameters confirmed that a signal has emerged in Europe, with a strong increase of the scale parameter, i.e a shift of the whole distribution to more intense precipitation, without distortion. In the Mediterranean, only a few small regions had significant change of scale or shape parameter, reinforcing the argument that a climate change signal on wet-days has not yet emerged from natural variability.

1.A Influence of the time period

In Figure 1.2, we can see the wet-days category maps computed for different time periods, covering the 1950–2020 periods:

- 1950-1970 vs 2000-2020
- 1950-1975 vs 1995-2020
- 1950-1980 vs 1990-2020
- 1950-1985 vs 1985-2020

At a given location, the category of the reference period is considered as robust if at least three of the four pairs of periods give the same category. This criterion is used to define both for wet-days and all-days category's robustness, which is represented by the gray hatches on Figure 1.3. For all-days regimes' definition, please refer to chapter 2.

On Figure 1.3 we see that both the wet-days and all-days category map are very robust with the time periods, over the northern part of Europe. However, in the Mediterranean, most places' categories are not as robust, especially when at the frontier between different categories. Overall, the North-South pattern of all-days and wet-days categories is robust to the time periods considered.

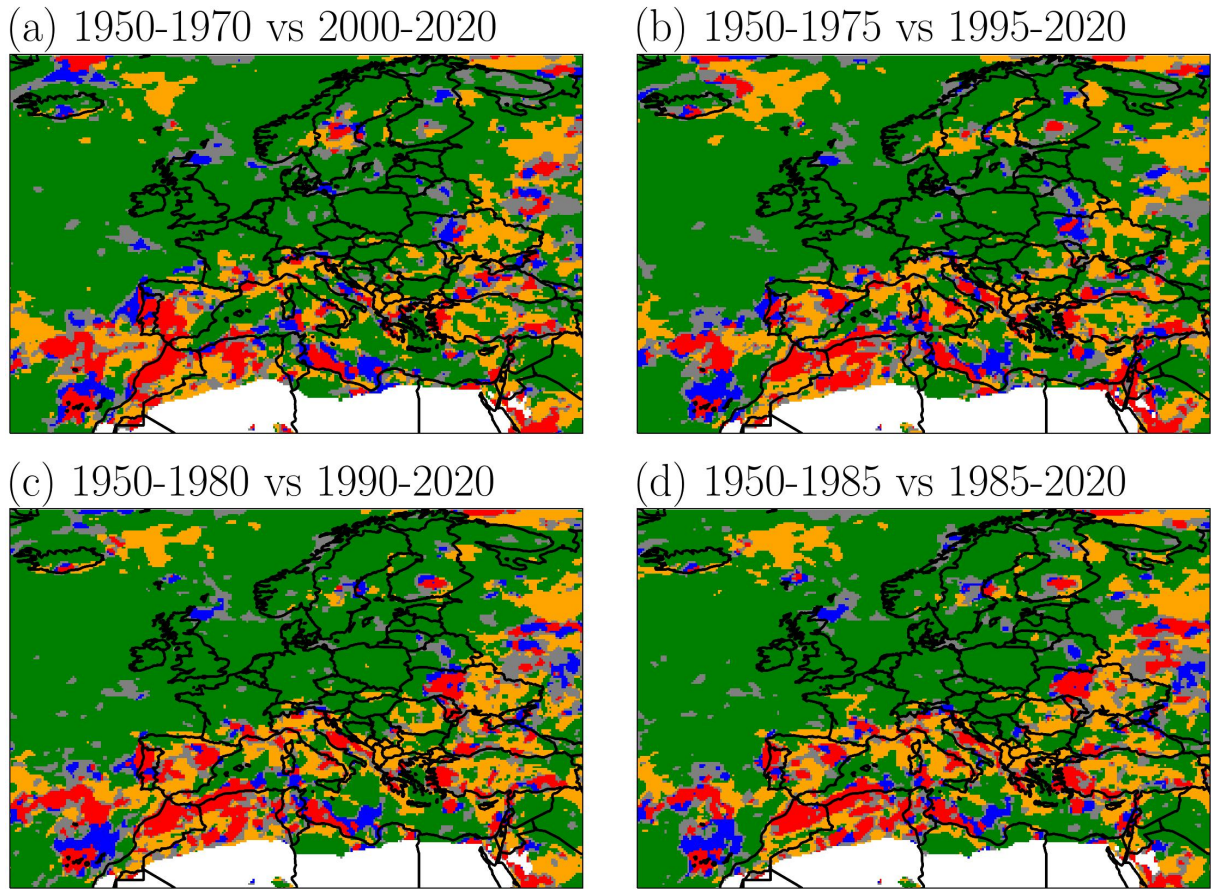


Figure 1.2: Category maps for wet-days quantile trends computed for different couples of time periods over 1950-2020. The quantile trends values leading to this map have been processed by a smoothing window of nine points. As before, green color corresponds to “all quantiles intensify” category, red to “all quantiles decrease”, orange to “U-shape” and blue to “reversed U-shape”.

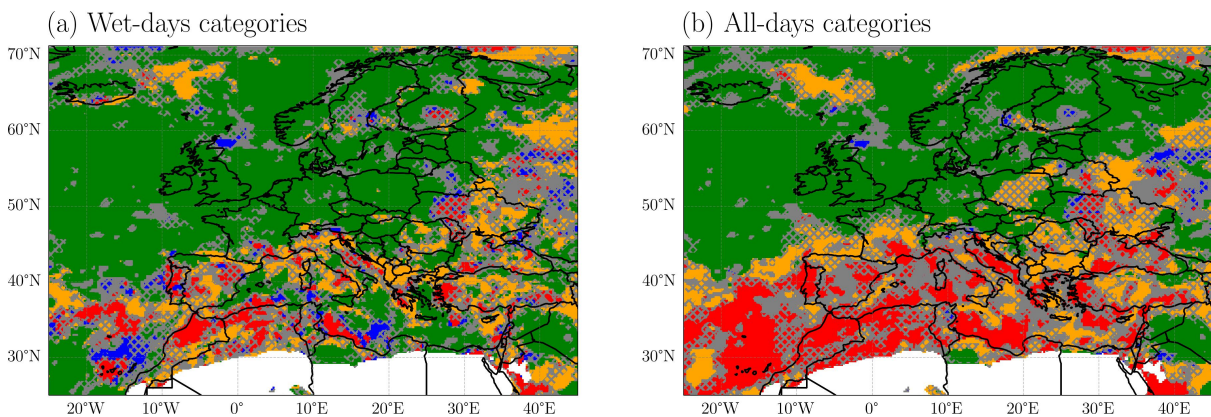


Figure 1.3: Category maps for the 1950–1980 and 1990–2020 periods. As before, green corresponds to “all quantiles intensify” category, red to “all quantiles decrease”, orange to “U-shape” and blue to “reversed U-shape”, while points whose category was unclear are in gray. White designates desert location (less than 2% of wet-days). The gray hatches denote places where the category detection is not very robust with regard to changes in the periods considered (cf Section 1.A).

1.B Comparison of distribution models for ERA5 precipitation

There is no *a priori* clear choice for a parametric model for the whole wet-days distribution of daily precipitation (above threshold, here 1 mm/day). The choice of a particular model may depend a lot on the region considered, on the origin of the data (station data, spatial interpolation from stations, satellite data, reanalysis, or climate projections), on its spatial and temporal resolution, etc. We have therefore tested on ERA5 daily precipitation data, a list of the most common models (as well as the distribution from (Naveau et al., 2016), called Naveau in the following). To compare the quality of the different models, we used two goodness-of-fit estimators, computed on cumulative distribution functions: Kolmogorov-Smirnov (a L1 distance) and Cramer von Mises (a L2 distance). When a location parameter was needed, we set it at the wet-days threshold (1 mm/day).

The inference is done on the period 1950–1980, pulling all wet-days of a given location together, irrespective of their seasonal occurrence. We do not make the assumption of equal distribution of wet-days precipitation across season; we simply disregard the potential seasonal variation of the parameters.

We found that in average, the best distribution for the Mediterranean region was the Naveau law, followed by the Weibull law and the Gamma law (Figure 1.4). As the Naveau model has more complexity (three parameters) than what we need to capture the quantile trends regimes, we decided not to select this model. We compared Weibull and Gamma laws pixel-wise across the whole Europe and Mediterranean. The ratio of the fitting error of Weibull vs. Gamma laws shows that the Weibull model is more suitable than Gamma law, in most of the Mediterranean domain. We therefore choose the Weibull law for our model.

Once we fitted the Weibull law on a time series and that we got its optimal fit parameters, we used the usual Kolmogorov-Smirnov distance as an adjustment test: if this distance is “small enough”, the fit is accepted. According to empirical tables, for a confidence level of 95%, the Kolmogorov-Smirnov distance is considered small enough if falling below $1.36/\sqrt{N}$, where N is the number of data points, as far as $N > 35$ (which is largely the case since we fit Weibull on daily data on several decades). The mask of where the Weibull fit doesn’t pass the adjustment test is shown by hatches on Figure 1.4. It shows that Weibull is indeed an acceptable model for most of the domain (except for some Mediterranean coastal areas and sea area in the Atlantic west of Portugal).

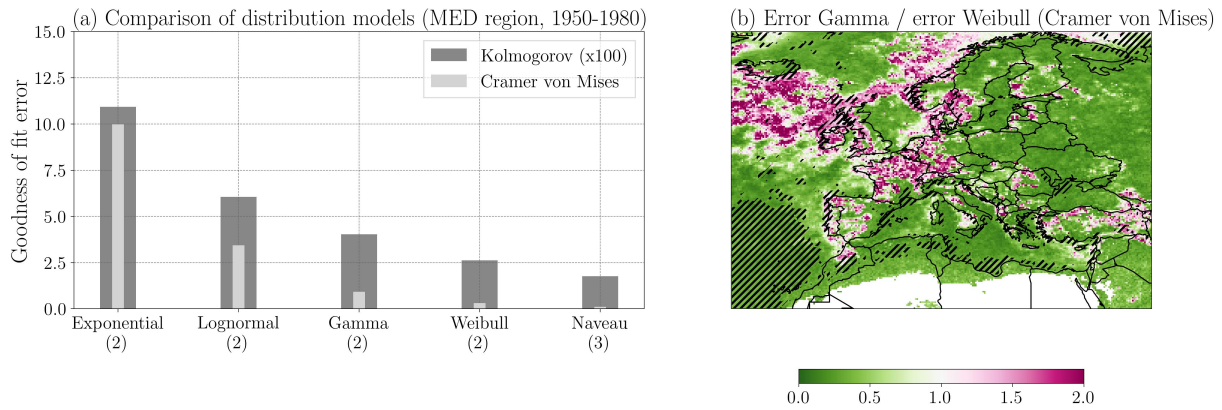


Figure 1.4: (a) Goodness-of-fit estimator for different wet-days distribution models in the Mediterranean region (as defined by the IPCC) on 1950-1980. Note that we used a scale factor for the Kolmogorov–Smirnov estimator, which was much smaller than Cramer von Mises estimator. In the x-axis, the number in parentheses is the number of parameters of the fit. (b) Map of the ratio of errors (here Cramer von Mises goodness-of-fit) between Gamma and Weibull models, across the whole domain, for the same period. In green are all the location where Weibull model is better suited for the data than Gamma. Black hatches show the locations where the adjustment test of the Weibull model fails, with a confidence level of 95%.

1.C Weibull parameters values and uncertainties

Figure 1.5 shows the values of the Weibull parameters for the wet-days distribution of ERA5 precipitation data, their trends and statistical significance (computed by a bootstrap test, as explained in Section 1.D) and the uncertainties of the fit.

The uncertainties on the fit were quantified by the standard errors of each parameter, estimated through the approximate normality of the log-likelihood function, as presented in Coles et al., 2001, chapter 2.6. Though the values of a precipitation time series are not independent and identically distributed, this method gives us an order of magnitude of the fit uncertainties. In practice, we used the Python package Reliability Reid, 2022 to compute the standard error of each parameter.

We then checked if the standard errors on α and β parameters could change the category deduced by diagonal separation. More precisely, we looked at whether the four points around $(\frac{\Delta\beta}{\beta}, \frac{\Delta\alpha}{\alpha s})$ i.e. $(\frac{\Delta\beta}{\beta}, \frac{\Delta\alpha \pm 2\sigma_\alpha}{\alpha s})$ and $(\frac{\Delta\beta \pm 2\sigma_\beta}{\beta}, \frac{\Delta\alpha}{\alpha s})$, lie in the same quadrant of the Weibull phase space. If the fit errors make the quadrant change, then we consider that the diagonal categorization is not robust to the inference uncertainty, for this location.

This happens for pixels which lie close to the diagonals and the center on the Weibull space, as shown in 1.6. When this figure is compared to 2.5, it becomes clear that the places where the uncertainty on fit parameters interfere with the diagonal category detection are the places where neither $\Delta\alpha$ nor $\Delta\beta$ is significant, i.e. the locations where the wet-days categories are considered are not significant. Therefore, the fit uncertainties do not impact the results presented in this article.

1.D Statistical significance test

We are interested in their statistical significance of different statistics computed on the data, such as the quantile trends or the Weibull parameters trends. As the precipitation data in the Mediterranean region is spatially and temporally correlated, we perform a bootstrap test. It consists in comparing the trend of the real data with the trends that would be obtained on a large number (typically a hundred) of artificial samples presenting a spatial and temporal variability similar to our original data. Each sample is an

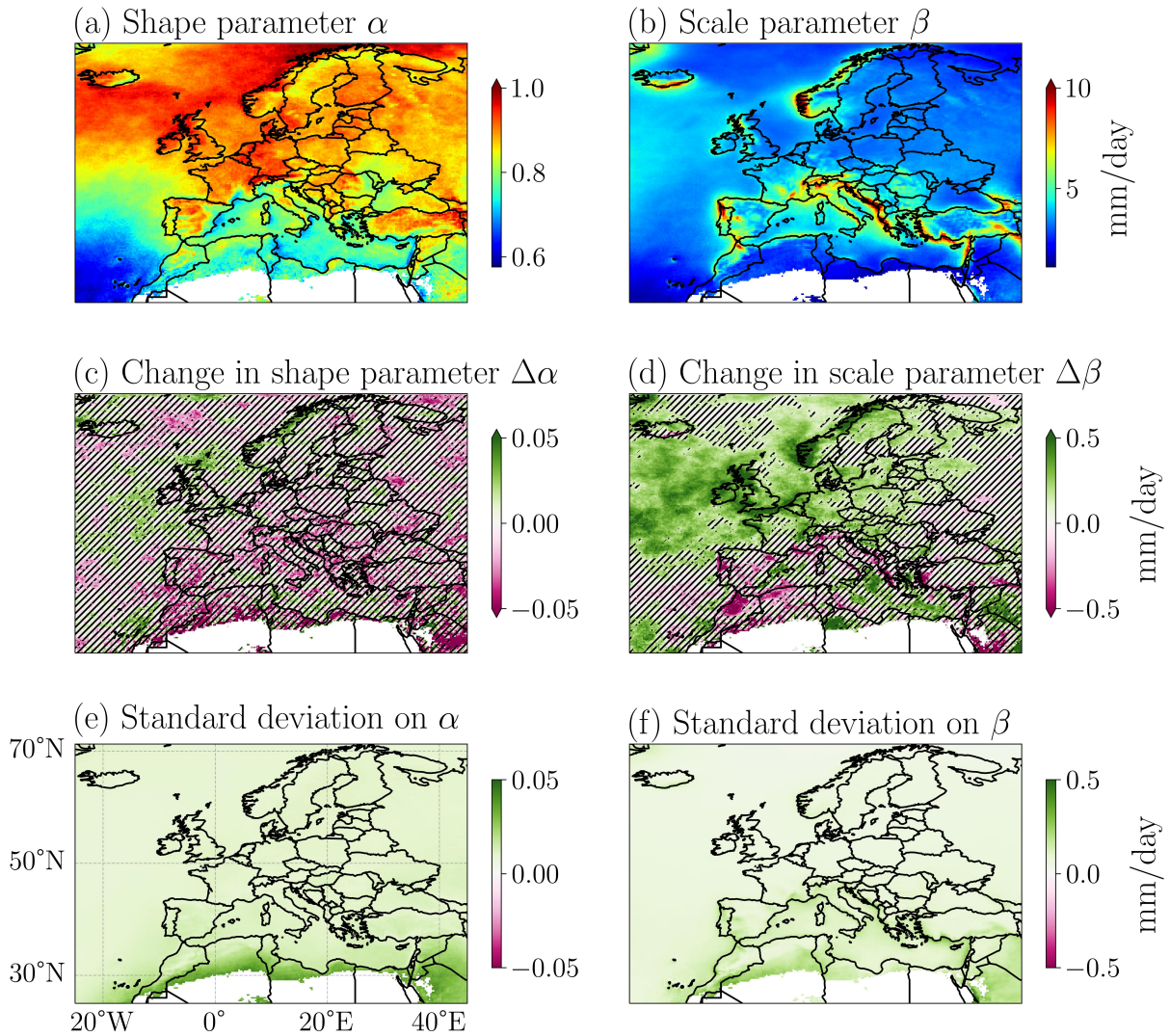


Figure 1.5: Results for the Weibull parameters fitted on ERA5 wet-days precipitation distribution. Top row: Weibull shape parameter α and scale parameter β on the period 1950–1980. Middle row: absolute changes between 1950–1980 and 1990–2020. The hatches denote the location where the change is not significant through a bootstrap test, at a confidence level of 90%. Bottom row: standard error of the Weibull parameters, on the period 1950–1980, estimated through the approximate normality of the log likelihood.

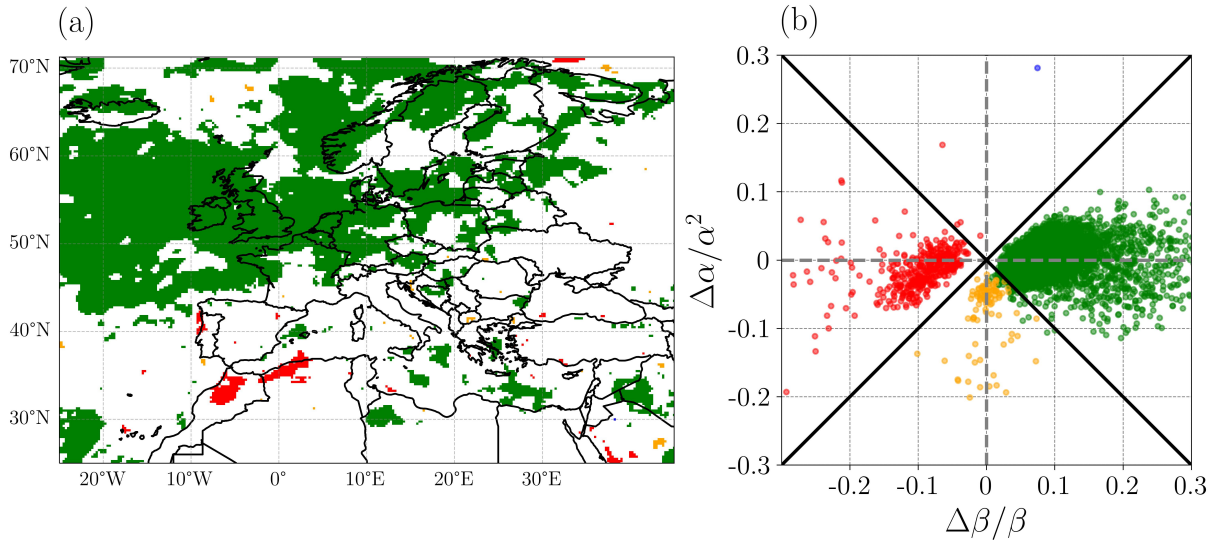


Figure 1.6: (a) Categories plotted for locations where diagonal separation method is robust with regard to the inference uncertainties. (b) These locations are plotted in the Weibull phase space.

artificial time series created by pulling random days (and the corresponding precipitation map over the domain) from our 1950–2020 original data. The random pulling is done with replacement. The artificial time series created have the same length as the original one.

Since the dates have been mixed in the artificial samples, their average linear trends are zero, but their variability gives us an estimation of the noise in our original data. The trend of the original data is said significant at a given level, for example 90%, if the original data lies within the 10% more extreme values of the bootstrap distribution, meaning that we could have the original data “by chance” from this random distribution only with low probability (less than 10%).

1.E Discontinuities in EOBS precipitations

As we started my work for this PhD, we began to work on EOBS gridded dataset, EOBS being seen as a reference for observation dataset based on station data in Europe. However, we realized that there were unfortunately spatial jumps in this precipitation data (version 23.1 at the time). For example, spatial jumps at the administrative borders between countries are clearly visible on the map of the change of the variance of daily precipitation intensity, between 1950–1980 and 1990–2020, as shown in figure 1.7.

After discussing with the ECAD project team, it became clear that the causes of these discontinuities could be quite diverse:

One possibility is the changes in station density (spatially and with time). This density can vary significantly between neighboring countries or regions (with for example a very denser network in Germany and Catalonia). The total station number also greatly changes over time, as is illustrated by the red curve in figure 1.8. Although a given gridpoint might be complete over later periods, its value in the earlier past may be derived using fewer stations, which might result in underestimating extreme events.

Another reason might be the differences in the type of the rain gauges. Unfortunately, the ECAD project team does not have information about the instruments that each data provider is using. Some gauges might be more precise than others: for example, the automatic rain gauges measure about 5-8% less precipitation than manual rain gauges in the Netherlands in annual totals, according to the ECAD responder. Besides, the change from manual rain gauges to automatic rain gauges in the last decades may have occurred at different time between the European countries, giving artificial trends.

A third possibility is the definition of the ‘day’ that is used between countries: some measure pre-

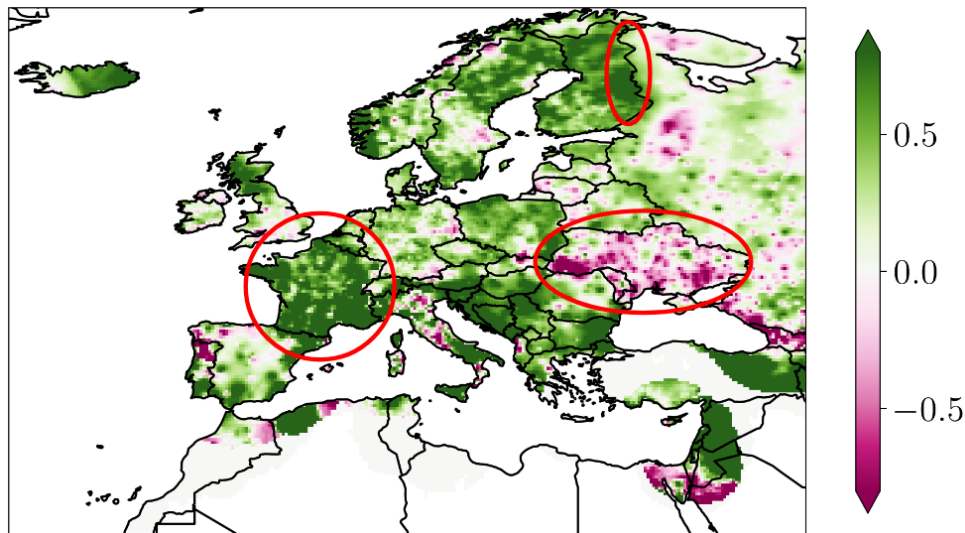


Figure 1.7: Change of the variance of daily precipitation between 1950–1980 and 1990–2020, on EOBS precipitation dataset, version 23.1. Location with less than 90% of days with valid value on the two considered time periods are removed. The red ellipses highlight several jumps between countries, which are not physical.

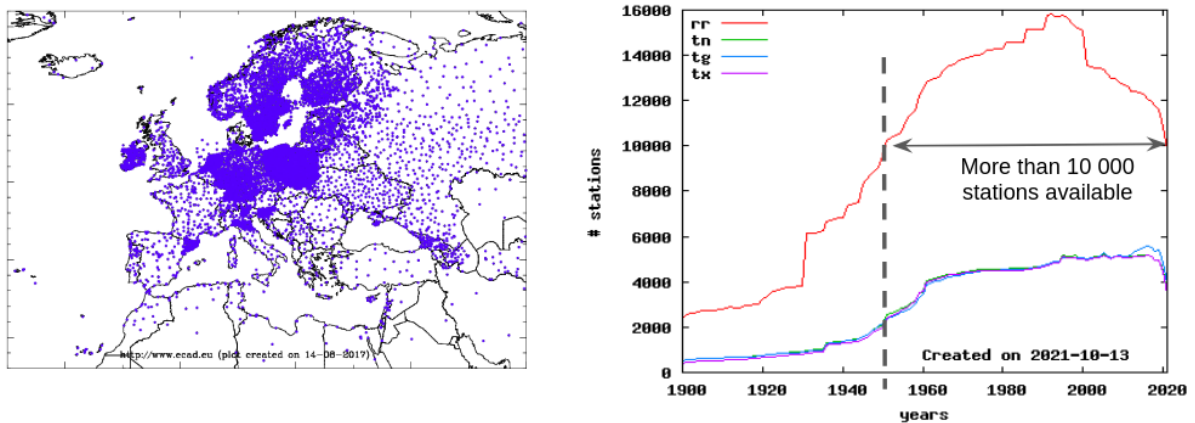


Figure 1.8: Left: map of all the stations which are used for the daily precipitation gridded dataset produced by ECAD. Right: evolution over time of the number of stations used for the daily gridded dataset produced by ECAD. rr designate the precipitation variable, while tn, tg and tx are respectively the daily minimum, mean, and maximum temperatures.

precipitation from midnight to midnight, while others measure from morning to morning (6AM usually). Depending on the timing of heavy rain events, this could impact the reported daily amount, especially for a rain event split between two days.

It is difficult to pinpoint the exact cause of these discrepancies.

As these spatial discontinuities make it difficult to have an homogenized view of the situation over the whole Mediterranean and European region, we stopped working with EOBS precipitation dataset.

Chapter 2

Regimes of precipitation distribution change in the past climate - impact of the dry-days frequency change

In this chapter, we develop further the methodological framework on the change of precipitation distribution, by incorporating the effects of dry-days frequency change in the all-days distribution.

This chapter essentially corresponds to the last section of the article published in JGR-Atmosphere. Note that the appendix corresponding to this article section was reintroduced within the text, for improved fluidity. At the end of this chapter, we also added supplementary materials, one about the seasonality of the changes, and another about the theoretical separation between the four all-days precipitation regimes.

2.1 Impact of dry-days frequency change on precipitation annual mean

In order to illustrate the importance of taking into account not only the wet-days distribution but also the change of the dry-days frequency, we study their relative contributions to the all-days mean precipitation (i.e., total annual precipitation), which is one of the most studied parameters in climate change studies.

The all-days mean \bar{x} is the mean of the daily precipitation intensity, and can be equivalently computed as the product of the wet-days frequency $f_w = 1 - f_d$ with the wet-days precipitation mean μ :

$$\bar{x} = (1 - f_d) \mu$$

The change of the all-days mean is due both to the change of dry-days frequency $f_d = 1 - f_w$ and to the change of wet-days mean:

$$\frac{\Delta \bar{x}}{\bar{x}} = -\frac{\Delta f_d}{(1 - f_d)} + \frac{\Delta \mu}{\mu} \quad (2.1)$$

Those two terms can either be of the same sign and add up to each other, or be of opposite signs and tend to cancel each other out. Indeed, there could be more wet-days but with less intense precipitation, which could result in an almost zero trend on the mean precipitation. Conversely, there could be regions with fewer wet-days but with higher precipitation intensity, as was shown in future projections by Pierce, Cayan, Das, Maurer, Miller, Bao, Kanamitsu, Yoshimura, Snyder, Sloan, et al., 2013b for California and by Polade et al., 2014 for Mediterranean type climates. The relative weight of the two terms is also important to study. For future projections, Polade et al., 2014 showed that the change in the occurrence

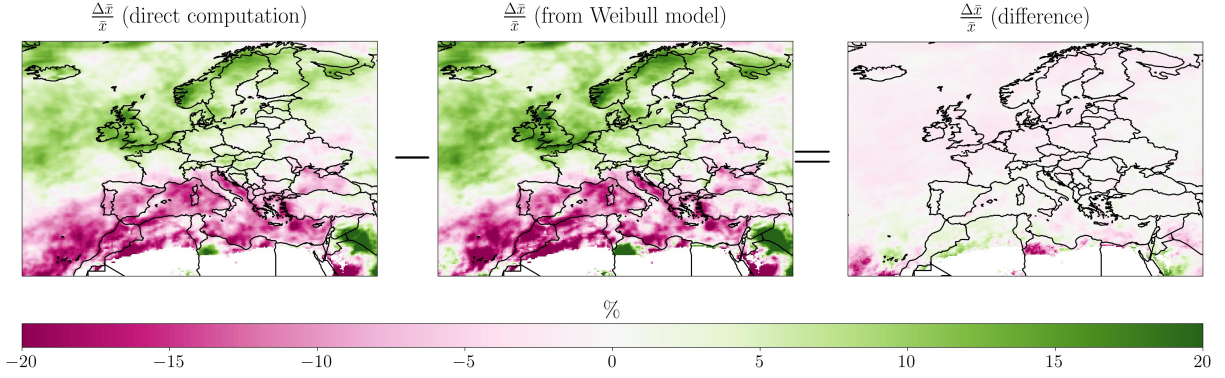


Figure 2.1: Relative change of all-days mean $\frac{\Delta\bar{x}}{\bar{x}}$, between 1950–1980 and 1990–2020, computed directly on data, compared to estimated from the Weibull model, i.e the three contributions from f_d , α and β .

term will dominate the change in intensity for the all-days mean, in most of the subtropics. However, there is very little literature on the behavior of these two terms in past data.

For a Weibull distribution, we can further detail the dependency of the wet-days mean on the shape and scale parameters. The expression of the Weibull mean is $\mu = \beta \Gamma(1 + 1/\alpha)$, where Γ denotes the Gamma function. Taking the logarithmic derivative of the mean, and using the definition of the Digamma function (usually noted ψ) as the derivative of the log of the Gamma function, we get:

$$\frac{\Delta\mu}{\mu} \approx \frac{\Delta\beta}{\beta} - \frac{\Delta\alpha}{\alpha^2} \left(\frac{d \ln \Gamma}{dz} \right)_{z=1+1/\alpha} = \frac{\Delta\beta}{\beta} - \frac{\Delta\alpha}{\alpha^2} \psi(1 + 1/\alpha) \quad (2.2)$$

Note that the Digamma function is strictly positive for the typical range of the shape parameter for ERA5 precipitation, thus the sign of the shape parameter contribution is given by $-\Delta\alpha$. Its typical values are $\psi(1 + 1/\alpha) \in [0.4, 1]$, for $\alpha \in [0.5, 1]$, which is the typical range for Europe and the Mediterranean. Thus, even in regions with a U-shape categories, where $\Delta\alpha$ dominates the wet-days trend curve as $\frac{|\Delta\beta|}{\beta} < \frac{|\Delta\alpha|}{\alpha^2}$, the change in wet-days mean is not necessarily dominated by $\Delta\alpha$, since the Digamma factor is smaller than 1.

Note that the first order approximation and the use of the Weibull model capture most of the signal of the relative change of mean precipitation, with an error of less than 1% on most parts of the domain, aside from desert. Indeed, we can compare the all-days mean (computed directly from data) to the sum of the f_d , α and β terms in Equation (2.3). Figure 2.1 shows that the Weibull model for the intensity plus the precipitation occurrence capture most of the features of the all-days mean. Except for the lower latitudes where the error can reach 10%, the difference between the direct computation and the sum term is indeed only of a few percent, in Europe and the Mediterranean.

Finally, the relative change of the all-days mean can be decomposed in three contributions, from the relative changes of f_d , α and β :

$$\frac{\Delta\bar{x}}{\bar{x}} \approx -\frac{\Delta f_d}{(1 - f_d)} + \frac{\Delta\beta}{\beta} - \frac{\Delta\alpha}{\alpha^2} \psi(1 + 1/\alpha) \quad (2.3)$$

Figure 2.2 shows the relative contributions of those terms to the all-days mean change, and the significance of these changes. We have a clear North-South pattern for the change of total precipitation and of dry-days occurrence.

For northern Europe, the contributions of occurrence and intensity changes are of same sign (decrease of dry-days frequency and more intense precipitation in average), but the all-days mean change is mainly due to the increase of the wet-days mean (the latter being mainly due to the increase of the Weibull scale

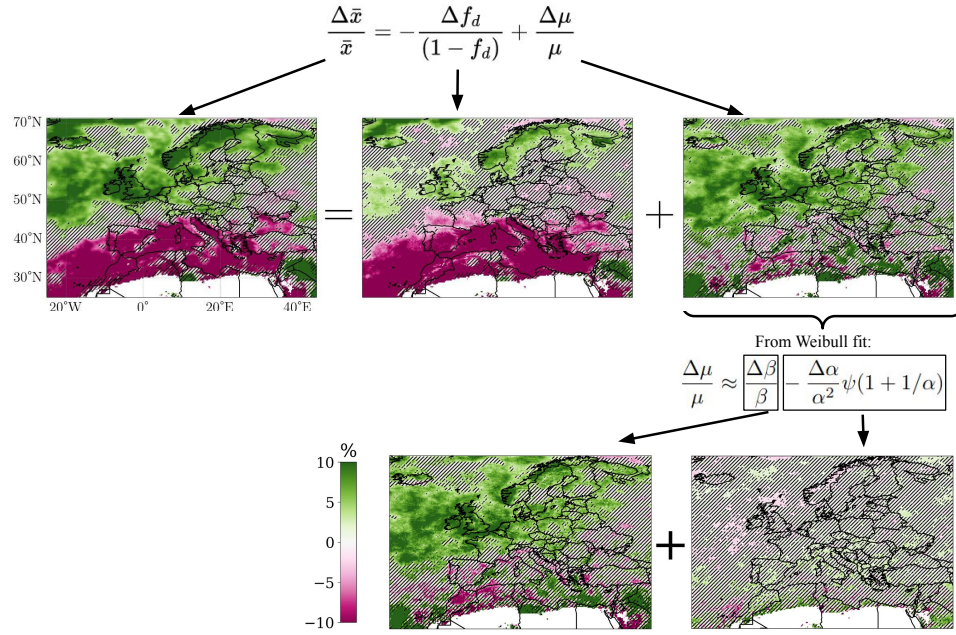


Figure 2.2: The relative change between 1950–1980 and 1990–2020 of the all-days precipitation mean \bar{x} , decomposed in its different contributions, from the changes of dry days frequency f_d and the wet-days mean μ , the latter further decomposed into contributions from Weibull two parameters, α and β . Every map has the same scale for the color-map. The hatches show the zones where the changes are not significant, with bootstrap test at 90% confidence level.

parameter β). We see also that the intensity change is significant over a larger region than the occurrence change, in Northern Europe.

For the Mediterranean region, on the contrary, the intensity change is mainly not significant, while the increase of dry-days frequency is homogeneous and significant, leading to a significant decrease of all-days mean. In a central European band between East France and Poland, the change of occurrence is close to zero, and the change in wet-days intensity is the sole contributor to the all-days mean.

Both in northern Europe and in the Mediterranean (even in U-shape regions), the changes of the wet-days mean are mainly due to the significant change of the scale parameter β , while the term due to the change of the scale parameter α is smaller in intensity and not significant.

Section sum up: Impact of dry-days frequency change on precipitation annual mean

In this section, we illustrated the importance of taking into account the change of dry-days frequency by decomposing the change of total precipitation into a term of the change of the wet-days mean and a term of the change of occurrence (wet-days frequency). ERA5 reanalysis displayed a statistically significant North-South dipole of the total precipitation change (decrease over the Mediterranean, increase in Northern Europe), which is due to a similar dipole of wet-days frequency change, amplified in Northern Europe by an increase of the wet-days mean precipitation. The Mediterranean signal for total precipitation is dominated by the increase of dry-days frequency.

We further decomposed the changed of wet-days mean into a contribution of the Weibull scale and the shape parameter, showing that the shape parameter's change had negligible contribution.

2.2 Influence on all-days quantiles trends of the dry-days frequency

In this section, we investigate in more detail the link between all- and wet-days precipitation quantiles. In order to understand and quantify how looking only at wet-days can impact the values of the trends for all-days quantiles, we follow the framework proposed by Schär et al., 2016, more precisely the derivation made in their first appendix.

The all-days precipitation distribution is linked to the wet-days' one by the dry-days frequency f_d . More precisely, the wet-days percentile p , which denotes the probability of having an event of intensity smaller or equal than x mm/day, and the all-days percentile p_a for the same precipitation intensity, are linearly linked by f_d :

$$p_a = (1 - f_d)p + f_d \quad (2.4)$$

Note that this formula is valid for any percentile rank as far as $p_a \geq f_d$. It gives indeed that for $p = 0$ we have $p_a = f_d$ and that the probability of the maximum precipitation value is the same ($p = 1$ when $p_a = 1$). This simple formula shows that a wet-days percentile p is linearly linked to the all-days percentiles p_a .

By definition, the wet-days quantile Q is equal to the all-days quantile Q_a for percentiles where they are both defined:

$$\forall p_a \in [f_d, 1], Q(p) = Q_a(p_a) \quad (2.5)$$

We now consider a change between the two time periods, 1 and 2, of the wet-days precipitation distribution and its quantiles Q : $\Delta Q = Q_2 - Q_1$, where Δ denotes again the change. For a fixed wet-days percentile p , ΔQ is related to the change of the all-days rank and quantile intensity, but also to the change in dry-days frequency. Rewriting with our notations the equation A7 from the appendix of Schär et al., 2016 gives:

$$\Delta Q(p) = \Delta Q_a(p_a) + \frac{\Delta f_d}{1 - f_d} (1 - p_a) \frac{\partial Q_{a,2}}{\partial p_a} \quad (2.6)$$

We would like to express analytically the slope of the quantile curve $\frac{\partial Q_{a,2}}{\partial p}$, with the Weibull model developed earlier. Thus, we come back to the slope of the wet-days quantiles, by using Equation (2.5) and the chain rule:

$$\frac{\partial Q_{a,2}(p_a)}{\partial p_a} = \frac{\partial Q_2(p)}{\partial p_a} = \frac{\partial Q_2(p)}{\partial p} \frac{\partial p}{\partial p_a}$$

Since the percentiles p and p_a are linearly linked, $\frac{\partial p}{\partial p_a} = \frac{1}{1 - f_d} = \frac{1 - p}{1 - p_a}$, we get the following relationship between the two quantiles slopes:

$$(1 - p_a) \frac{\partial Q_{a,2}}{\partial p_a} = (1 - p) \frac{\partial Q_2}{\partial p}$$

Thus, Equation (2.6) becomes:

$$\Delta Q(p) = \Delta Q_a(p_a) + \frac{\Delta f_d}{1 - f_d} (1 - p) \frac{\partial Q_2}{\partial p} \quad (2.7)$$

Finally, we can apply the general formula in Equation (2.7) to a Weibull distribution of shape parameter α and scale parameter β . Putting all the terms depending on the wet-days percentile p on the same side, it yields:

$$\Delta Q_a(p_a) = \Delta Q(p) - \frac{\Delta f_d}{(1 - f_d)} \underbrace{\frac{\beta_2}{\alpha_2} \left[\ln \left(\frac{1}{1 - p} \right) \right]^{1/\alpha_2 - 1}}_{\text{distorting term}} \quad (2.8)$$

This equation shows that the quantile trends in all-days can differ from the wet-days trends due to the change of precipitation occurrence, which acts as a weight in front of a distorting term (underlined by a curly brace in equation Equation (2.8)). Note that the distorting term is growing with p and its form changes with the shape parameter α , giving even larger additive trends for the heavy precipitation percentiles as α is small. Note that in the limit case where $\alpha \rightarrow 1$, this distorting term becomes a shift of constant value β_2 : it is not anymore distorting the wet-days trend curve.

Section sum up: Influence on all-days quantiles trends of the dry-days frequency

In this section, we quantified analytically the influence of a dry-days frequency change on the quantile trends, by applying the framework from Schär et al., 2016 to a Weibull distribution model. We obtained a simple equation linking the all-days and wet-days quantile trends, where the dry-days frequency change plays the role of a distorting term.

2.3 Modified regimes for all-days quantile trends

On historical data, it is important to quantify when and where the change of occurrence is large enough, compared to the wet-days quantile trends, to create relevant changes on the all-days quantile curves. We also want to analyze which percentiles' all-days trends will be the most impacted by Δf_d . We thus need to compare the Δf_d term to the $\Delta Q(p)$ term, in Equation (2.7).

The all-days trend is given by the wet-days trend if and only if, $\Delta Q_a(p_a) \approx \Delta Q(p)$ i.e. $|\Delta Q(p)| \gg \left| \frac{\Delta f_d}{1-f_d} \frac{\beta_2}{\alpha_2} \left[\ln \left(\frac{1}{1-p} \right) \right]^{1/\alpha_2-1} \right|$. To first order, this is true if and only if :

$$\left| \frac{\partial Q}{\partial \alpha}(p) \Delta \alpha + \frac{\partial Q}{\partial \beta}(p) \Delta \beta \right| \gg \left| \frac{\Delta f_d}{1-f_d} \frac{\beta}{\alpha} \left[\ln \left(\frac{1}{1-p} \right) \right]^{1/\alpha-1} \right|$$

where we noted $\alpha = (\alpha_1 + \alpha_2)/2 \approx \alpha_2$ and similarly for β . Let's look whether at least one of the two left-hand side terms is dominant over the term in Δf_d . The term due to the change of the scale parameter of the wet-days distribution, $\left| \frac{\partial Q}{\partial \beta}(p) \Delta \beta \right|$, dominates over the change of occurrence term for percentiles p such as:

$$\left| \ln \left(\frac{1}{1-p} \right) \right| \gg \left| \frac{\Delta f_d}{1-f_d} \frac{\beta}{\Delta \beta} \frac{1}{\alpha} \right|. \quad (2.9)$$

This is verified at least for rank a rank $p < 1$ since $\lim_{p \rightarrow 1} \ln \left(\frac{1}{1-p} \right) = +\infty$. This independence of the maximum precipitation event trend from the precipitation occurrence was to be expected from Equation (2.4): $p = 1$ and $p_a = 1$ both describe the same event in wet-days and all-days. In addition, since the function $p \rightarrow \ln \left(\frac{1}{1-p} \right)$ is strictly growing on $[0, 1]$ up to infinity, there exists a percentile $p_{\text{lim}, \Delta \beta}$ above which the function becomes larger than $\left| \frac{\Delta f_d}{1-f_d} \frac{\beta}{\Delta \beta} \frac{1}{\alpha} \right|$.

$$\exists p_{\text{lim}, \Delta \beta} \in [0, 1[\left| \ln \left(\frac{1}{1-p_{\text{lim}, \Delta \beta}} \right) \right| = \left| \frac{\Delta f_d}{1-f_d} \frac{\beta}{\Delta \beta} \frac{1}{\alpha} \right|. \quad (2.10)$$

Thus, all quantiles of ranks $p \in [p_{\text{lim}, \Delta \beta}, 1]$ can be considered as not impacted by the change of dry-days frequency.

As for the term due to the change of the shape of the wet-days distribution, it is only dominant over the change of occurrence term for percentiles p such as:

$$\left| \ln \left(\frac{1}{1-p} \right) \ln \left(\ln \left(\frac{1}{1-p} \right) \right) \right| \gg \left| \frac{\Delta f_d}{1-f_d} \frac{\alpha}{\Delta \alpha} \right|. \quad (2.11)$$

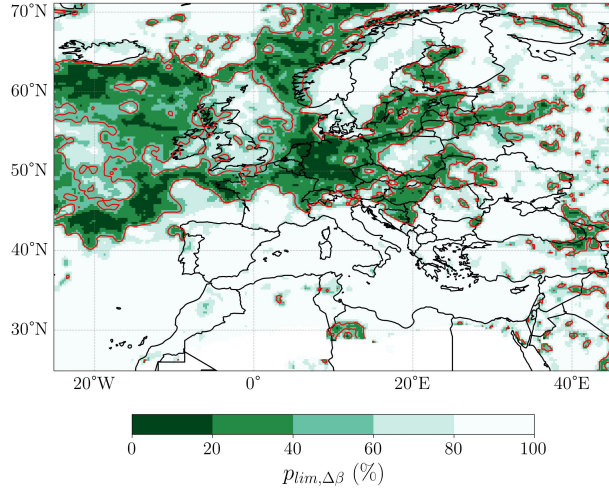


Figure 2.3: Limit percentiles $p_{\text{lim},\Delta\beta}$ after which the impact of the precipitation occurrence trend can be neglected for a wet-days quantile trends, thanks to the large trend of Weibull parameter β . The thin red contour denotes the value of 50%.

The left-hand side function is strictly growing on $[1 - e^{-1}, 1]$ and tends to infinity at 1, thus there also exists a percentile rank $p_{\text{lim},\Delta\alpha}$ above which this term becomes larger than $|\frac{\Delta f_d}{1 - f_d} \frac{\alpha}{\Delta\alpha}|$.

These two limit percentiles, which we will call $p_{\text{lim},\Delta\alpha}$ and $p_{\text{lim},\Delta\beta}$, can be inverted either analytically or numerically (for example using the segment or tangent methods).

On ERA5 precipitation data, the resulting percentile $p_{\text{lim},\Delta\alpha}$ is very high in both Europe and the Mediterranean (mostly above 95%, not shown) which means that the term in $\Delta\alpha$ is almost never dominant compared to the one in Δf_d for the all-days trend $\Delta Q_a(p_a)$.

On the other hand, the limit percentile $p_{\text{lim},\Delta\beta}$ can reach lower values and has more spatial variability (see Figure 2.3). For the Mediterranean, $p_{\text{lim},\Delta\beta}$ is very large (close to 100%). Thus, for the great majority of percentile ranks in the Mediterranean, the all-days trends are mainly due to the decrease of dry-days frequency and not to a change of intensity when it rains. This is consistent with the low statistical significance of $\Delta\alpha$ and $\Delta\beta$ over the Mediterranean on ERA5 data, while Δf_d is strong and significant.

For most of central and north Europe (aside of the Scandinavia), $p_{\text{lim},\Delta\beta}$ reaches much lower values: it is below 50% on about half of these regions' surface, and can go as low as 10%. Thus, in these regions, the influence of the change of dry-days frequency can be neglected compared to the change of the wet-days scale parameter, for wet-days percentiles larger than $p_{\text{lim},\Delta\beta} \approx 50\%$.

Let us now study the all-days trend curves, and how the all-days categories can differ from the wet-days' in the case of a strong change of occurrence. Figure 2.4 displays three typical cases, depending on the sign of the occurrence change.

It shows that in regions where the precipitation occurrence increases strongly enough, some locations with U-shape wet-days regime can become "all-increase" all-days regime (provided that the Δf_d term is large enough), while the wet-days "all-increase" trends can be even stronger. Similarly, wet-days "all-decrease" will merge with "reversed U-shape" to give a new all-days "reversed U-shape". Thus, only two main regimes could exist for such regions in all-days distribution: "all-increase" and "reversed U-shape".

In regions where the precipitation occurrence decreases strongly (like in the Mediterranean), the opposite occurs: the "all-increase" wet-days regime will disappear in favor of an all-days "U-shape" regime, while wet-days U-shape's inversion percentile will become even larger in all-days. Similarly, the "reversed U-shape" will merge with the "all-decrease" category. Thus, only two all-days regimes would be expected in regions with a strong decrease of f_d : "U-shape" and "all-decrease".

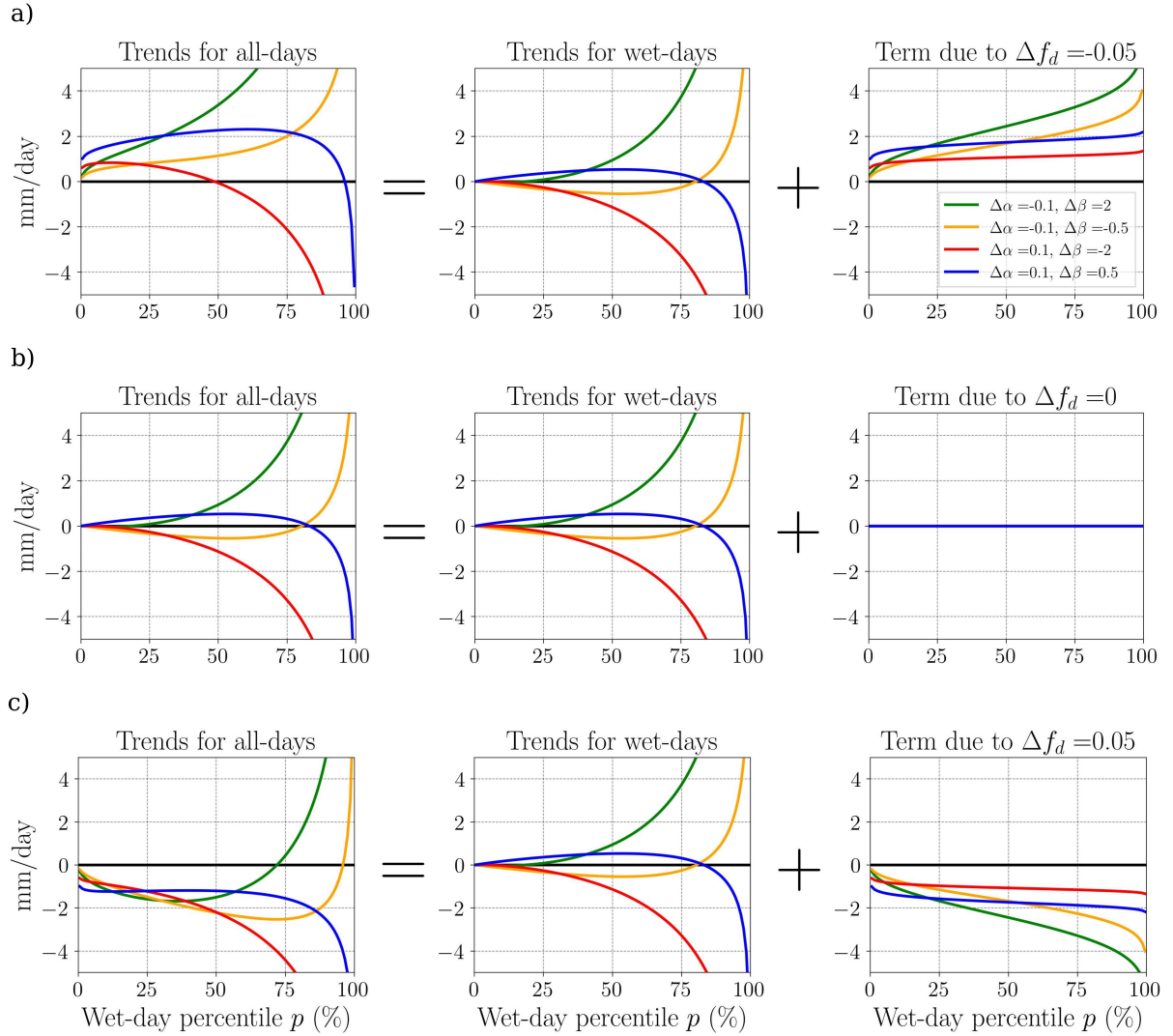


Figure 2.4: Illustration of the influence of the dry-days frequency term on the all-days quantile trend curves, for the four categories, for different values of the dry-days frequency change Δf_d : $\Delta f_d = -5\%$ (a), $\Delta f_d = 0\%$ (b), $\Delta f_d = 5\%$ (c). The values of the wet-days Weibull parameters ($\alpha, \beta, \Delta\alpha$ and $\Delta\beta$) are the same for all the subplots and are given on the top row, and are synthetic.

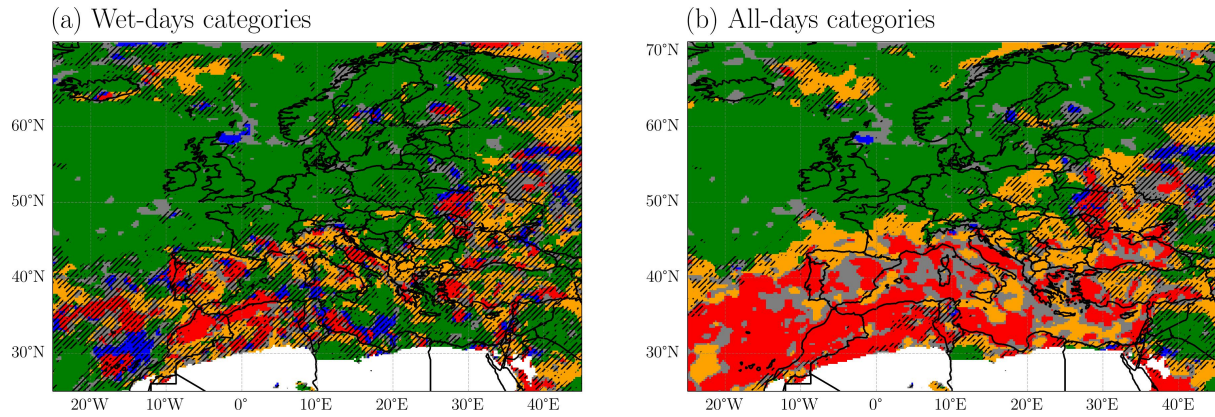


Figure 2.5: Category maps for the 1950–1980 and 1990–2020 periods. As before, green corresponds to “all quantiles intensify” category, red to “all quantiles decrease”, orange to “U-shape” and blue to “reversed U-shape”, while points whose category was unclear are in gray. White designates desert location (less than 2% of wet-days). The hatches on the left figure (resp. right figure) denote the location where neither $\Delta\alpha$ nor $\Delta\beta$ (resp. neither $\Delta\alpha$ nor $\Delta\beta$ nor Δf_d) are significant through a bootstrap test, at a confidence level of 90%.

Therefore, we expect that the Mediterranean all-days quantile trend curves will be mainly due to the increase of dry-days frequency, leading to a “all-decrease” category, different from the wet-days non-significant categories.

In opposition, for most of northern Europe, all-days quantile trend curves are expected to be very similar to the wet-days’, as the influence of $\Delta\beta$ is dominant over the change of dry-days there.

We can check this theoretical conclusion again on the all-days categories maps. We can naturally define an extension of the detection algorithm from wet-days quantile curves (as presented in Section 1.3) to all-days quantiles curves. It consists in computing the all-days quantile trends (from percentiles $p_a \in [0, 1]$) and then applying the algorithm only the right part of the curve: only on the equivalent wet-days percentiles p corresponding to $p_a \in [f_d, 1]$, with f_d the dry-days frequency of the reference period (1950–1980). This all-days detection algorithm enables to focus on the rainy quantiles, nevertheless incorporating the change of dry-days frequency.

Figure 2.5 shows the results for the all-days category map, and the already shown wet-days category map. The maps are put side by side to better highlight the differences due to the change of dry-days frequency, which are as we predicted above. In terms of spatial pattern, the overall North-South pattern of all-days category map is even clearer than the wet-days’, and the map is overall smoother. In all-days categories, there is a continuous transition in latitude, from “all increase” in the North to “all decrease” in the South, and “U-shape” or “Mediterranean paradox” transition zone in between. Thus, the Mediterranean paradox is found in this transitional zone between the wetting in northern Europe (due to the increase of both precipitation intensity and occurrence) and the strong drying in the Mediterranean (due to the decrease of occurrence).

The significance of the wet-days categories is associated to the one of the Weibull scale parameter change $\Delta\beta$, while we consider all-days categories as significant when either $\Delta\beta$ or Δf_d are significant. The significance results in Figure 2.5 highlight the fact that the signal of precipitation change in the Mediterranean in the last 70 years is not due to the change in wet-days distribution, but to the decrease of the dry-days frequency (which impacts the whole all-days distribution).

Section sum up: Consequences for the wet-days categories

In this section, we build further from the equation of all-days quantile trend, and showed that the dry-days frequency change had an influence on all-days quantiles up to a given percentile, which depends on the ratio of occurrence and intensity change. For most of central and north Europe, the influence of the change of dry-days frequency can be neglected compared to the change of the wet-days scale parameter, for wet-days percentiles larger than about 50%. For the Mediterranean, on the contrary, the dry-days frequency change is dominant for almost all quantiles (except the very extreme ones).

In the Mediterranean, this resulted in different all-days regimes compared to the wet-days one. We found a clear and robust North-South pattern for all-days regimes, with “all quantiles intensify” in northern Europe, mainly “all quantiles decrease” in the Mediterranean, and a small transition zone with a “U-shape” regime in between. In the Mediterranean, we showed that these all-days regimes were significant due to the strong change of the dry-days frequency.

2.4 Conclusion of the chapter

In this chapter, we aimed at better understanding how the strong trends of drying of the Mediterranean can influence the distribution of precipitation, all-together with the change of the whole wet-days distribution itself (from the low and medium percentiles to the most extreme precipitation). Using the ERA5 reanalysis, we studied the different contributions of dry-days frequency and wet-days distribution in the recent past, since the 1950s. Similarly to the wet-days regimes defined in chapter 1, we show that we could define all-days quantile change regimes, i.e. on the whole distribution, keeping the dry-days events in the distribution. The resulting all-days category map shows a clearer signal with latitude, from the Mediterranean (mainly “all decrease”) with a smooth transition (through a “U-shape” regime) to northern Europe (“all increase” regime). The greater spatial uniformity of the all-day regime map in the Mediterranean comes from the stronger and more robust signal of dry-days frequency change, which dominates the all-day distribution trends.

We quantified how much some all-days important variables, such as the trends of the annual mean or of quantiles, are influenced by both the change of wet-days distribution and of dry-days frequency (the latter significantly increases in the Mediterranean but decreases in northern Europe). The two effects can add up (as for the all-days mean in most of northern Europe) or counterbalance each other (as in southern Italy or in Poland).

One of the key findings of this work is that the change of dry-days frequency is predominant for the all-days trends of most quantiles in the Mediterranean, while in northern Europe its effect can be neglected compared to the strong increase of the Weibull scale parameter, for all quantiles with wet-days rank above about 50%.

In a nutshell, the framework developed in this study establishes a connection between changes in wet-days precipitation and a few critical parameters that capture the shift and distortion of the precipitation distribution, as well as changes in precipitation occurrence. It has the potential to be employed in different geographical regions and time spans.

In chapter 3, we will apply this framework to the future climate projections for the 21st century, in order to have a stronger and more robust signal over the Mediterranean.

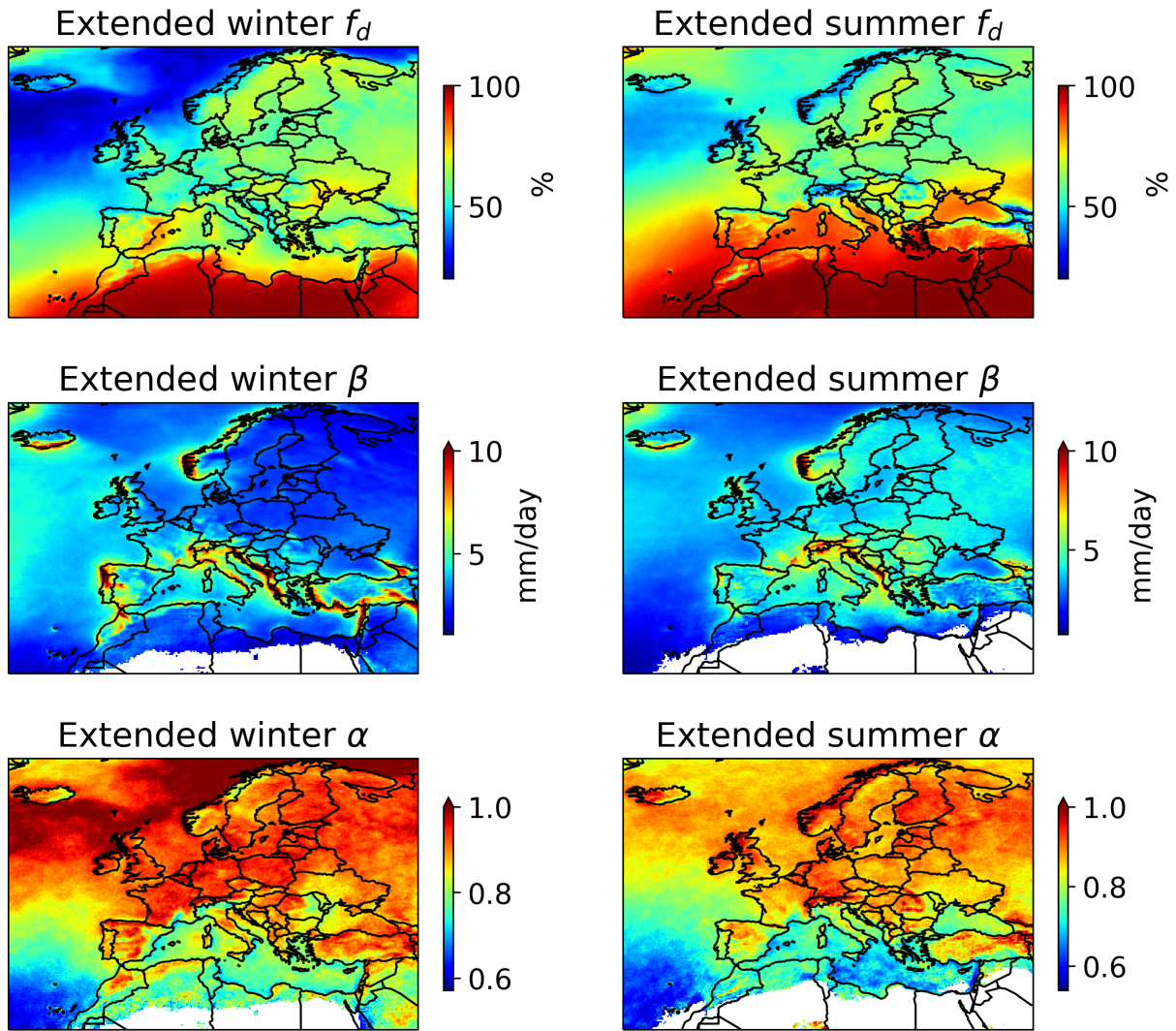


Figure 2.6: Maps of the parameters of the precipitation distribution, for period 1950–1980. First row: frequency of dry-days (days with more than 1 mm/day); Second row: Weibull scale parameter β ; Third row: Weibull shape parameter α .

2.A Seasonality of the climate change signal on precipitation

The annual analysis of wet-days and all-days distribution which we performed in the preceding chapter can be completed at seasonal scale. It will have the advantage of separating the different types of precipitation: large-scale stratiform precipitation occurring mainly in winter, and local-scale convective precipitation occurring mainly with warmer temperatures in an unstable atmosphere. Thus, looking separately at the seasons can give us more insights on the physical mechanisms which could explain parts of the trends observed.

As we focus mainly on the Mediterranean region, we decided to study two extended seasons: an extended summer (from May to October) and an extensive winter (from November to April). These correspond to a wetter and a drier season in the Mediterranean region.

Seasonality of the distribution parameters

We see in figure 2.6 the values of the dry-days frequency and Weibull parameters for wet-days, for the two extended seasons. The figures display known pattern of precipitation climatology.

The frequency of dry-days f_d has a strong latitudinal component, with an almost continuous decrease

from South to North, from about 95% in the Sahara to about 30% in the ocean off Norway (winter' values). f_d is higher in extended summer than winter over most of the domain, which is well-known: in the Mediterranean specifically, most of the precipitation days occur in the extended winter season, while the summer is much drier. Note that the only places where there are less dry-days in extended summer than in extended winter are the Alps. This may be due to the higher proportion of precipitation due to convection favored by the orography of the Alpine area in extended summer.

The scale parameter β , which can be associated to the median of wet-days precipitation (it is more precisely the quantile of rank 63%), is also higher in winter than in summer. This shows that the median intensity of precipitation is higher within the extended winter. We also observe a stronger East-West β contrast during winter in coastal areas such as Portugal, western Norway, the Balkan or south-west Turkey. This is consistent with the westerlies transporting humidity (from the Atlantic Ocean and even from the Mediterranean), which leads to more precipitation on the western coasts in winter.

Seasonality of the distribution parameter's changes

In figure 2.7, we show the changes between 1950–1980 and 1990–2020 in the dry-days frequency and in the two Weibull parameters for the wet-days precipitation.

The annual North-South pattern of the dry-days frequency change, previously described in chapter 2, is very similar to what we observe for the changes in extended winter: a large and significance zone with more dry-days in the Mediterranean region, and a significant increase of wet-days frequency over the United Kingdom, Iceland, the Scandinavia. Therefore, it appears that the dry-days frequency changes at the annual scale are driven by the extended winter.

There are also significant changes of dry-days frequency during extended summer:

- like in the annual case, there is a significant decrease of occurrence in summer for the Mediterranean, but this time with a lesser spatial extension, with signal only over the Mediterranean Sea.
- like in the annual case, an increase in wet-days frequency over Scandinavia and around Britain. However, we also find a significant increase of occurrence in a large region in the east Atlantic Ocean, in the Alpine region, and over Turkey.

In a nutshell, we can say that the results in summer occurrence changes differ from winter and the annual analysis mainly with a signal of increase occurrence on the east Atlantic waters, and with a smaller extension of the drying in the Mediterranean region, restricted to precipitation above the sea.

As for the seasonal changes in the Weibull parameters, we see that the changes in the shape parameter, $\Delta\alpha$, are overall much smaller than the scale parameter, $\Delta\beta$, and they are not significant almost anywhere. In winter, $\Delta\beta$ is positive over most of Western, Central and Northern Europe and in parts of the Mediterranean, at the exception to a few areas such as the Maghreb and the Western Iberian Peninsula. In summer, again the main trend for $\Delta\beta$ is an increase, except for the Mediterranean Sea and most of its coastal regions, where it decreases. However, most of the $\Delta\beta$ Mediterranean changes are not statistically significant. In the contrary, its increase signal is significant in Northern Europe in winter, and in the Atlantic in summer.

Seasonality of the decomposition of total precipitation change

We show in figure 2.8 the decomposition of the total mean precipitation into a change of occurrence and of intensity, with an annual and seasonal analysis.

Note that the relative change of the wet-days mean precipitation μ is expected to be approximately equal to the relative change of the Weibull scale parameter β , as the changes in α are negligible: $\frac{\Delta\mu}{\mu} \approx$

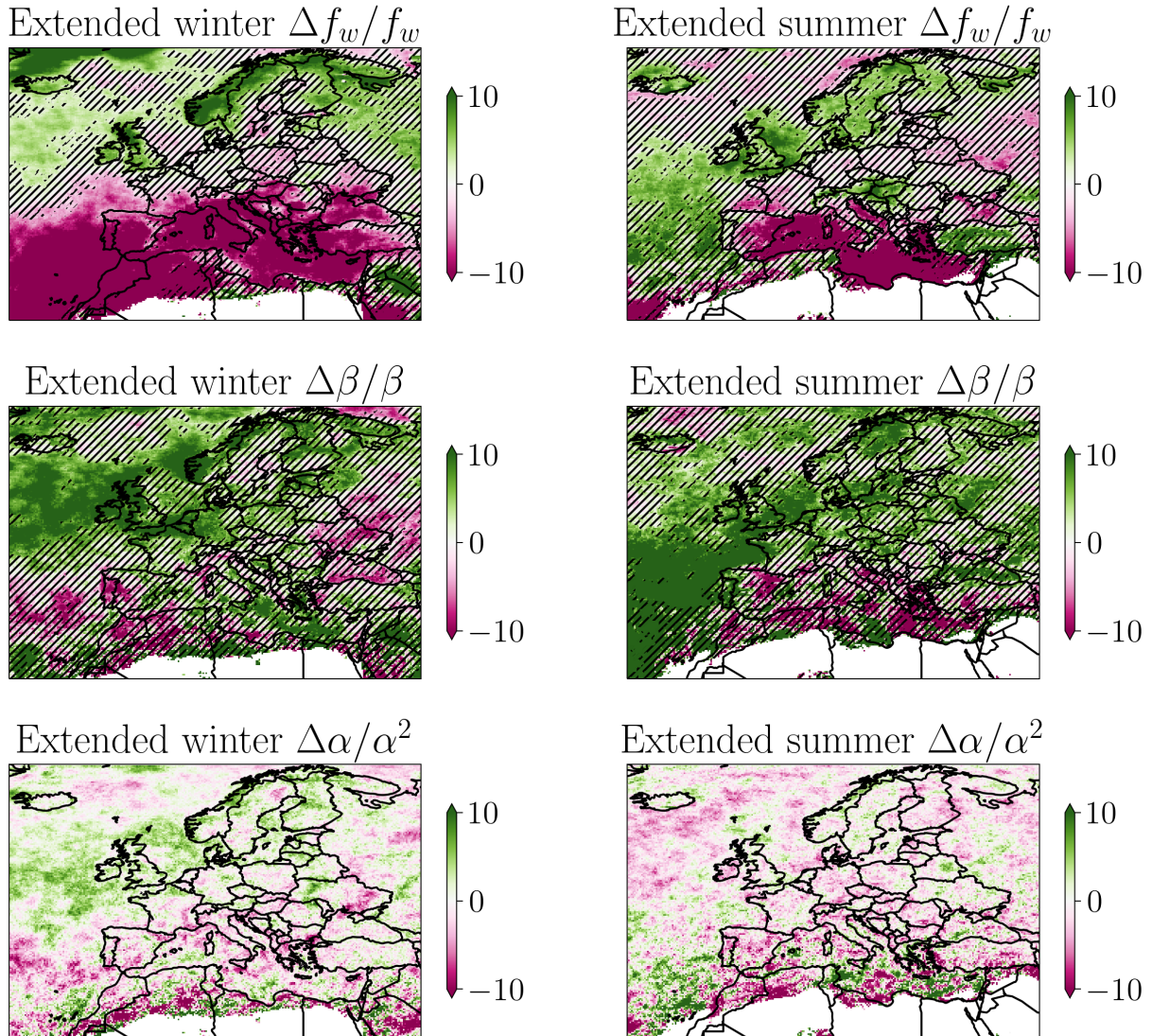


Figure 2.7: Maps of the relative changes of the precipitation distribution parameters, for periods 1950–1980 vs 1990–2020. First row: change in frequency of dry-days (days with more than 1 mm/day). Second row: change in Weibull scale parameter β . Third row: change in Weibull shape parameter α . We used $\Delta\alpha/\alpha^2$ instead of $\Delta\alpha/\alpha$ because this term is more comparable in terms of impacts with $\Delta\beta/\beta$, as seen from the equations before. The hatches show where the changes are not significant by Bootstrap test of confidence level 90% (except for $\Delta\alpha$, where it's always all not significant, therefore we did not plot the hatches at all).

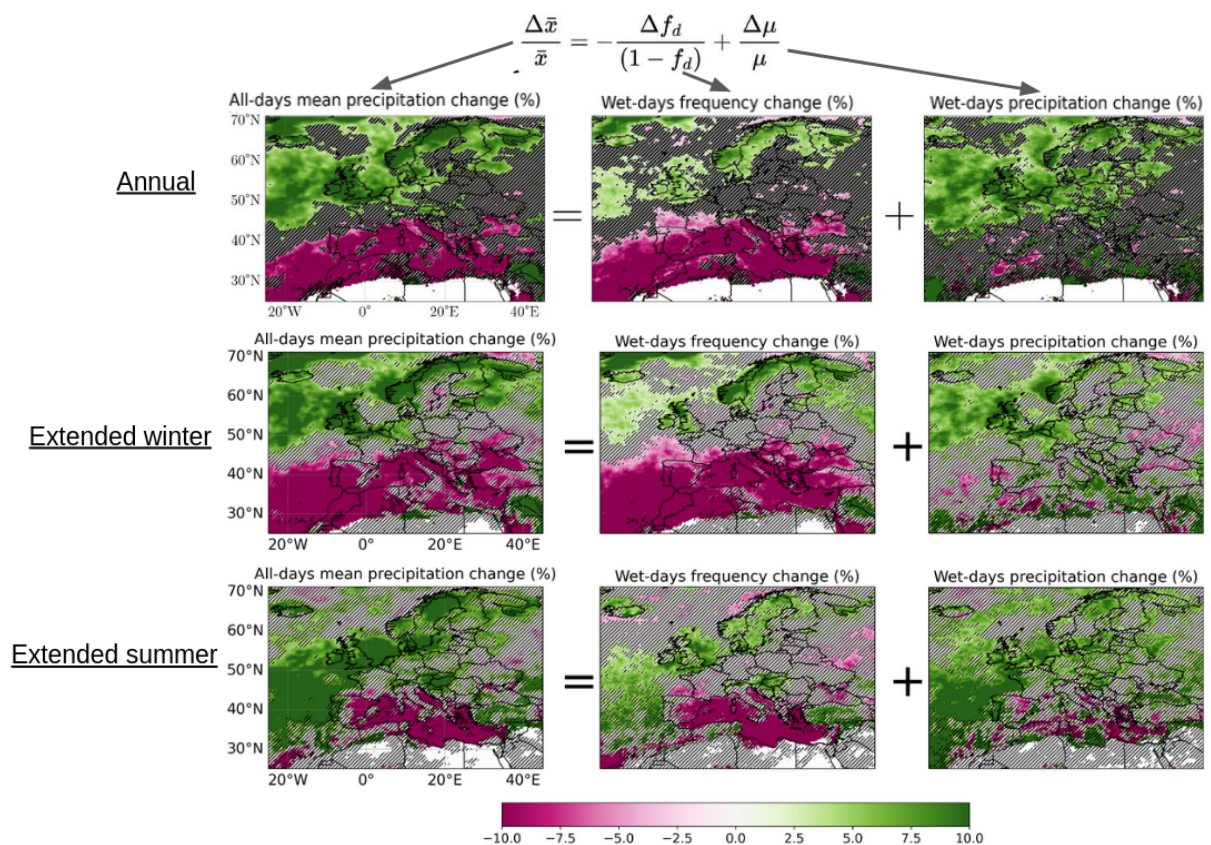


Figure 2.8: Decomposition of the total precipitation relative change in an occurrence term and an intensity term. The changes are between 1950–1980 and 1990–2020. Analysis is made at the annual scale (upper row), extended winter (middle row) and extended summer (lower row). Hatches show the area where the change of the relevant parameters are not significant by Bootstrap test, at a 90% confidence level.

$\frac{\Delta\beta}{\beta} - \frac{\Delta\alpha}{\alpha^2}\psi(1 + 1/\alpha) \approx \frac{\Delta\beta}{\beta}$. Thus, we are not surprised to find the same map structure and significance areas as in figure 2.7.

Concerning total precipitation changes, the winter and annual patterns are very similar to each other, thus again we can say that the winter precipitation are leading the changes.

We see that, like at the annual scale, the leading term within the Mediterranean is not the intensity change but the occurrence change. There is one exception for this statement, which is Portugal and the ocean off Portugal, where the intensity change in summer is responsible for an increase of total precipitation in summer (contrary to winter).

Still, it is interesting that the signal in summer differs from the one in winter, mainly by:

- the position of the zone of increasing total precipitation, shifted more to the south in summer, up to Portugal coasts. Therefore, in the Eastern Atlantic (off Portugal and African coasts), the change of total precipitation is positive in summer but negative in winter, resulting in a negative trend at the annual scale.
- the smaller extent of the Mediterranean zone with decrease of mean precipitation, restricted in summer to the sea and the eastern part of Spain.

Seasonality of the wet-days and all-days categories

Maps of the precipitation quantile trend regimes at the annual, extended winter and summer scales are shown on figure 2.9. We find again very clearly the North-South pattern of increase dry-days frequency in the all-days categories, with mainly “all quantiles intensify” in Northern Europe and “all quantiles decrease” in the Mediterranean. For the summer all-days map, the main difference with the annual map is the regimes of the Easter Atlantic Ocean and parts of the Mediterranean coast: they are not anymore in the “all quantiles decrease” regime but mostly in the “all quantiles intensify” regime. Once again, the winter categories are leading the largest part of the annual maps, both in all-days and wet-days.

In terms of statistical significance, there is no large gain to be at seasonal scale. Actually, the annual significant masks seem to be the combination of the extended winter and summer ones. This is logical, since a strong and significant signal in one season, while no large change is registered in the other season, leads the annual signal and its significance.

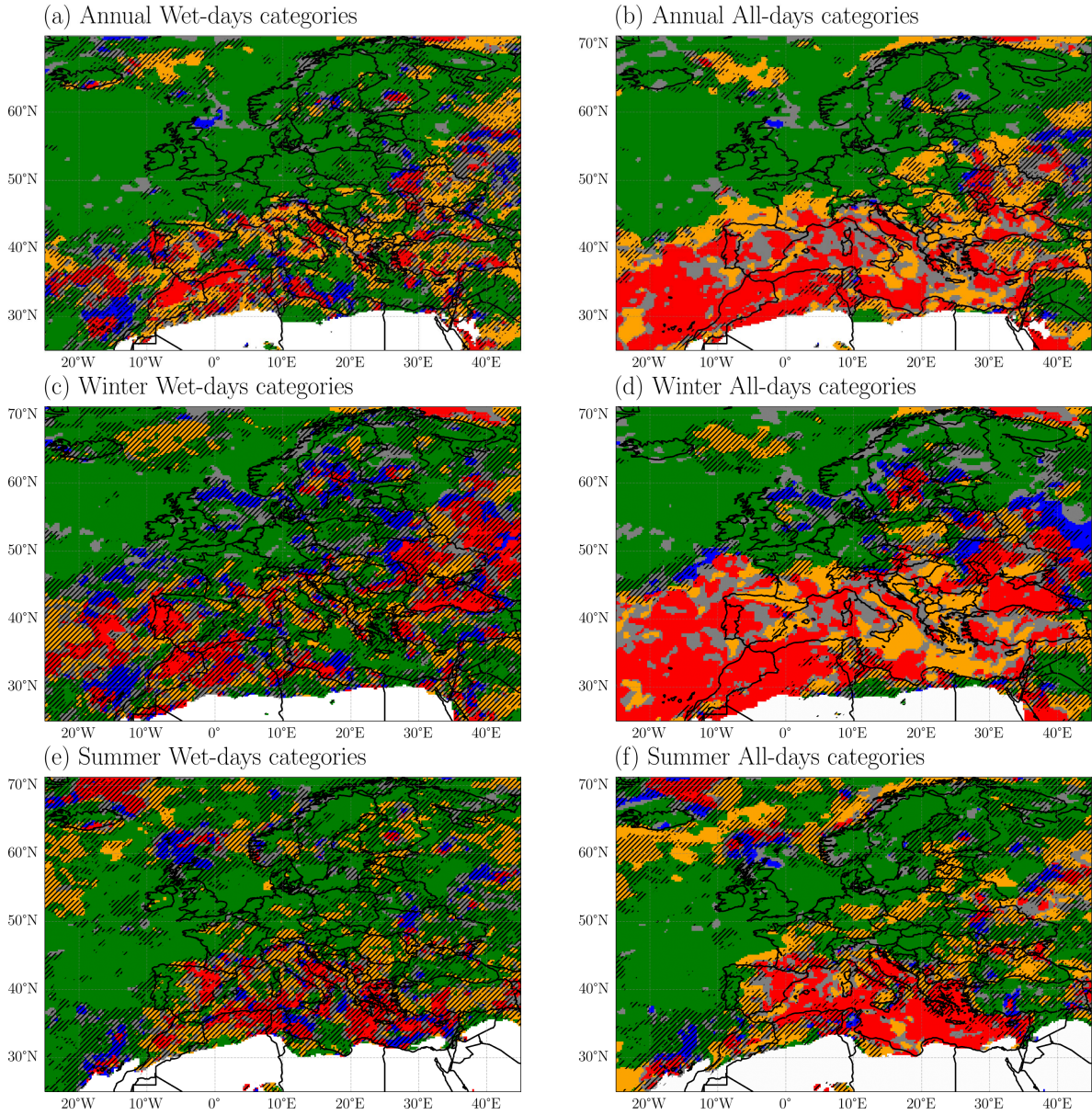


Figure 2.9: Wet-day categories (left) and all-days categories (right) for the periods 1950–1980 vs 1990–2020. Analysis is made at the annual scale (upper row), extended winter (middle row) and extended summer (lower row). On wet-days regimes, hatches show the area where neither $\Delta\beta$ nor $\Delta\alpha$ are significant by Bootstrap test, at a 90% confidence level. Similarly, on the all-days regimes, hatches show the area where neither $\Delta\beta$ nor $\Delta\alpha$, nor Δf_d , are significant.

Physical explanation - hypotheses

It would be interesting to understand the physical processes leading to these seasonal patterns and explaining these two main differences in total precipitation change between extended summer and winter. More precisely, we would like to explain:

1. the increase of wet-days intensity over northern Europe and Atlantic Ocean, which location and extent can vary between winter and summer seasons.
2. the large scale North-South pattern of the annual dry-days frequency change, with significant increase over the whole Mediterranean region (latitudes between 30° and 45°) while there is a increase of wet-days over some parts of northern Europe.
3. the smaller extent of this increasing dry-days frequency over the Mediterranean region in summer compared to winter (restricted to the Mediterranean Sea in summer), while there is a summer increase of wet-days frequency over the eastern Atlantic Ocean.

During my PhD, we didn't have the time to investigate these questions more thoroughly, but we can propose a few hypotheses.

- Hypothesis for item 1: the expected increase of humidity and extreme precipitation with Clausius Clapeyron relationship (as explained in the introduction), with a surface temperature, consistent with "all quantiles intensify" and "U-shape" regimes, and with the increase of wet-days mean intensity.
- Hypothesis for item 2: the decrease in precipitation occurrence could be due to the poleward expansion of the Hadley cell, which limits are different between summer and winter. As the subsiding branch of the Hadley cell reaches the Southern Mediterranean, it would inhibit convective updrafts and precipitation.
- Hypothesis for item 3: the Mediterranean land in summer is very dry, but also warmer than the sea, favoring atmospheric instability, which could tend to enhance convection processes on land, and could slightly counterbalance larger scale effects.
- Hypothesis for item 3: this could be due to an increased occurrence of a heat low phenomenon over the Iberian Peninsula (Drobinski et al., 2020), i.e. a cyclonic blocking, which also advects dry air from the Sahara to Mediterranean Sea.
- Hypothesis for item 3: it has been shown that there is an increase in the last decades of the frequency of occurrence of summer atmospheric lows (high troposphere) over the Atlantic Ocean off the European coast (D'Andrea et al., 2024). These lows could be associated with more frequent summer rainfall over this part of the Atlantic.

Delving into these different hypotheses could be the focus of future work related to this PhD thesis, as discussed further in part III.

2.B Separation between all-days regimes and value of the inversion percentile

This section comes in complement to the methodology described in the first two chapters of this manuscript. We can go one step further in the analytical analysis of all-days regimes.

The main question is: can we deduce the all-days regime from the analytical link between all-days and wet-days quantile trends, given by equation (2.12)?

$$\Delta Q_a(p) = \Delta Q(p) + \frac{\Delta f_w}{f_w} \underbrace{\frac{\beta}{\alpha} [\ln(\frac{1}{1-p})]^{1/\alpha-1}}_{\text{distorting term}} \quad (2.12)$$

Yes, and it is actually quite simple. Let us be in the case where the changes in the scale parameter β are dominant over those of the shape parameter α . Then equation (2.12) simplifies to:

$$\Delta Q_a(p) = \Delta\beta [\ln(\frac{1}{1-p})]^{1/\alpha} + \frac{\Delta f_w}{f_w} \frac{\beta}{\alpha} [\ln(\frac{1}{1-p})]^{1/\alpha-1} \quad (2.13)$$

Note that, as the wet-days percentile $p \in [0, 1]$, $\ln(\frac{1}{1-p})$ is positive. Therefore, if $\Delta\beta$ and Δf_w are both positive, so will be $\Delta Q_a(p)$, thus giving a “all quantiles intensify” regime. Likewise, if $\Delta\beta$ and Δf_w are both negative, it will give a “all quantiles decrease” regime.

It becomes slightly more complicated if $\Delta\beta$ and Δf_w are of opposite signs, as it leads to an inversion percentile, as we will see just below.

All-days inversion percentile

Let’s take for instance, $\Delta\beta > 0$ and $\Delta f_w < 0$, which is the very common case found in our data, where there are more numerous dry-days, while wet-days precipitation get more intense. The sign of the change of all-days precipitation quantile $\Delta Q_a(p)$ can be computed easily:

$$\begin{aligned} \Delta Q_a(p) \geq 0 &\iff \frac{\Delta\beta}{\beta} \geq \frac{-\Delta f_w}{f_w} \frac{1}{\alpha} [\ln(\frac{1}{1-p})]^{-1} \\ &\iff \ln(\frac{1}{1-p}) \geq \frac{-\Delta f_w}{f_w} \frac{\beta}{\Delta\beta} \frac{1}{\alpha} \\ &\iff p \geq 1 - \exp\left(\frac{-\Delta f_w}{f_w} \frac{\beta}{\Delta\beta} \frac{1}{\alpha}\right) \\ &\iff p \geq p_{inv,all-days} \end{aligned}$$

Therefore, in this case, the quantile trend curve is positive for percentiles larger than what we define as the inversion percentile, $p_{inv,all-days}$, and negative below this percentile. This describes a “U-shape” all-days regime.

We thus also found the expression for the inversion percentile of all-days “U-shape” regime, which happens to be the same as the limit percentile presented previously in chapter 2:

$$p_{inv,all-days} = 1 - \exp\left(\frac{-\Delta f_w}{f_w} \frac{\beta}{\Delta\beta} \frac{1}{\alpha}\right) = p_{lim,\Delta\beta} \quad (2.14)$$

The inversion percentile decreases with $\frac{-\Delta f_w}{f_w} \frac{\beta}{\Delta\beta}$, i.e. on the ratio of the change of the wet-days frequency and median intensity. If the change of frequency dominates, i.e. $|\frac{\Delta f_w}{f_w}| \gg |\frac{\Delta\beta}{\beta}|$, the expression boils down to $p_{inv,all-days} = 1$ consistent with an “all quantiles decrease” regime, while if the increase of intensity dominates, it leads to $p_{inv,all-days} = 0$, consistent with an “all quantiles intensify” regime. This highlights that the “U-shape” regime is a transition between the “all quantiles decrease” and “all quantiles intensify” regimes. Note that the inversion percentile does depend also on the value of α , but not on its change.

As before, the expression of the inversion regime $p_{inv,all-days}$ is given here in wet-days percentile,

while some application may require an expression in all-days, for example to come back to the return period of an event. We can easily translate this inversion percentile to its corresponding all-days percentile $p_{a,inv,all-days}$, thanks to equation (2.4), which gives:

$$p_{a,inv,all-days} = (1 - f_d) p_{inv,all-days} + f_d \quad (2.15)$$

In this section, we had taken the common case where $\Delta\beta > 0$ and $\Delta f_w < 0$. In the opposite case, when $\Delta\beta < 0$ and $\Delta f_w > 0$, we understand through the same reasoning that we get a “reversed U-shape” regime, and the expression for the inversion percentile given in equation (2.14) is still valid.

Adapted phase space for the all-days regimes

To sum up, we have identified the link between the signs of $\Delta\beta$ and Δf_w and the all-days regimes:

- When Δf_w and $\Delta\beta$ are both positive, the all-days regime is “all quantiles intensify”;
- When Δf_w and $\Delta\beta$ are both negative, the all-days regime is “all quantiles decrease”;
- When $\Delta f_w < 0$ and $\Delta\beta > 0$, the all-days regime is “U-shape”;
- When $\Delta f_w > 0$ and $\Delta\beta < 0$, the all-days regime is “reversed U-shape”.

Therefore, we have the theoretical all-days regimes given by the x and y axis of a new phase space, $(\frac{\Delta f_w}{f_w}, \frac{\Delta\beta}{\beta})$. This is illustrated in the left plot of figure 2.10.

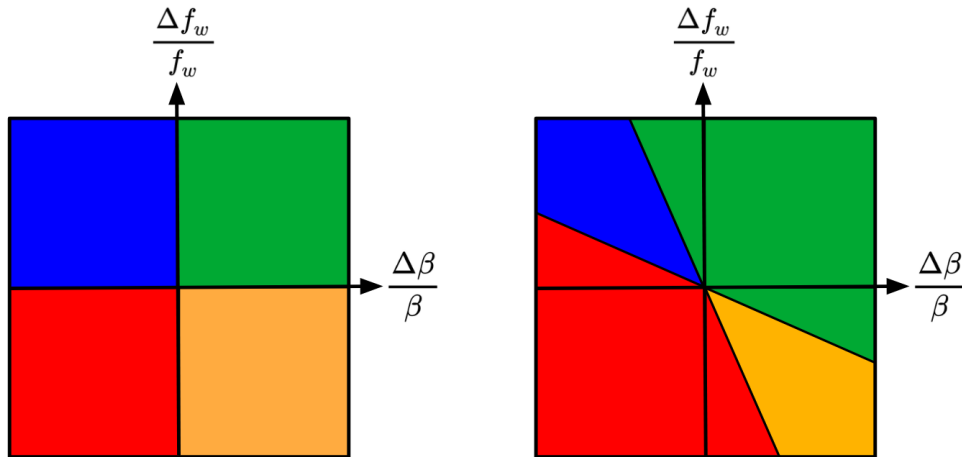


Figure 2.10: Schematic view of the separation of all-days regimes in the phase space $(\frac{\Delta f_w}{f_w}, \frac{\Delta\beta}{\beta})$. Green corresponds to “all quantiles intensify” category, red to “all quantiles decrease”, orange to “U-shape” and blue to “reversed U-shape”.

Left: the most theoretical expectation, if one could detect a U-shape regime with an inversion percentile very close to $p = 0\%$ and $p = 100\%$. Right: expectation with a detection of a U-shape only for percentile not too close to $p = 0\%$ and $p = 100\%$.

However, this theoretical phase space has to be slightly corrected. Indeed, when we are in the orange corner but close to the x axis, $\frac{\Delta f_w}{f_w} \ll \frac{\Delta\beta}{\beta}$, thus the percentile of inversion is almost $p_{inv,all-days} = 0$, with negative trends only for a very small range of percentiles. Our algorithm cannot detect that on a quantile trend curve (neither can our eyes). Therefore, a more practical regime distinction is illustrated in the right plot of figure 2.10, with smaller “U-shape” and “reversed U-shape” zones.

The precise limit between a “U-shape” and its two neighboring regimes can be roughly assessed, by looking back at the definition of our algorithm. For “belly” of the quantile trend curve was defined as

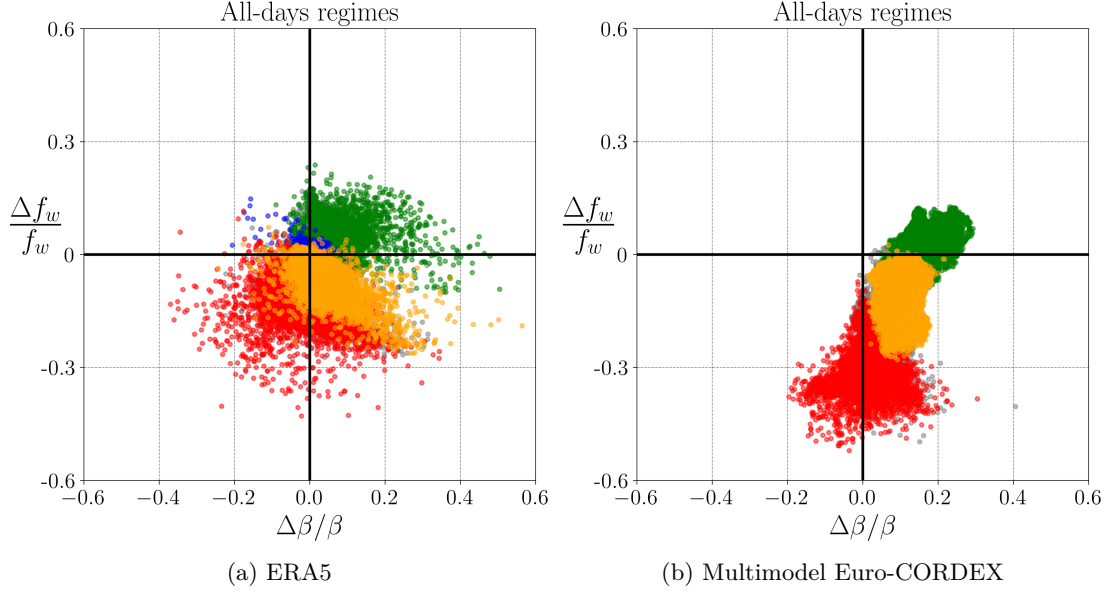


Figure 2.11: All-days regimes detected over the whole domain, plotted on the phase space $(\frac{\Delta f_w}{f_w}, \frac{\Delta \beta}{\beta})$. Trends are computed between 1950–1980 and 1990–2020 for ERA5, and between 1970–2000 and 2070–2100 for Euro-CORDEX (more details about the selection of models and their bias-correction in chapter 3).

Green corresponds to “all quantiles intensify” category, red to “all quantiles decrease”, orange to “U-shape” and blue to “reversed U-shape”. Note that there are very few blue points for ERA5, and not any for multimodel CORDEX.

$p \in [10\%, 60\%]$ and the “tail” as $p \in [80\%, 99\%]$, and the regime is detected as “U-shape” if, basically, the “belly” and the “tail” are of opposite signs. If we imagine a “U-shape” regime with a very small inversion percentile (for instance smaller than 10%), then the “belly” will be of positive sign, and our algorithm will wrongly classify as a “all quantiles intensify”. We can therefore estimate that our algorithm can only detect “U-shape” regime if the inversion percentile is larger than about 30% and smaller than about 95% (i.e. taking the middle of the “belly” range, and slightly more for the “tail” as the slope can be much larger at the tail). This was sufficient to detect correctly the wet-days “U-shape” regimes, which inversion percentile is theoretically bounded, between 30% and 93%. For all-days “U-shape” regime, there is no such bound as we’ve seen.

This simple analysis gives us the limit values of the ratio $\frac{\Delta f_w}{f_w} \frac{\beta}{\Delta \beta}$ which can be detected as a “U-shape” regime: two practical limits expected from our algorithm classification, one close to the y axis, with a slope of $\frac{\Delta f_w}{f_w} \frac{\beta}{\Delta \beta} \approx -\frac{1}{\alpha} \ln \frac{1}{(1-0.95)} \approx -\frac{2.3}{\alpha}$, the second close to the x axis: $\frac{\Delta f_w}{f_w} \frac{\beta}{\Delta \beta} \approx -\frac{1}{\alpha} \ln \frac{1}{(1-0.4)} \approx -\frac{0.4}{\alpha}$. Note that the frontier depends on the value α ; for an order of magnitude, we’ll take its value in the Mediterranean region, with α between 0.7 and 0.9. Therefore, the first slope of separation of the “U-shape” regime is around -0.3 and -0.4, and the second between -2.1 and -2.7. In terms of angle from the horizontal, this gives a first limit around -20° and the second around -67° .

We have plotted the all-days categories detected on ERA5 precipitation in this $(\frac{\Delta f_w}{f_w}, \frac{\Delta \beta}{\beta})$ phase space, as well as for the future on a selection of Euro-CORDEX projections (more details about the selection of models and their bias-correction in chapter 3). The results show indeed a cloud with colors very similar to the right plot of figure 2.11, with separations between “all quantiles decrease”, “U-shape” and “all quantiles intensify” which are consistent with the -20° and -67° limits that we estimated above.

Therefore, the $(\frac{\Delta f_w}{f_w}, \frac{\Delta \beta}{\beta})$ phase space can be a visual way to separate between all-days regime. Note that this phase space is valid when the relative changes in (f_w, β) are much larger than those in α , which is the case for ERA5 reanalysis and in past and future CORDEX simulations.

Chapter 3

Regimes of precipitation distribution change with future global warming

The objective of this chapter is to apply the methodology, which we developed in the two previous chapters, to future projections, where the level of global warming and its consequences on the water cycles are much higher than in the recent past (Ali et al., 2022). Parts of this work have implied Nicolas Chiabrande, who we supervised during his master internship.

In section 3.1, we select and bias-correct a subset of projections to perform a multimodel analysis. In section 3.2, we apply the methodology to the past period of the models, to compare the CORDEX selection to the ERA5 reanalysis. This enables a validation of the selected dataset. Besides, thanks to the multimodel approach, depending on the robustness of the changes between projections, we can rule out the internal multi-decadal variability as a cause of the changes in the past periods.

Then, we turn to future projections. In section 3.3, we aim at characterizing the future evolution of the whole precipitation distribution, taking into account both wet-days distribution change and dry-days frequency change. As we have seen in previous chapters, for the Mediterranean and the recent past, the significant precipitation change signal was restricted to a dry-days frequency change only. We are therefore interested in whether the future projections provide a robust signal in the change in both the occurrence and the intensity of precipitation, especially for the Mediterranean. We are also curious about the evolution of the contribution of dry-days frequency and wet-days intensity changes to the whole distribution. Finally, in section 3.4, we study the emergence of these potential future signals with time.

Key points

- In future climate projections, there is a robust signal on wet-days rain distribution change: it shifts toward more intense rainfall, in both Northern Europe up to northern Mediterranean. No robust signal is found on the southern Mediterranean in the wet-days distribution.
- In the past and the future, the evolution of precipitation distribution in the Mediterranean is essentially dominated by the dry-days frequency change, which affects wet-days quantile up to rank 80% at least.
- The climate change signal in all-days distribution changes emerges sooner for Europe than for the Mediterranean, with a few decades of lead for Northern and Central Europe.

3.1 Selection and correction of a multimodel projection datasets

The aim of this section is to explain the choices we made on the selection and bias-correction of a set of future projections. We also explain the choices made in terms of multimodel analysis and define what we call the robustness between models.

3.1.1 Selection of a dataset of climate projections

In the following, we use the daily accumulated surface precipitation variable from climate simulations from the Euro-CORDEX experiment (“EURO-CORDEX: new high-resolution climate change projections for European impact research”, 2014). Euro-CORDEX is part of the international effort of the Coordinated Regional Climate Downscaling Experiment (Giorgi et al., 2009; Gutowski Jr et al., 2016). It aims at providing high resolution projections for regional analysis, by dynamical downscaling some of the Global Climate Models (GCM) of the CMIP5 project, using Regional Climate Models (RCM). In the high resolution runs of Euro-CORDEX, data is available over an European domain at 0.11° of horizontal resolution, on a rotated grid. The runs span the period from 1950 (or 1970 depending on the RCMs) to 2100.

We use projections with the future emissions’ scenario representative concentration pathway (RCP) 8.5, considering a continuing rise of greenhouse gas emissions during the twenty-first century, and reaching an additional global forcing due to human emissions of 8.5 W/m^2 by 2100, compared to pre-industrial levels. The RCP8.5 scenario projections give a global average increase of about 4.5°C by 2080–2100, compared to 1850–1900 (very likely values of 2.6°C and 4.8°C). We choose the RCP8.5 scenario as with a higher level of global warming, we expect to see a stronger and clearer signal on precipitation changes, as was shown for extreme precipitation in Trambly and Somot, 2018.

As precipitation projections are greatly affected by inter-model spread and internal variability, an ensemble of models is needed to assess uncertainties. More than 70 simulations are available in Euro-CORDEX for scenario RCP8.5; using all of them would be computationally costly and would not necessarily result in an improvement compared to a smaller selection. As advised by Pierce et al., 2009, we preferred using a large model ensembles rather than what could be defined as the best-performing simulations on observed climate.

For this study, a sub-ensemble of 15 regional climate simulations from the Euro-CORDEX have been selected: figure 3.1. Note that the six GCMs used in Euro-CORDEX were found to be realistic over Europe in terms of circulation patterns, and suitable to capture the maximum possible range of changes in temperature and precipitation (McSweeney et al., 2015). We did not choose the GCM/RCM couples in function of the RCMs’ parametrization schemes, though it is known that the schemes used to represent convection can induce large uncertainties in precipitation extremes (Beranová et al., 2018). Instead, we constructed the selection to allow i) considering all the six general circulation models (GCM) included in Euro-CORDEX, and ii) offering a large diversity of regional climate models (RCM), with in our selection each of the six GCMs forcing at least two RCMs.

3.1.2 Bias-correction of the models

The quality of the Euro-CORDEX simulations has been discussed in literature, for example in Vautard et al., 2021, or with a focus on daily precipitation in Stephens et al., 2010; Casanueva et al., 2016.

In Vautard et al., 2021, 55 Euro-CORDEX simulations from a matrix of 8 GCMs \times 11 RCMs were evaluated over the 1981–2000 period, where they were found to perform relatively well in terms of classical variables, with yet some systematic biases. For example, the simulations compared to observations or

RCM -GCM	CNRM	EC-EARTH	HADGEM	IPSL	MPI	NORESM
ALADIN53	r1i1p1					
ALADIN63			r1i1p1			
CCLM	r1i1p1	r12i1p1			r1i1p1	
HIRHAM		r1i1p1				r1i1p1
RACMO		r1i1p1	r1i1p1	r1i1p1		
RCA	r1i1p1	r12i1p1				
REMO				r1i1p1	r1i1p1	r1i1p1

Figure 3.1: Table of the different runs selected from Euro-CORDEX, from different General Circulation Models (GCMs) and Regional Climate Models (RCMs). The emission scenario used is RCP8.5. We use only daily precipitation.

reanalyses, were found to be overall too cold and too windy. Compared to EOBS precipitation (a dataset based on the interpolation of rain gauges), simulations were also found to be too wet, with up to a factor 1.5 in total winter precipitation in some part of Europe (Central France, the Alps, Eastern Europe). These biases were shown to have shared responsibilities among RCMs and GCMs.

Another common bias in climate models is the overestimation of wet-days frequency, and the wet-days precipitation is predicted too lightly. This is known as the “drizzle problem” in climate modeling Polade et al., 2014; Casanueva et al., 2016; Bastin et al., 2019; Pichelli et al., 2021. Biases on precipitation also concern all quantiles up to the extremes: actually, the whole distribution of precipitation.

Considering the biases in climate simulations, bias adjustment methods are often used for climate studies, especially for impacts study, or for evaluation of the climate models on th epast periods. A list of some of the correction methods used by studies on Euro-CORDEX runs can be read in [Summary of bias adjustment methods applied to CORDEX simulations](#).

We performed a bias-correction of the daily precipitation with the now commonly used Cumulative Density Function Transform method (called also CDF-t), developed by Michelangeli et al., 2009. The CDF-transform is based on quantile mapping, a method based on the correction of the whole distribution. Quantile mapping bias-correction algorithms have been reviewed in the context of hydrological impacts studies and have been found to outperform the simpler bias-correction method that corrects only the mean of the precipitation series (Teutschbein & Seibert, 2012; Chen et al., 2013). Compared to quantile mapping, CDF-t has the advantage of allowing the CDF of the model to evolve in time, between the historical period and the future one (see more detailed explanation in section 3.A.1).

Besides, as precipitation is a variable which distribution has a strong discontinuity in 0 (there are many dry-days), the classical bias-correction methods must be adapted. We therefore applied the CDF-t method through the Singularity Stochastic Removal (SSR) method developed by Vrac et al., 2016, which aim to correct precipitation (or any other variable with a singularity), wether the model predicts too few or too many dry-days. The SSR method has been shown to provide improved results for both the precipitation occurrence and intensity compared to the classical application of CDF-t (Vrac et al., 2016), and to provide a good compromise between the correction of occurrence and intensity. Compared to other methods to take into account the singularity (such as threshold adaptation or positive approach), SSR allows dealing in the same way with the situations where the precipitation model has too many wet-days or not compared to the reference data.

We used daily precipitation data from ERA5 reanalysis (Hersbach et al., 2018) as the reference for past precipitations. The choice not to use EOBS gridded dataset (used for example in Vautard et al., 2021) was driven by the temporal and spatial inhomogeneities that we observed in this precipitation dataset over 1950–2020 (more details in section 3.A).

For the bias-correction, we chose 1971–2005 as the reference period, which corresponds to the last 35 years of the historical runs of CORDEX, and to a period with a better quality of observations assimilated in the ERA5 reanalysis. The models were projected on ERA5 coarser grid (0.25° horizontal resolution) through bilinear interpolation, with the package Climate Data Operators (CDO) developed by the Max Planck Institute for Meteorology (Schulzweida, 2023). Note that the influence of the interpolation method is negligible on the results (not shown here). Then the CDF-t-SSR bias-correction was applied on each individual Euro-CORDEX model’s precipitation data, using the python Statistical Statistical Bias Correction Kit (“SBCK: Statistical Bias Correction Kit”, 2023). Note that we performed the bias-correction without separating between seasons, for simplicity’s sake. Besides, we did not remove the potential trends in precipitation in the period 1971–2005, neither in the reference reanalysis nor in the Euro-CORDEX models. We checked that the changes in precipitation distribution are small during the period 1971–2005 (usually of a few percents for Weibull parameters and the dry-days frequency), thus we neglected them in the bias-correction procedure.

Note that we studied the effect of the bias-correction (and of the reference dataset) on the distribution regimes, in section 3.A. Using EOBS gridded dataset indeed gives slightly different results for our methodology, especially on wet-days regimes. Still, the main messages of our work remain valid.

3.1.3 Choices made in the multimodel analysis

We present here the choices we made for the multimodel analysis and give a definition of what is the robustness between models.

For a continuous variable, such as the change of wet-days frequency, we simply perform a multimodel mean. We use the standard deviation to assess the uncertainties between models. To quantify the robustness between models on a given trend, we compute the Signal-to-Noise Ratio (SNR), as presented in Kendon et al., 2008; Laux et al., 2017; Christensen et al., 2019; Matte et al., 2019. It is defined as the ratio of the multimodel mean (considered as the signal) divided by the inter-model standard deviation (considered as the noise). We considered a trend robust between models if the SNR value is larger than 1 (as usually done in the papers using SNR). On our results, we observed that the criteria of $SNR > 1$ gave very similar results than the agreement on the sign of the trends by at least 12 out of the 15 models.

However, as the quantile trends classification is not a continuous variable (the category is for example “all quantiles intensify” or “all quantiles decrease”), we need to use another framework to assess multimodel values and robustness. We choose to define a multimodel category value, in each location, as the main category found in the different models if at least 10 out of the 15 models agree on the category. If less than 10 models agree on the category, then the category is defined as none, as we consider that in this case, the models have a too large spread in their results.

3.2 Validation of the selected projections on the past period for wet-days and all-days distribution changes

As a first step, we will apply most of the methodology presented in chapter 1 and chapter 2 to Euro-CORDEX models on the same past periods as previously, 1950–1980 vs 1990–2020. It will enable the comparison of the methodology’s result between the selected models with ERA5 reanalysis. It is a way to check whether the selected Euro-CORDEX simulations give consistent results with ERA5 on the past period, and thus to validate our selection. We will study both the wet-days and all-days category maps, as well as the amplitude of the relative changes between wet-days frequency and intensity.

3.2.1 Analysis of the wet-days category maps in Euro-CORDEX and comparison with ERA5

We applied the classification algorithm to each model separately, giving 15 different wet-days category maps, shown in figure 3.2, for period 1950–1980 compared to 1990–2020. Note that the two simulations with SMHI-RCA4 as a RCM were not available from 1950 on but from 1970. Therefore, the trend analysis is done by comparing the shorter period 1970–1980 with 1990–2020.

A large variation between the different models is visible in the results of the classification, both for Europe and the Mediterranean. The difference seems larger between simulations with different forcing GCMs than for different RCMs sharing the same forcing GCM. For example, the two runs forced by the MOHC-HadGEM2 model both display a higher homogeneity of category than the other models, with a dominant “all quantiles intensify” regime in most of Europe. On the contrary, the three runs forced by the CNRM-CERFACS model each have much more spotty wet-days category maps, with a larger fraction of “U-shape” and “reversed U-shape” regimes in Northern Europe.

This strong dependency on the forcing GCM would mean that the wet-days category, i.e. the change in the wet-days distribution, is more strongly linked to the changes in the large-scale dynamics than to regional and local processes represented by the RCM. Indeed, large-scale atmospheric dynamics in a GCM/RCM simulation is mainly given by the GCM, for midlatitude regions such as the European domain of CORDEX (Demory et al., 2020).

The multimodel category map on the past periods is shown in figure 3.4. It shows that there is some robustness, though not very strong, between the 15 models. At least 10 out of 15 models agree that the regime “all quantiles intensify” is present in parts of Northern Europe, while there is no agreement on which regimes are dominant in the Mediterranean. As a reminder, in ERA5 reanalysis, we found the same regime “all quantiles intensify” to be statistically significant in Northern Europe, while in the Mediterranean region, the different regimes detected were proven to be not significant. Therefore, on the past periods, the wet-days regime maps of ERA5 and multimodel Euro-CORDEX are overall consistent with each other.

Besides, the agreement between models for Northern Europe enables us to attribute the “all quantiles intensify” signal in ERA5 to climate change. Indeed, in our multimodel approach, the regional climate models are forced by different Global Circulation Model (GCM) runs, which all have their own internal variability, such as the North Atlantic Oscillation (NAO) or the Atlantic multidecadal oscillation. While these natural variability modes can have influence on European precipitation, their oscillations in each GCM can be different, and are a priori disconnected from those of the reanalysis. Therefore, a common signal between the 6 different GCMs and ERA5 reanalysis cannot be due to internal variability (or with only an extremely low probability). Thus, this common signal can be attributed to the climate change signal due to anthropogenic forcing.

With the same reasoning, we deduce that for the Mediterranean, the lack of robustness in the wet-days maps in the historical runs of Euro-CORDEX confirms our hypothesis that the noisy wet-days precipitation distribution changes in this region were not due to climate change, but to natural variability.

3.2.2 Analysis of the all-days category maps in Euro-CORDEX and comparison with ERA5

In figure 3.3, are shown the all-days categories for each CORDEX model, over the same past periods (1950–1980 vs 1990–2020). We observe that, similar to the wet-days categories, the variation between the different models is quite substantial. Again, stronger differences appear for runs with different forcing Global Circulation Models, suggesting major effects of the large-scale dynamics. In the Mediterranean,

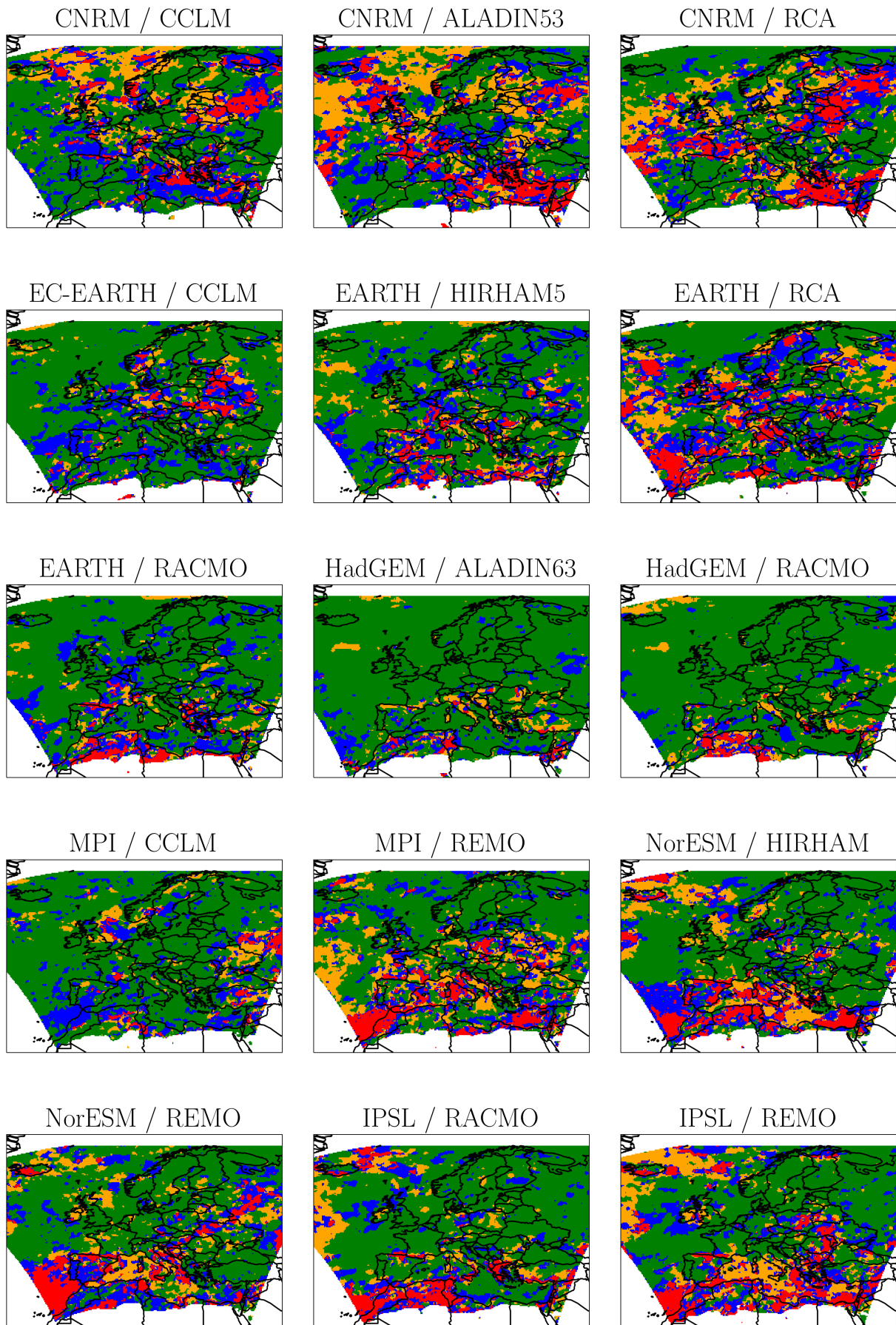


Figure 3.2: Wet-days category map for the 15 selected Euro-CORDEX models, for quantile trends computed between 1950–1980 and 1990–2020, with a sliding window of nine grid-points. Green corresponds to “all quantiles intensify” category, red to “all quantiles decrease”, orange to “U-shape” and blue to “reversed U-shape”. The white color displays the borders of the Euro-CORDEX simulation domain, and desert areas (defined as where the wet-days frequency in 1950–1980 is less than 2%).

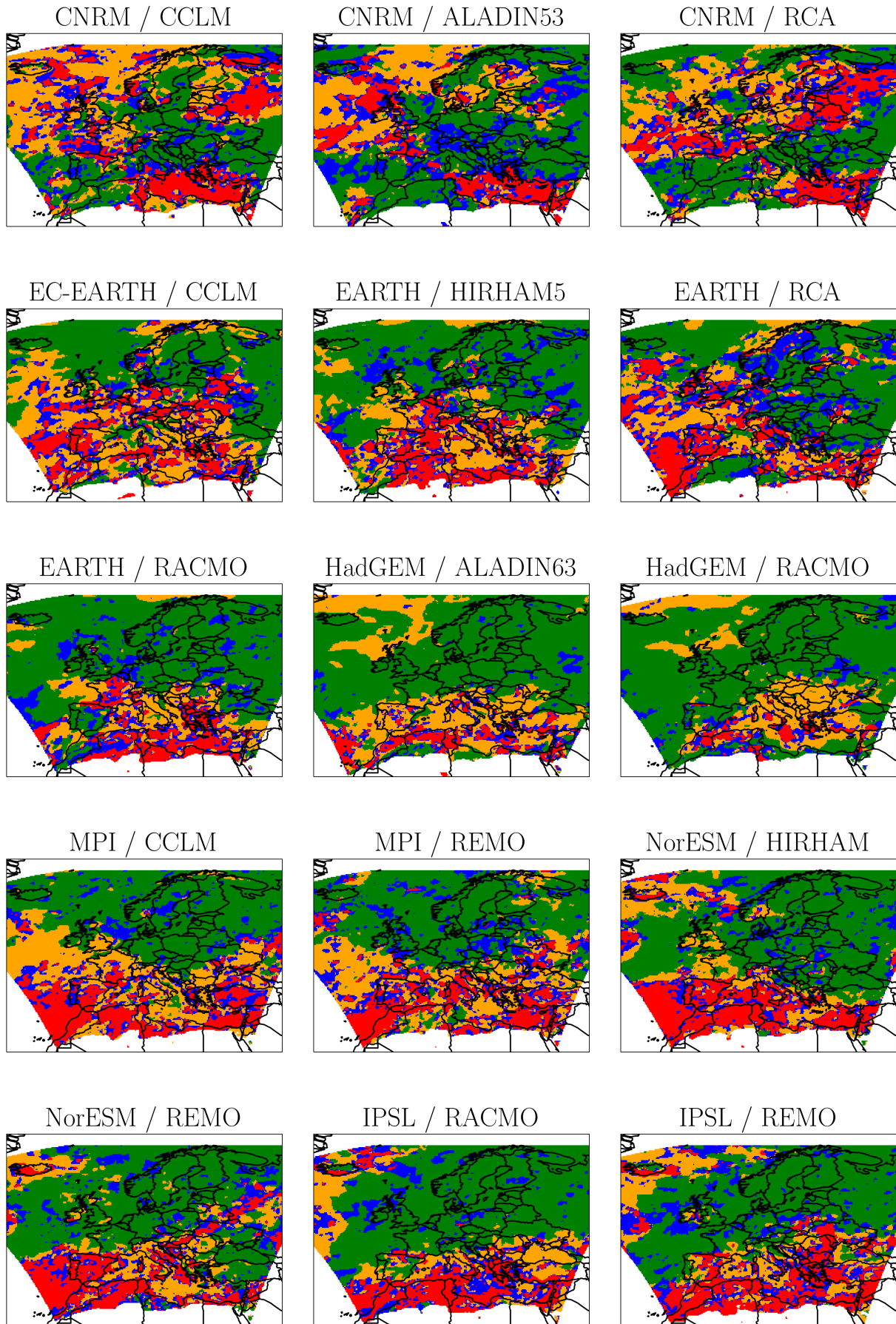


Figure 3.3: Like in figure 3.2 but for all-days category maps.

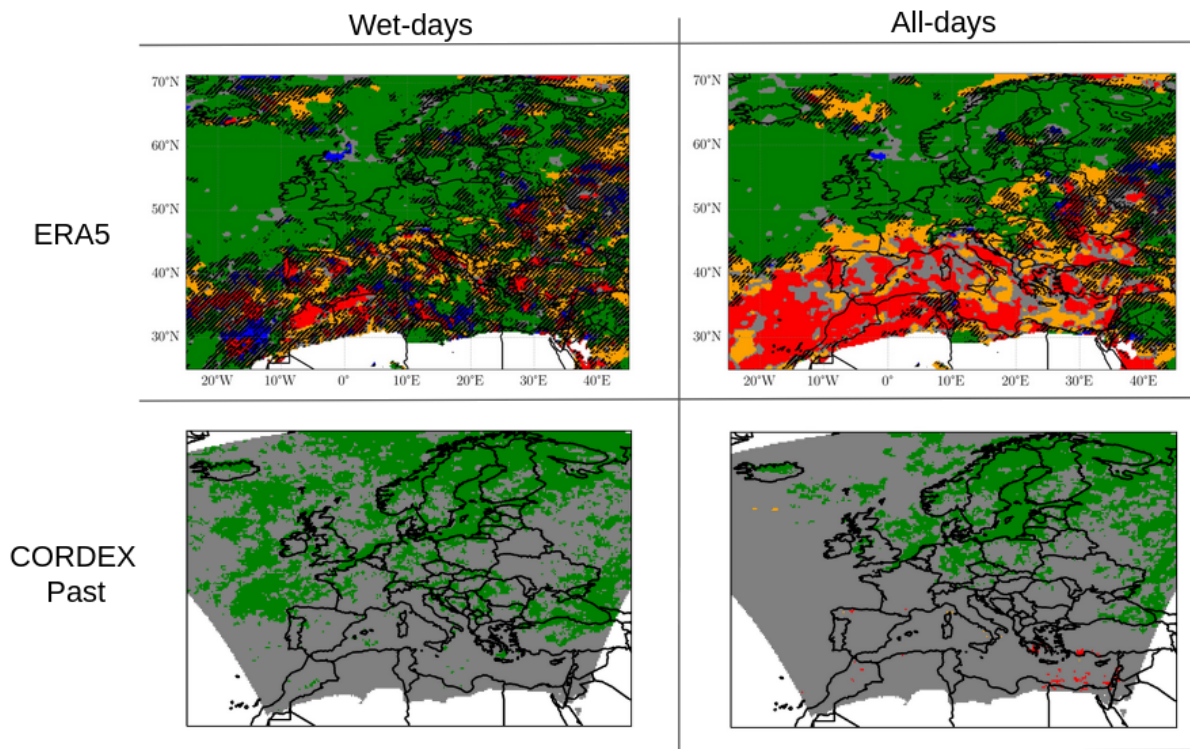


Figure 3.4: Category map for wet-days trends or all-days trends computed on ERA5 data or the selection of 15 Euro-CORDEX models, between 1950–1980 and 1990–2020. On ERA5 figures, the hatches show the places where neither the change of $\Delta\beta$ nor $\Delta\alpha$ are statistical significant (with a bootstrap test of confidence level 90%). On the CORDEX figures, the gray color shows the places where less than 10 out of the 15 models agree on the regime, while white color displays desert areas, or for CORDEX the border of the regional simulation domain. The green, red, orange and blue colors are the same as in figure 3.2.

most models display some part of the region in the “all quantiles decrease” category, though the position of this regime is changing from model to model (for example, this regime concerns mainly the Eastern Mediterranean according to CNRM-CERFACS, while it touches most of the Mediterranean basin according to MPI, NCC or IPSL). When comparing the all-days category maps with the wet-days frequency change maps in figure 3.6, it becomes clear that the spatial patterns of all-days categories in the Mediterranean are highly correlated to the models’ representation of the wet-days frequency change’s spatial pattern. This already gives the intuition that the dry-days frequency change dominates the distribution change in the Mediterranean.

The multimodel category map is presented in figure 3.4 and compared with the results on ERA5 reanalysis. Despite the significant inter-model variation, a common pattern emerges in the multimodel all-days category map shown in figure 3.4: most models agree on the presence of an “all quantiles intensify” regime in parts of Northern Europe and over the Northern Atlantic, which is consistent with ERA5 results. However, contrary to ERA5, Euro-CORDEX doesn’t show any robust signal on a “all quantiles decrease” regime in the Mediterranean, neither on a “U-shape” as a transition regime.

As a sum up, the all-days categories map of multimodel CORDEX is broadly consistent with ERA5’s, but with less signal on the Mediterranean, probably due to a lower agreement between the models, especially the GCMs, on the amplitude and location of the reduction in wet-days frequency.

3.2.3 Why is there less robust signal in Euro-CORDEX models, for the Mediterranean in the past, in all-days regimes?

One hypothesis is that the categories, especially the all-days categories, are very dependent to the large-scale dynamics aspects, which are represented differently between the six General Circulation Models used in Euro-CORDEX experiments. The differences between GCMs can be due to both the different models’ choices for the representation of the dynamics, but also to the random multi-decadal variability that different runs of a same GCM can create.

To assess the first aspect and cancel out the effect of the forcing GCM, one could perform the analysis on the evaluations runs of Euro-CORDEX, which are simulations with RCM forced at their boundaries by the ERA-Interim reanalysis. Their large-scale natural variability, such as the North Atlantic Oscillation or the Multi-decadal Atlantic Oscillation, would be mainly given by the forcing of ERA-Interim. Thus, we would expect category maps of individual evaluation runs to be closer to the one of ERA5 reanalysis, and that they show a smaller variation for all-days categories between the different regional models.

To assess the second aspect, it would be interesting to compare all-days category maps for multi-ensemble runs composed of runs with the same GCM and RCM. These runs would sample various possible natural variability, and the agreement between these runs would highlight the climate change signal, as represented by the GCM/RCM.

Another hypothesis could be that Euro-CORDEX models may have a time latency in their level of global warming in the past periods, compared to ERA5 reanalysis. Indeed, CORDEX simulations are downscaled from CMIP5 models, which in average predict a weaker future warming over Europe than CMIP6 (Coppola et al., 2021). For instance, this article found a mean winter warming of 4.5°C for Euro-CORDEX and CMIP5 by 2071–2100, compared to 6°C predicted by CMIP6 (scenario SSP5-8.5, comparable to RCP8.5). For summer, there is again a difference of warming, especially over the Mediterranean land region, with +4°C for Euro-CORDEX, +4.5°C for CMIP5, and +6.5°C for CMIP6. Besides, on the historical period, Euro-CORDEX was found to be cooler than CMIP5 (Sørland et al., 2018).

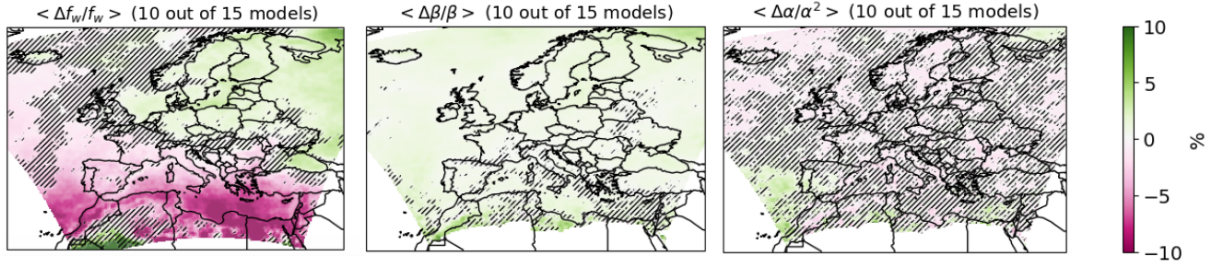


Figure 3.5: Maps of the relative change of the wet-days frequency f_w , the Weibull scale parameter β and the shape parameter α . The trends are computed over the past periods (1950–1980 vs 1990–2020). The values represent the multimodel mean, and the hatches, the places where the multimodel agreement is low, i.e. where signal-to-noise ratio is smaller than 1. The grey color here displays the borders of the Euro-CORDEX domain, for improved readability.

A latency in the regional warming in CORDEX could induce a latency in the impacts on the water cycle, as shown for mean precipitation in Coppola et al., 2020, and thus probably on the change of wet and all-days precipitation quantiles. This time latency could be more visible in the Mediterranean than in Europe, because the signal there emerges later. A way to check this hypothesis could be to change slightly the methodology: instead of comparing the trends over fixed periods (here 1950–1980 and 1990–2020) we could define a second study period specific to each GCM, corresponding to the 30 years period with the same level of global warming than represented in ERA5 global reanalysis during 1990–2020. This would homogenize the level of warming between all CORDEX runs and the ERA5 reanalysis. Unfortunately, we did not have time to perform such an analysis.

3.2.4 Comparison of the contributions of the changes in wet-days frequency and intensity

In this section, we go a step further in the methods developed in chapter 1 and chapter 2, to compare quantitatively the influences of the change in wet-days distribution and dry-days frequency.

We come back to equation (2.1), the decomposition of the total precipitation into a frequency term and an intensity term (at first order):

$$\frac{\Delta \bar{x}}{\bar{x}} \approx \frac{\Delta f_w}{f_w} + \frac{\Delta \mu}{\mu}$$

where we note \bar{x} the all-days precipitation mean, μ wet-days precipitation mean, and f_w the wet-days frequency ($\bar{x} = f_w \mu$). A wet-day is again defined as a day with more than 1 mm of precipitation. For a Weibull distribution of shape parameter α and scale parameter β , as shown before in equation (2.2), we can express the change of wet-days mean μ in terms of the parameters, giving:

$$\frac{\Delta \bar{x}}{\bar{x}} \approx \frac{\Delta f_w}{f_w} + \frac{\Delta \beta}{\beta} - \frac{\Delta \alpha}{\alpha^2} \psi(1 + 1/\alpha)$$

This equation highlights that the three terms ($\frac{\Delta f_w}{f_w}$, $\frac{\Delta \beta}{\beta}$, $\frac{\Delta \alpha}{\alpha^2}$) are crucial to compare with each others to understand the relative contribution of occurrence and intensity changes to the total precipitation change (and actually also to the precipitation distribution change).

The CORDEX multimodel maps of these three terms in the past periods are presented in figure 3.5. As explain in section 3.1, the inter-model robustness is defined by a large enough signal-to-noise ratio (larger than 1). This also corresponds approximately to the places where most of the models (12 out of 15 models) agree on the sign of the change (tested but not shown here).

The patterns in these maps are overall consistent with the ones from ERA5 reanalysis. Indeed, as in ERA5, we find a robust signal of $\frac{\Delta\beta}{\beta} > 0$ over Northern Europe, while the signal on $\frac{\Delta\alpha}{\alpha^2}$ is of smaller amplitude and is not robust between models. This is consistent with the signal obtained in ERA5, where only the change in the scale parameter β was significant, and only in Northern Europe. This also aligns logically with the wet-days category maps where models only agree on a “all quantiles intensify” regime in Northern Europe, i.e. where the signal of $\frac{\Delta\beta}{\beta}$ is robust.

Concerning the wet-days frequency change, the CORDEX models agree on a North-South dipole of change, with a strong decrease in the Mediterranean region and a (smaller) increase in the North. This North-South dipole compares well with the one in ERA5, even if the position of the frontier curve is more to the North-West than for the reanalysis.

In terms of amplitude, the multimodel changes are less intense compared to the ones in ERA5, both for $\frac{\Delta f_w}{f_w}$ and $\frac{\Delta\beta}{\beta}$. For example, multimodel CORDEX’s $\frac{\Delta f_w}{f_w}$ value is below 5% over Scandinavia, while ERA5 reanalysis’s value reaches up to 11% on land. The amplitude of multimodel $\frac{\Delta\beta}{\beta}$ is also about two to three times less than the one in ERA5.

This is probably due to the averaging effect of computing the multimodel mean. For instance, individual models have much higher maxima for the change of f_w , such as MPI-ESM with up to a 20% relative decrease in the southern Mediterranean, which is comparable with ERA5’s values. As models don’t agree on the localization of the peak of increase of f_w in the Mediterranean (figure 3.6), the multimodel mean results in a smaller value compared to individual models and ERA5.

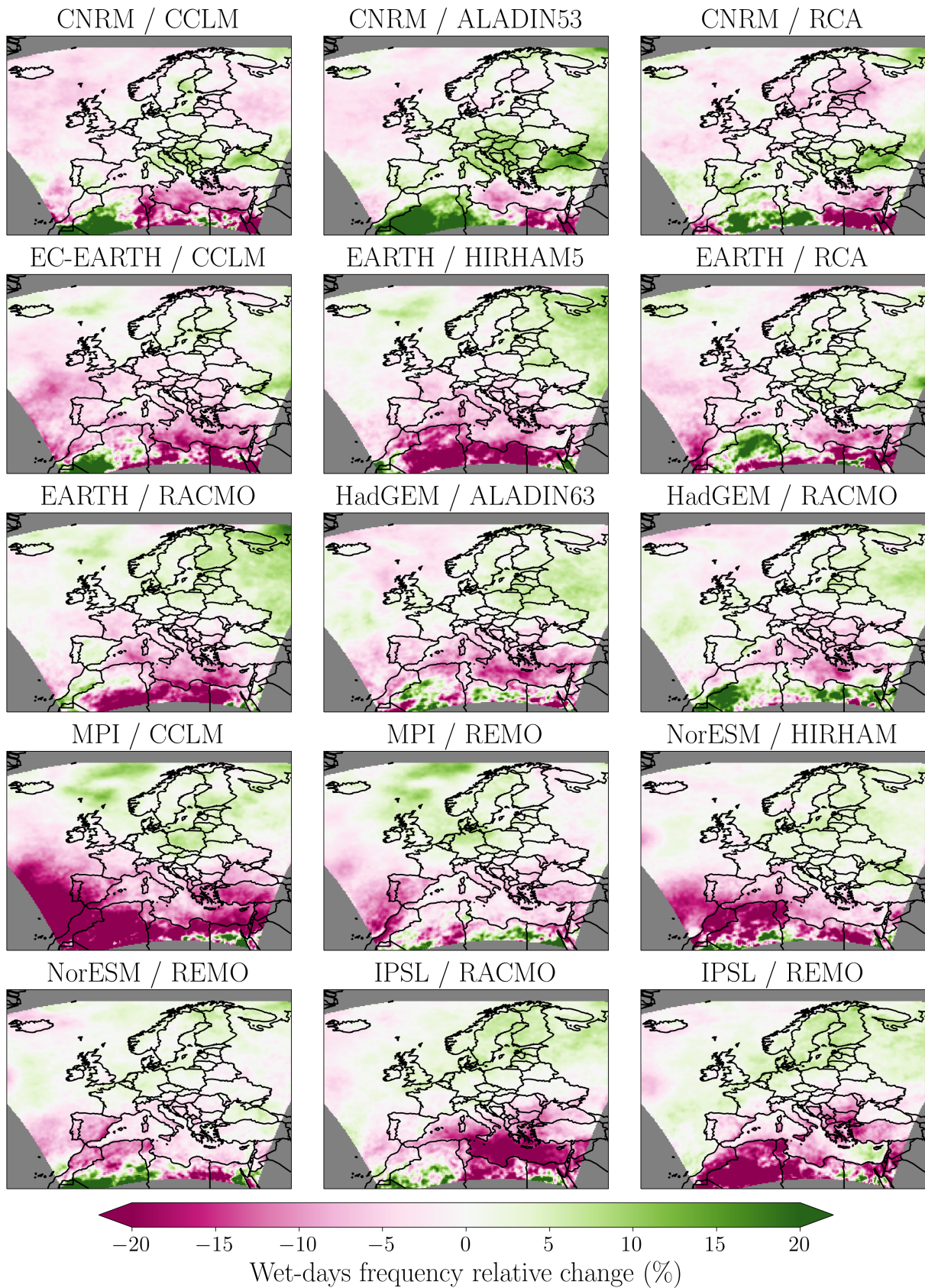


Figure 3.6: Maps of the relative change of the wet-days frequency f_w , over the past periods (1950–1980 vs 1990–2020), for the 15 selected Euro-CORDEX models.

The grey color here displays the borders of the Euro-CORDEX domain, for improved readability.

We now compare the amplitude of the relative changes between the wet-days frequency and the scale parameter β in the multimodel maps. It appears clearly that the amplitude of the changes of precipitation occurrence is much higher compared to intensity in the whole Mediterranean region, which is consistent with ERA5 reanalysis. Once again, we can state that the Mediterranean precipitation distribution is dominated by the dry-days frequency change.

As the multimodel mean of $\frac{\Delta f_w}{f_w}$ is larger than $\frac{\Delta \beta}{\beta}$ and $\frac{\Delta \alpha}{\alpha^2}$ in the Mediterranean, we could expect there a multimodel all-days “all quantiles decrease” regime. As seen on figure 3.4, it is not the case. This is due to the large deviation around the mean between the models, on the location of the strongest decrease in f_w , with even some models showing an increase in f_w in southern Mediterranean (like CNRM-CERFACS). Therefore, the lack of robustness between models in all-days regime in the Mediterranean is indeed due to the large variation between models on the regional pattern of the wet-days frequency change.

Section sum up: Validation of the selected projections on the past period

To sum up, we qualitatively find a good agreement between the historical runs of Euro-CORDEX and ERA5 reanalysis, both for wet-days and all-days categories, as for the signs of the changes of dry-days frequency and wet-days Weibull parameters. The agreement between the selected CORDEX models and ERA5 on a “all quantiles intensify” regime in Northern Europe (both for wet-days and all-days) validates the fact that this signal cannot be due only to natural variability (which is different in each run) but includes a climate change component. CORDEX multimodel analysis also confirms that the Mediterranean distribution change is dominated by the decrease in wet-days frequency, as highlighted in chapter 2 with ERA5 reanalysis.

Quantitatively, the models disagree on the precise regional pattern of the change in wet-days frequency in the Mediterranean, leading to a lack of robustness in all-days regimes in this region compared to ERA5 reanalysis.

The overall coherence of the CORDEX multimodel results and those of ERA5 gives some confidence that the selected projections are capable to represent the future regimes of changes in precipitation distribution. Studying the future projection is the focus of the next section.

3.3 Analysis of the precipitation distribution changes in projections at the end of the 21st century

In the past section and in the previous chapter, we studied the changes in the recent past, by comparing periods 1950–1980 and 1990–2020. There, we found climate change signal in the Mediterranean for dry-days frequency changes and all-days distribution, but not for wet-days distribution. Is this still the case in the future, with a higher level of global warming, or does a signal on wet-days intensity appear as well?

In this section, we want to study the future change of precipitation distribution corresponding to the highest level of warming of the simulations, where we expect the changes to be much more intense than in the recent past. We will thus focus on the changes between the last thirty-one years of the simulations, 2070–2100, compared to one hundred years before, 1970–2000. Once again, the choice of periods of about three decades is done to filter out natural variability of annual and decadal timescales. We chose to keep all the 15 models, instead of restricting the selection to those which past trends are the more similar to the one of ERA5 reanalysis. This choice was made to keep the larger diversity as possible to have a better representation of the possible spread in the projected future changes, as advised by Pierce et al., 2009.

3.3.1 Analysis of the wet-days and all-days precipitation change regimes

We apply the classification into four regimes to the precipitation time series from each model, for quantile trends between 2070–2100 and 1970–2100. This gives 15 maps of categories, both for wet-days and all-days, shown respectively in figure 3.7 and figure 3.8. We can note again the influence of the forcing GCM, with for example a wet-days “all quantiles decrease” regime in models forced by IPSL and NCC, while it is much less common in the other GCMs. Still, a better homogeneity within models is visible compared to the past periods, both for wet-days and all-days regimes.

Once again, we can construct the associated multimodel category maps (figure 3.9) by defining the multimodel regime as the dominant regime, when at least 10 out of 15 models agree on the classification. These multimodel maps of the future regimes display a much better robustness between models compared to the past periods, as expected since the associated global warming and its consequences are much stronger.

The multimodel wet-days category map can be seen as the amplification of the past results, but with increased robustness, and a signal going even more south. Indeed, this wet-days map displays a robust “all quantiles intensify” across most of the domain, from Northern Europe up the Mediterranean Sea (up to about 35°N). This brings the question of when this wet-days signal emerges in the Northern Mediterranean. On the Southern Mediterranean part, however, there is still no robust signal of a change of wet-days distribution.

As for the multimodel all-days category map, it also has much more robustness than for the past. It presents a clear pattern with a North-South triptych of regimes:

- a robust “all quantiles intensify” in the North East part of Europe;
- a robust “all quantiles decrease” in the African coasts;
- a robust “U-shape” regime (which can be seen as a transition regime), in between: on Eastern Atlantic, on the Northern coast of the Mediterranean and up to Turkey.

As a reminder, the “all quantiles decrease” regime doesn’t exclude that a given extreme quantile can intensify, but these extremes quantiles are very rare. The classification algorithm only states that the

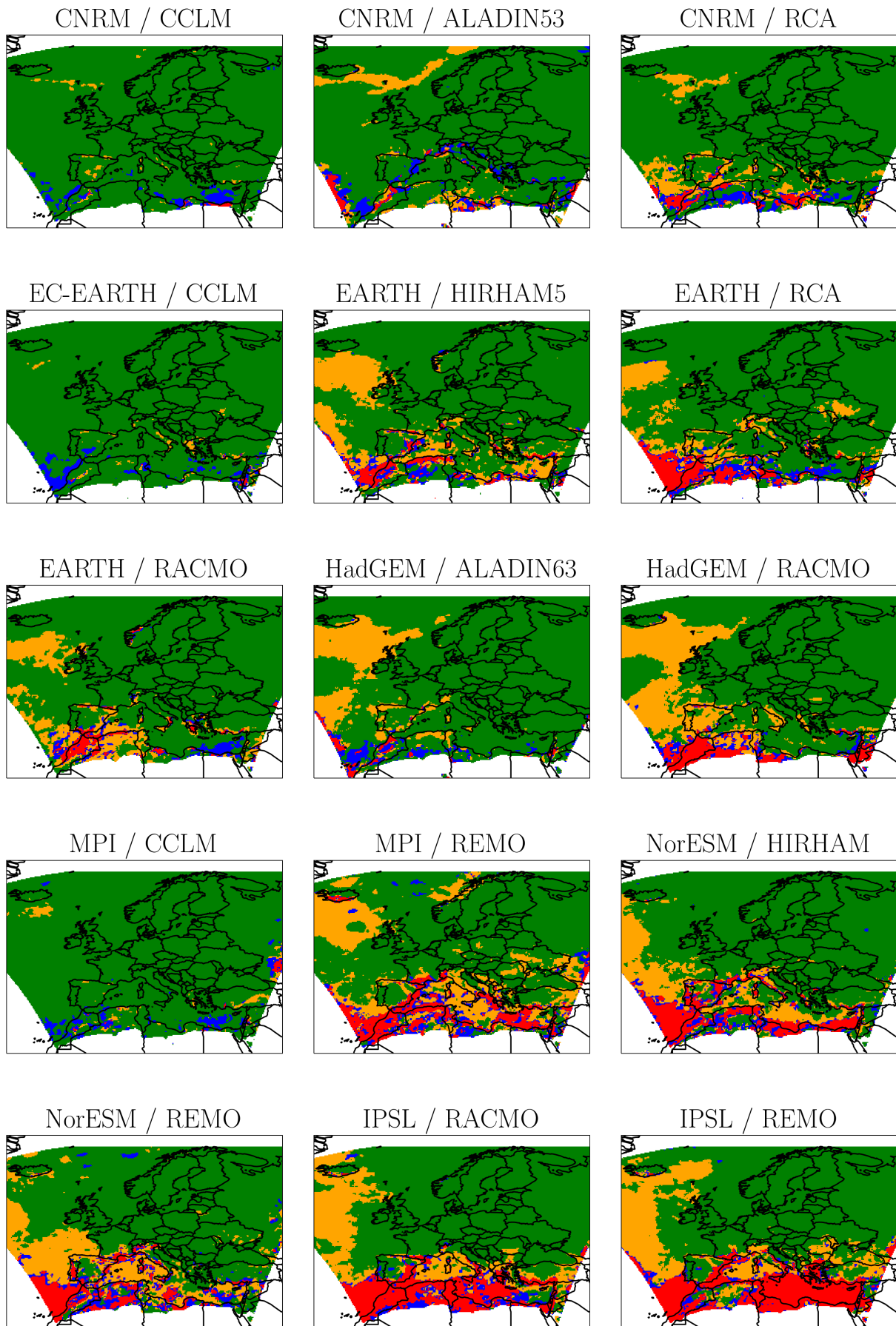


Figure 3.7: Wet-days category map for the selection of 15 Euro-CORDEX models, for trends computed between 1970–2100 and 2070–2100. Green corresponds to “all quantiles intensify” category, red to “all quantiles decrease”, orange to “U-shape” and blue to “reversed U-shape”. The white color displays the borders of the Euro-CORDEX simulation domain, and desert areas.

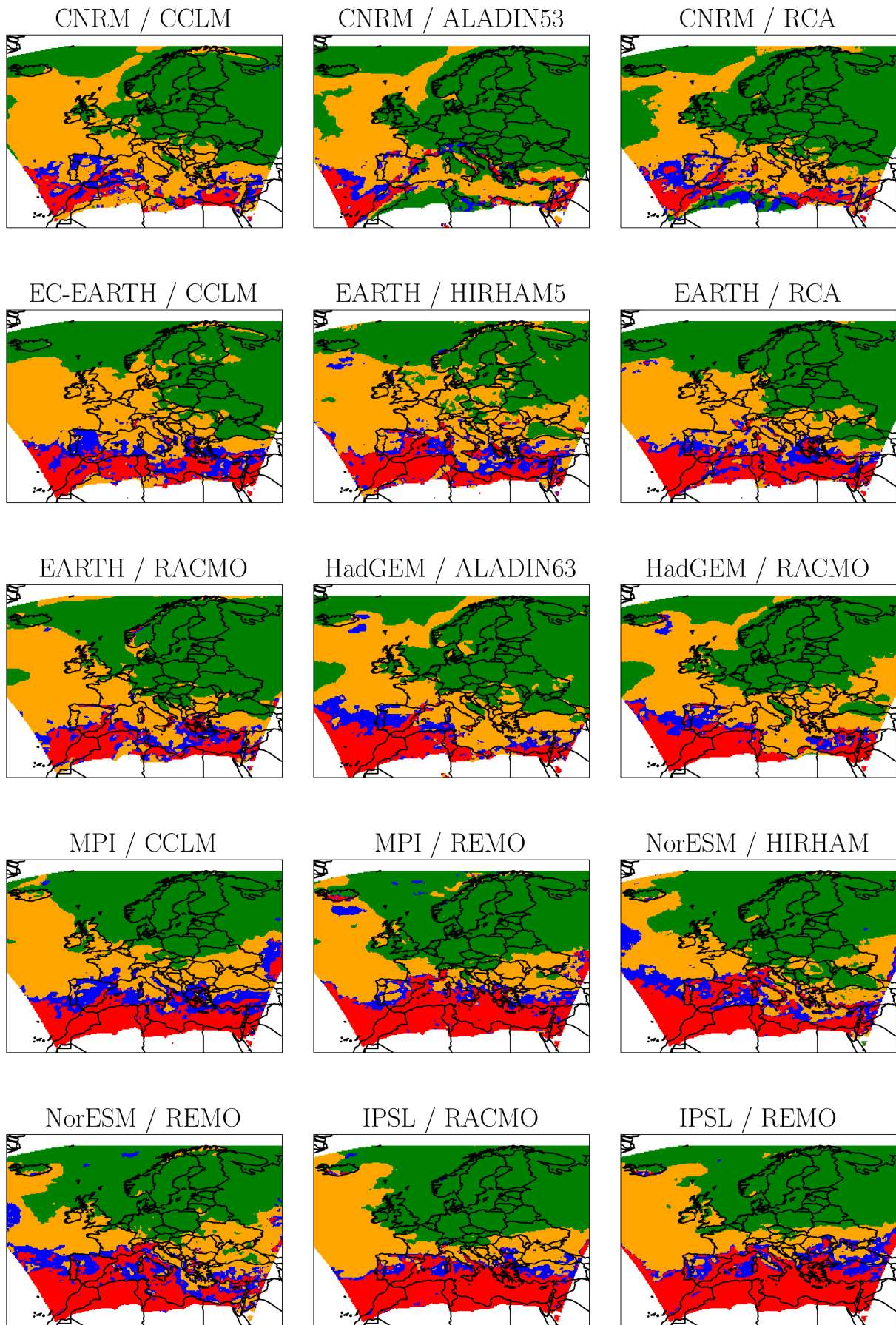


Figure 3.8: All-days category map for the selection of 15 Euro-CORDEX models, for trends computed between 1970–2100 and 2070–2100. Green corresponds to “all quantiles intensify” category, red to “all quantiles decrease”, orange to “U-shape” and blue to “reversed U-shape”. The white color displays the borders of the Euro-CORDEX simulation domain, and desert areas.

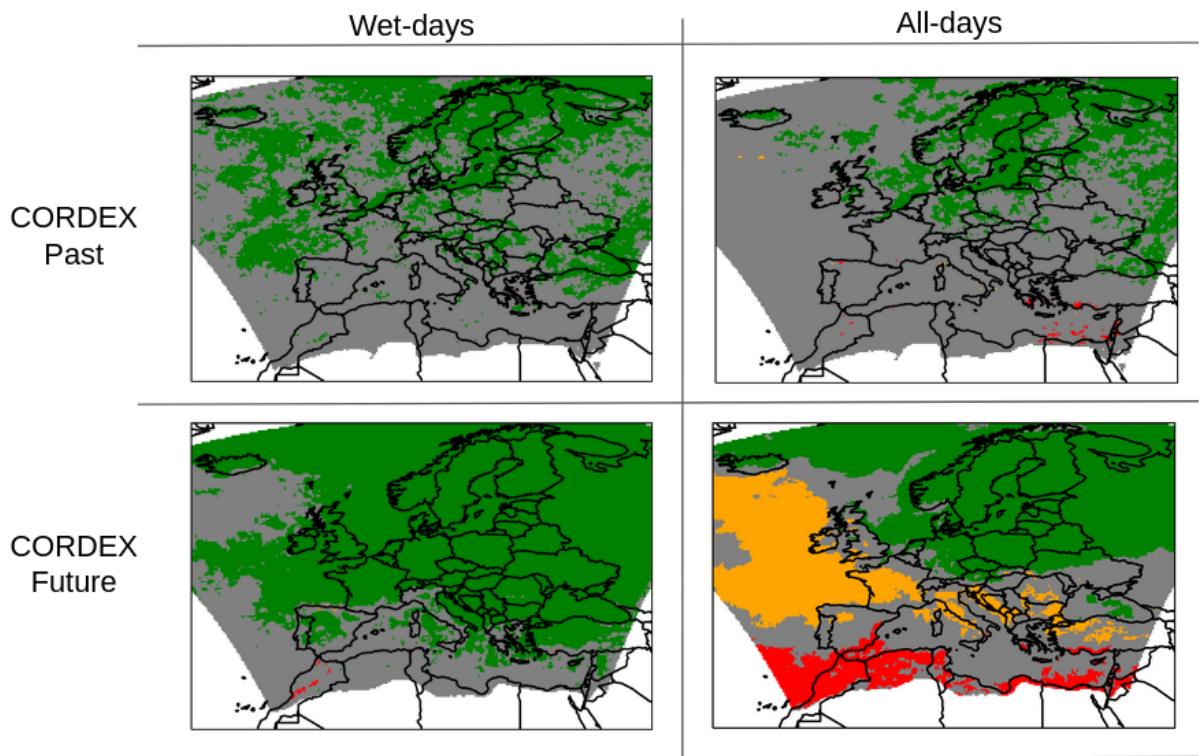


Figure 3.9: Category maps for wet-days trends and all-days trends computed on the selection of 15 Euro-CORDEX models, for past periods (trends between 1950–1980 and 1990–2020) and future periods (1970–2000 and 2070–2100).

Green corresponds to “all quantiles intensify” regime, red to “all quantiles decrease”, orange to “U-shape” and blue to “reversed U-shape”. The gray color shows the places where less than 10 out of the 15 models agree on the regime. White color displays desert areas and the border of the regional simulation domain.

mean trends of quantiles of rank $p \in [85\%, 99\%]$ and the slope of the trends of quantile with $p \in [60\%, 99\%]$ are both negative. Therefore, a few extremes could get more intense, but they will be probably at the very tail of the distribution. There could even be an inversion percentile, but it may be so close to 100% that the algorithm doesn't detect it.

To come back to the results, these all-days “U-shape” and “all quantiles decrease” regimes, visible and robust in future projections, were not present in the multimodel maps of the past periods. This brings forward the question of when these signals emerge from the noise of natural variability. This question will be studied in the next section.

Finally, from the methodology based on the Weibull decomposition presented in chapter 1 and chapter 2, we can have intuition on the signs of the changes of the important parameters. We expect the all-days “all quantiles intensify” regime to be due to the wet-days “all quantiles intensify” regime, due to $\Delta\beta > 0$, maybe with an additional contribution of an increase of wet-days frequency. For the all-days “all quantiles decrease” in the Southern Mediterranean, since there was no robust signal of a wet-days “all quantiles decrease”, we can hypothesize that it is due to a future decrease of the wet-days frequency. As for the all-days “U-shape” transition zone, as it is not linked to a wet-days “U-shape” regime, it can only come from the competition of two opposite contributions, which we can imagine as an increase in intensity (due to α or β) and a decrease of wet-days frequency change.

We will now check these different hypotheses by studying the values of the changes of the different parameters f_w, β, α .

3.3.2 Comparison of the amplitude of the changes in wet-days frequency and wet-days parameters

To better understand the category maps shown above, and to identify where each aspect (occurrence vs intensity) dominates the distribution change, we now compare the amplitude of the changes in the wet-days frequency and in Weibull parameters.

The multimodel values of $(\frac{\Delta f_w}{f_w}, \frac{\Delta\beta}{\beta}, \frac{\Delta\alpha}{\alpha^2})$ are plotted in figure 3.10. As in the previous subsection, an estimation of the inter-model robustness is given by a large enough signal-to-noise ratio (larger than 1), which also corresponds to an estimation of where most of the models agree on the sign of the changes.

The results show a very good agreement between models on the signs of the changes on most of the domain. The models agree on a robust increase of the shape parameter α (except on the African coasts where there is no signal), with a multimodel mean $\frac{\Delta\alpha}{\alpha^2}$ of about -2% to -5% in Europe and the Mediterranean region, and up to -10% in the Northern Atlantic. This signal on the shape parameter is new, compared to the CORDEX and ERA5 results on the past periods. Still, the relative change of α remains smaller than the relative change in β , which is about +10% in Southern Europe, up to +30% in Scandinavia. These amplitudes of $(\frac{\Delta\beta}{\beta}, \frac{\Delta\alpha}{\alpha^2})$ explain the multimodel wet-days map: the smaller relative change of α and the robust positive change of β explains perfectly well the wet-days “all quantiles intensify” regime from figure 3.9. We can indeed note that the places where this wet-days regime is found correspond to the places where the change in the scale parameter β is positive and robust between models. In addition, the Southern Mediterranean, where no robust regime is found, corresponds to the place where models do not agree the sign of on neither $\frac{\Delta\beta}{\beta}$ nor $\frac{\Delta\alpha}{\alpha^2}$.

We can also study the form of the models' data in the Weibull phase space $(\frac{\Delta\beta}{\beta}, \frac{\Delta\alpha}{\alpha^2})$, which gives indication about the wet-days regime, as explained in chapter 1. From this Weibull plot in figure 3.11, we could anticipate a small zone of wet-days “U-shape” regime in the Atlantic Ocean, south of Iceland, where $\frac{\Delta\beta}{\beta}$ is smaller while $\frac{\Delta\alpha}{\alpha^2}$ is robust and negative. Although this regime is not visible in figure 3.9 with the robustness criteria of “10 out of 15 models agree”, it appears if we relax this condition to “8

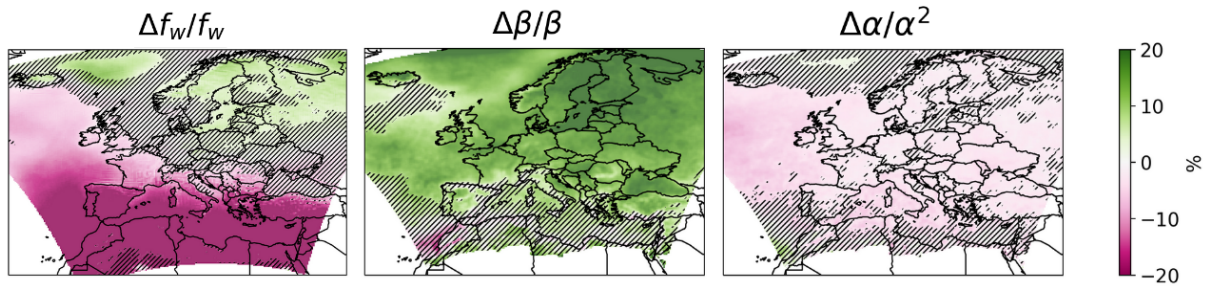


Figure 3.10: Maps of the relative change of the wet-days frequency f_w , the Weibull scale parameter β and the shape parameter α . The trends are computed over the future period. The values represent the multimodel mean, and the hatches, the places where the multimodel agreement is low, i.e. where signal-to-noise ratio is smaller than 1.

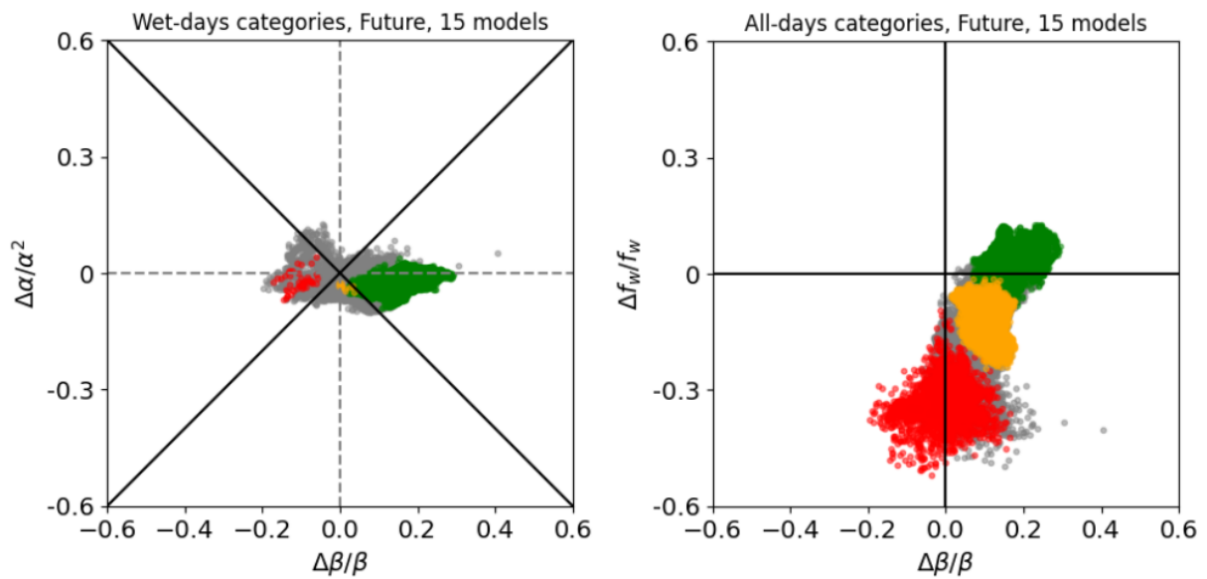


Figure 3.11: (Left) Relative change of multimodel mean Weibull parameters, $(\frac{\Delta\beta}{\beta}, \frac{\Delta\alpha}{\alpha^2})$, plotted on the whole Euro-CORDEX domain. The colors indicate the multimodel values of the wet-days categories from the classification algorithm.

(Right) Values of the multimodel mean $(\frac{\Delta\beta}{\beta}, \frac{\Delta f_w}{f_w})$, plotted on the whole CORDEX domain. The colors indicate the multimodel values of the all-days categories from the classification algorithm.

For both subplots, if less than 10 out of the 15 models agree on a regime, the gridpoint is plotted to grey. Otherwise, green corresponds to “all quantiles intensify” regime, red to “all quantiles decrease”, orange to “U-shape” and blue to “reversed U-shape”.

out of 15 of the models agree on the category” (map not shown here). This Northern Atlantic region has thus a lower agreement between models than the rest of the domain.

Concerning the wet-days frequency change, the uncertainties between models can be seen on figure 3.12. Most models agree on a strong dipole of increase of wet-days frequency in North-Eastern Europe, and a decrease in the Southern-Western Europe and the Mediterranean region (except CNRM-CERFACS, which has a different behavior in Northern Africa). In the overall, the models show robust results in terms of amplitude and sign, visible in the multimodel mean. It highlights a dipole of change, with a relative increase of f_w of about 5% to 15% in the North East part of Europe, and an even larger relative decrease in the rest of the domain, with higher values as we go South (reaching up -40% to -50% in the Mediterranean region).

We can also study the form of the models’ data in the intensity/occurrence phase space ($\frac{\Delta\beta}{\beta}, \frac{\Delta f_w}{f_w}$) (figure 3.11), which gives indication about the all-days regimes. The cloud of gridpoints is much more spread along the $\frac{\Delta f_w}{f_w}$ direction than the $\frac{\Delta\beta}{\beta}$ direction, while the cloud in the Weibull phase plot is more elongated in the $\frac{\Delta\beta}{\beta}$ than the $\frac{\Delta\alpha}{\alpha^2}$ direction. This illustrates that the changes in frequency have higher relative amplitude than those of wet-days intensity. For a interpretation of the separation of the all-days regimes in this phase space, the reader is invited to go to section 2.B.

We have now all the ingredients needed to properly interpret the all-days category map. In the Southern Mediterranean, the amplitude of $\frac{\Delta f_w}{f_w}$ is much stronger than the one of $\frac{\Delta\beta}{\beta}$, leading to an “all quantiles decrease” all-days regime. In northern Eastern Europe, where both the wet-days frequency and the scale parameter β increase, their contributions add up to give an “all quantiles intensify” all-days regime. Finally, the “U-shape” all-days regime in the transition latitudes corresponds indeed to a competition between two opposite contributions: the contribution of a decreasing wet-days frequency and the one of an increasing wet-days intensity, mainly through the β parameter.

Therefore, our methodology with the use of the Weibull distribution and the estimation of the contribution of the wet-days frequency explains very well the projected distribution change regimes for Euro-CORDEX.

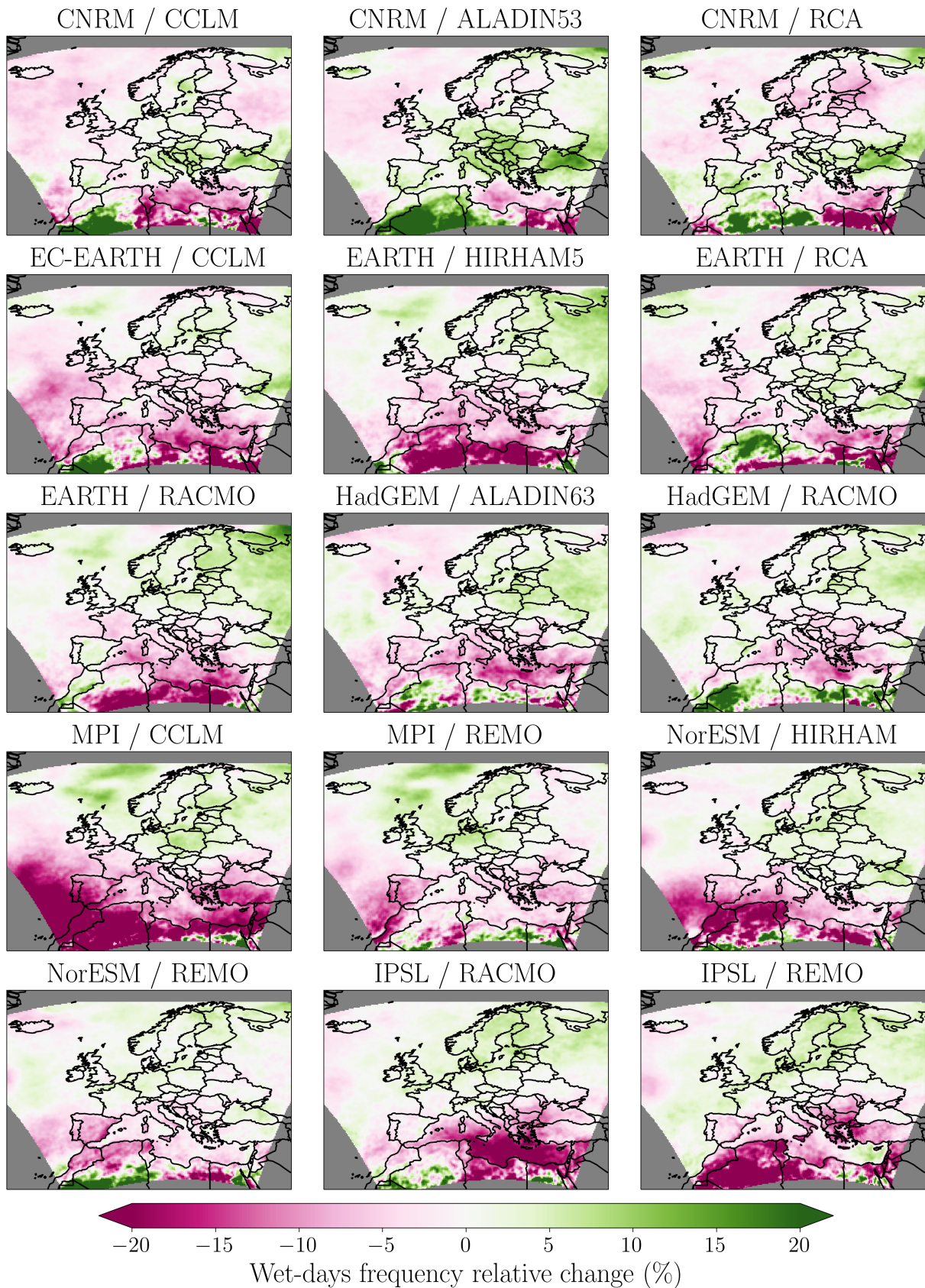


Figure 3.12: Maps of the relative change of the wet-days frequency f_w , over the future period (1970-2000 vs 2070-2100), for the 15 selected Euro-CORDEX models.

3.3.3 The Mediterranean precipitation distribution change is dominated by the wet-days frequency change

We have seen that in the Mediterranean, the wet-days frequency relative change was of higher magnitude than the change of intensity (due to the scale parameter β) leading to an all-days “all quantiles decrease” regime in the Southern Mediterranean and a “U-shape” regime in the Northern Mediterranean. This means that the wet-days frequency change is paramount for the precipitation distribution change in the Mediterranean, in the future as in the recent past.

We can go one step further in the quantification of the importance of the wet-days frequency change, by computing the quantile rank p_{lim} up to which the effect of this change still impacts the all-days trends more than the intensity change. As a reminder from chapter 2, the wet-days frequency change is considered to impact the all-days quantiles $Q_a(p)$ more than the wet-days intensity changes $Q(p)$, for a certain rank p , in the case where we have the following inequality:

$$\left| \frac{\partial Q}{\partial \alpha}(p)\Delta\alpha + \frac{\partial Q}{\partial \beta}(p)\Delta\beta \right| < \left| \frac{\Delta f_w}{f_w} \frac{\beta}{\alpha} \left[\ln \left(\frac{1}{1-p} \right) \right]^{1/\alpha-1} \right|$$

The highest percentile which respects this inequality is called the limit percentile and noted p_{lim} .

At first order, we can neglect one of the left-hand side term, for example the $\frac{\partial Q}{\partial \alpha}(p)\Delta\alpha$ term (respectively the $\frac{\partial Q}{\partial \beta}(p)\Delta\beta$ term), and compare directly the wet-days change due to $\Delta\beta$ (respectively $\Delta\alpha$) with the wet-days frequency term. The smaller the limit percentile, the less impact the wet-days frequency change will have on the distribution, compared to the wet-days intensity change. This leads to the estimation of a limit percentile $p_{lim,\Delta\beta}$ (resp. $p_{lim,\Delta\alpha}$) above which the wet-days frequency doesn’t impact the distribution change anymore. This limit percentile can be computed analytically (respectively inverted numerically).

As we have seen above, the changes due to $\Delta\alpha$ are much smaller than the one of $\Delta\beta$ in CORDEX projections over the whold domain, and thus can be neglected. Therefore, we will focus on the limit percentile due to the change of β , noted $p_{lim,\Delta\beta}$. The results for $p_{lim,\Delta\beta}$ are shown in figure 3.13. The limit wet-days percentile up to which Δf_w has an impact on the all-days quantiles is very large in the Mediterranean, up to 80% to 100%. It is not the case in Northern Europe, where only the quantiles between 0% and about 20% are impacted by the dry-days frequency change.

These results are one more argument in favor of the strong domination of the Mediterranean precipitation distribution change by the wet-days frequency change.

3.3.4 Comparison with literature for Mediterranean projections

Here, we discuss our two main results with regard to the literature.

[1] **We have shown that in the Mediterranean, the all-days distribution changes (precipitation total, but also most quantiles up to the extreme ones) are driven by the decrease of the wet-days frequency.** The fact that the dry-days change controls the total precipitation is consistent with the results of different studies, such as Polade et al., 2014 or Polade et al., 2017. In these papers, the authors studied trends in dry-days frequency in Global Circulation Models of CMIP5, with scenario RCP8.5. They showed that the future changes in dry-days dominate the changes in precipitation totals compared to the change in wet-days intensity, over much of the subtropics (especially the Mediterranean), and that these decrease of wet-days is mainly in winter. The present work’s results build further on the literature, as we emphasize that the dry-days frequency increase’s impact in the Mediterranean is not limited to the total precipitation but concerns the whole distribution.

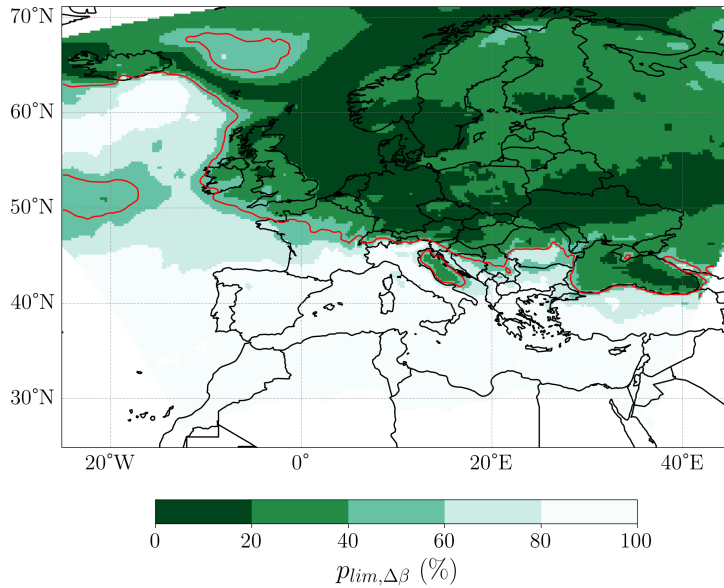


Figure 3.13: Limit wet-days percentiles $p_{lim,\Delta\beta}$ above which the impact of the precipitation occurrence trend can be neglected for a wet-days quantile trends, thanks to the large trend of Weibull scale parameter β . The thin red contour denotes the value of 50%. This variable is computed on the future period, with the CORDEX multimodel mean values of $\Delta\beta$, Δf_w , etc.

Besides, in Drobinski et al., 2018, the authors showed that the Mediterranean had a smaller than Clausius-Clapeyron rate for the function of extreme precipitation and temperature in summer. They suggested that it could be due to a loss of precipitation efficiency because of the very dry environment, pointing to a link between drying and extreme precipitation intensity. The present framework goes in this direction, as we show that the increase of the dry-days frequency in the Mediterranean impacts the whole distribution up to quite high precipitation extremes..

[2] **We have also shown that there is a contrasting behavior of all-days distribution change between the northern part of the Mediterranean and the southern part, mainly due to opposite behavior in their extreme precipitation.** More precisely, the southern part experiences an “all quantiles decrease” behavior due to the strong reduction in wet-days frequency. The northern part, however, experiences a “U-shape” all-days regime, with a decrease of low to medium quantiles due to a decreased wet-days frequency, while its extreme quantile intensify due to the increase of the wet-days scale parameter.

These North-South distinctions in terms of extremes’ behavior for the Mediterranean have already been mentioned in the literature (Giorgi et al., 2014; Vautard et al., 2014; Drobinski et al., 2018; Trambly & Somot, 2018; Myhre et al., 2019; Pichelli et al., 2021; Ali et al., 2022). For example, in Trambly and Somot, 2018, the authors studied the trends of precipitation intensities of extremes (both yearly maxima and 20-years return period extremes) on Euro-CORDEX projections with scenarios RCP4.5 and RCP8.5, across the 21st century and specifically on the Mediterranean basin’s catchments. Their results showed a dipole of these extreme precipitation trends, with a significant positive trends in the northern catchments and a negative trends on the southern catchments.

Our results are consistent with this literature and bring more light on the causes of these changes. We understand that in the southern part of the Mediterranean, the decrease of the extreme precipitation comes from the increase of the dry-days frequency, not from a change within the wet-days distribution. In opposition, in the northern part, the projected signal is coming from both the change in the wet-days distribution and the dry-days frequency.

The physical reasons of the strong decrease of frequency in the Mediterranean region were not investi-

gated in this work. However, previous studies suggest that it is mainly due to changes on the large-scale dynamics (Pfahl et al., 2017). Different mechanisms could be at stake. One mechanism could be the poleward extension of the Hadley cell: the Hadley subsidence branch would shift from the Sahara desert to the North, up to the Southern Mediterranean, reducing the precipitation occurrence in this region. Another hypothesis is a meridional contraction of the winter storm track, which is responsible for most of the winter precipitation in Europe and the Mediterranean. For example, the Mediterranean storm track has been shown to be projected to give less frequent extratropical cyclones in the whole Mediterranean basin (Zappa et al., 2013; Zappa et al., 2015), and thus a decrease of winter wet-days frequency.

Section sum up: Analysis of the precipitation distribution changes in projections

We showed that by the end of the 21st century, the selected CORDEX models give a robust signal of wet-days distribution change categories, with a “all quantiles intensify” regime in most of Europe and in the northern Mediterranean, due to an increasing scale parameter, while no robust wet-days signal is visible on the southern part of the Mediterranean.

The models give also a robust signal on all-days categories, with a North-Central-South pattern over the domain, with “all quantiles intensify” in Northern Eastern Europe (mainly due to the increase of intensity through the scale parameter), “U-shape” in central and western Europe and the northern Mediterranean (competition between less wet-days but with higher intensity), and finally a “all quantiles decrease” in the Southern Mediterranean (due to the decrease of wet-days frequency). Our results therefore feature a contrast between the northern and the southern Mediterranean, like the literature, which mainly concerns the extreme trends.

Our results prove that the wet-days frequency change dominates the distribution signal in most of the Mediterranean, which impacts both the total precipitation but also the trends on the wet-days extremes. This contrasts with central and northern Europe, where the signal is dominated by the wet-days intensification, with only a secondary contribution of the change of wet-days frequency.

These different aspects bring forward the question of when, these robust signals for the Mediterranean emerge from the natural variability noise, in the simulation of the 21st century. This is the subject of the next section.

3.4 Study of the emergence of the distribution change signal throughout the 21st century

In this section, we will focus on the apparition of a robust signal of all-days precipitation regimes throughout the 21st century. We chose to focus on all-days regimes as they were not robust within the Mediterranean in the historical part of the models, but have become robust by the end of the 21st century (illustration in figure 3.14). As the regimes are discontinuous and qualitative data, we cannot apply standard methods to quantify the emergence of a continuous signal. Instead we have to imagine a way to assess the emergence of a robust signal in these qualitative results of the classification.

We first compute the maps of all-days regimes for eight different 31 years periods ranging from 2000–2030 to 2070–2100 (the latter corresponding to the future period studied in the previous section), compared to a fixed period of reference, defined as 1970–2000. This is done for all the 15 models, giving for each period considered, 15 individual maps and a multimodel map. Note that two consecutive periods are separated by 10 years, thus have 21 years in common; they are not independent, which can be a limitation of this approach. The question, now, is how to analyze the emergence of a robust signal in these time series of eight periods’ all-days regime maps.

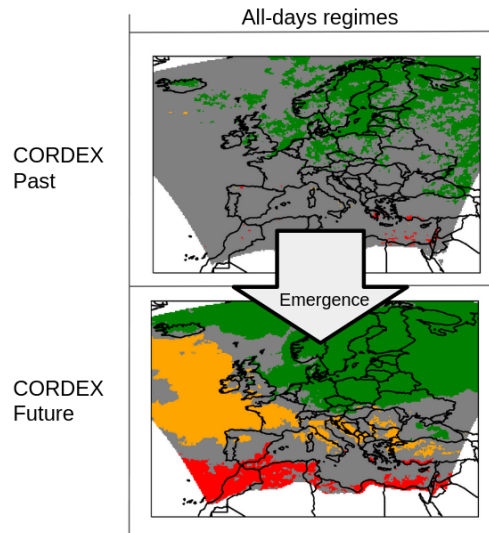


Figure 3.14: Illustration of the emergence of a signal, on the all-days regime maps, between the past periods (where there is no agreement between models on the regimes in Southern Europe and the Mediterranean) and the future periods (where the robustness between model is strong). Same colorcode as in figure 3.9.

3.4.1 First metric: proportion of gridpoints per category

As a first type of approach, we propose to study the evolution in time, for each all-days category, of the proportion of gridpoints in a given region which are classified in this category. As a first try, we compute these proportions on three European regions defined by the IPCC: Northern Europe (NEU), West Central Europe (WCE) and the Mediterranean region (MED). The delimitations of these three regions are shown in figure 3.15, along with the evolution of their different categories.

In Northern Europe (NEU), there is a very good agreement of models from early on, with about 80% of the domain in the “all quantiles intensify” regime. Most of the 20% remaining gridpoints are in the

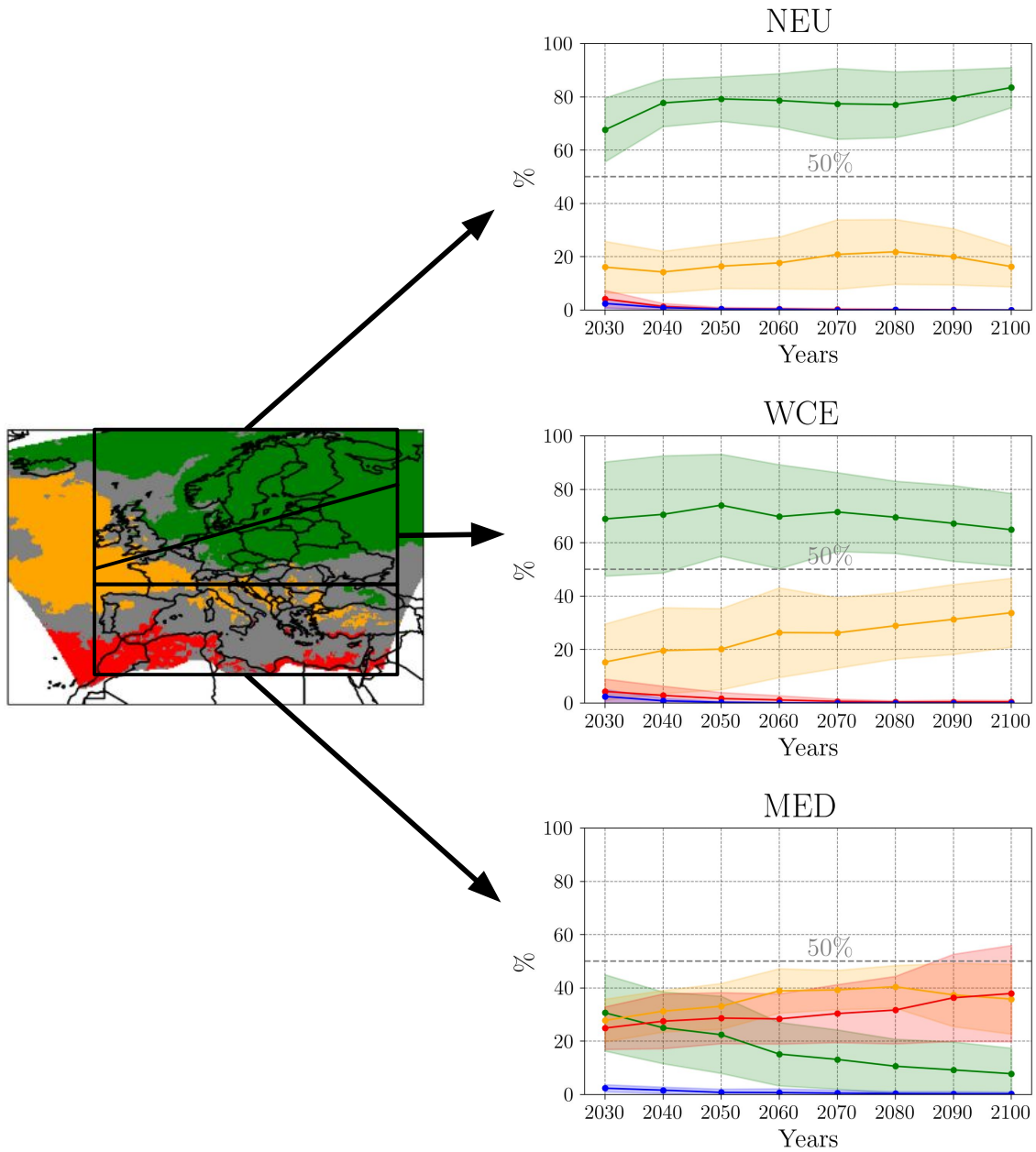


Figure 3.15: Multimodel mean of the proportion of grid points in each wet-days trend category, with trends computed from a fixed first period (1970-2000) to different 30 years periods, from 2000-2030 (first point on the left) up to 2070-2100 (last point on the right). The filled areas correspond to the standard deviation between the models. Each subplot corresponds to one of the IPCC regions: NEU for Northern Europe, WCE for West Central Europe and MED for Mediterranean.

“U-shape” regime, and we can deduce by looking at the different maps that they are situated at the western limit of NEU. We observe some multi-decadal variations which superpose with the monotonous trend: for instance, the proportion of gridpoints within the “U-shape” regime increases around period 2050–2080 to exceed 20% and then decreases slightly. However, these variations of the multimodel mean stay within the standard deviation of the models, thus we will not dwell on them. The fact that the dominant curve reaches a plateau could be interpreted as an equilibrium in the type of changes for this region.

In West Central Europe (WCE), the dominant regime during the 21st century is the “all quantiles intensify”. Its proportion tends to slightly decrease with time, yet, this decrease stays within the intermodel uncertainties. However, there is a robust increase with time of the proportion of gridpoints in an other regime, the “U-shape”. It means that this regime emerges throughout the century, and becomes the secondary dominant regime for this region. By the end of the simulation (2070–2100), WCE is actually separated into two parts (as visible in figure 3.14), with about 65% of gridpoints (North part of WCE) in “all quantiles intensify” regime, and about 35% in “U-shape” (South part of WCE). Note that the intermodel standard deviation in WCE proportions is larger than in NEU (about $\pm 20\%$ compared to about $\pm 12\%$), especially for the earliest time periods. This means that, throughout the simulation, there is a stronger agreement between models on the Northern part of Europe compared to its Southern part, concerning the all-days precipitation regimes.

Finally, for the Mediterranean (MED), we observe the emergence of two coexisting regimes: a “U-shape” regime and a “all quantiles decrease” regime, with a little less than 40% of the gridpoints by 2070–2100 for each of the regime. We notice a strong reduction with time of the proportion of a third regime, the “all quantiles intensify” regime, which we interpret as a noise for the MED region. From figure 3.14 and from the literature, we deduce that these two different regimes correspond to the different behaviors of the Northern and Southern parts of the Mediterranean.

As we see, for this approach, the IPCC regions may not be the best choice, as these regions, especially WCE and MED, display a cohabitation of two main regimes by 2070–2100. Therefore, we will refine the study, by selecting from now on sub-regions which have a homogeneity in terms of regimes by 2070–2100. The question will then be: when does the given regime become the dominant one, i.e. when is the 50% threshold crossed?

We select four regions with homogenous regimes by 2070–2100: Northern and Southern Mediterranean, the region centered on the Scandinavian, and an oceanic region South of Island and West from England. The results are displayed in figure 3.16. As expected, all these regions display an increase with time in the proportion of one specific all-days regime.

In the Scandinavia region, the proportion of gridpoints in the “all quantiles intensify” regime increases, from 70% in 2000–2030 to 90% in 2070–2100. The proportion of “all quantiles decrease” and “reversed U-shape” regimes were low from the beginning and decrease rapidly. The “U-shape” regimes capture the rest of the gridpoints, with about 10 to 15%. The fact that a plateau is reached for the dominant regime can be again interpreted as the fact that Scandinavia reaches an equilibrium in the types of its precipitation changes.

It is in the Atlantic region that the emergence is the clearest, with a steady temporal increase of the “U-shape” regime, which reaches 80% of the gridpoints by the end of the simulation. The threshold of 50% of gridpoints in this regime is passed very early, in the period 2010–2040. This region also have the lowest intermodel spread, showing a strong intermodel agreement on the future all-days behavior of this region.

In the Northern Mediterranean, the “U-shape” dominant regime struggles to exceed the 50% become. We note that after 2050–2080, the proportion of “U-shape” gridpoints slightly decreases in favor of those

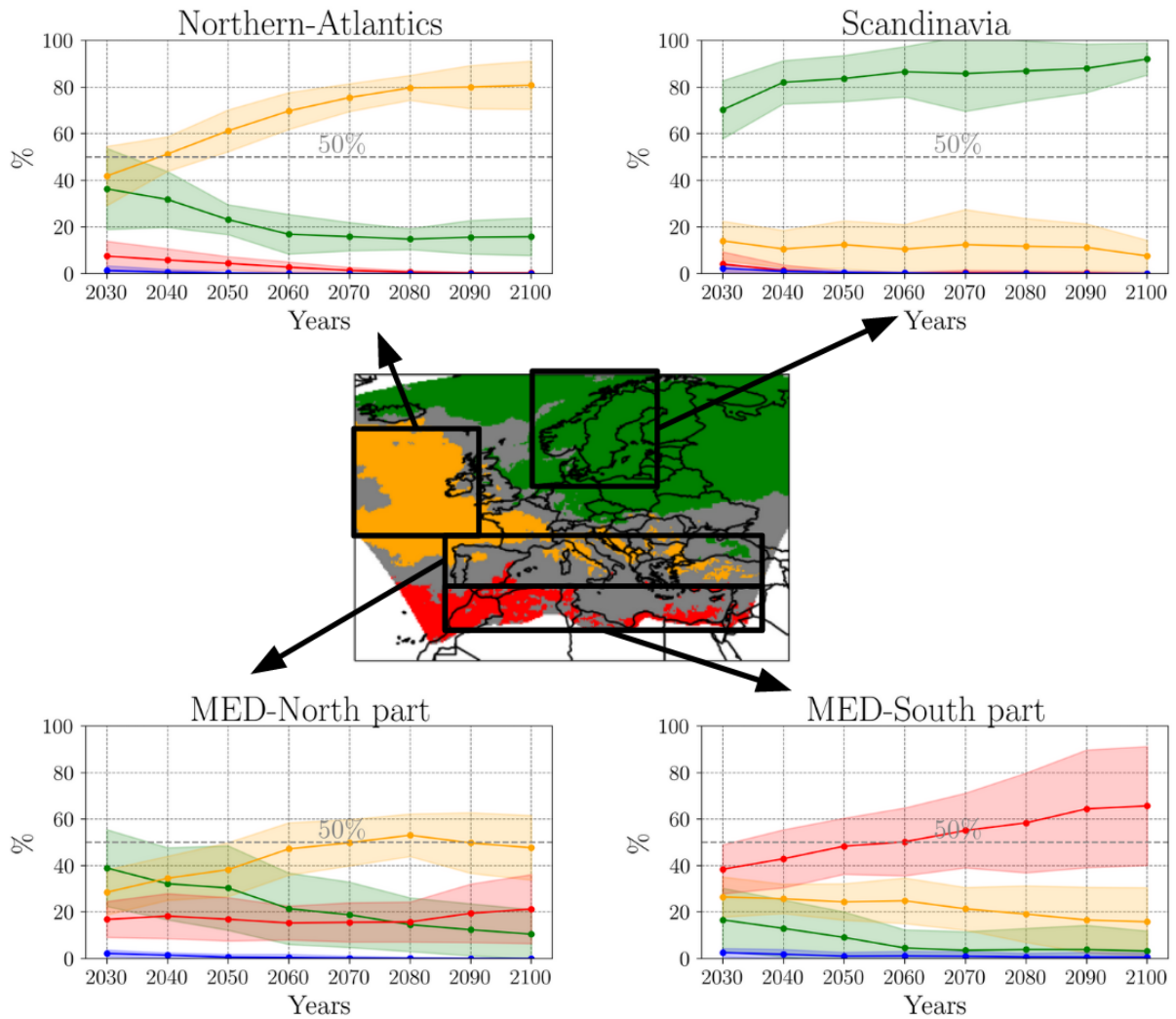


Figure 3.16: Same as in figure 3.15 but on four selected subregions: the Scandinavia, an Atlantic oceanic region south of Island, the Northern and Southern part of the Mediterranean region.

in the “all quantiles intensify” regime. Still this is within the intermodel uncertainties. We can conclude that the Northern Mediterranean has less robust results in terms of all-days regimes, which is consistent with the low robustness of the models visible in the maps in figure 3.9, especially on the sea.

In the Southern Mediterranean we observe a clear emergence of an “all quantiles decrease” regime, with more than 50% of the gridpoints in this regime by 2030–2060 (for the multimodel mean). This regime finally covers 65% of the region by the end of the projection. Still, the standard deviation between models becomes quite large (about 25%) indicating a weaker agreement between models.

Note that the comparison between the two parts of the Mediterranean highlights that the all-days precipitation distribution change emerges faster and clearer in the Southern part of the Mediterranean.

This approach is interesting as it quantifies when one specific regime becomes dominant in terms of spatial area, in a specific region. However, as we have seen, we are forced to pre-define regions which have a majority of its gridpoints in a given regime, thus it is not applicable to regions where two or more regimes cohabitate. Besides, even if a region has a very dominant regime (let say about 70% of the gridpoints), we could still imagine the extreme case where, from decade to decade, the location of the dominant and “noisy” gridpoints could totally change within the region. This would be the sign of a region with large temporal variation and no clear climatic signal. With this first metric based on a proportion of gridpoints and not on spatial patterns, we can not capture these potential changes.

3.4.2 Second metric: distance between maps of all-days regime

Therefore, we propose a second approach, which we think is complementary, and which takes into account the potential change of geographical pattern with time.

The all-days regime maps of the 21st century can be identified as a sequence of a two-dimensional vector, for which we study the convergence in time to a potential equilibrium state. As we don’t know the equilibrium state (if it exists), we chose to take the latest map as a proxy.

We thus simply compute the distance from the all-days regimes map from a given period to the final one (2070–2100, which corresponds to the highest level of warming), and we study the evolution with the time period. The distance between two all-days regime maps is defined as the fraction of gridpoints with distinct values between the two maps (it is bounded by 0 and 1). This distance is computed for each model individually and for each of the 8 time periods, giving us 8 distance values per model. The last distance is zero by definition, as we compare the all-days regime map of 2070–2100 with itself.

Note also that every three consecutive points’ distance can be correlated. Indeed, their time periods overlap, thus they have a part of their precipitation distribution in common. For example, there are 1/3 of the days in common between 2060–2080 and 2070–2100, and 2/3 between periods 2060–2090 and 2070–2100. This correlation aspect could be reduced by taking shorter time periods, for example of 20 years. Still, we decided to keep the 30 years periods to be consistent with the rest of the work.

The results of this inter-maps distance computation are shown in figure 3.17. We see that for MED, the first two regime maps have more than 50% of their gridpoints with a different regime than the ones of 2070–2100. For WCE and NEU, the distances start from a lower value, and stay below the threshold of a third of the gridpoints, throughout the 21st century. The distance in the earliest periods is thus much higher for MED than for WCE and NEU. This makes sense, as in the multimodel regime map of the past periods (figure 3.4), there were a good agreement between models on a dominant all-days “all quantiles intensify” regime for parts of WCE and NEU, but no robust signal in the Mediterranean.

What is striking in this curve is the continuous and steady decreasing of the distances, in all regions. As this sequence of distance is finite, we cannot properly talk about convergence in the mathematical

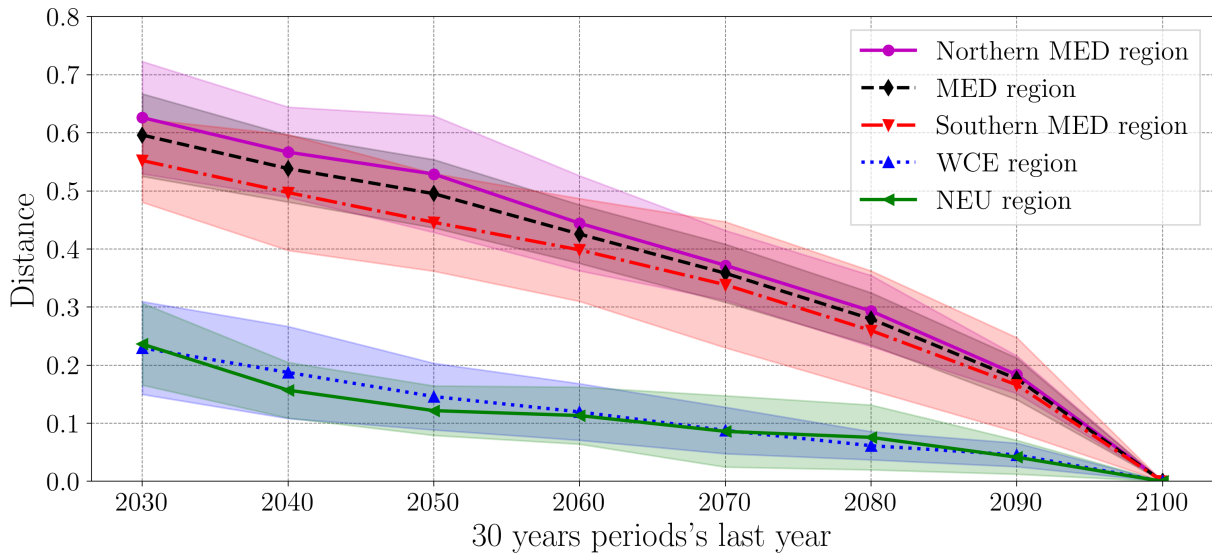


Figure 3.17: Evolution with time of the distance between a given periods' all-days regime map (1970—2000 vs (date-30 years)–date) and the final all-days regime map (1970—2000 vs 2070–2100). The distance between two regime maps is computed as the fraction of gridpoints with different categories. The distance curves are plotted for the three IPCC regions (NEU for Northern Europe, WCE for West Central Europe, MED for Mediterranean) and the northern and southern part of the MED. The main line is the multimodel mean, and the spreading is given by the standard deviation between models. The colors used in this figure have no link with our usual regime color-code.

sense. Still, this shows that as the global warming intensifies, the trends regime maps get closer to the one of the end of the century, regardless of the region considered.

Another aspect we can extract from this graph is the year at which each region's distance becomes lower than a fixed threshold. It can give an idea of the difference in emergence time of the robust signal. For example, if we take the threshold of 0.5 (50% of common gridpoints with the final regime maps) then the distance is below the threshold from the beginning in WCE and NEU, but for MED we must wait until 2030–2060 for the multimodel mean (or from 2000–2030 to 2040–2070 according to the inter-models standard deviation). As for a smaller distance threshold of 0.2 (i.e. 80% of the gridpoints have the same regime as the latest map), it is reached by 2010–2040 for WCE and NEU, and only by 2060–2090 for MED (with for each region, ± 10 years according to the inter-models standard deviation).

Whatever the threshold chosen, we conclude that the climate change signal on all-days regimes emerge at least a few decades later for the Mediterranean than for the rest of Europe. We can also highlight that the Southern Mediterranean's signal emerges about a decade before the Southern Mediterranean.

To be more rigorous in the definition of the year of emergence, a proper threshold should be defined to take into account the internal variability of the precipitation, and thus the sampling errors we can make. We could propose the following construction of a threshold, inspired by classical Bootstrap tests:

- Keep the period 1970–2000 as a past period, as the reference for precipitation quantile intensity ; Keep the map of 1970–2000 vs 2070–2100 as the regime map of the end of the simulation (called “final map” in the following).
- Pull N samples of 30 artificial years, by sampling with replacement 30×365 days from the 2000–2100 time series of daily precipitation maps.
- On each sample, compute the regime map of this artificial period, compared to the reference. Then compute the distance of this artificial regime map to the final map.

- The distribution of the N samples distances gives us the probability of having a certain value of distance by random sampling of the future. These distances can theoretically cover values from 1 (all gridpoints have different regime than the final map) to 0 (we pulled by chance exactly the same days as in the final time period 2070–2100).
- The threshold we look for could be defined as the 5th percentile of the samples' distance. Indeed, having a smaller distance than this threshold would happen by chance only with a 5% probability.

This would indeed sample the variability of the precipitation data and show what noise we can have on the resulting computed distances.

One of the limits of the test is the fact that the samples periods are not continuous 30 years, and thus we miss the temporal correlation between daily precipitation. This could be easily overcome by performing a block-bootstrap time of sampling, i.e. sampling 30 years by blocks of, for example, seven days.

An other limit is the fact that we still don't take into account the correlation of each 3 subsets of consecutive periods.

Implementing this bootstrap construction of the threshold would be needed to finalize this emergence study, but this won't be done in the current thesis document.

Section sum up: Study of the emergence of the distribution change signal

In this section, we studied how the signal of robust all-days precipitation regimes appear throughout the 21st century, transitioning from a non-robust signal in the Mediterranean in the past to a more defined pattern. We employed two different metrics to assess this emergence: the evolution of the proportion of gridpoints by regime, or the evolution of the distance of regime maps to the final one. Both metrics provided consistent results.

Our analysis shows that the signal for all-days regimes becomes increasingly robust as the century progresses, but the pace of this emergence varies by region. The emergence of all-days signal occurs much earlier in Northern Europe than in the Mediterranean, with at least a few decades of lead. Within the Mediterranean, there is also a noticeable difference in the pace of emergence between the northern and southern parts. The southern Mediterranean, characterized by a "all quantiles decrease" regime, sees this signal emerging about a decade sooner than the "U-shape" regime projected in the northern Mediterranean.

3.5 Conclusions

In this chapter, we applied the previously developed methodology to climate models, both on the historical and future periods. We selected a subset Euro-CORDEX simulations, which we validated by comparing the models' distribution changes over 1950–2020 with ERA5 reanalysis. The analysis shows a good qualitative agreement between historical runs of Euro-CORDEX models and ERA5 reanalysis for both wet-days and all-days categories, especially over Northern Europe with an “all quantiles intensify” regime. Quantitatively, there are disagreements among models on the exact regional changes in wet-days frequency in the Mediterranean, leading to less robust all-days regimes in this region compared to ERA5. Despite this, the agreement between CORDEX and ERA5 on the signs of the parameters' trends suggests that the changes in dry-days frequency and wet-days Weibull parameters observed in ERA5 reanalysis in previous chapters are not solely due to natural variability but also include a climate change component. Besides, the overall coherence between CORDEX multimodel results and ERA5 reanalysis provides confidence in the models' ability to represent future changes in precipitation distribution.

By the end of the 21st century, the selected CORDEX models indicate a robust signal of changes in wet-days distribution across Europe. Most of Europe, including the northern Mediterranean, is projected to experience an “all quantiles intensify” regime. This intensification is due to an increase in the distribution's scale parameter, which suggests that precipitation events will become more intense across all wet-days quantiles. However, the southern Mediterranean does not exhibit a robust wet-days signal, indicating significant regional variability.

For all-days categories, the models reveal a North-Central-South pattern. In Northern and Eastern Europe, the “all quantiles intensify” regime is driven by increased precipitation intensity through the scale parameter, with a smaller contribution from the increased wet-days frequency. Central and Western Europe, along with the northern Mediterranean, show a “U-shape” regime, i.e. a decrease of low and medium quantiles but an increase of extremes. We showed that this “U-shape” signal is primarily driven by the strong decrease of wet-days frequency, with a secondary contribution from the wet-days intensification. The Southern Mediterranean has a non robust change of wet-days intensity but a strong and robust decline in the precipitation occurrence, thus is expected to have an all-days “all quantiles decrease” regime.

This highlights a contrast between the northern and southern Mediterranean, consistent with existing literature on extreme weather trends. In addition, our study brings to light the fact that the strong decrease in wet-days frequency dominates the whole precipitation distribution signal in the Mediterranean, affecting both total precipitation, most wet-day quantiles and even wet-days extremes. This slower pace of emergence for the northern part of the Mediterranean compared to the southern basin is consistent with the lower robustness of the future all-days regimes in this region, especially over the Mediterranean sea.

The study also examined the emergence of robust all-days regimes throughout the 21st century, noting that these signals appear sooner in Northern Europe than in the Mediterranean, with Northern Europe leading by a few decades. Within the Mediterranean, the southern part sees a “all quantiles decrease” regime emerging about a decade earlier than the “U-shape” regime in the northern part.

3.A Study of the influence of the bias-correction on the results

3.A.1 Different effects of bias-correction on wet-days and all-days regimes

In this section, we assess the potential effects of bias-correction on the results. It has been noted in the literature that quantile mapping methods can affect trends in extreme quantiles differently than trends

in the mean (Maurer & Pierce, 2014), which with our methodology could possibly result in a difference of distribution regime. We thus want to know if the results on the wet-days and all-days regime can be impacted by the method of bias-correction, and by the reference dataset used.

For this study, we focus on a subset of 6 out of the 15 Euro-CORDEX models and on the future regimes (both wet-days and all-days). We compare the results for (1) raw models, i.e. without any bias-correction, (2) bias-corrected models, with the CDF-t-SSR method and ERA5 reanalysis as the reference, (3) bias-corrected models with the same method but with EOBS gridded dataset as the reference. The bias-corrections are done with 1971–2005 as the period of reference. Note that, as EOBS is a dataset based on rain gauges only, the models bias-corrected with EOBS as the reference won't have any on the sea and ocean.

The differences of wet-days and all-days regimes for these three ensembles are displays in figure 3.18. The first important point is that the multimodel regimes are essentially the same between the raw models and the models bias-corrected with ERA5, whether in wet-days or all-days. The fact that bias-correcting the Euro-CORDEX models with ERA5 reanalysis gives the same classification results than the raw models, is a result in itself.

The second point is that the models corrected with EOBS differ from the two other sets, especially:

- for wet-days regimes, in the northern Mediterranean shore (especially in Iberia, southern France, Italy, Greece, and Turkey), where the EOBS-corrected models predict a “U-shape” instead of an “all quantiles intensify” regime.
- for all-days regimes, in Northern Africa, where no agreement is found within models, compared to the “all quantiles decrease” regime agreement for raw models and ERA5-bias-corrected ones.

So, indeed, there can be differences due to the reference dataset used in the bias-correction. We know that EOBS is based on rain gauges, while precipitation in ERA5 reanalysis and Cordex are an output of the model. Therefore, there is a higher dry-days frequency in EOBS than in Euro-CORDEX and ERA5. Could that be the reason we have different results? Can we understand those differences by coming back to how precisely the bias-correction is modifying the data?

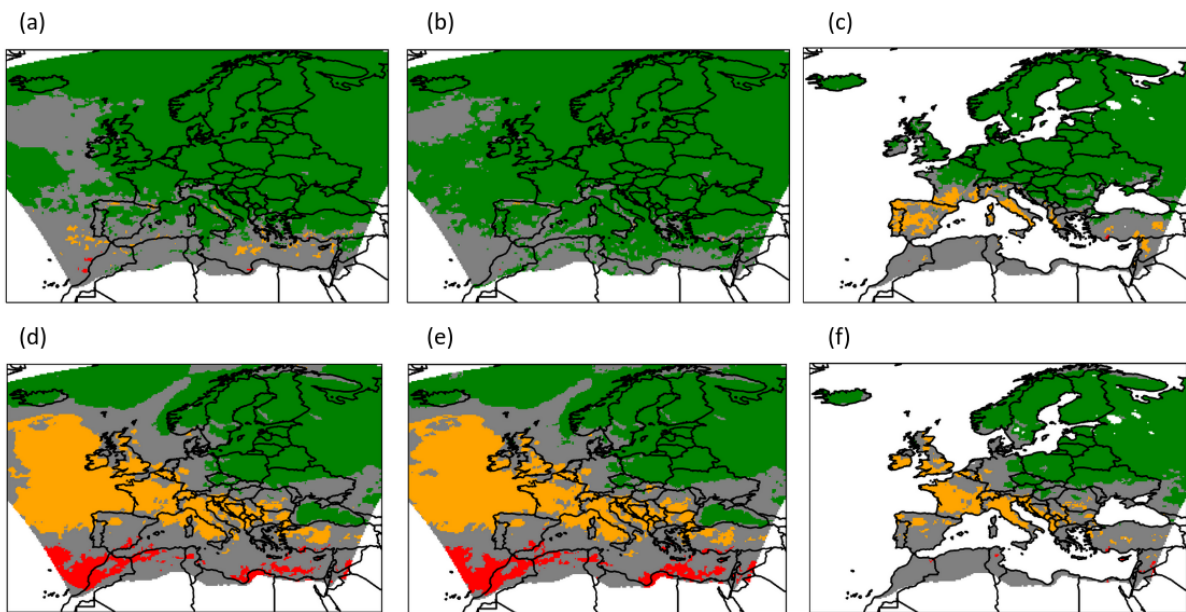


Figure 3.18: Subfigures (a), (b), (c): Multimodel wet-days category maps for trends computed between 1970–2100 and 2070–2100, for 6 selected Euro-Cordex models, either without correction (a), with bias-correction using ERA5 (b) or EOBS as the reference dataset (c). Subfigures (d), (e), (f): Same, but on all-days category maps. White color displays the border of the Euro-CORDEX simulation domain and desert areas, and of the EOBS domain for figures (c) and (f). Grey color shows locations where less than 4 out of the 6 models agree on the regime.

3.A.2 Reminder: CDF-t and quantile mapping definition

Let's come back to the definition of the CDF-t method used for the correction. The CDF-t method can be seen as an extension of the idea of quantile mapping (also called quantile matching) applied to a climate variable, for example by Déqué et al., 2007. We will use similar notation to Cannon et al., 2015: we use the subscript o for the reference observations, m for the model, h for the historical period and f for the future period. For quantile mapping, the principle is very simple: it consists in equating cumulative the two distribution functions (CDFs) of the observations and the model in the historical period, $F_{o,h}$ and $F_{m,h}$, respectively, on the observed data $x_{o,h}$ and modeled data $x_{m,h}$ (x is the precipitation daily intensity in mm/day in our case). This correction means that for a value $x_{m,h}$ of the model, the bias-corrected value $\hat{x}_{m,h}$ is taken as :

$$\hat{x}_{m,h} = x_{o,h} = F_{o,h}^{-1}(F_{m,h}(x_{m,h})) \quad (3.1)$$

Quantile mapping then also equates the CDF of the model in the future period $F_{m,f}$ to the historical observation one, $F_{o,h}$, to correct the future precipitation intensity. The bias-corrected precipitation intensity in the future is thus defined as:

$$\hat{x}_{m,f} = F_{o,h}^{-1}(F_{m,h}(x_{m,f})) \quad (3.2)$$

Therefore, in both cases, the same correction $F_{o,h}^{-1}F_{m,h} : \mathbb{R}^+ \rightarrow \mathbb{R}^+$ is applied to a given intensity of precipitation. Note that the CDFs can be estimated empirically from the time series (non-parametric quantile mapping).

In CDF-t however, the correction doesn't aim at equating the model future CDF to the observation historical one, but takes into account the fact that the model's CDF may have changed between the historical period and the future. Therefore, the corrected value for the future period is different. As described in Michelangeli et al., 2009, the transformation applied to the percentile rank $u \in [0, 1]$ (or p_a with this thesis notations), is defined on the historical period by once again equating the CDFs for any data value x : $T(F_{m,h}(x)) = F_{o,h}(x)$, giving the definition of T :

$$T(u) = F_{o,h}(F_{m,h}^{-1}(p_a)) \quad (3.3)$$

Assuming T is stationary in time (i.e. the model conserves the same types of bias in the future compared to the historical period), the transformation can be applied to the future period: $T(F_{m,f}(x)) = F_{o,f}(x)$. What we note $F_{o,f}(x)$ here is the equivalent of the CDF of the observations, but in the future (of course we don't have it). By inverting for $F_{o,f}(x)$, we get the value of the corrected intensity with CDF-t:

$$\hat{x}_{m,f} = \left(F_{m,f}^{-1} F_{m,h} F_{o,h}^{-1} F_{m,f} \right) (x_{m,f}) \quad (3.4)$$

which is a more complex expression than the quantile mapping correction. Still, in the case where the changes with time in the model's CDF can be neglected, i.e. if $F_{m,f} \approx F_{m,h}$, then the CDF-t method boils down to the exact same correction as the quantile mapping.

3.A.3 Partial explanation of the stronger impact of bias-correction on wet-days regimes

Then, what is the effect of these two bias-correction methods on the precipitation quantile trends $\Delta Q = Q_2 - Q_1$ in wet-days and all-days?

3.A.3.1 All-days quantiles

For a fixed percentile, the correction of precipitation with quantile mapping can actually be seen as multiplying by a correcting factor $c(p_a) \in \mathbb{R}^+$, which depends only on the percentile rank p_a . Note that this is equivalent to a correcting factor depending only on the intensity of precipitation, x , as the CDF is a strictly growing function. Therefore, we will now note: $c(p_a) \in \mathbb{R}^+$: $\hat{x}_{m,f} = c(p_a)x_{m,f}$.

For the quantile mapping method, the correcting factor is the same for the reference period and the future period. Thus, the all-days quantile trends will be corrected the following way:

$$\begin{aligned}\Delta\hat{Q}_a(p_a) &= \hat{Q}_{a,2}(p_a) - \hat{Q}_{a,1}(p_a) \\ &= c(p_a) Q_{a,2}(p_a) - c(p_a) Q_{a,1}(p_a) \\ &= c(p_a) \Delta Q_a(p_a).\end{aligned}$$

The effect of the bias-correction on all-days quantile trends is just to multiply each of the terms by the same correction factor $c(p_a) \geq 0$, giving a trend of different amplitude but with the same sign.

For the CDF-t method, we can follow the same reasoning, but with a correction factor that changes between the historical and the future period: $c_h(p_a)$ vs $c_f(p_a)$, giving:

$$\begin{aligned}\Delta\hat{Q}_a(p_a) &= \hat{Q}_{a,2}(p_a) - \hat{Q}_{a,1}(p_a) \\ &= c_f(p_a) Q_{a,2}(p_a) - c_h(p_a) Q_{a,1}(p_a)\end{aligned}$$

Thus with CDF-t, the corrected trends have a changed amplitude, and potentially a change in sign. We also note that the all-days quantile relative trends remain unchanged by quantile mapping, but can be impacted by CDF-t method.

As our classification algorithm is mainly defined on the mean trends' signs over some parts of the quantile trend curve (except for a criterion on the slope of the distribution tail), the all-days classification should not be impacted by quantile mapping. Besides, the CDF-t method boils down to quantile mapping, if the temporal change in CDF is very small. At first order approximation, we can suppose that this is the case. We will also suppose that the SSR correction doesn't change the results (this was not investigated). Thus, at a first order approximation, we would expect the same all-days regimes with the CDF-t-SSR correction than on raw models.

This is consistent with the results shown in figure 3.18, for most of the domain: in Europe, the all-days regimes are essentially the same between the raw models and the models corrected, with EOBS or with ERA5 as the reference. The only difference is for EOBS-corrected models in Southern Mediterranean, which is a region where the EOBS's rain gauges observations are of much lower density, therefore the gridded dataset is not as trustful. Besides, Southern Mediterranean is also the place where the temporal change in all-days distribution is the biggest (driven by a strong drying), therefore where the CDF-t method becomes a priori really different from the quantile mapping; this may explain the difference.

3.A.3.2 Wet-days quantiles

With the same reasoning, we will now look at the effect of bias-correction on wet-days precipitation trends. Note that the threshold of definition of wet-days (1 mm/day) is applied after the bias-correction. When we take a fixed wet-days percentile rank p , the wet-days quantiles trend ΔQ_w is defined as:

$$\Delta Q_w(p) = Q_{w,2}(p) - Q_{w,1}(p)$$

with $p_a = (1 - f_d)p + f_d$. If the dry-days frequency f_d has changed between the two periods of time, then the wet-days rank p doesn't correspond anymore to the same all-days percentile p_a . Thus, the quantile mapping correction factor for the two periods would differ, which can impact the sign of the trend:

$$\begin{aligned} \Delta \hat{Q}_w(p) &= c(p_{a_2}) Q_{w,2}(p) - c(p_{a_1}) Q_{w,1}(p) \\ &\neq \text{factor } \Delta Q_w(p) \end{aligned}$$

The difference in the correction factor will increase with the amplitude of the change in dry-days frequency between the two periods. Thus, the definition of the wet-days quantile trends makes them dependent to the bias-correction, both for quantile mapping and CDF-t. This is consistent with figure 3.18, which shows that EOBS-corrected models have different wet-days regimes than raw models (and ERA5-corrected models), especially in the Mediterranean where the change in f_d is the strongest.

This being said, the bias-correction has little influence on our results, as we see on figure 3.18 that the all-days and wet-days regimes are extremely similar between the raw models and the ERA5-corrected models used for this study.

Part III

Conclusions and perspectives

Conclusions

The overarching goal of this thesis was to enhance the understanding of the change in precipitation due to climate change in the Mediterranean. The main approach of the thesis was to study the whole distribution of daily precipitation, instead of focusing on only the extreme precipitation, or the absence of rain associated to drought. This work has eventually participated in clarifying how the changes in wet-days intensity and dry-days frequency contribute to the evolution of the whole distribution of precipitation, highlighting the importance of the increasing dry-days frequency in the Mediterranean.

The first chapter of this thesis focused on developing a simple methodology to characterize the change of the whole wet-days distribution, with a special focus on both low, medium and extreme quantiles. It consisted in a classification into different regimes depending on the shape of the wet-days quantile trend curve, which we applied to daily precipitation from the ERA5 reanalysis. We also modeled the wet-days distribution with a Weibull law with two parameters (a shape and a scale parameter) whose relative changes are directly linked to the quantile trend curve classification. This analytical model enabled us to test the statistical significance of the wet-days regime through the significance of the Weibull parameters' trends. It showed that the “all quantiles intensify” regime of northern Europe was significant, thanks to the increase of the scale parameter, while no wet-days change was found significant in the Mediterranean, probably due to a larger natural variability of precipitation in this region.

In the second chapter, we then extended our methodological framework to take into account the potential impacts of the change in dry-days frequency, in all-days distribution. We first highlighted that for the total mean precipitation, the main observed changes in the Mediterranean were not due to a wet-days intensity change, but to the increase of dry-days frequency, underlining the necessity to take into account this occurrence change. Then, following the paper of Schär et al., 2016, we analytically derived the effects of dry-days frequency change on the all-days distribution, for any rank of quantile. We showed that the all-days quantile trends could be dominated by the change in dry-days frequency up to a certain percentile. This limit percentile scaled with the relative importance of the dry-days frequency change compared to the wet-days scale parameter change. This analysis enabled us to conclude that the change of dry-days frequency is predominant in the past period for most quantiles all-days trends in the Mediterranean. We therefore found a significant signal of an all-days “all quantiles decrease” regime in the Mediterranean in ERA5 reanalysis, meaning that most precipitation quantiles become less intense. This strongly contrasted with northern Europe, where the effect of the increase of wet-days frequency can be neglected, compared to the increase of the Weibull scale parameter for most quantiles.

The third chapter of this thesis applied our developed methodology on climate projections, to study the changes of daily precipitation distribution in the future, in the Mediterranean. We selected an ensemble of Euro-CORDEX simulations with emission scenario RCP8.5, and evaluated them in terms of precipitation regimes over their historical period. The models showed wet-days and all-days regimes overall consistent with those of ERA5 reanalysis, except for all-days regimes in the Mediterranean where no robust signal was found, probably due to the lower agreement between models on the precise pattern of drying within the Mediterranean. This good agreement of the CORDEX models with ERA5 reanalysis enables to attribute to anthropogenic climate change the northern Europe's “all quantiles intensify” signal in the past period.

By the end of the 21st century, the CORDEX ensemble predicts robust distribution regimes across Europe, with all-days and wet-days “all quantiles intensify” regimes in Europe, a robust all-days “all quantiles decrease” signal in the southern Mediterranean, and a transition region in between, where the increase of dry-days frequency and the increase of wet-days intensity result in a robust all-days “U-shape” regime and a wet-days “all quantiles intensify” regime. These results highlight a contrast between the

northern and southern Mediterranean, with dry-days frequency changes dominating in the South while it is competing with the wet-days intensification in the northern part. The emergence of a robust signal of all-days regimes between Euro-CORDEX models was finally studied. The pace of emergence was shown to be slower for the Mediterranean than for Northern Europe, and even slower for the northern Mediterranean part, which can be seen as a transition region between two clear but opposing aspects.

This thesis work helped to give a clearer view of the observed and projected changes in precipitation distributions with global warming, within the Mediterranean region. It highlighted the paramount importance of the drying aspect for precipitation change in this region, even when studying extreme precipitation. The use of the quantile trend classification also helped to identify areas that have similar behaviors, enabling to overpass the spatial and orographic complexity of the Mediterranean region to deduce robust large-scale changes common to large parts of the Mediterranean. This study highlighted two main large-scale changes of importance for the precipitation distribution: (1) the North-East to South-West dipole of change of the wet-days frequency, and (2) the increase in wet-days intensity, which is projected to affect Europe and (with a smaller intensity) the northern part of the Mediterranean. These patterns and their physical causes would need to be investigated, though it was not done within this thesis.

Overall, this thesis work highlighted the regional disparities in the timing and nature of precipitation regime changes, emphasizing the importance of region-specific climate models and projections. Understanding these differences is crucial for developing effective climate policies and strategies to address the diverse impacts of climate change across Europe.

We would also like to highlight that the methodological framework developed in this thesis can be a new tool to propose a diagnostic on the whole distribution change, whatever the region. Indeed, this methodology is not restricted to Mediterranean or European application, but can also be useful to study the ongoing or future changes in other region of the world, with different climatology and societal challenges, as for example the Sahel Monsoon, the tropical rainfalls in the Inter Tropical Convergence Zone, etc.

Finally, this work also undoubtedly generated new questions, spanning the shorter and longer term, which we will discuss in the next section.

Perspectives

Perspectives in direct line with the thesis

Due to the finite duration of a PhD thesis, several questions raised by this work could not be addressed but would deserve further investigation. These include assessing the robustness of the results found, notably to the dataset and to the projection ensemble. More work is also desirable to investigate the sensitivity to the timescale of precipitation considered (daily precipitation here), and to clarify the physical processes behind the observed precipitation changes. In this section, we discuss potentially promising avenues to address these important questions.

Improve the robustness of the past classification results using other datasets

One of the questions raised with the first two chapters is the possible change of parts of the regime signal depending on the precipitation dataset used. It would be interesting to apply the methodology to an ensemble of observations and reanalyses, for instance, comparing the all-days and wet-days regimes between them. Using an ensemble would enable to better assess the uncertainties in the observations, which for precipitation usually can be substantial between rain-gauges *in situ* data, satellite data (corrected with rain gauges or not) and especially among different reanalyses (Alexander et al., 2020; Bador et al., 2020). These uncertainties among precipitation observational dataset can be even larger than inter-model spread in climate projections.

The main expected difficulty is to find datasets with long enough records to enable the selection of two periods where we filter out natural climate variability. The choice made in this study to compare two 30 years periods could be simplified to two 20 years periods, which would require less temporal extension in the data (1984 – 2024 would be enough, enabling the use of some satellite products such as CHIRPS).

We could also remove the condition of selecting data covering the whole Mediterranean region, and instead focus on some specific countries or subregions where higher-quality observations are available. For example, we could use the Iberia01 gridded dataset, which incorporates a much higher density of rain gauges in Portugal and Spain than EOBS gridded dataset. Iberia01 has been shown to better represent the spatial gradient and the values of daily precipitation intensity and extremes (Herrera et al., 2012; Herrera et al., 2019). Similarly, for France, we could use the SAFRAN dataset (Vidal et al., 2010), which incorporate a much higher density of station than in EOBS.

Finally, as the methodology is not restricted to gridded datasets, we could also validate the trends on a few high-quality stations across the domain, quality-controlled by national meteorological agencies for their temporal homogeneity.

In terms of methodology, it is possible that the best model for the wet-days distribution in terms of fit may not be always the Weibull law, as this can depend on the type of data (for example, for EOBS gridded dataset, our preliminary work suggested that a Lognormal law obtained a better score). Still, we would suggest keeping this Weibull model as it offers a classification of the regimes with only two parameters, whose relative changes can be compared to that of the dry-days frequency to determine whether changes in dry-days frequency or wet-days intensity are dominant.

Improve the robustness of the future classification results using other projections

Our methodological framework is general, and could thus be used to study another ensemble of climate simulations than Euro-CORDEX. Note that there is no other large ensemble of regional simulations covering Europe and the Mediterranean based on more recent global simulations than CMIP5.

A straightforward path would be to work directly on CMIP6 simulations, which are the current state of the art in long-term global climate modelling. Using CMIP6 model would enable a global overview of the precipitation changes over the different continents and oceans, which would enable to compare regions with similar behaviors, and probably highlight the importance of large-scale circulation changes.

However, the CMIP6 models' resolutions (from 0.70° to 3.75° depending on simulations), are much coarser than ERA5 or Euro-Cordex (0.22° and 0.11° respectively). Therefore, the impact of scale is not negligible, especially on convective precipitation which can happen at a very local scale. The potential impacts on the classification could possibly be reduced by applying statistical downscaling on the Mediterranean, to reach the same resolution as ERA5 for instance. We could use the same method as for the bias-correction in chapter 3, i.e. the CDF-Transform with the Statistical Singularity Removal method. A validation on the historical period would of course be needed to assess the downscaling effects.

Another natural step would be to turn then to higher resolution projections, as far as they allow a few decades of simulation in present and future climate. A good candidate for this study could be the convection permitting models simulations at kilometer resolution on the greater Alpine domain, from the international CORDEX Flagship Pilot Study. These simulations have been shown to better represent the fine scale details of daily mean precipitation, occurrence, and precipitation extremes on a seasonal scale, compared to Euro-CORDEX simulations (Pichelli et al., 2021).

Using some of these different projections would help to confirm the robustness of the results found in the CORDEX simulation in our study.

What about hourly precipitation distribution change?

Hourly and daily extremes of precipitation do not necessarily respond to warming similarly. Indeed, daily precipitation extremes can arise from a long-lasting event with weak precipitation rates for most of the day, or from an intense hourly convective event lasting a few hours. Besides, some studies showed that the anthropogenic forcing on extreme precipitation is expected to lead to a higher intensification of hourly extremes than daily extremes (Lenderink & Van Meijgaard, 2008; Utsumi et al., 2011; Drobinski et al., 2016; Drobinski et al., 2018; Intergovernmental Panel On Climate Change (IPCC), 2023), probably due to a stronger response in convective systems than in stratiform systems (Berg et al., 2013). Therefore, we may have a clearer signal of change at hourly temporal scale. In addition, with hourly precipitation, the link between extremes and convection is more straightforward, as an extreme hourly precipitation intensity likely results from an intense convective event. Therefore, our approach of distribution change could be applied to hourly precipitation, to investigate in more detail how convective events and short-term precipitation extremes respond to warming.

A few adaptations would need to be done on our methodology, for example, adapting from dry-days to dry-hours in order to compare the relative importance of the changes of hourly precipitation occurrence and of intensity, in the whole distribution change. Whether the Weibull distribution is still adapted to hourly precipitation should also be investigated.

Explore the physical mechanisms responsible for the changes observed

In this thesis work, we have highlighted that large-scale patterns seem to drive the signal in precipitation daily distribution changes over Europe and the Mediterranean: we found a clear dipole of change of the dry-days frequency (approximately North-South), and a spatially homogenous increase (resp. decrease) of the wet-days scale (resp. shape) parameter in Europe.

We would like to understand the physical mechanisms explaining these two large-scale changes. To that end, we have some hypotheses that we would like to test. The first hypothesis is that the dry-days frequency change dipole is due to the northward shift of the winter storm track, or to the polar extension of the Hadley Cell’s subsiding branch (Johanson & Fu, 2009; Xian et al., 2021). Note that in the literature, some papers mentioned the responsibility of the storm track position change for either winter drought or extreme precipitation trends in the Mediterranean region (Zappa et al., 2013; Zappa et al., 2015), but the link with the dry-days frequency has not been studied, to our knowledge.

The second hypothesis is that the thermodynamics (through Clausius-Clapeyron relation) explains parts of the intensification of wet-days precipitation, which is projected in both northern and central Europe but also in the northern Mediterranean. Therefore, we could try to link the intensification of the Weibull scale parameter to thermodynamics effects.

In practice, if we were to delve into these questions, we would probably start on the last 70 years with ERA5 reanalysis, where we already showed that the dry-days change dipole is clear and statistically significant. The reanalysis would enable us to work with physical fields such as the winds and moisture profiles. We could first study how ERA5 represents the evolution of the European storm track, and if this change is correlated to the dry-days frequency signal. We could then use Euro-CORDEX or CMIP6 simulations in the future period, which would give a stronger signal of large-scale change, and enable a multimodel comparison for more robustness.

Perspectives toward hydrological impacts

More broadly, one question that this thesis work brings forward is the potential increase of hydrological extremes (droughts and floods) due to the changes in the precipitation distribution. This section discusses important implications of these changes that would be interesting to investigate in the long term.

In the northern Mediterranean region, as we have seen, future increased heavy precipitation is projected to be associated with an increased dry-days frequency and a higher evaporative demand. The drying effects of climate change could lead to a decrease in the soil water content and to a change in the water-holding and infiltration capacity. This could change the response of the land to an extreme heavy precipitation event, both in terms of groundwater recharge and flooding impacts. In Northern Europe, all precipitation quantiles are projecting to intensify, together with a decrease of dry-days frequency, which could lead to a different signal in terms of groundwater recharge and flooding than for the Mediterranean. These hydrological aspects are of great interest for countries, both for water managements and risk-based flooding managements.

It would be scientifically interesting to use the framework we constructed in this thesis to study the hydrological impacts of the precipitation distribution changes. We could make a diagnostic of the trends of hydrological variables (such as soil moisture, of river flow) by conditioning on a given all-days precipitation regime. For this, we could use already available projections from Euro-Cordex, or other simulations at higher resolutions made with the IPSL land surface model ORCHIDEE. For example, we could group together the pixels of a subregion of “all quantiles intensify” regime, such as the Netherlands, and compare its hydrological trends with a region of “U-shape” regime, such as the South part of France, and with regions with a strong “all quantiles decrease”, such as South West Iberia or the Maghreb. We would also use high resolution simulations on metropolitan France, computed in the context of the Explore2 project, which studied the evolution of future French water resources using many hydrological models of different complexity (from parsimonious models to Land-Surface Models), forced by bias-corrected Euro-CORDEX atmospheric fields. This simple project could help to get a first intuition on how the trends in precipitation distribution are related to trends in hydrological variables.

Another project would be to study climate change effect on flood risk through its impact on soil moisture conditions. More precisely, we could study the effect of different antecedent soil moisture conditions on the vulnerability to a heavy rainfall event, potentially leading to more impactful floods. For instance, an extreme heavy rainfall will have a higher impact if it occurs on already saturated soils from previous months of higher than usual precipitation. Indeed, saturated soils will generate more runoff. Furthermore, already filled water reservoirs reduce their potential to mitigate floods. The opposite preconditioning is also possible: an extreme heavy rainfall on very dry soils with degraded vegetation would also generate more runoff during a heavy rainfall and possible high impact flash floods.

In terms of risk prevention, it would be indeed useful to assess, at the end of the wet-season, if a given catchment is more or less vulnerable to potential heavy precipitation in the coming summer or autumn (a season typically prone to very intense rainfall in the Mediterranean), in order to take water management decisions beforehand to reduce the potential flooding's impacts (e.g. empty the water reservoirs so it can mitigate the excess of rainfall). As heavy rainfall is expected to intensify in the Northern Mediterranean, it is also important to determine how the likelihood of antecedent soil moisture conditions favoring flooding will evolve, in order to obtain more reliable projections of future flood risks.

In practice, as a case study, we could select an impactful flood event from recent years, due to a heavy rainfall accumulation on a few days. We could reproduce this event with different hydrological models, and test the effects on flooding when we change the rivershed soil moisture conditions a few months before the heavy rainfall event occurs. The memory effect of the rivershed could thus be studied, enabling to identify which types of soil moisture conditions can lead to more impactful flooding in the rivershed. We could finally estimate whether these conditions would become more frequent with future global warming, by looking at the evolution of their probability of co-occurrence in climate projections.



Bibliography

- Betts, A. K., & Harshvardhan. (1987). Thermodynamic constraint on the cloud liquid water feedback in climate models. *Journal of Geophysical Research: Atmospheres*, *92*(D7), 8483–8485.
- Ben-Gai, T., Bitan, A., Manes, A., Alpert, P., & Rubin, S. (1998). Spatial and temporal changes in rainfall frequency distribution patterns in israel. *Theoretical and Applied Climatology*, *61*, 177–190.
- Groisman, P. Y., Karl, T. R., Easterling, D. R., Knight, R. W., Jamason, P. F., Hennessy, K. J., Suppiah, R., Page, C. M., Wibig, J., Fortuniak, K., et al. (1999). Changes in the probability of heavy precipitation: Important indicators of climatic change. *Weather and climate extremes: changes, variations and a perspective from the insurance industry*, 243–283.
- Karl, T. R., Nicholls, N., & Ghazi, A. (1999). Clivar/gcos/wmo workshop on indices and indicators for climate extremes workshop summary. *Weather and climate extremes: Changes, variations and a perspective from the insurance industry*, 3–7.
- Trenberth, K. E. (1999). Conceptual framework for changes of extremes of the hydrological cycle with climate change. *Climatic Change*, *42*(1), 327–339. <https://doi.org/10.1023/A:1005488920935>
- Brunetti, M., Buffoni, L., Maugeri, M., & Nanni, T. (2000). Precipitation intensity trends in northern Italy. *International Journal of Climatology*, *20*(9), 1017–1031. [https://doi.org/10.1002/1097-0088\(200007\)20:9<AID-JOC515>3.0.CO;2-S](https://doi.org/10.1002/1097-0088(200007)20:9<AID-JOC515>3.0.CO;2-S)
- Coles, S., Bawa, J., Trenner, L., & Dorazio, P. (2001). An introduction to statistical modeling of extreme values. *208*.
- Kistler, R., Kalnay, E., Collins, W., Saha, S., White, G., Woollen, J., Chelliah, M., Ebisuzaki, W., Kanamitsu, M., Kousky, V., et al. (2001). The ncep–ncar 50-year reanalysis: Monthly means cd-rom and documentation. *Bulletin of the American Meteorological society*, *82*(2), 247–268.
- Allen, M. R., & Ingram, W. J. (2002). Constraints on future changes in climate and the hydrologic cycle. *Nature*, *419*(6903), 224–232. <https://doi.org/10.1038/nature01092>
- Alpert, P., Ben-Gai, T., Baharad, A., Benjamini, Y., Yekutieli, D., Colacino, M., Diodato, L., Ramis, C., Homar, V., Romero, R., Michaelides, S., & Manes, A. (2002). The paradoxical increase of Mediterranean extreme daily rainfall in spite of decrease in total values. *Geophysical Research Letters*, *29*(11), 31-1-31–4. <https://doi.org/10.1029/2001GL013554>
- Wilcox, B. P., Breshears, D. D., & Seyfried, M. S. (2003). Rangelands, water balance on. *Encyclopedia of water science*, 791–794.
- Brunetti, M. (2004). Changes in daily precipitation frequency and distribution in Italy over the last 120 years. *Journal of Geophysical Research*, *109*(D5), D05102. <https://doi.org/10.1029/2003JD004296>
- d’Andrea, F., Provenzale, A., Vautard, R., & De Noblet-Decoudré, N. (2006). Hot and cool summers: Multiple equilibria of the continental water cycle. *Geophysical Research Letters*, *33*(24).
- Giorgi, F. (2006). Climate change hot-spots. *Geophysical research letters*, *33*(8).
- Held, I. M., & Soden, B. J. (2006). Robust responses of the hydrological cycle to global warming. *Journal of Climate*, *19*(21), 5686–5699. <https://doi.org/10.1175/JCLI3990.1>

- Pohlmann, H., & Greatbatch, R. J. (2006). Discontinuities in the late 1960's in different atmospheric data products. *Geophysical research letters*, *33*(22).
- Déqué, M., Rowell, D., Lüthi, D., Giorgi, F., Christensen, J., Rockel, B., Jacob, D., Kjellström, E., De Castro, M., & Van Den Hurk, B. (2007). An intercomparison of regional climate simulations for europe: Assessing uncertainties in model projections. *Climatic Change*, *81*, 53–70.
- Giorgi, F., & Lionello, P. (2008). Climate change projections for the mediterranean region. *Global and planetary change*, *63*(2-3), 90–104.
- Kendon, E. J., Rowell, D. P., Jones, R. G., & Buonomo, E. (2008). Robustness of future changes in local precipitation extremes. *Journal of climate*, *21*(17), 4280–4297.
- Lenderink, G., & Van Meijgaard, E. (2008). Increase in hourly precipitation extremes beyond expectations from temperature changes. *Nature Geoscience*, *1*(8), 511–514.
- Nastos, P., & Zerefos, C. (2008). Decadal changes in extreme daily precipitation in greece. *Advances in Geosciences*, *16*, 55–62.
- Sheffield, J., & Wood, E. F. (2008). Global trends and variability in soil moisture and drought characteristics, 1950–2000, from observation-driven simulations of the terrestrial hydrologic cycle. *Journal of Climate*, *21*(3), 432–458.
- Bocheva, L., Marinova, T., Simeonov, P., & Gospodinov, I. (2009). Variability and trends of extreme precipitation events over bulgaria (1961–2005). *Atmospheric Research*, *93*(1-3), 490–497.
- Giorgi, F., Jones, C., Asrar, G. R., et al. (2009). Addressing climate information needs at the regional level: The cordex framework. *World Meteorological Organization (WMO) Bulletin*, *58*(3), 175.
- Johanson, C. M., & Fu, Q. (2009). Hadley cell widening: Model simulations versus observations. *Journal of Climate*, *22*(10), 2713–2725.
- Michelangeli, P.-A., Vrac, M., & Loukos, H. (2009). Probabilistic downscaling approaches: Application to wind cumulative distribution functions. *Geophysical Research Letters*, *36*(11).
- O’Gorman, P. A., & Schneider, T. (2009). The physical basis for increases in precipitation extremes in simulations of 21st-century climate change. *Proceedings of the National Academy of Sciences*, *106*(35), 14773–14777.
- Pierce, D. W., Barnett, T. P., Santer, B. D., & Gleckler, P. J. (2009). Selecting global climate models for regional climate change studies. *Proceedings of the National Academy of Sciences*, *106*(21), 8441–8446.
- Boberg, F., Berg, P., Thejll, P., Gutowski, W. J., & Christensen, J. H. (2010). Improved confidence in climate change projections of precipitation further evaluated using daily statistics from ENSEMBLES models. *Climate Dynamics*, *35*(7), 1509–1520. <https://doi.org/10.1007/s00382-009-0683-8>
- O’Gorman, P., & Muller, C. J. (2010). How closely do changes in surface and column water vapor follow clausius–clapeyron scaling in climate change simulations? *Environmental Research Letters*, *5*(2), 025207.
- Sabater, S., & Barceló, D. (2010). *Water scarcity in the mediterranean: Perspectives under global change* (Vol. 8). Springer Science & Business Media.
- Stephens, G. L., L’Ecuyer, T., Forbes, R., Gettelmen, A., Golaz, J.-C., Bodas-Salcedo, A., Suzuki, K., Gabriel, P., & Haynes, J. (2010). Dreary state of precipitation in global models. *Journal of Geophysical Research: Atmospheres*, *115*(D24).
- Vidal, J.-P., Martin, E., Franchistéguy, L., Baillon, M., & Soubeyroux, J.-M. (2010). A 50-year high-resolution atmospheric reanalysis over france with the safran system. *International journal of climatology*, *30*(11), P–1627.
- Colin, J. (2011). *Etude des événements précipitants intenses en Méditerranée : Approche par la modélisation climatique régionale* (Doctoral dissertation). Université de Toulouse, Université Toulouse III - Paul Sabatier.

- Muller, C. J., & O’Gorman, P. (2011). An energetic perspective on the regional response of precipitation to climate change. *Nature Climate Change*, 1(5), 266–271.
- Sousa, P. M., Trigo, R. M., Aizpurua, P., Nieto, R., Gimeno, L., & García Herrera, R. (2011). Trends and extremes of drought indices throughout the 20th century in the Mediterranean. *Natural hazards and earth system sciences*, 11(1), 19.
- Trenberth, K. E. (2011). Changes in precipitation with climate change. *Climate Research*, 47(1-2), 123–138. <https://doi.org/10.3354/cr00953>
- Utsumi, N., Seto, S., Kanae, S., Maeda, E. E., & Oki, T. (2011). Does higher surface temperature intensify extreme precipitation? *Geophysical research letters*, 38(16).
- Zhang, X., Alexander, L., Hegerl, G. C., Jones, P., Tank, A. K., Peterson, T. C., Trewin, B., & Zwiers, F. W. (2011). Indices for monitoring changes in extremes based on daily temperature and precipitation data. *WIREs Climate Change*, 2(6), 851–870. <https://doi.org/10.1002/wcc.147>
- Crétat, J., Pohl, B., Richard, Y., & Drobinski, P. (2012). Uncertainties in simulating regional climate of southern africa: Sensitivity to physical parameterizations using wrf. *Climate dynamics*, 38, 613–634.
- Durack, P. J., Wijffels, S. E., & Matear, R. J. (2012). Ocean salinities reveal strong global water cycle intensification during 1950 to 2000. *science*, 336(6080), 455–458.
- Ferguson, C. R., & Villarini, G. (2012). Detecting inhomogeneities in the twentieth century reanalysis over the central united states. *Journal of Geophysical Research: Atmospheres*, 117(D5).
- Herrera, S., Gutijze nérrez, J. M., Ancell, R., Pons, M., Frías, M., & Fernández, J. (2012). Development and analysis of a 50-year high-resolution daily gridded precipitation dataset over spain.
- Hoerling, M., Eischeid, J., Perlwitz, J., Quan, X., Zhang, T., & Pegion, P. (2012). On the increased frequency of mediterranean drought. *Journal of Climate*, 25(6), 2146–2161. <https://doi.org/10.1175/JCLI-D-11-00296.1>
- Sheffield, J., & Wood, E. F. (2012). *Drought: Past Problems and Future Scenarios*. Routledge.
- Tanarhte, M., Hadjinicolaou, P., & Lelieveld, J. (2012). Intercomparison of temperature and precipitation data sets based on observations in the mediterranean and the middle east. *Journal of Geophysical Research: Atmospheres*, 117(D12).
- Teutschbein, C., & Seibert, J. (2012). Bias correction of regional climate model simulations for hydrological climate-change impact studies: Review and evaluation of different methods. *Journal of hydrology*, 456, 12–29.
- UNEP/MAP. (2012). State of the mediterranean marine and coastal environment. *Barcelona Convention, Athens*.
- Ambrosino, C., & Chandler, R. E. (2013). A nonparametric approach to the removal of documented inhomogeneities in climate time series. *Journal of Applied Meteorology and Climatology*, 52(5), 1139–1146.
- Berg, P., Moseley, C., & Haerter, J. O. (2013). Strong increase in convective precipitation in response to higher temperatures. *Nature Geoscience*, 6(3), 181–185.
- Chen, J., Brissette, F. P., Chaumont, D., & Braun, M. (2013). Finding appropriate bias correction methods in downscaling precipitation for hydrologic impact studies over north america. *Water Resources Research*, 49(7), 4187–4205.
- Fischer, E. M., Beyerle, U., & Knutti, R. (2013). Robust spatially aggregated projections of climate extremes. *Nature Climate Change*, 3(12), 1033–1038.
- Krueger, O., Schenk, F., Feser, F., & Weisse, R. (2013). Inconsistencies between long-term trends in storminess derived from the 20cr reanalysis and observations. *Journal of Climate*, 26(3), 868–874.
- Pierce, D. W., Cayan, D. R., Das, T., Maurer, E. P., Miller, N. L., Bao, Y., Kanamitsu, M., Yoshimura, K., Snyder, M. A., Sloan, L. C., et al. (2013a). The key role of heavy precipitation events in climate

- model disagreements of future annual precipitation changes in california. *Journal of Climate*, 26(16), 5879–5896.
- Pierce, D. W., Cayan, D. R., Das, T., Maurer, E. P., Miller, N. L., Bao, Y., Kanamitsu, M., Yoshimura, K., Snyder, M. A., Sloan, L. C., Franco, G., & Tyree, M. (2013b). The Key Role of Heavy Precipitation Events in Climate Model Disagreements of Future Annual Precipitation Changes in California. *Journal of Climate*, 26. <https://doi.org/10.1175/JCLI-D-12-00766.1>
- Tramblay, Y., El Adlouni, S., & Servat, É. (2013). Trends and variability in extreme precipitation indices over maghreb countries. *Natural Hazards and Earth System Sciences*, 13(12), 3235–3248.
- Tramblay, Y., Neppel, L., Carreau, J., & Najib, K. (2013). Non-stationary frequency analysis of heavy rainfall events in southern france. *Hydrological Sciences Journal*, 58(2), 280–294.
- Zappa, G., Shaffrey, L. C., Hodges, K. I., Sansom, P. G., & Stephenson, D. B. (2013). A multimodel assessment of future projections of north atlantic and european extratropical cyclones in the cmip5 climate models. *Journal of Climate*, 26(16), 5846–5862.
- Di Luca, A., Flaounas, E., Drobinski, P., & Brossier, C. L. (2014). The atmospheric component of the mediterranean sea water budget in a wrf multi-physics ensemble and observations. *Climate dynamics*, 43, 2349–2375.
- Euro-cordex: New high-resolution climate change projections for european impact research. (2014).
- Fischer, E. M., & Knutti, R. (2014). Detection of spatially aggregated changes in temperature and precipitation extremes. *Geophysical Research Letters*, 41(2), 547–554.
- Giorgi, F., Coppola, E., Raffaele, F., Diro, G. T., Fuentes-Franco, R., Giuliani, G., Mamgain, A., Llopart, M. P., Mariotti, L., & Torma, C. (2014). Changes in extremes and hydroclimatic regimes in the crema ensemble projections. *Climatic Change*, 125, 39–51.
- Jiménez Cisneros, B. E., Oki, T., Arnell, N. W., Benito, G., Cogley, J. G., Doll, P., Jiang, T., & Mwakalila, S. S. (2014). Freshwater resources.
- Maurer, E. P., & Pierce, D. W. (2014). Bias correction can modify climate model simulated precipitation changes without adverse effect on the ensemble mean. *Hydrology and Earth System Sciences*, 18(3), 915–925.
- Miralles, D. G., Van Den Berg, M. J., Gash, J. H., Parinussa, R. M., De Jeu, R. A., Beck, H. E., Holmes, T. R., Jiménez, C., Verhoest, N. E., Dorigo, W. A., et al. (2014). El niño–la niña cycle and recent trends in continental evaporation. *Nature Climate Change*, 4(2), 122–126.
- on Climate Change (IPCC), I. P. (2014a). Europe. In *Climate change 2014 – impacts, adaptation and vulnerability: Part b: Regional aspects: Working group ii contribution to the ipcc fifth assessment report* (pp. 1267–1326). Cambridge University Press.
- on Climate Change (IPCC), I. P. (2014b). Freshwater resources. In *Climate change 2014 – impacts, adaptation and vulnerability: Part a: Global and sectoral aspects: Working group ii contribution to the ipcc fifth assessment report* (pp. 229–270). Cambridge University Press.
- Pendergrass, A. G., & Hartmann, D. L. (2014). The atmospheric energy constraint on global-mean precipitation change. *Journal of climate*, 27(2), 757–768.
- Polade, S. D., Pierce, D. W., Cayan, D. R., Gershunov, A., & Dettinger, M. D. (2014). The key role of dry days in changing regional climate and precipitation regimes. *Scientific Reports*, 4(1), 4364. <https://doi.org/10.1038/srep04364>
- Vautard, R., Gobiet, A., Sobolowski, S., Kjellström, E., Stegehuis, A., Watkiss, P., Mendlik, T., Landgren, O., Nikulin, G., Teichmann, C., & Jacob, D. (2014). The european climate under a 2°c global warming. *Environmental Research Letters*. <https://doi.org/10.1088/1748-9326/9/3/034006>
- Cannon, A. J., Sobie, S. R., & Murdock, T. Q. (2015). Bias correction of gcm precipitation by quantile mapping: How well do methods preserve changes in quantiles and extremes? *Journal of Climate*, 28(17), 6938–6959.

- L'Ecuyer, T. S., Beaudoin, H., Rodell, M., Olson, W., Lin, B., Kato, S., Clayson, C., Wood, E., Sheffield, J., Adler, R., et al. (2015). The observed state of the energy budget in the early twenty-first century. *Journal of Climate*, *28*(21), 8319–8346.
- Mariotti, A., Pan, Y., Zeng, N., & Alessandri, A. (2015). Long-term climate change in the mediterranean region in the midst of decadal variability. *Climate Dynamics*, *44*(5-6), 20.
- McSweeney, C., Jones, R., Lee, R. W., & Rowell, D. (2015). Selecting cmip5 gcms for downscaling over multiple regions. *Climate Dynamics*, *44*, 3237–3260.
- Vautard, R., van Oldenborgh, G.-J., Thao, S., Dubuisson, B., Lenderink, G., Ribes, A., Planton, S., Soubeyroux, J.-M., & Yiou, P. (2015). Extreme fall 2014 precipitation in the cévennes mountains. *Bulletin of the American Meteorological Society*, *96*(12), S56–S60.
- Zappa, G., Hawcroft, M. K., Shaffrey, L., Black, E., & Braysshaw, D. J. (2015). Extratropical cyclones and the projected decline of winter mediterranean precipitation in the cmip5 models. *Climate Dynamics*, *45*, 1727–1738.
- Bartolomeu, S., Carvalho, M., Marta-Almeida, M., Melo-Gonçalves, P., & Rocha, A. (2016). Recent trends of extreme precipitation indices in the iberian peninsula using observations and wrf model results. *Physics and Chemistry of the Earth, Parts A/B/C*, *94*, 10–21.
- Casanueva, A., Kotlarski, S., Herrera, S., Fernández, J., Gutiérrez, J. M., Boberg, F., Colette, A., Christensen, O. B., Goergen, K., Jacob, D., et al. (2016). Daily precipitation statistics in a euro-cordex rcm ensemble: Added value of raw and bias-corrected high-resolution simulations. *Climate Dynamics*, *47*, 719–737.
- Drobinski, P., Alonzo, B., Bastin, S., Silva, N. D., & Muller, C. (2016). Scaling of precipitation extremes with temperature in the french mediterranean region: What explains the hook shape? *Journal of Geophysical Research: Atmospheres*, *121*(7), 3100–3119.
- Gutowski Jr, W. J., Giorgi, F., Timbal, B., Frigon, A., Jacob, D., Kang, H.-S., Krishnan, R., Lee, B., Lennard, C., Nikulin, G., et al. (2016). Wcrp coordinated regional downscaling experiment (cordex): A diagnostic mip for cmip6.
- Khodayar, S., Fosser, G., Berthou, S., Davolio, S., Drobinski, P., Ducrocq, V., Ferretti, R., Nuret, M., Pichelli, E., Richard, E., et al. (2016). A seamless weather–climate multi-model intercomparison on the representation of a high impact weather event in the western mediterranean: Hymex iop12. *Quarterly Journal of the Royal Meteorological Society*, *142*, 433–452.
- Naveau, P., Huser, R., Ribereau, P., & Hannart, A. (2016). Modeling jointly low, moderate, and heavy rainfall intensities without a threshold selection. *Water Resources Research*, *52*(4), 2753–2769. <https://doi.org/10.1002/2015WR018552>
- Raymond, F., Ullmann, A., Camberlin, P., Drobinski, P., & Smith, C. C. (2016). Extreme dry spell detection and climatology over the Mediterranean Basin during the wet season. *Geophysical Research Letters*, *43*(13), 9. <https://doi.org/10.1002/2016GL069758>
- Schär, C., Ban, N., Fischer, E. M., Rajczak, J., Schmidli, J., Frei, C., Giorgi, F., Karl, T. R., Kendon, E. J., Tank, A. M. G. K., O’Gorman, P. A., Sillmann, J., Zhang, X., & Zwiers, F. W. (2016). Percentile indices for assessing changes in heavy precipitation events. *Climatic Change*, *137*(1), 201–216. <https://doi.org/10.1007/s10584-016-1669-2>
- Vrac, M., Noël, T., & Vautard, R. (2016). Bias correction of precipitation through singularity stochastic removal: Because occurrences matter. *Journal of Geophysical Research: Atmospheres*.
- Zhang, Y., Peña-Arancibia, J. L., McVicar, T. R., Chiew, F. H., Vaze, J., Liu, C., Lu, X., Zheng, H., Wang, Y., Liu, Y. Y., et al. (2016). Multi-decadal trends in global terrestrial evapotranspiration and its components. *Scientific reports*, *6*(1), 19124.
- Klingaman, N. P., Martin, G. M., & Moise, A. (2017). ASoP (v1.0): A set of methods for analyzing scales of precipitation in general circulation models. *Geoscientific Model Development*, *10*(1), 57–83. <https://doi.org/10.5194/gmd-10-57-2017>

- Laux, P., Nguyen, P. N., Cullmann, J., Van, T. P., & Kunstmann, H. (2017). How many rcm ensemble members provide confidence in the impact of land-use land cover change?
- Pfahl, S., O’Gorman, P. A., & Fischer, E. M. (2017). Understanding the regional pattern of projected future changes in extreme precipitation. *Nature Climate Change*, 7(6), 423–427. <https://doi.org/10.1038/nclimate3287>
- Polade, S. D., Gershunov, A., Cayan, D. R., Dettinger, M. D., & Pierce, D. W. (2017). Precipitation in a warming world: Assessing projected hydro-climate changes in california and other mediterranean climate regions. *Scientific reports*, 7(1), 10783.
- Beranová, R., Kyselý, J., & Hanel, M. (2018). Characteristics of sub-daily precipitation extremes in observed data and regional climate model simulations. *Theoretical and applied climatology*, 132, 515–527.
- Blanchet, J., Molinié, G., & Touati, J. (2018). Spatial analysis of trend in extreme daily rainfall in southern france. *Climate Dynamics*, 51, 799–812.
- Caloiero, T., Caloiero, P., & Frustaci, F. (2018). Long-term precipitation trend analysis in europe and in the mediterranean basin. *Water and Environment Journal*, 32(3), 433–445. <https://doi.org/10.1111/wej.12346>
- Cavicchia, L., Scoccimarro, E., Gualdi, S., Marson, P., Ahrens, B., Berthou, S., Conte, D., Dell’Aquila, A., Drobinski, P., Djurdjevic, V., et al. (2018). Mediterranean extreme precipitation: A multi-model assessment. *Climate Dynamics*, 51, 901–913.
- Cornes, R., Schrier, G., Van den Besselaar, E., & Jones, P. (2018). An Ensemble Version of the E-OBS Temperature and Precipitation Data Sets. *Journal of Geophysical Research Atmospheres*, 123. <https://doi.org/10.1029/2017JD028200>
- Drobinski, P., Silva, N. D., Panthou, G., Bastin, S., Muller, C., Ahrens, B., Borga, M., Conte, D., Fossier, G., Giorgi, F., Güttler, I., Kotroni, V., Li, L., Morin, E., Önlol, B., Quintana-Segui, P., Romera, R., & Torma, C. Z. (2018). Scaling precipitation extremes with temperature in the mediterranean: Past climate assessment and projection in anthropogenic scenarios. *Climate Dynamics*, 51(3), 21. <https://doi.org/10.1007/s00382-016-3083-x>
- Hersbach, H., Bell, B., Berrisford, P., Biavati, G., Horányi, A., Muñoz Sabater, J., Nicolas, J., Peubey, C., Radu, R., Rozum, I., et al. (2018). Era5 hourly data on single levels from 1959 to present [dataset]. copernicus climate change service (c3s) climate data store (cds). 10.24381/cds.adbb2d47 (accessed on 05-jul-2022).
- Lionello, P., & Scarascia, L. (2018). The relation between climate change in the mediterranean region and global warming. *Regional Environmental Change*, 18, 1481–1493.
- Sørland, S. L., Schär, C., Lüthi, D., & Kjellström, E. (2018). Bias patterns and climate change signals in gcm-rcm model chains. *Environmental Research Letters*, 13(7), 074017.
- Tramblay, Y., Jarlan, L., Hanich, L., & Somot, S. (2018). Future scenarios of surface water resources availability in north african dams. *Water resources management*, 32, 1291–1306.
- Tramblay, Y., & Somot, S. (2018). Future evolution of extreme precipitation in the mediterranean. *Climatic Change*, 151(2), 289–302. <https://doi.org/10.1007/s10584-018-2300-5>
- Zittis, G. (2018). Observed rainfall trends and precipitation uncertainty in the vicinity of the Mediterranean, Middle East and North Africa. *Theoretical and Applied Climatology*, 134(3), 1207–1230. <https://doi.org/10.1007/s00704-017-2333-0>
- Bastin, S., Drobinski, P., Chiriaco, M., Bock, O., Roehrig, R., Gallardo, C., Conte, D., Domínguez Alonso, M., Li, L., Lionello, P., et al. (2019). Impact of humidity biases on light precipitation occurrence: Observations versus simulations. *Atmospheric Chemistry and Physics*, 19(3), 1471–1490.
- Benestad, R. E., Parding, K. M., Erlandsen, H. B., & Mezghani, A. (2019). A simple equation to study changes in rainfall statistics. *Environmental Research Letters*, 14(8), 084017. <https://doi.org/10.1088/1748-9326/ab2bb2>

- Berthou, S., Rowell, D. P., Kendon, E. J., Roberts, M. J., Stratton, R. A., Crook, J. A., & Wilcox, C. (2019). Improved climatological precipitation characteristics over west africa at convection-permitting scales. *Climate Dynamics*, *53*, 1991–2011.
- Christensen, J. H., Larsen, M. A., Christensen, O. B., Drews, M., & Stendel, M. (2019). Robustness of european climate projections from dynamical downscaling. *Climate Dynamics*, *53*(7), 4857–4869.
- Dagan, G., Stier, P., & Watson-Parris, D. (2019). Analysis of the atmospheric water budget for elucidating the spatial scale of precipitation changes under climate change. *Geophysical research letters*, *46*(17-18), 10504–10511.
- Herrera, S., Cardoso, R. M., Soares, P. M., Espírito-Santo, F., Viterbo, P., & Gutiérrez, J. M. (2019). Iberia01: A new gridded dataset of daily precipitation and temperatures over iberia. *Earth System Science Data*, *10*.
- Matte, D., Larsen, M. A. D., Christensen, O. B., & Christensen, J. H. (2019). Robustness and scalability of regional climate projections over europe. *Frontiers in Environmental Science*, *6*, 163.
- Myhre, G., Alterskjær, K., Stjern, C. W., Hodnebrog, Ø., Marelle, L., Samset, B. H., Sillmann, J., Schaller, N., Fischer, E., Schulz, M., & Stohl, A. (2019). Frequency of extreme precipitation increases extensively with event rareness under global warming. *Scientific Reports*, *9*(1), 16063. <https://doi.org/10.1038/s41598-019-52277-4>
- Raymond, F., Ullmann, A., Trambly, Y., Drobinski, P., & Camberlin, P. (2019). Evolution of mediterranean extreme dry spells during the wet season under climate change. *Regional Environmental Change*.
- Ribes, A., Thao, S., Vautard, R., Dubuisson, B., Somot, S., Colin, J., Planton, S., & Soubeyroux, J.-M. (2019). Observed increase in extreme daily rainfall in the french mediterranean. *Climate Dynamics*, *52*, 1095–1114.
- Shangguan, M., Wang, W., & Jin, S. (2019). Variability of temperature and ozone in the upper troposphere and lower stratosphere from multi-satellite observations and reanalysis data. *Atmospheric Chemistry and Physics*, *19*(10), 6659–6679.
- Zhang, Y., Kong, D., Gan, R., Chiew, F. H., McVicar, T. R., Zhang, Q., & Yang, Y. (2019). Coupled estimation of 500 m and 8-day resolution global evapotranspiration and gross primary production in 2002–2017. *Remote sensing of environment*, *222*, 165–182.
- Alexander, L. V., Bador, M., Roca, R., Contractor, S., Donat, M. G., & Nguyen, P. L. (2020). Intercomparison of annual precipitation indices and extremes over global land areas from in situ, space-based and reanalysis products. *Environmental Research Letters*, *15*(5), 055002.
- Azzopardi, B., Balzan, M. V., Cherif, S., Doblas-Miranda, E., dos Santos, M., Dobrinski, P., Falder, M., Hassoun, A. E. R., Giupponi, C., Koubi, V. V., et al. (2020). Climate and environmental change in the mediterranean basin—current situation and risks for the future. first mediterranean assessment report. *Chapter 2*.
- Bador, M., Alexander, L. V., Contractor, S., & Roca, R. (2020). Diverse estimates of annual maxima daily precipitation in 22 state-of-the-art quasi-global land observation datasets. *Environmental Research Letters*, *15*(3), 035005.
- Berthou, S., Kendon, E. J., Chan, S. C., Ban, N., Leutwyler, D., Schär, C., & Fosser, G. (2020). Pan-European climate at convection-permitting scale: A model intercomparison study. *Climate Dynamics*, *55*(1), 35–59. <https://doi.org/10.1007/s00382-018-4114-6>
- Coppola, E., Nogherotto, R., Ciarlo', J. M., Giorgi, F., van Meijgaard, E., Kadyrov, N., et al. (2020). Climate hazard indices projections based on cordex-core, cmip5 and cmip6 ensemble. *Journal of Geophysical Research: Atmospheres*. <https://doi.org/10.1029/2019JD032356>
- Demory, M.-E., Berthou, S., Fernández, J., Sørland, S. L., Brogli, R., Roberts, M. J., Beyerle, U., Seddon, J., Haarsma, R., Schär, C., et al. (2020). European daily precipitation according to euro-cordex regional climate models (rcms) and high-resolution global climate models (gcms) from the high-

- resolution model intercomparison project (highresmp). *Geoscientific Model Development*, 13(11), 5485–5506.
- Drobinski, P. (2020). État actuel des connaissances en matière de réchauffement climatique. *Revue d'économie financière*, (2), 19–40.
- Drobinski, P., Da Silva, N., Bastin, S., Mailler, S., Muller, C., Ahrens, B., Christensen, O. B., & Lionello, P. (2020). How warmer and drier will the Mediterranean region be at the end of the twenty-first century? *Regional Environmental Change*, 20(3), 12. <https://doi.org/10.1007/s10113-020-01659-w>
- Hersbach, H., Bell, B., Berrisford, P., Hirahara, S., Horányi, A., Muñoz-Sabater, J., Nicolas, J., Peubey, C., Radu, R., Schepers, D., Simmons, A., Soci, C., Abdalla, S., Abellan, X., Balsamo, G., Bechtold, P., Biavati, G., Bidlot, J., Bonavita, M., . . . Thépaut, J.-N. (2020). The ERA5 global reanalysis. *Quarterly Journal of the Royal Meteorological Society*, 146(730). <https://doi.org/10.1002/qj.3803>
- Muller, C., & Takayabu, Y. (2020). Response of precipitation extremes to warming: What have we learned from theory and idealized cloud-resolving simulations, and what remains to be learned? *Environmental Research Letters*, 15(3), 035001.
- Peña-Angulo, D., Vicente-Serrano, S. M., Domínguez-Castro, F., Murphy, C., Reig, F., Trambly, Y., Trigo, R. M., Luna, M. Y., Turco, M., Noguera, I., Aznárez-Balta, M., García-Herrera, R., Tomas-Burguera, M., & Kenawy, A. E. (2020). Long-term precipitation in Southwestern Europe reveals no clear trend attributable to anthropogenic forcing. *Environmental Research Letters*, 15(9), 094070. <https://doi.org/10.1088/1748-9326/ab9c4f>
- Tencaliec, P., Favre, A.-C., Naveau, P., Prieur, C., & Nicolet, G. (2020). Flexible semiparametric generalized pareto modeling of the entire range of rainfall amount. *Environmetrics*, 31(2), e2582.
- Chinita, M. J., Richardson, M., Teixeira, J., & Miranda, P. M. (2021). Global mean frequency increases of daily and sub-daily heavy precipitation in era5. *Environmental Research Letters*, 16(7), 074035.
- Coppola, E., Raffaele, F., Giorgi, F., Giuliani, G., Xuejie, G., Ciarlo, J. M., Sines, T. R., Torres-Alavez, J. A., Das, S., di Sante, F., et al. (2021). Climate hazard indices projections based on cordex-core, cmip5 and cmip6 ensemble. *Climate Dynamics*, 57, 1293–1383.
- Da Silva, N. A., Muller, C., Shamekh, S., & Fildier, B. (2021). Significant amplification of instantaneous extreme precipitation with convective self-aggregation. *Journal of Advances in Modeling Earth Systems*, 13(11), e2021MS002607.
- Pichelli, E., Coppola, E., Sobolowski, S., Ban, N., Giorgi, F., Stocchi, P., Alias, A., Belušić, D., Berthou, S., Caillaud, C., Cardoso, R. M., Chan, S., Christensen, O. B., Dobler, A., de Vries, H., Goergen, K., Kendon, E. J., Keuler, K., Lenderink, G., . . . Vergara-Temprado, J. (2021). The first multi-model ensemble of regional climate simulations at kilometer-scale resolution part 2: Historical and future simulations of precipitation. *Climate Dynamics*, 56(11), 3581–3602. <https://doi.org/10.1007/s00382-021-05657-4>
- Rivoire, P., Martius, O., & Naveau, P. (2021). A Comparison of Moderate and Extreme ERA-5 Daily Precipitation With Two Observational Data Sets. *Earth and Space Science*, 8(4), e2020EA001633. <https://doi.org/10.1029/2020EA001633>
- Taszarek, M., Allen, J. T., Marchio, M., & Brooks, H. E. (2021). Global climatology and trends in convective environments from era5 and rawinsonde data. *NPJ climate and atmospheric science*, 4(1), 35.
- Taszarek, M., Pilguy, N., Allen, J. T., Gensini, V., Brooks, H. E., & Szuster, P. (2021). Comparison of convective parameters derived from era5 and merra-2 with rawinsonde data over europe and north america. *Journal of Climate*, 34(8), 3211–3237.

- Vautard, R., Kadygrov, N., Iles, C., Boberg, F., Buonomo, E., Bülow, K., Coppola, E., Corre, L., van Meijgaard, E., Nogherotto, R., et al. (2021). Evaluation of the large euro-cordex regional climate model ensemble. *Journal of Geophysical Research: Atmospheres*, *126*(17), e2019JD032344.
- Vicente-Serrano, S. M., Domínguez-Castro, F., Murphy, C., Hannaford, J., Reig, F., Peña-Angulo, D., Tramblay, Y., Trigo, R. M., MacDonald, N., Luna, M. Y., et al. (2021). Long-term variability and trends in meteorological droughts in western europe (1851–2018). *International journal of climatology*, *41*(S1), E690–E717.
- Xian, T., Xia, J., Wei, W., Zhang, Z., Wang, R., Wang, L.-P., & Ma, Y.-F. (2021). Is hadley cell expanding? *Atmosphere*, *12*(12), 1699.
- Zittis, G., Bruggeman, A., & Lelieveld, J. (2021). Revisiting future extreme precipitation trends in the mediterranean. *Weather and Climate Extremes*, *34*, 100380.
- Ali, E., Cramer, W., Carnicer, J., Georgopoulou, E., Hilmi, N., Cozannet, G. L., & Piero, L. (2022). Cross-chapter paper 4: Mediterranean region. *Climate Change 2022: Impacts, Adaptation and Vulnerability*, 2233–2272. <https://doi.org/10.1017/9781009325844.021>
- Bandhauer, M., Isotta, F., Lakatos, M., Lussana, C., Båserud, L., Izsák, B., Szentes, O., Tveito, O. E., & Frei, C. (2022). Evaluation of daily precipitation analyses in e-obs (v19. 0e) and era5 by comparison to regional high-resolution datasets in european regions. *International Journal of Climatology*, *42*(2), 727–747.
- Reid, M. (2022). Reliability – a python library for reliability engineering. <https://doi.org/10.5281/zenodo.3938000>
- Rivoire, P., Le Gall, P., Favre, A.-C., Naveau, P., & Martius, O. (2022). High return level estimates of daily era-5 precipitation in europe estimated using regionalized extreme value distributions. *Weather and climate extremes*, *38*, 100500.
- Contribution of Working Groups I, I., & to the Sixth Assessment Report of the Intergovernmental Panel on Climate Change, I. (2023). *Climate change 2023: Synthesis report, summary for policymakers* (1st ed.). Cambridge University Press. <https://doi.org/10.59327/IPCC/AR6-9789291691647.001>
- Intergovernmental Panel On Climate Change (IPCC). (2023). *Climate Change 2021 – The Physical Science Basis: Working Group I Contribution to the Sixth Assessment Report of the Intergovernmental Panel on Climate Change* (1st ed.). Cambridge University Press. <https://doi.org/10.1017/9781009157896>
- Sbck: Statistical bias correction kit.* (2023). <https://doi.org/10.32614/CRAN.package.SBCK>
- Schulzweida, U. (2023). Cdo user guide. <https://doi.org/10.5281/zenodo.10020800>
- André, J., D’Andrea, F., Drobinski, P., & Muller, C. (2024). Regimes of precipitation change over europe and the mediterranean. *Journal of Geophysical Research Atmospheres*. <https://doi.org/10.1029/2023JD040413>
- Bao, J., Stevens, B., Kluft, L., & Muller, C. (2024). Intensification of daily tropical precipitation extremes from more organized convection. *Science Advances*, *10*(8), eadj6801.
- D’Andrea, F., Duvel, J.-P., Rivière, G., Vautard, R., Cassou, C., Cattiaux, J., Coumou, D., Faranda, D., Hap pe, T., J z quel, A., et al. (2024). Summer deep depressions increase over the eastern north atlantic. *Geophysical Research Letters*, *51*(5), e2023GL104435.
- Mathbout, S., Lopez-Bustins, J., Roy , D., Martin-Vide, J., Bech, J., & Rodrigo, F. (20a18). Observed changes in daily precipitation extremes at annual timescale over the eastern mediterranean during 1961–2012. *Pure and Applied Geophysics*, *175*, 3875–3890.

Part IV

Other contributions in climate change research

In this part, we shift the focus on two scientific works related to climate change impacts, but not specifically on precipitation distribution. During my three years of PhD, I have had the chance to work on two side projects related to climate impacts.

How to disseminate the research results on climate change impacts in cities to guide adaptation public policies ? Application to the Paris region (France)

The first paper is the natural continuation of a project developed during the Master Politique et Action Publique pour le Développement Durable (MPAPDD) in early 2021, with the team “Equipe Ville” of Météo-France, and deals with the dissemination of research results on urban climate change to public stakeholder in the Paris area. Continuing this work with the impulse of Dr Aude Lemonsu finally led to a paper submitted to Climate Services, in 2023, accepted in October 2024. The version submitted in 2023 is available in [How to disseminate the research results on climate change impacts in cities to guide adaptation public policies ? Application to the Paris region \(France\)](#).

Winter climate preconditioning of summer vegetation extremes in the Northern Hemisphere

The second side project was born through the three-weeks summer school of the Damocles European project on climate change and the impact of compound extreme events, which I attended in Budapest in 2022. It started during the group project allocated time, under the supervision of Dr Ana Bastos and Dr Freya Garry, aiming at better understanding the preconditioning of summer vegetation extremes by winter climate on observational data. The five PhD students and our supervisors continued the collaboration afterward. With additional feedbacks from Jakob Zscheischler, we finally submitted an article in Environmental Research Letter, which was published in 2024. It is in open-access here: [Winter climate preconditioning of summer vegetation extremes in the Northern Hemisphere](#).

The PDF of these two papers are given in the following.

How to disseminate the research results on climate change
impacts in cities to guide adaptation public policies ? Application
to the Paris region (France)

Julie André^{1,2}, Benjamin Le Roy^{3*}, Aude Lemonsu³,
Morgane Colombert^{4,5}, Valéry Masson³

November 26, 2024

¹ Laboratoire de Météorologie Dynamique / Institut Pierre Simon Laplace, ENS - PSL Université, Ecole Polytechnique - Institut Polytechnique de Paris, Sorbonne Université, CNRS, France

² Ecole des Ponts, France

³ CNRM, Université de Toulouse, Météo-France, CNRS, Toulouse, France

⁴ Efficacity, 14 Boulevard Newton, F-77420 Champs-sur-Marne, France

⁵ LAB'URBA, Université Gustave Eiffel, Université Paris Est Creteil, EIVP, F-77454 Marne-la-Vallée, France

Corresponding author: Benjamin Le Roy, benjamin.le-roy@hereon.de

* Benjamin Le Roy's current affiliation is Climate Service Center Germany (GERICS), Helmholtz-Zentrum Hereon, Hamburg, Germany

Abstract

The construction of efficient climate services often relies on the interaction between decision-makers and scientists. Urban overheating is an issue that is already preoccupying public authorities and is likely to be exacerbated by climate change. Taking into account its evolution is essential for urban policy-making, especially to implement and size adaptation measures in conjunction with urban planning. In this study, we present the analysis of an interview campaign, realized with a panel of 13 public actors in the Paris area (France). The actors' current practices and their needs of urban climate data are explored. Their feedback on high resolution climate projections on the Paris area are presented. Climate projections can be difficult to apprehend by the general public, thus an effort of explanation is necessary. Stakeholders usually do not use projections up to 2100, instead are in demand of short and medium-term prospective, in coherence with the temporality of public policies and political mandates. Depending on the aim for which the data are used by public actors (raise awareness, territory diagnosis, decision support, or public action evaluation), the type and format of the data must be adapted, from maps to key figures. Indicators on extreme impacts and risks, are a strong demand of public actors, especially in the health and energy sectors. Finally, resources from former urban climate research are still not visible to most public actors. We advise improving their dissemination through urban planning agencies and local actors, whose expertise is recognized by policy-makers for urban climate issues.

Keywords: climate change; urban heat island; public action; policymaking; climate services

Practical Information

This study investigates how climate information could be better communicated and used by public stakeholders for decision-making, particularly in the case of adapting cities to climate change. Cities are indeed places with significant societal, economic and environmental importance and could be particularly impacted by the effects of climate change across various different sectors. Furthermore, urban areas are already subject to a phenomenon known as the urban heat island (UHI): with nighttime urban temperatures being a few degrees higher than the surrounding countryside. The intensity of the UHI can vary according to different factors depending on the city itself, the geographical context, and weather conditions. The effect is particularly exacerbated during heatwaves [Li and Bou-Zeid, 2013] which can worsen the consequences associated with these extreme events (health risks, energy overconsumption, infrastructure breakdowns, etc.). As heatwaves become more frequent and intense with climate change, the exposure of urban areas to strong heat is expected to increase. Public stakeholders in charge of regional and urban planning are already facing these growing challenges, and have to think about how to adapt their areas. To do so, they need science-based information that is both robust and appropriate.

In order to design and develop an urban climate service, scientific data must be disseminated as resources for stakeholders to help public action at the regional and local level. The aim of the study is to investigate what the needs of urban stakeholders in climate data are, how recent research results on the UHI phenomenon and its evolution with climate change could better meet the needs and expectations of public stakeholders, and be communicated effectively.

To answer these questions, a case study was performed on the Paris region (France) by interviewing a panel of public stakeholders in charge of different thematics, from urban planning to energy consumption management, and also local climate plan. The analysis of the interviews enabled an inventory of current practices. It showed that, in the Paris region, urban or climate data are used 1) mainly in an attempt to raise awareness about climate change impacts both on local population and on elected representatives, 2) to establish a territorial diagnostic of local vulnerabilities to urban overheating, and 3) less often for decision-making, e.g. to choose between different urban planning or urban design scenarios, in which case climate data are needed at a very fine scale (building scale). Yet, climate change, albeit crucial

to the future evolution of city living conditions, is usually not directly present in the data used by stakeholders. The case study showed that urban public actors have a need for climate information on a more regional and local scale than is currently available, and if possible tailored to their specific sectors (energy consumption, urban planning, etc.).

In a second stage, the results of the surveys were used to draw up practical recommendations on how to better communicate and disseminate climate projection results from research institutes to stakeholders. Firstly, the time periods covered by climate projections could be more in line with the temporality of public action. Indeed, stakeholders are in demand of short and medium-term prospective data that fits in with the public policy timetable and that can actually be used for decision-making. The next few decades are of particular interest for public actors, which highlights the need to foster and improve projections at the decadal scale. Then, data on the impacts of extreme climate conditions usually seem of better use to decision-makers than average values, both for raising awareness (a human being is more sensible to a more intense heatwave than to an average warming of 2°C) and for supporting specific technical studies on the vulnerability of infrastructures to these extremes (e.g. can the electricity supply system meet higher demand during an extreme heatwave) and the sizing of adaptation solutions. A climate service must be able to respond to diverse needs and applications, intended for users with different levels of expertise. For effective dissemination and provision of climate data and information, two types of resources have been targeted: a) notes dedicated to public actors, with graphics that are clear and well explained, with key messages, so that they can be used directly by public actors without specific scientific skills; and b) reworkable and geo-referenced projection data that can be used by technical services or scientific teams to perform specific impact studies on a given sector. Finally, the study highlighted that it is essential for (urban) climate scientists and service providers to rely on local and regional urban planning agencies for the dissemination of new data and resources, which are clearly identified by stakeholders in the Paris area as key providers of urban climate data.

1 Introduction

Decision-making and action for risk prevention and adaptation to climate change should rely on current knowledge from scientific research. To promote the integration of climate information into development policies and enable the implementation of relevant adaptation measures, the Global Framework for Climate Services (GFCS) was established in 2009 [WCC3, 2009, Hewitt et al., 2012]. Since then, many initiatives have been conducted in this direction, for climate services at different territorial scales (from global to regional), to meet as much as possible the needs of a wide range of users and sectors. The initial approach to developing this type of product and service was mainly based on a top-down approach [Jacobs and Street, 2020], where scientific data is produced by “experts” and supplied to potential users. More recent works show the importance of an iterative and interactive approach between data-providing scientists and data users in a context of operationalization and decision-making [Brosseur and Gallardo, 2016, Giordano et al., 2020]. It is necessary to take into account users’ acculturation to climate data, their practices and their constraints in terms of resources, legislation or levels of governance [Carter, 2011, Cortekar et al., 2016]. Responding appropriately to expectations also means going beyond raw scientific data and crossing expertise by considering local social, economic and environmental specificities [Swart et al., 2021]. This is particularly true for urban environments, which are already facing major challenges due to the concentration of assets, socio-economic activities and population.

The specificities of urban areas linked to the strong artificialization and imperviousness of soils, to the complex morphology, and to the local emissions of heat and humidity, are deeply disrupting the local environmental conditions [Oke et al., 2017]. The actors in charge of urban planning and urban design are for the most part already aware and concerned about these issues, which could become even

more serious with climate change [IPCC, 2022]. The urban heat island (UHI), that results in an urban overheating occurring predominantly at night, is certainly the local climate issue that has been most discussed and addressed in recent years in the orientation choices of urban planning policies. Worsened by global warming and increased heatwaves, the urban-scale climate conditions can lead to multiple sectoral impacts, e.g. on energy, thermal comfort, health, economic productivity, etc [Takakura et al., 2017, Vigi   et al., 2020, Pascal et al., 2021a]. Many urban climate research studies investigate strategies and action levers to reduce urban overheating, with spatial scales of action that vary from the very local street or urban space, to the neighborhood, or the entire city [Lemonsu et al., 2021]. In this field of research, the link with stakeholders such as urban policymakers and urban planning professionals is already partially in place. Many research initiatives make an effort to transfer knowledge and make data available to assist in decision-making [Eliasson, 2000, Zhang and Yuan, 2023]. Nevertheless, these are usually based on case studies, mainly covering large cities, and the generalization of these results to other cities and other environmental conditions is little discussed. In addition, although the studies in question are often performed by the “climate service” of a city, an explicit account of the effects of climate change on the UHI is overwhelmingly absent from these works.

At the same time, climate change studies are approaching increasingly finer scales, by the use of various statistical, dynamic or combined spatial downscaling techniques [Maurer et al., 2007, Hoffmann et al., 2018, Duch  ne et al., 2022]. The objective is to investigate regional and local phenomena and their evolution with climate change, and to conduct impact studies focused on specific issues and sectors. The description and treatment of urban areas in spatial downscaling approaches and in high-resolution regional climate modeling [Masson et al., 2020, Lucas-Picher et al., 2021] now offers the possibility to conduct more robust studies on the impacts of climate change in cities. In this context, the question arises as to how to effectively disseminate and communicate these new results to users and stakeholders in order to guide in the implementation of city-scale adaptation measures. There is a real challenge in designing climate services that are adapted to urban issues. They should be understandable, respond to the expectations and fit current practices of local actors. Nonetheless, they should provide relevant and scientifically sound information on expected vulnerabilities and impacts. There are two important issues to consider: providing reliable climate projections and impacts on time scales of interest to decision-makers [Brasseur and Gallardo, 2016], and communicating appropriately about the spread of climate model results and the associated uncertainties [Carter, 2011].

The research presented here examines both the role of climate communication strategies and use of climate information in decision-making. It is focused on the specific context of cities, where the challenges of adapting to climate change interact with the challenges of mitigating the effects of urban climate, especially the UHI already inherent in today’s cities. Using the Paris region (France) as a case study and selecting a panel of public stakeholders in charge of local planning policies, the study seeks to clarify their current practices in integrating these issues, the existing climate data and climate services used, and the gaps and needs identified. Based on recent research work combining climate projections and dedicated modeling of urban climate to assess local multi-sectoral impacts of climate change on the Paris region, this study investigates how these new data could better meet the needs of stakeholders and be communicated effectively. Section 2 describes the methodology used to select the public players and to draw up and analyze the semi-structured interviews, as well as the scientific material used as input. Section 3 presents the key findings of this analysis, from which some recommendations are drawn to improve the dissemination and use of current research results and prepare more generic future studies and support new climate services, in section 4.

2 Material and methodology

The technical goal of this methodology is to identify the diverse viewpoints of stakeholders, rather than ensuring the representativeness of these viewpoints and of the actors sample. As a result, the method of semi-structured interviews, commonly used in social sciences to produce a qualitative analysis on a reduced number of interviews, is chosen. Indeed, it does not require a large size of actors sample, but rather a diverse range of participants.

In the following, we present how the panel of public stakeholders was selected (section 2.1), how the interview grid was constructed (section 2.2) based on some recent research results (section 2.3) and how the interview material was finally analyzed (section 2.4).

2.1 Identification of relevant public actors for the Paris region

The study is focused on Île-de-France, the most populous of the eighteen regions of France, centered on Paris, which gathers more than 12 millions inhabitants. A panel of public stakeholders was selected to cover a wide diversity of interlocutors of public action in the field of urban climate:

- urban development actors and urban planning agencies,
- local authorities in charge of planning documents (urban planning or climate plans) and operational projects,
- state services that support local authorities in their efforts.

Here, the decision was made to focus on institutional actors, which allowed for a clearer understanding of governance scales, areas of intervention, connections, and key stakeholders for information dissemination. While it would also have been valuable to include private stakeholders, that would have constituted a separate study.

To avoid a potential bias of the study that would consist in staying too close to climate change experts, we were careful to select in the panel people with various backgrounds and expertises, dealing with broader or related issues to UHI, such as sustainability or urban planning and development.

We identified actors in structures covering the four main territorial scales of action against UHI: (1) national level through an incentive for local actors to take mitigation and adaptation measures, or through research funding (e.g. ADEME, see in next paragraph for definition); (2) regional level as an intermediate scale of support for municipalities in the Île-de-France region in terms of climate-sensitive urban planning and reducing energy consumption; (3) departmental or intercommunal level through a close and tailored support of municipalities, for ex. Plaine Commune, Saint-Quentin-en-Yvelines, chosen for having previously worked on urban climate adaptation; (4) communal level where actions can be initiated by the municipalities themselves, depending on in-house skills and financial resources.

Figure 1 summarizes the public institutes that were selected for the interviews, according to the spatial scale of action or support and the status of these institutes. The ADEME (agency for the environment and energy management) is a central actor for ecological transition through support for innovation and research to application. The FNAU (national federation of urban planning agencies) leads the national network of urban planning agencies by promoting the exchange of expertise and collective projects. The DRIEAT (regional and interdepartmental directorate for the environment, planning and transport) is an organization that helps local authorities in the Paris region, for example, with regulatory aspects and territorial planning. Institut Paris Region is the urban planning agency commissioned by the Region, of which APUR (Parisian agency of city planning and renovation) is the Paris equivalent at the city level. The regional council is the deliberative assembly of the region, responsible for issues such as regional transport, secondary and higher education, regional planning, etc.

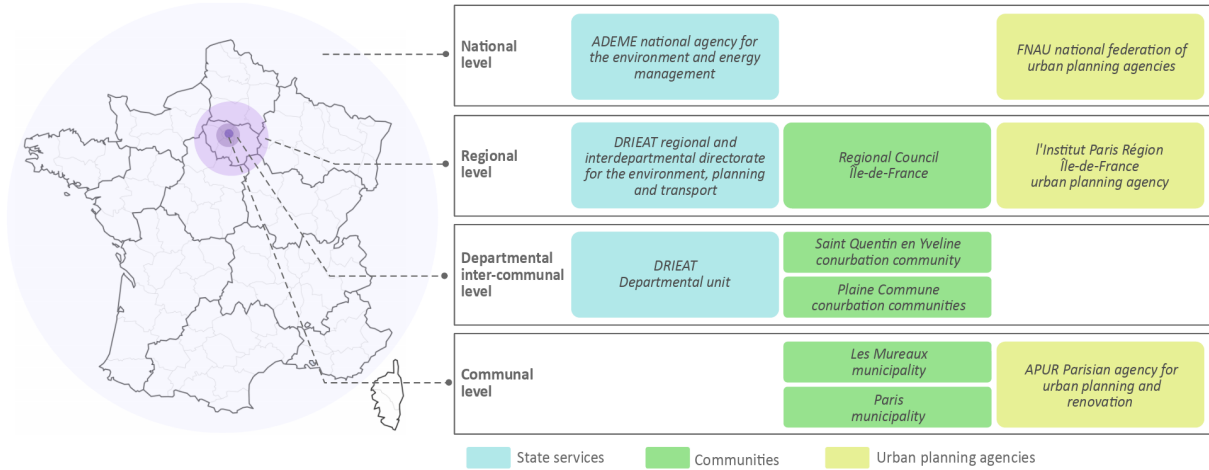


Figure 1: Inventory of public institutes covered by the study through the people interviewed.

2.2 Construction of the interview grid

The interview grid was structured in two main parts to address the two objectives of the study. For both parts, the questionnaire was constructed based on several starting hypotheses, with the idea to investigate each of these through open questions. This approach allows for multiple sub-themes to be covered, while remaining open to any other comments than those previously anticipated.

Part 1 aimed to establish a diagnosis of the current use of urban climate data by public stakeholders and their possible needs. It was conducted without any visual of urban climate data, not to influence the interlocutor. The starting hypotheses were as follows:

- (1) Stakeholders have climate data needs for different areas of activities depending on their missions (e.g. development, planning, awareness of elected officials).
- (2) These data are mainly used for diagnosis but rarely for decision support, which requires more substantial work and resources (e.g. modeling and comparison of different urban planning scenarios).
- (3) The type of data used depends on the training and skills of people in charge of collecting and using/valuing them. An expertise in climate (or even in data processing) can facilitate the appropriation.
- (4) Climate data are preferentially chosen for their ease of use and understanding, confidence in their sources, but also by historical practice. There is potentially a lack of knowledge of the (new) data available, including those provided by Météo-France, the French institute for meteorology and climate.
- (5) To obtain tailored data to address local issues, the public actors can turn to local or national research centers (for example Météo-France climate services).
- (6) The need for local climate data on a target city may not yet be met, despite the data and devices at the disposal of public actors.

Part 2 aimed to get feedback on the new research outcomes to define recommendations and orientations. It was conducted with a presentation of schematic views of the model used and its hypothesis, and a variety of samples presenting the new research results (with different types of content and presentation forms). This led the interlocutor to answer the questions of the interview grid. The starting hypotheses were as follows:

- (1) The actors do not have a clear view of all the information resulting from urban climate modelling, but can take a critical look at the choice of indicators and results formatting.
- (2) Both the geographical zoom level and the spatial resolution of the data are important factors in its use by public actors.
- (3) Stakeholders need tailored sectorial indicators that are not yet addressed by climate science (which

usually deals with weather hazards without necessarily going as far as the impacts).

(4) The representation of uncertainty is central in climate studies to investigate possible futures, but can confuse the messages for a non-expert audience.

The main questions that were asked to the interviewees are presented in a logical framework diagram, in appendix A.

2.3 Research material as support to interviews

The research work that motivated and fed the reflection on the information dissemination to potential actors and users comes from the PhD thesis of Le Roy [2021]. For the first time, multi-model and multi-scenario climate simulations with a high spatial resolution have been performed over the Paris (France) urban area in order to provide indicators of urban climate evolution and of urban-scale impacts of climate change. These climate simulations were based on an original and innovative methodology that took into account the evolution of the regional climate and its interactions with the local urban climate generated by the city itself (see appendix B for the detailed methodology of the simulations). The study domain

is covering the entire Île-de-France administrative region (that contains the Paris urban area). A 1 km resolution was used over the domain as illustrated in fig. 2, showing the main land use patterns in Île-de-France. The climate simulations ran from 1970 to 2099 and consisted of 55 unique combinations of general circulation and regional climate models that projected both a scenario of moderate greenhouse gas emissions (RCP4.5, 14 simulations) and a scenario of high emissions (RCP8.5, 41 simulations). For each projection, the climate conditions in the urban areas were simulated with the dedicated Town Energy Balance urban model (TEB, Masson [2000], Lemonsu et al. [2012], Redon et al. [2017, 2020], Schoetter et al. [2017]). TEB can calculate, among other things, the street-level air temperature as well as the outdoor thermal comfort, and the energy consumption of buildings for air-conditioning and heating.

The raw data coming from these urban simulations were stored with a 1-hour time step over the time period 1970–2099, and at each grid mesh of the study domain. Nonetheless, a post-processing was applied to derive multi-sectoral indicators of local-scale climate change impacts (summarized in table 1). These indicators can take the form of maps, time series, or integrative values (either spatially and/or temporally).

2.4 Methodology for analyzing interviews

A total of 13 interviews were conducted in French, each lasting approximately 1.5 hours. For each of them, a written report of a few pages was made to summarize the discussion, according to the interview grid structure. The audio recordings of the interviews were useful for reporting and quoting accurately the respondents' answers, and were deleted afterward.

A cross-analysis of the 13 interview reports was conducted using a qualitative approach. This non-numeric exploratory approach is often used in sociology to understand social phenomena or the experiences of individuals, through the collection and analysis of nonnumerical data, such as polls, interview, observations, etc. Looking back at all reports in a transversal manner, we cross-referenced the answers point by point. The aim was (1) to check whether the answers of the different stakeholders were consistent or not ; and (2) in case of discrepancy, to link them if possible with the difference between the actors' missions or the profiles of their structure (objectives, history, means of actions). The quotations that best illustrated the shared or different points of view for each question were selected. The stakeholders' quotations that are given in this paper are our own English translations from the French original verbatim.

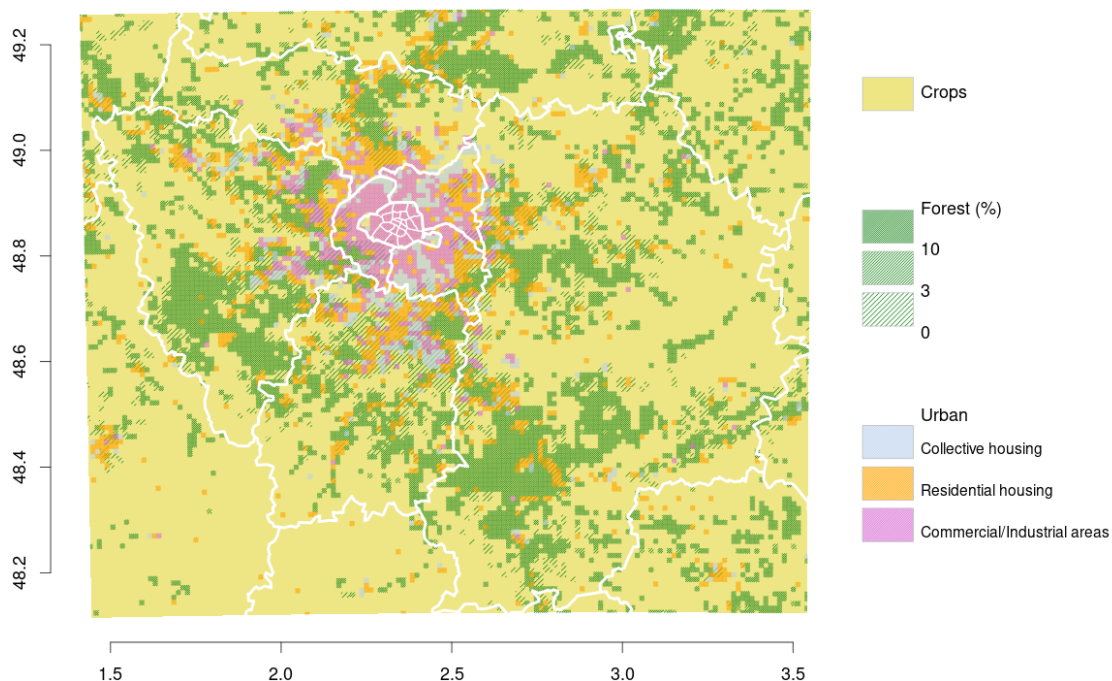


Figure 2: Map showing the study area and the main land use patterns on the 1-km resolution modelling grid. The white lines represent the administrative boundaries of the counties (thicker lines) and of the districts of the city of Paris (thinner lines). More details in appendix B

Sector	Indicators (Units)
Urban climate	<ul style="list-style-type: none"> • Average air temperature over urban areas ($^{\circ}\text{C}$) • Average air temperature over rural areas ($^{\circ}\text{C}$) • Intensity of UHI computed as the difference between urban and rural temperatures ($^{\circ}\text{C}$) • Spatial extent of UHI for a given threshold above rural temperature and expressed as a proportion of the city (%)
Thermal comfort	<ul style="list-style-type: none"> • Average number of hours per day spent above medium heat stress, i.e. for $\text{UTCI} \geq 26^{\circ}\text{C}$ (hours per day) • Average number of hours per day spent below low cold stress, i.e. for $\text{UTCI} \leq 9^{\circ}\text{C}$ (hours per day) • Average number of hours spent in different UTCI classes (hours per day)
Energy	<ul style="list-style-type: none"> • Average energy consumption due to heating (kWh) • Average energy consumption due to cooling (kWh)

Table 1: List and description of multi-sectoral impacts indicators derived from the climate simulation. UTCI, or Universal Thermal Comfort Index, is a measure used to evaluate the temperature as it is perceived by humans; it is detailed further in appendix B.

The results of this qualitative analysis are presented in sections 3.1 and 3.2. This analysis provided a broad view of the needs of stakeholders and the resources necessary to address them more effectively. On the basis of these results, several recommendations were drawn, intended for research teams on urban climate, in order to make the dissemination of the new climate results more efficient.

3 Results

3.1 Inventory of current practices of public actors

The first part of the survey made it possible to make an inventory and analyze the current practices of public actors, the data used and the identified needs, with regard to the issue of UHI or urban overheating.

3.1.1 Which applications involve urban climate data used by public actors ?

From the interviews, it appeared that urban climate data was used for four main applications: raise awareness, territorial diagnosis, decision support, and evaluation of implemented policies (fig. 3). These four applications will be described in the following.

Climate data are used to raise awareness by local authorities and urban planning professionals on UHI and climate change. This can take the form of educational materials or recommendation guides, such as those produced and distributed by ADEME or APUR for example. The data can also be presented at times of discussion and consultation that accompany the urban planning process (at regional or intercommunal level, for example) to alert newly elected officials and technical staff ¹. Finally, climate data are used to raise awareness among a wider audience, to communicate on a city's actions, and to encourage public support ².

Climate data are useful to assess the vulnerability of the territory, and thus meet the diagnostic obligation set by French urban planning documents at all levels (e.g. local urbanism plan at city scale, territorial coherence scheme at intercommunal level). The UHI estimation can be included in the diagnosis as a vulnerability factor for urbanized areas. City services need such tangible elements to mobilize their elected officials on the urban overheating issue ³. Spatial climate data on the target territory can also be used to identify the most impacted areas, and helps orientate and prioritize public measures accordingly ⁴. Some organizations even go beyond legal obligation, with initiatives to better understand how their territory is affected by UHI.

Urban climate data can be used as a decision support in construction or renovation projects. The examples given by the interviewees are modelling specific constructions at the neighborhood scale or cities development scenarios, to compare them through their impact on temperature and thermal comfort. In addition, they can be valuable for labelling processes as those required for the construction of eco-neighborhood or high energy quality buildings (for considering UHI impacts).

At last, climate data may be used by public actors for the evaluation of implemented policies, that is a necessary step for public action. A good example is the schoolyard greening OASIS project (commissioned by the city of Paris, supported by the EU's European Regional Development Fund) for which sensors were installed to measure local conditions before and after schoolyard greening and evaluate the cooling

¹As an example, the master plan for the Île-de-France region is seen as "an opportunity to get messages across, because there is a lot of collaborative work going on, with the territorial authorities of the Île-de-France." (Regional Council)

²"Having all this data, it allows us to launch training, awareness and communication programs on a large scale for all users in the Paris area." (City of Paris)

³"to be able to tell them [their elected officials]: look, we're not talking nonsense, there really is a problem of urban overheating in such and such a place. We can see it, it's quantified, it's that many degrees [...]. It allows us to cut short endless political debates" (ADEME)

⁴"It can be an opportunity to have zoning for problematic areas, where any development that would contribute to aggravate the UHI in these sectors, we could answer: watch out!" (Paris Region Institute)

	Local measurements		Satellite imagery	LCZ GIS-mapping	Numerical modelling	
	Short-term	Long-term	Land surface temperature	Link LCZ-microclimate	Current state	Scenarios
Raise awareness	Green	Green	Green	Green	Green	Green
Territory diagnosis	Green	Green	Green	Green	Green	Green
Decision support for public action	Orange	Yellow	Orange	Yellow	Orange	Green
Public action evaluation	Orange	Green	Green	Orange	Orange	Orange

Figure 3: Summary of the different types of urban climate data used by public actors and the objectives targeted by this use, with the following color code: green if used for this objective, red if not used, yellow if it can be used in certain cases. Local measurements can be conducted through a short-term campaign lasting a few days or weeks, such as during a heatwave or in the summer (referred to as “short-term” measurements). Alternatively, instruments can be installed for extended periods, collecting data over several years or decades. This allows for the creation of a longer time series and more comprehensive analysis (referred to as “long-term” measurements). Local Climate Zones (LCZ) is a method for mapping the territory according to the land cover and morphology of urban areas to group together neighborhoods whose thermal response is assumed to be similar. GIS (geographic information science) is a technology that enables the visualization and analysis of complex spatial data, and is often used in urban planning.

potential, especially during summer and heatwaves. The measurement-based evaluation of local impacts helps public authorities to quantify and demonstrate the effectiveness of implemented measures and justify their financial cost. It also enables the proposition of possible improvements.

By taking a step back on the interviews, the use of climate data for awareness raising emerges as the most frequent of the four identified areas of application in Île-de-France public action. Conversely, the use of climate data for decision support is so far rather punctual (as mentioned by the FNAU). Another key point is that the timetable for the development of planning documents and public policies influences the receptivity and needs of public actors in terms of climate data. If the release of new data is not in line with these time constraints, the data is simply not used.

3.1.2 What types and formats of climate data are used by public actors ?

The climate data used by public actors (which are mainly temperatures or derived indicators) are mainly presented in the form of key figures and maps, depending on the purpose. The maps fit both with awareness raising and territorial diagnosis. The key numbers allow rising awareness, but also to objectively and quantitatively evaluate the action. More marginally, mainly for climate projections, the data are presented as temporal evolution curves of meteorological parameters. The format and content are also adapted to the target audience. For example, the online dissemination of the climate plan of the Saint-Quentin intercommunality required a reworking of the data to make them understandable and effectively reach the general public ⁵.

The results of the interviews show that four main types of urban climate data are used by stakeholders (fig. 3) depending on the needs and objectives but also on the human and financial resources available. According to the interviews, the most meaningful and expected data for public actors is a direct measurement of the UHI on their territories by in-situ stations. Some French cities launched their own measurement campaign (ex. airborne thermal image of the Paris area acquired for a summer day) or deploy their own station network (ex. Toulouse, Grenoble, Nantes, Clermont-Ferrand, etc.). One-off campaigns characterizing the city at a given point in time, which provides diagnostic and awareness-raising elements, while permanent networks enable to monitor the evolution of physical variables over longer periods such as years or decades, which allows for the evaluation of local actions. These two

⁵ “When we made it available to the public for consultation, we got a lot of feedback from people who said: ‘We don’t understand it, there are too many figures, too many documents’ ” (Saint Quentin en Yvelines)

time-scales for local measurement are referred to as “short-term” and “long-term” in fig. 3. Nevertheless, these initiatives require expertise and funding, so that they are mainly implemented by large cities.

With no in situ measurements, medium-sized communities often turn to free satellite data. They are generally land surface temperature maps retrieved from infrared measurements. Depending on the satellite products and their spatial and temporal resolution, they can allow monitoring long-term evolution (from the 1990s) and ongoing changes, and possibly evaluate local projects. The resulting territorial diagnoses frequently lead to a confusion between surface temperature and air temperature, which are, however, quite different information ⁶. Despite this risk of confusion, land surface temperature maps are widely used by many municipalities as a way to talk about the concepts of urban heating ⁷.

The classification into Local Climate Zones (LCZ) is another approach used to compensate for the lack of urban-scale measurements. Proposed in 2012 [Stewart and Oke, 2012], this classification is based on knowledge of the urban climatology concepts. LCZ was constructed as a logical and universal classification of both urban and rural areas, based only on surface and urban properties, with the aim to differentiate locations in terms of their energy response to incoming radiation (thermal admittance, surface albedo) and thus in terms of local thermal response. The urban properties used for the classification are for example: building characteristics and construction material, street dimensions and geometry, vegetation and pervious surface fraction, but also human activities and heat production. Note that this classification in LCZ does not incorporate directly any weather or climate information, but highlights the different thermal responses of locations to a typical clear and calm evening. The typical effect on the 2 meters temperature that one can expect from different LCZ classes were assessed from urban measurements and numerical modeling, in the simple setting of a clear night [Stewart and Oke, 2012]. Note that the effects on other meteorological variables (such as wind or humidity) were not assessed, as it was not the focus of the LCZ classification.

The main advantage of the LCZ classification is that it allows for a first-order assessment of overheating risk, using geographical data that urban planners typically have access to or can easily gather through field visits. For French urban planning agencies with Geographic Information Systems (GIS) skills, LCZ classification has therefore become a “classic method” (interview ADEME) for the analysis at scale of a few hundreds of meters to a few kilometers. For example, the Paris Region Institute developed an interactive map of the Île-de-France region that provides indicators reflecting the effects of urban overheating in relation to LCZ, urban parameters, and a land surface temperature map from the 2003 heatwave (<https://www.institutparisregion.fr/environnement/changement-climatique/chaleur-sur-la-ville/>). This LCZ approach offers a diagnosis for a fixed mapping of the city at a given time, yet it cannot be used for evaluation of implemented policies.

Finally, results of numerical modelling of the urban climate are also used by some public actors. They have the advantage of covering areas where measurements are sparse or non-existent, or even of simulating and evaluating prospective scenarios. Simulations from research projects such as MAPUCE [Masson et al., 2015] and PÆNDORA (Suher-Carthy et al. [2023], Gardes et al. [2020], Project page) are used for the cities of Paris and Toulouse. Yet, “many urban planning agencies do not have the chance to have access to modelling data made on their territories by Météo-France [...]” (interview FNAU). Modelling is more often provided by engineering firms, or more rarely by certain urban planning agencies. This is the case of the Paris agency APUR which is developing a simplified model to simulate the city-scale overheating for favorable weather conditions. However, the interviews revealed a reluctance to use data resulting from complex climate modelling, as they are generally considered as too complicated and mathematical

⁶ “I have seen a lot of nonsense circulating about UHI data. With infrared measurements, people confuse UHI and energy loss of buildings. . .” (ADEME)

⁷ “Why do we still use this data? Well, simply because they are accessible and because they enable to talk about the subject, and being anchored in the territories. Otherwise, we would remain in concepts!” (FNAU)

⁸. Simpler models that are better understood and mastered are preferred by non-technical people ⁹. The mistrust of non-scientist people can also stem from the perception that these models are based on too many assumptions and are subject to important uncertainties. The dissemination of climate modelling results to a non-expert audience is therefore much more delicate than for measurements, and requires progressive acculturation and guidance.

3.1.3 Which needs have the public actors expressed ?

The public actors interviewed expressed the need for a more detailed territorial diagnosis in order to target and prioritize the areas where intervention is needed ¹⁰. They underline the scarcity of local measurements for monitoring the temperature in the cities and UHI. In particular, it was deplored by several respondents that the only station in Paris of the Météo-France weather network is located in a large urban park (Montsouris), that does not allow for an accurate measurement of the UHI. On the other hand, some public actors would like finer UHI modelling to get closer to the local scale, but with imprecise and disparate requests regarding the spatial resolution (from the municipality to the neighborhood level) ^{11 12}.

Concerning the use of urban development scenario studies as a support for decision-making, the expectations of public actors are for the production of more operational scenarios than what can be achieved by some prospective scientific studies (i.e. less generic and more localized), better in line with public action and implementation constraints ¹³.

The link between UHI and climate change can rarely be made explicitly because the available data do not allow it. Public actors are increasingly demanding urban climate data that integrate trends in climate projections, and take place in an adaptation perspective. This dimension becomes a prerequisite for the calls for research projects funded by ADEME. Nevertheless, in the absence of such data, the public actors now complement their territorial diagnoses on UHI with a discussion on the expected increase in the occurrence of weather situations (especially, heatwaves) that exacerbate the UHI and associated impacts ¹⁴.

3.1.4 Who do public actors turn to for urban climate data ?

The results from interviews show that there is a very wide disparity in terms of in-house technical and scientific skills and human and financial resources between structures ¹⁵. The city of Paris is a driving force in city-scale impacts studies of climate change. It has a dedicated department on these issues, which can itself contribute to the UHI diagnosis and the implementation of local actions. On the contrary, the absence of a geomatics department for many organizations is a significant barrier for efficient access and processing of urban climate raw data, and adapt it to the specific needs of the actors concerned. Therefore, although some planning agencies have the capacity to produce data or process existing data,

⁸ “When you present data from modelling to elected officials, there are some who are very perplexed, and who say to us, but how can you be sure that this will go this way?” (Saint-Quentin-en-Yvelines)

⁹ “we don’t necessarily like very complicated models. For people in urban planning, we prefer them to be able to grasp the ins and outs [...] We are wary of black box phenomena”

¹⁰ “having climate projections [...] that are very localized would be very interesting, I think. It would allow us to prioritize our actions even more, to really know where to start first” (City of Paris)

¹¹ “10 km would be really good already” (ADEME)

¹² “What we are really interested in is having a downscaling with a fine mesh, let’s say, almost to the district level” (City of Paris)

¹³ “When you talked about doubling the green spaces in Paris, well, that’s interesting, let’s admit it. But it’s not operational enough: we don’t have a project that is either double or not double the green surface!” (Les Mureaux)

¹⁴ “Now we have a systematic discussion about climate change in our diagnoses: the heat phenomena that we encounter today, tomorrow are likely to be multiplied, to concern new territories” (FNAU)

¹⁵ “I’ve seen some [communities] take ownership of datasets, have a geographic information system engineer who deals a little with climate data. There are really very different levels of involvement, and very different needs depending on the territories.” (ADEME)

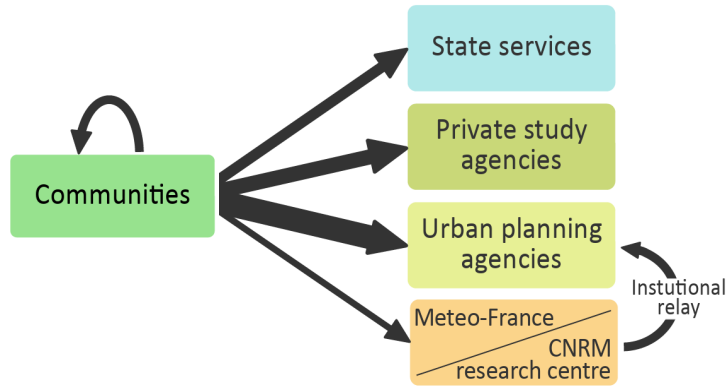


Figure 4: Schematic view of the actors toward which communities would generally turn to, if they want some urban climate data. The larger the arrow, the stronger the link.

many structures turn to consultancy firms. This may involve data from measurement campaigns, or climate modelling on different scales, or modelling on a very local scale for a particular project.

The time constraints may dictate the choice of entrusting an analysis to a private study agency rather than a research team¹⁶. Research projects (typically 3–4 years long) do not necessarily respond to the dynamics of public action, which is notably punctuated by local and regional elections. Nevertheless, the cost of consulting firms is a limiting factor and encourages the local authorities or State services to turn instead to institutional partners. Some structures are identified as resources for providing or producing UHI data: the State technical agency CEREMA (Center for studies and expertise on risks, the environment, mobility and planning) with a recognized expertise on urban thermal issues, the ADEME for energy issues, the AIRPARIF regional air quality monitoring association, or the Teddif network (Territories, environment and development in Île-de-France). The State services can play a role in redirecting communities to these expert resources.

For public actors, Météo-France is the reference for reliable meteorological and climatic data and products¹⁷. Still, except for public actors who have been involved in research projects, Météo-France is not identified as a resource on UHI-related issues, especially regarding its practical translation for development and planning actions. According to the Paris Region Institute, which has collaborated a lot with the research center of Météo-France and CNRS (National center for scientific research), the project reports are not efficiently publicized to the urban planning community. Although reports and main results are accessible on Météo-France website and published in the scientific literature, the results and data from those projects are not clearly identified as available and retrievable by most public actors.

Instead, the interlocutors considered as the real reference on UHI issues in the Paris region are the urban planning agencies (fig. 4). Both Paris Region Institute and APUR (for the regional and Paris urban level, respectively) are very well identified by the local authorities, particularly for their expertise on the link between UHI and public planning policies¹⁸. The local authorities rely on the technical notes and publications relayed by the Paris Region Institute, which are highly appreciated because they are truly adapted to operational needs.

¹⁶ “consultancies generally work faster [...]. For example, the study with Ranboll took only about four to six months.” (City of Paris)

¹⁷ “Obviously when you also have a study stamped from Météo-France, it is always reassuring for everyone. It’s Météo-France, so it’s reliable” (City of Paris)

¹⁸ “It is true that we work more particularly with Arc [Energy Climate Regional Agency] or the Paris Region Institute when we want data like that, that are so specialized. So they are quite the experts. This is part of the missions delegated to them by the Region.” (Regional Council)

3.2 Feedback of stakeholders to new research outcomes

The second part of the survey made it possible to collect the reactions of the same actors interviewed to the presentation of new data resulting from research work on the urban climate and its expected evolution with climate change. The objective here is to clarify to what extent this data, its method of calculation, its representation and format can meet the needs of the actors. For this part of the survey, we presented to the actors some visuals based on research results to illustrate the different aspects discussed.

3.2.1 About the setup of the simulations

Before considering the results, the interviewees were asked about some important configuration elements for the simulation, i.e., the geographic area covered, the spatial resolution chosen, the main assumptions of the model. They first reacted on the description of the study area. The use of a fixed land cover mapping for the region that is based on the current state (as shown previously in fig. 2), with no change in urbanization during the climate simulation, is unanimously seen as an important limitation¹⁹. The actors would have appreciated taking into account the old land use for the simulation of the past period, and a projection of the land use in the future combined with some generic assumptions of urbanization, thermal renovation of buildings, increasing installation of air conditioning equipment, etc. The comparison of different evolution scenarios (e.g. land use planning, energy renovation plan, urban greening) would also have been very interesting for the public actors²⁰.

Despite this, stakeholders were very keen on the results presented, provided that the assumptions made were highlighted. The 1-km horizontal resolution of the simulation was generally highly appreciated and considered as an important step in raising awareness about UHI and climate change in the Paris region²¹²². Nevertheless, some actors, mainly those with a background in urban planning, would like to go to an even finer resolution (typically, at street level)²³. They therefore insist on the importance of completing the results at 1 km by local modelling or by measurements.

As for the potential need to aggregate the data from the 1-km grid to an administrative unit, the stakeholders were unanimous that it was better to keep the native resolution to preserve the maximum precision²⁴. Any further change of scale or aggregation of the data may be relevant depending on the needs and applications, but at a later stage and preferably by the users themselves (section 4). For example, aggregated numbers on a municipality's territory could be of use by local geomatics services to compare more quantitatively different territories, using the raw simulation results.

The presentation of a given result at different levels of zooms appeared very useful to local actors (fig. 5). They are primarily interested in the issues specific to their own territory²⁵. But that way, they can also compare the impacts and urban effects in their municipality (or department) with those of neighboring municipalities.

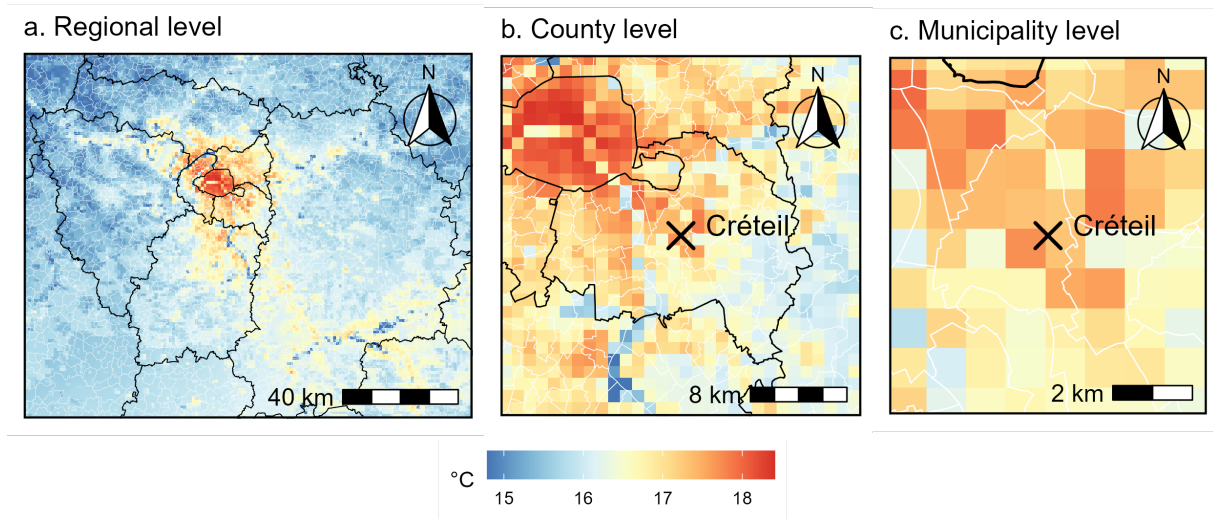


Figure 5: Visual presented during the interviews, showing the same 1 km resolution simulation data at three zoom levels. Average nighttime temperature for the hottest summer simulated by one model over the historical period 1976–2005.

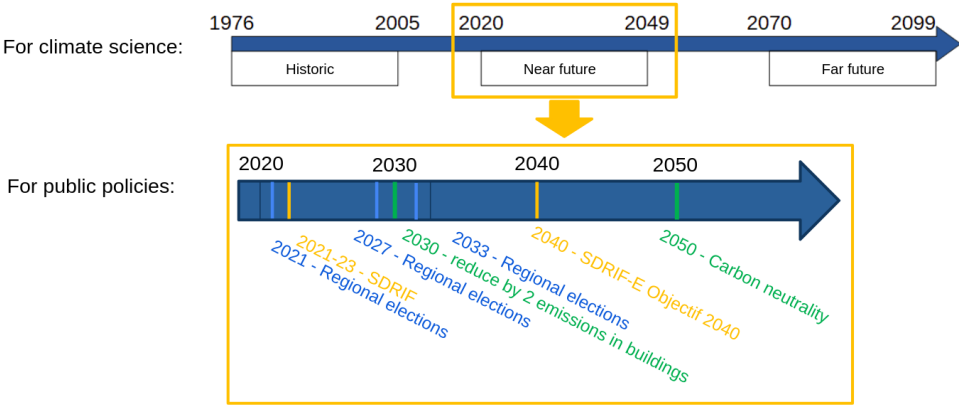


Figure 6: Illustration of the different time scales at scales for Climate sciences compared to public policies, with regular elections, urban plans (such as the SDRIF -Schéma directeur Île-de-France-, carbon emission reduction objectives, etc.

3.2.2 About the hypothesis and temporal characteristics of the climate projections

In a second stage, the question of the choice of emission scenarios and climate projections, as well as the temporality of these projections and their analysis, was addressed. Stakeholders did not express a strong preference for one of the greenhouse gas emission scenarios, and seem satisfied with the scientific results often based on the RCP8.5 scenario with the highest emission levels and the strongest warming signal, as far as the definitions are explained. However, this extreme scenario may be difficult to back up by the State services given its incompatibility with the carbon neutrality objectives by 2050²⁶. As a result, they could be more comfortable with medium (RCP4.5) to low (RCP2.6) emission scenarios. Stakeholders agreed that showing different possible futures raises awareness of the importance of mitigation actions and of a scalable and flexible adaptation²⁷. Nonetheless, they preferred the results to be limited to a few scenarios (three at maximum) for the sake of clarity²⁸. In their opinion, it is not necessarily useful to systematically overlay the results of several emission scenarios. They suggested illustrating the main message based on a single selected scenario, then showing how this can be amplified or reduced with other emission scenarios on a few chosen examples.

The climate simulations that led to the results presented in the survey covered the period 1970–2099. As most climate analyses based on a statistical approach of trends, the results were presented as averages of three 30-years periods, i.e. historical (1976-2005), near future (2020-2049), and far future (2070-2099) as illustrated on fig. 6. The survey revealed that this presentation of the results in the form of a 30-year time-slice was very difficult to grasp for stakeholders, because it is such a long period compared to the timescale of most public actions²⁹. There is a gap between the information expected by the actors on the one hand, and the scientific results and analysis methods on the other. Due to the inter-annual climate variability, it is not statistically robust to reduce significantly the length of the periods over which climate trends and impacts are calculated. Therefore, to speak of “time horizons” instead of “periods” by referring to the central year of the 30-years time-slice (e.g. “2020-2049” becomes “horizon 2035”) is a simple communication element that allows to take up the usual codes in public policy.

Climate projections to the end of the 21st century did not emerge as deadlines that interested and challenged most of the public actors³⁰. The temporality that was relevant for them had to be linked to the rhythm of public action and elections³¹ and planning documents (for ex. 20 years for the SCOT, a local urban planning document). Therefore, from the perspective of adaptation decision-making by elected public actors, it appeared to be more effective and relevant to present them with short and medium-term projections (until 2040, even 2050) rather than long-term. Nevertheless, the projection data up to 2100

¹⁹ “The city extent of 1970 is not one of today! The year 1990 can only be used if you have access to the urbanization of that time, otherwise it is strongly recommended to run the model only on recent years.” (APUR)

²⁰ “If you make several scenarios, it would be very interesting. There are big debates about nature in the city, these are electoral and political issues.” (DRIEAT - Energy Climate)

²¹ “I think that what you are presenting, this downscaling [to 1 km], is really capable of moving the lines.” (DRIEAT - Energy Climate)

²² “1 km is already something very interesting, especially for a planning exercise.” (FNAU)

²³ “You should in fact give a degree of precision that makes it possible to deal with the district, [otherwise] the project leaders, the elected representatives, they will find it difficult to use what we bring them.” (DRIEAT - departmental unit)

²⁴ “Temperature does not stop at the municipal boundary! If we take the average at the commune level, we risk having a wrong interpretation afterward, within the same territory, the results are heterogeneous. No, I don’t see the point of aggregation.” (FNAU)

²⁵ “the map zoomed in on Paris, that’s absolutely certain, because that’s our territory, and that’s where we’re competent.” (City of Paris)

²⁶ “We need to be in line with what the SNBC [Stratégie Nationale Bas Carbone] and the government say about our climate targets.” (DRIEAT - Departmental unit)

²⁷ “If you show two scenarios, you show a range of possible, credible futures.” (DRIEAT - Energy Climate)

²⁸ “We could present a few scenarios, but not too many, because if you present more of them, people are lost. Two, three, but not more!” (Saint-Quentin-en-Yvelines)

²⁹ “When you say 2020–2049, I find it hard to see what it means. Can’t we work on time horizons that are a little more precise?” (City of Paris)

³⁰ “2080, it’s a long way off. The further away the targets are, the less concerned the people.” (Regional Council)

³¹ “Town representatives are in place for 6 years: they want to do things now, that have an impact now.” (Saint-Quentin-en-Yvelines)

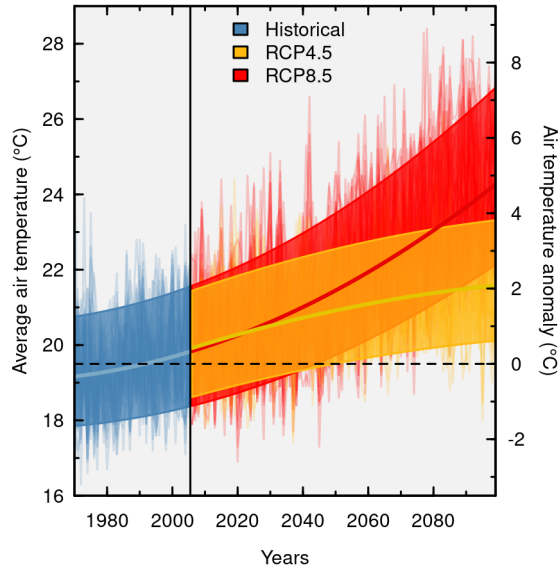


Figure 7: Temporal evolution of the average summer urban air temperature over Paris. The background lines represent the variability associated with the multiple models used and their natural variability. Two scenarios are represented: RCP4.5 in orange and RCP8.5 in red. The smooth lines and envelope represent the multimodel mean and the 90% uncertainty range smoothed by polynomial regression. The dashed horizontal line indicates the temperature anomaly relative to the 1976–2005 mean.

should remain available for technical services and for actors of long-term energy prospective or urban planning.

As for the temporal integration of a result, the interlocutors generally advised against the use of averages, when aiming at raising awareness: the concept of mean seems not easy to grasp³². Instead, the interviewees’ advice to highlight the results on extremes, which can impact people, health and activity sectors a lot: for example heatwaves or extreme temperatures³³.

Last but not least, the presentation of models uncertainties to elected officials or the general public appeared to be counterproductive, based on the survey feed-backs. These uncertainties based on statistical notions made the information more cumbersome and complex, which could confuse the core of the message for a non-technical public³⁴. On an evolution curve, a colored band around the average value could be enough to remind people of the dispersion of the models without making the graph too heavy (fig. 7). Still, for technical services, uncertainty assessment would be necessary to define robust adaptation strategies³⁵.

3.2.3 About the choice of indicators

Respondents were asked about the relevance and interest of the different indicators that have been selected in the research work to assess the local impacts of climate change on the Paris region (see table 1). First, the surface air temperature was presented and discussed, and by extension the associated UHI (fig. 8).

³² “In my experience, when you communicate with the general public or policymakers, people do not understand what an average is.” (APUR)

³³ “There are times when the thresholds of acceptability are crossed. [...] If we say that there will be 32 days in the summer when our infrastructure will be at the breaking point, when the rails will bend because it will be too hot [...] this can really mark people.” (DRIEAT - Energy Climate)

³⁴ “I think you need to have the clearest message possible. The min and max will confuse a more complete reading of the graph.” (DRIEAT - Departmental unit)

³⁵ “The mustache box [showing the standard deviation around the mean for a given value, as presented during the interview] is of no use to the elected representatives I think, but for the technical services of the climate plans it is worth having this report in detail” (ADEME)

The surveys showed that these data over the region was already of great interest to the actors. The surface air temperature and UHI maps were considered to be relevant tools for awareness and diagnosis. All respondents found these maps to be very meaningful and useful for diagnosing and viewing the geographic sectors affected by UHI hazard, even in areas that may not be perceived as problematic in peri-urban municipalities. Some respondents felt that confusion or misunderstandings are still possible, depending on the vocabulary used. Stakeholders and municipality services usually work with their own definition, for example a local-scale evaluation of UHI on their own territory and for a specific weather situation, as opposed to the evaluation that was proposed here for the whole region and for a summer average. Besides, for energy and transports operators, the surface air temperature appeared to be of great interest to estimate the risk of rupture of specific infrastructures ³⁶.

Two other meteorological indices related to temperature emerged as particularly relevant for some stakeholders because they are frequently used in their territorial studies: heatwave days and tropical nights. According to the French warning system, a heatwave is defined as a period of at least three consecutive days when the daily mean temperature does not fall below a threshold prescribed for each county by the national health agency [Pascal et al., 2021b]. The tropical nights corresponds to days when the minimum temperature does not fall below 20°C (ETCCDI: <https://etccdi.pacificclimate.org/indices.shtml>, Karl et al. [1999], Zhang et al. [2011]).

Indicators relating to thermal comfort (or heat stress) were presented in a second step. They are similar to the notion of perceived temperature depending on environmental conditions (i.e. combination of temperature, humidity, wind, and radiation). This concept is still emerging in France and needs a minimum of guidance, but it was very well received by the respondents because it addresses the individual's scale ³⁷. The feedback from the surveys indicated that comparing spatial data (map) and temporal data (evolution over a day) helped to understand the exposure of individuals according to their mobility and the time of day. In addition, integrated over the day, they provided daily exposure maps under heat stress conditions which was very informative for urban planning. Respondents emphasized the complementarity of these results to the nighttime temperature maps, with the influence of urban form and compactness on wind and sunlight sometimes leading to counter-intuitive results on urban comfort. Nevertheless, there was a strong demand to give even more informative data concerning the impact of thermal discomfort on health, if possible in a quantitative way ³⁸.

The last indicators concerned energy. The evolution of energy consumption for air-conditioning and heating has undoubtedly emerged as a prospective data much awaited by municipalities and operators to prepare for the energy transition ³⁹, ⁴⁰. An important point of vocabulary was underlined by some respondents: it would be more appropriate to speak of cooling demand rather than air conditioning demand. The message thus referred to a more systemic reflection on the renovation of buildings to ensure summer comfort, rather than an incentive for the systematic development of air conditioning systems. The respondents reminded that two levels of information could be useful, i.e. (1) the evolution in annual energy consumption to support municipalities in their planning and (2) the evolution of peak power to address the electricity supply issues of grid operators. For energy, the question of the unit and the appropriation of these quantities is crucial to communicating to a non-technical audience. An analogy with concrete quantities would help for a better understanding of the consumption volumes (expressed

³⁶ "If you say, it will reach 50°C around the regional trains catenaries, or if the tar melts too fast in some areas, that will be of great interest for them." (DRIEAT - Energy Climate)

³⁷ "[Universal Thermal Comfort Index is interesting] because it's on a human scale, and not just on the physical scale of Météo-France [laughs]: it's not just a thermometer." (Plaine Commune)

³⁸ "What does it mean to spend 3 hours in thermal stress? Personally, I don't know if there is a clear difference between 2 hours and 6 hours. One needs to give a framework, a context that is established." (Plaine Commune)

³⁹ "All these elements of the evolution of the demand for air-conditioning in a changing climate, in the urban and periurban areas, these are very, very precious elements to situate the extent of the challenges today!" (Paris Region Institute)

⁴⁰ "This will be of great interest to Énédis [a French electricity distributor] and RTE [the French electricity grid operator], who will have to make sure that they can supply the necessary electricity." (DRIEAT - Energy Climate)

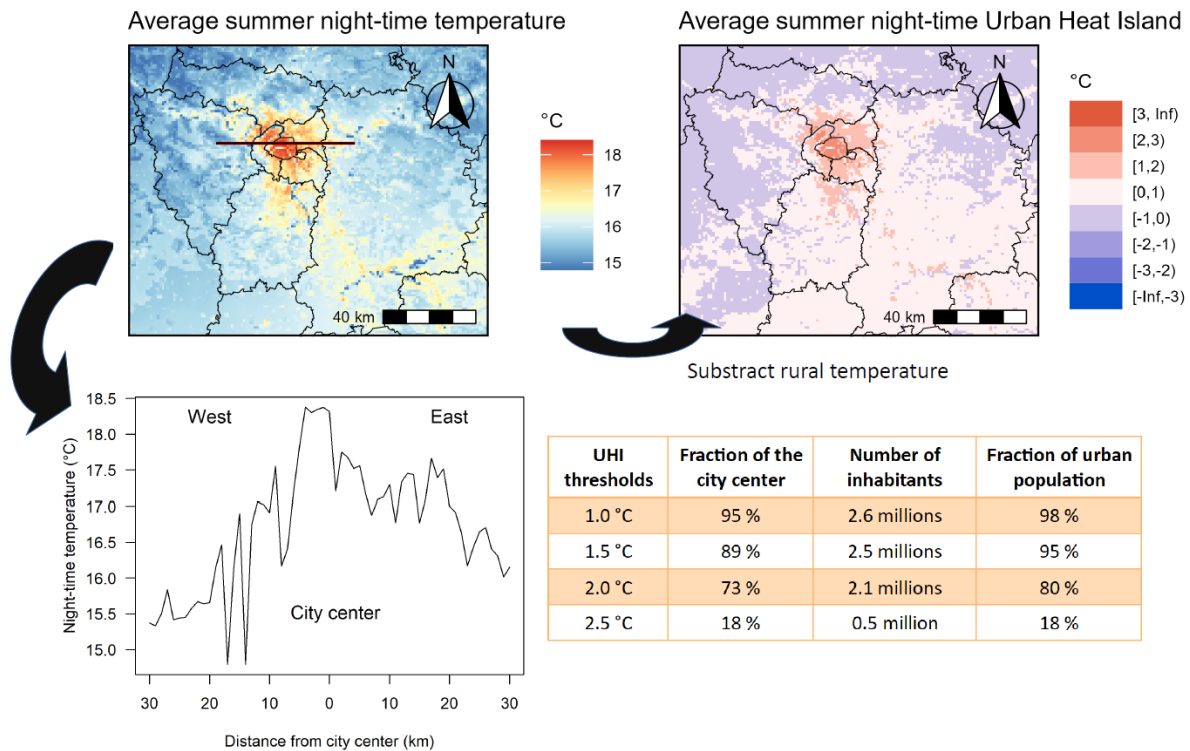


Figure 8: Visual presented during the interviews, showing different ways of representing the impacts of nighttime Urban Heat Islands. Average nighttime temperature for the hottest summer simulated by one model over the historical period. Top left: the temperature at 2 meter from the ground, with a continuous color-scale; top right: the same temperature field to which its regional mean has been subtracted, giving the Urban Heat Island field, with a discrete color-scale. Bottom left: a transect of the temperature field through Paris city center, from West to East; bottom right: table with the number of people in the Paris area affected by given levels of UHI.

in kWh m⁻² yr⁻¹) for instance by referring to an equivalent number of nuclear reactors, or a number of wind turbines or a surface area of solar panels.

The indicators mentioned above were all welcomed with interest but also led to an expression of needs from the actors in relation to their fields of intervention. Stakeholders expressed a strong demand to cross-reference climate data with sectorial data to assess new types of impacts (e.g. the effect of high temperatures on urban infrastructure and transport networks). Not surprisingly, the impact on health emerged as a central issue. Even if thermal comfort is already a very relevant information, the transition to the evaluation and understanding of the vulnerability of the inhabitants is at the heart of the concerns. Putting sociodemographic data or data on sensitive equipment into perspective with climate data could support action for risk prevention.

3.2.4 About the visualization and data accessibility

In a last stage, the respondents also commented on the proposed visual media and formats for presenting indicator information. The first important result is that the cartographic medium is clearly the easiest to access and the most meaningful for the actors (but also for the general public)⁴¹. This is in line with current practices in the urban planning sector, where this type of medium is widely used. The scientific curve - such as a temperature transect across the region - is much less common and more complex for a non-expert audience.

⁴¹ "This section curve chart speaks much less than the map. You would have to be used to reading graphs. Besides, this form of graph is not often used. I think that the average person who does planning will find it difficult to understand." (DRIEAT - Planification)

To facilitate reading and interpretation, but also to reinforce the message, the maps (or other graphic media) should be supplemented by reading elements in the form of combined map data, key messages, diagnosis, etc. For example, superimposing land use and occupation information on UHI maps (location of parks and urban centers by colored or hatched areas) raises awareness of the link between soil sealing and urban overheating. Technical services could rely on these media to support the preservation of natural areas. Another example, the data on the population affected by different UHI levels (Table in fig. 8) is a key figure highly appreciated by respondents ⁴² because it reinforces in a concrete way the information provided by the map. Even if the respondents would like these figures to be refined especially by accounting for sociodemographic variability, they considered the figures to already provide crucial information on a first level of impact, and could feed into more detailed studies carried out directly by the municipalities.

For map plotting, the survey outputs highlighted that the choice of color scales and temperature ranges (with continuous or discrete values) was important in reading the map and the resulting perception. Although the zoning effect associated with discrete thresholds can help identify high-stakes areas, it can also be counterproductive for taking action in areas where mitigation goals may seem unattainable. This point emerged from the respondents' feedback on the UHI maps, for which a discrete scale may be suitable for a regional overview, while a continuous scale is preferred when the maps are zoomed in on smaller areas.

Finally, concerning the way to show the evolution of indicators over time, three approaches were presented at the interviews: maps at different time frames, tables of key figures, and curves of temporal evolution. Again for stakeholders, the comparison of maps for the current state and the expected future stood out as the most meaningful medium, as map visualization is widely used in planning so that elected officials are familiar with it ⁴³. A key figure extracted from curves or maps could also be sufficient to convey a message, to raise awareness among all types of actors ⁴⁴ ⁴⁵. In contrast, the respondents recommended avoiding the graph as time evolution curve (perceived as too mathematical) when addressing elected officials or the general public ⁴⁶. The presentation of time series to a non-specialist audience requires a real work of formatting. The reader must be guided through the graph to make it more accessible, for instance with storytelling.

Lastly, the respondents were asked about how they would like to access this kind of data. The first mode of diffusion should be ready-to-use information at the Île-de-France regional level, in the form of a synthetic summary, that would be of use for most type of actors. This summary should present the project results in broad terms; it should explain where the simulation data comes from (model principle, hypothesis and inherent limits) and give general results, such as the spatial structure of UHI and its projected evolution in the future⁴⁷. It should also highlight the kind of output that could be provided from these simulations, with an example for each variable. The respondents highlighted that for such a document to be used by technical agencies or public actors, it had to be very clear and self-explanatory. Any impact map (e.g., a UHI map with localized maxima in certain areas) that may highlight areas that are more vulnerable than others should therefore be accompanied by explanatory information ⁴⁸. In

⁴² "That's the first thing people ask us: but how many people does your thing impact?" (Paris Region Institute)

⁴³ "The map is what speaks, and it is what makes it possible to illustrate to elected representatives." (DRIEAT - Departmental unit)

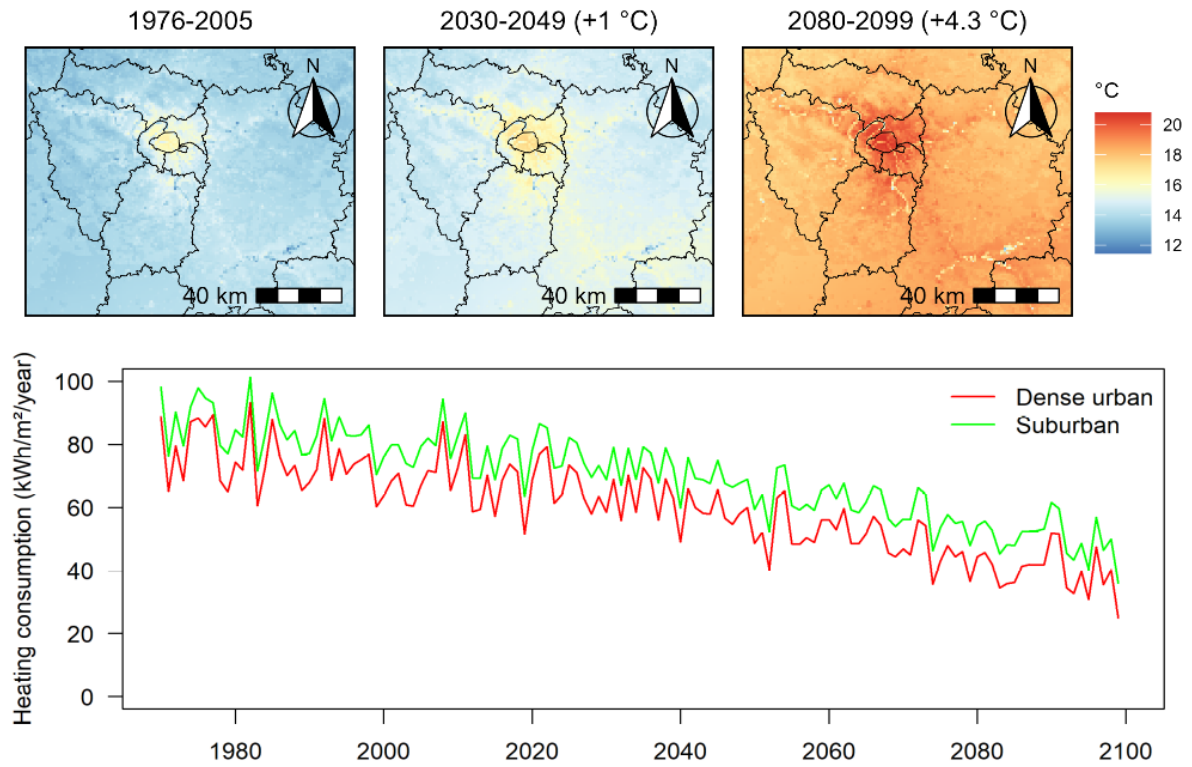
⁴⁴ "Some key figures that elected members could feed back into their speeches." (FNAU)

⁴⁵ "It's more like key figures that we give to show the need for action [...], it's meant to reinforce the message." (Plaine Commune)

⁴⁶ "I really think that there is not a great culture of mathematical graphs in urban planning and the population in general." (DRIEAT - Energy Climate)

⁴⁷ "For technicians like me, it allows us to understand how it was set up. It shouldn't be 70 pages long because we won't have the time. I read the quick notes that the Paris Region Institute makes, which are between 6 and 10 pages long." (Saint-Quentin-en-Yvelines)

⁴⁸ "If there are maps, we need explanations. To enable us to use them, to present them, and to answer the questions we will be asked." (Saint-Quentin-en-Yvelines)



	Number of hours in heat stress in summer		
	1976-2005	2020-2049	2070-2099
Dense urban	4 h 20 min	5 h	10 h 30 min
Suburban	4 h	4 h 50 min	9 h

Figure 9: Visual presented during the interviews, showing different ways of representing the future evolution of a given variable. By row: average summer nighttime temperature, yearly energy consumption due to heating, average number of hours in heat stress per summer day.

this way, the technical staff of a municipality can truly take ownership of these results and explain them themselves to their elected officials.

The second mode of diffusion should be raw data, that anyone can work on. Indeed, the interviews revealed that some of the stakeholders needed to perform their own tailored analysis at a smaller scale, or to cross-reference with sociodemographic or technical data ⁴⁹. Thus, a selection of interesting simulation outputs should be made available freely online. It would make sense to incorporate this into already existing platforms like DRIAS (<https://www.drias-climat.fr/>) from Météo-France, especially as it is becoming well-known by French public services. It is noteworthy to highlight that the respondents were not necessarily familiar with the format usually used for climate data (NetCDF files), therefore data should also be provided in a georeferenced format more common in the field of urban planning (e.g., Shapefiles, ASCII or geodatabase). Finally, once the data is available online, it appears imperative to publicize its existence and availability on a regular basis.

4 Recommendations and conclusions

These analyses gave a better understanding of the current practices of Île-de-France stakeholders in terms of their use of climate information for public policies in territorial development and urban planning, of their potential needs and expectations, and of who are the actors considered as reference for the UHI issue. This work made it possible to formulate a set of recommendations with a view to disseminating and promoting the current research results more effectively, and to provide guidelines for future studies.

With regard to the general dissemination strategy, several levels of information and data are expected. The results must be disseminated first as a level of information that is accessible and usable directly by all local authorities. The major issue is that every stakeholder can appropriate and use the data without the need for specific technical expertise, such as an internal geomatics department or a consulting firm, which not all municipalities have at their disposal. A second level of provision, with reworkable and geo-referenced data, is also expected by some of the stakeholders to carry out processing and analyzes based on their own expertise. Lastly, some of the scientific data produced can be shared in open access to other scientific communities of users (in particular by engineering firms) for feeding into new impact studies on finer spatial scales that address more diversified sectoral impacts.

To succeed in this transfer of data and knowledge, it is necessary to reinforce the visibility of the work already done, which is currently very insufficient because it is too restricted to the academic research community. With this aim, researchers must rely on key local interlocutors as relays between the field of research and the field of operationalization. Urban planning agencies can play this strategic role: they have both a very good understanding of scientific results, perfect knowledge of territorial policies, and a very well-established network of stakeholders and users. A generalization of this dissemination process to other cities in France will therefore require to systematically identify the entities that are located in these territories and active on climate and urban-overheating issues, in order to work with them. These could be the urban planning agencies in priority, some decentralized State services, but also local and regional climate and energy associations.

Several ways to improve the presentation of results were identified. Numerical modeling tools and their results are complex, therefore it is essential to clearly explain the configuration and the main concepts and assumptions of the simulations with the implications on the results (for example, the choice of a fixed land use and urbanization map must be justified). Besides, to effectively raise awareness on vulnerabilities, it seems more relevant to communicate on extreme conditions (e.g. during heatwaves) which often results

⁴⁹ "Planning agencies will want reusable data, where they can adapt the mode of representation, cross-reference with other data, etc." (FNAU)

in increased risks for population, urban systems and networks, rather than presenting annual average values that are usually not appropriately understood.

The stakeholder feedback highlighted that surface air temperature is considered to be a relevant tool for awareness and diagnosis of UHI and its evolution with climate change. In this way, a shortcut is too often made between surface temperature and UHI. To avoid confusion and in the absence of increased skills among stakeholders, we strongly suggest not to use surface temperature from satellite data to deal with UHI, as it does not represent the temperature felt by citizens, and does not compare with either modeled or measured surface air temperature. The selected panel of climate and impacts indicators is already very relevant and informative according to our results and does not necessarily need to be completed. Still, suggestions have been made to guide the calculation of indicators based on the stakeholders' needs, particularly for energy where municipalities are interested in annual consumption at the scale of their territory, when energy suppliers are rather interested in peaks of consumption in the region during extreme events. Respondents regularly express new perspectives and areas of interest on risk and impact assessment. The current tools and results do not meet all these expectations, but could serve as a basis for further studies by experts in the concerned fields.

To sum up, it is crucial to work for a good comprehension and accessibility of the data, to reinforce its diffusion through local operational actors, and to adapt the format to the different needs.

A final important point concerns climate projections. The time frames chosen for the presentation of climate change and impacts should be reviewed. Stakeholders are in demand of short- and medium-term prospective data that are in coherence with the temporality of political action and public policies, and could be a relevant support in decision-making for adaptation. The next few decades are of particular interest for public actors, which highlights the need to foster and improve projections at the decadal scale. Yet if such results are given, the uncertainties linked to natural variability must be properly highlighted. Regarding terminology, it could be more meaningful and understandable to speak of a "time horizon" (using a central year, e.g. "horizon 2035") rather than the corresponding 30-years climate period over which the analyses were performed (2020-2049). Finally, the feedback from respondents highlights the difficulty to deal with complex uncertainty representation (whether related to the dispersion of multimodel climate projections or to the different emission scenarios). When the aim is to raise awareness, we recommend simplifying the representations of uncertainties (showing for example the multimodel mean and a single scenario or level of warming). However, scientists should explain the importance of uncertainty in climate projections and convince stakeholders of the need to take it into account for the appropriate planning and sizing of adaptation levers. How to deal with uncertainties and communicate this information to decision makers is still an open question.

CRedit authorship contribution statement

J. André: Conceptualization, Data curation, Formal analysis, Investigation, Methodology, Visualization, Writing - original draft, Writing - review & editing. **B. Le Roy:** Data curation, Visualization, Writing - original draft, Writing - review & editing. **A. Lemonsu:** Conceptualization, Formal analysis, Funding acquisition, Investigation, Methodology, Project Administration, Supervision, Writing – original draft, Writing – review & editing. **M. Colombert:** Funding acquisition, Investigation, Methodology, Writing – review & editing. **V. Masson:** Funding acquisition, Writing – review & editing.

References

- E. Bocher, G. Petit, J. Bernard, and S. Palominos. A geoprocessing framework to compute urban indicators: The mapuce tools chain. *Urban climate*, 24:153–174, 2018.
- M. Bossard, J. Feranec, J. Othahel, et al. *CORINE land cover technical guide: Addendum 2000*, volume 40. European Environment Agency Copenhagen, 2000.
- G. P. Brasseur and L. Gallardo. Climate services: Lessons learned and future prospects. *Earth’s Future*, 4(3):79–89, 2016.
- P. Bröde, D. Fiala, K. Błażejczyk, I. Holmér, G. Jendritzky, B. Kampmann, B. Tinz, and G. Havenith. Deriving the operational procedure for the universal thermal climate index (utci). *International journal of biometeorology*, 56(3):481–494, 2012.
- B. Bueno, G. Pigeon, L. Norford, K. Zibouche, and C. Marchadier. Development and evaluation of a building energy model integrated in the teb scheme. *Geoscientific model development*, 5(2):433–448, 2012.
- J. G. Carter. Climate change adaptation in european cities. *Current Opinion in Environmental Sustainability*, 3(3):193–198, 2011.
- J. L. Champeaux, V. Masson, and F. Chauvin. Ecoclimap: a global database of land surface parameters at 1 km resolution. *Meteorological Applications: A journal of forecasting, practical applications, training techniques and modelling*, 12(1):29–32, 2005.
- J. Cortekar, S. Bender, M. Brune, and M. Groth. Why climate change adaptation in cities needs customised and flexible climate services. *Climate Services*, 4:42–51, 2016.
- M. Daniel, A. Lemonsu, M. Déqué, S. Somot, A. Alias, and V. Masson. Benefits of explicit urban parameterization in regional climate modeling to study climate and city interactions. *Climate Dynamics*, 52(5):2745–2764, 2019.
- F. Doblans-Reyes, A. Sörensson, M. Almazroui, A. Dosio, W. Gutowski, R. Haarsma, R. Hamdi, B. Hewitson, W.-T. Kwon, B. Lamptey, D. Maraun, T. Stephenson, I. Takayabu, L. Terray, A. Turner, and Z. Zuo. Linking global to regional climate change. In V. Masson-Delmotte, P. Zhai, A. Pirani, S. Connors, C. Péan, S. Berger, N. Caud, Y. Chen, L. Goldfarb, M. Gomis, M. Huang, K. Leitzell, E. Lonnoy, J. Matthews, T. Maycock, T. Waterfield, O. Yelekçi, R. Yu, and B. Zhou, editors, *Climate Change 2021: The Physical Science Basis. Contribution of Working Group I to the Sixth Assessment Report of the Intergovernmental Panel on Climate Change*, page 1363–1512. Cambridge University Press, Cambridge, United Kingdom and New York, NY, USA, 2021. doi: 10.1017/9781009157896.012.
- F. Duchêne, R. Hamdi, B. Van Schaeybroeck, S. Caluwaerts, R. De Troch, L. De Cruz, and P. Termonia. Downscaling ensemble climate projections to urban scale : Brussels’s future climate at 1.5 °c, 2 °c, and 3 °c global warming. *Urban Climate*, 46:19, 2022.
- I. Eliasson. The use of climate knowledge in urban planning. *Landscape and Urban Planning*, 48(1): 31–44, 2000. ISSN 0169-2046. doi: [https://doi.org/10.1016/S0169-2046\(00\)00034-7](https://doi.org/10.1016/S0169-2046(00)00034-7). URL <https://www.sciencedirect.com/science/article/pii/S0169204600000347>.
- D. Fiala, G. Havenith, P. Bröde, B. Kampmann, and G. Jendritzky. Utc-fiala multi-node model of human heat transfer and temperature regulation. *International journal of biometeorology*, 56(3):429–441, 2012.

- T. Gardes, R. Schoetter, J. Hidalgo, N. Long, E. Marquès, and V. Masson. Statistical prediction of the nocturnal urban heat island intensity based on urban morphology and geographical factors—an investigation based on numerical model results for a large ensemble of french cities. *Science of The Total Environment*, 737:139253, 2020.
- R. Giordano, K. Pilli-Sihvola, I. Pluchinotta, R. Matarrese, and A. Perrels. Urban adaptation to climate change: Climate services for supporting collaborative planning. *Climate Services*, 17:100100, 2020.
- C. Hewitt, S. Mason, and D. Walland. The global framework for climate services. *Nature Climate Change*, 2:831–832, 2012.
- P. Hoffmann, R. Schoetter, and K. Schlünzen. Statistical-dynamical downscaling of the urban heat island in hamburg, germany. *Meteorologische Zeitschrift*, 27(2):89–109, 07 2018.
- IPCC. *Climate Change 2022: Impacts, Adaptation and Vulnerability. Contribution of Working Group II to the Sixth Assessment Report of the Intergovernmental Panel on Climate Change*. Cambridge University Press, Cambridge, UK and New York, NY, USA, 2022. doi: 10.1017/9781009325844. URL https://report.ipcc.ch/ar6/wg2/IPCC_AR6_WGII_FullReport.pdf.
- D. Jacob, J. Petersen, B. Eggert, A. Alias, O. B. Christensen, L. M. Bouwer, A. Braun, A. Colette, M. Déqué, G. Georgievski, et al. Euro-cordex: new high-resolution climate change projections for european impact research. *Regional environmental change*, 14(2):563–578, 2014.
- D. Jacob, C. Teichmann, S. Sobolowski, E. Katragkou, I. Anders, M. Belda, R. Benestad, F. Boberg, E. Buonomo, R. M. Cardoso, et al. Regional climate downscaling over europe: perspectives from the euro-cordex community. *Regional environmental change*, 20(2):1–20, 2020.
- K. L. Jacobs and R. B. Street. The next generation of climate services. *Climate Services*, 20:100199, 2020.
- T. R. Karl, N. Nicholls, and A. Ghazi. Clivar/gcos/wmo workshop on indices and indicators for climate extremes workshop summary. *Weather and climate extremes: Changes, variations and a perspective from the insurance industry*, pages 3–7, 1999.
- Y. T. Kwok, R. Schoetter, K. K.-L. Lau, J. Hidalgo, C. Ren, G. Pigeon, and V. Masson. How well does the local climate zone scheme discern the thermal environment of toulouse (france)? an analysis using numerical simulation data. *International Journal of Climatology*, 39(14):5292–5315, 2019.
- G. S. Langendijk, D. Rechid, and D. Jacob. Urban areas and urban–rural contrasts under climate change: what does the euro-cordex ensemble tell us?—investigating near surface humidity in berlin and its surroundings. *Atmosphere*, 10(12):730, 2019.
- B. Le Roy. *Méthodologie d’étude des impacts du changement climatique sur la ville par descente d’échelle statistico-dynamique: application à la région parisienne*. PhD thesis, Université Paul Sabatier-Toulouse III, 2021.
- B. Le Roy, A. Lemonsu, R. Kouunkou-Arnaud, D. Brion, and V. Masson. Long time series spatialized data for urban climatological studies: a case study of paris, france. *International Journal of Climatology*, 40(7):3567–3584, 2020.
- B. Le Roy, A. Lemonsu, and R. Schoetter. A statistical–dynamical downscaling methodology for the urban heat island applied to the euro-cordex ensemble. *Climate Dynamics*, 56(7):2487–2508, 2021.

- B. Le Roy, A. Lemonsu, R. Schoetter, and T. Machado. Study of the future evolution of the urban climate of paris by statistical-dynamical downscaling of the euro-cordex ensemble. *Journal of Applied Meteorology and Climatology*, 2024.
- A. Lemonsu, V. Masson, L. Shashua-Bar, E. Erell, and D. Pearlmutter. Inclusion of vegetation in the town energy balance model for modelling urban green areas. *Geoscientific Model Development*, 5(6):1377–1393, 2012.
- A. Lemonsu, C. de Munck, R. Koukoku-Arnaud, V. Masson, and V. Vigié. What alternatives does paris have to adapt to future heat waves? *Urban Climate Science for Planning Healthy Cities*, pages 239–258, 2021.
- D. Li and E. Bou-Zeid. Synergistic interactions between urban heat islands and heat waves: The impact in cities is larger than the sum of its parts. *Journal of applied Meteorology and Climatology*, 52(9):2051–2064, 2013.
- P. Lucas-Picher, D. Argüeso, E. Brisson, Y. Trambly, P. Berg, A. Lemonsu, S. Kotlarski, and C. Caillaud. Convection-permitting modeling with regional climate models: Latest developments and next steps. *WIREs Climate Change*, 12(6):e731, 2021.
- V. Masson. A physically-based scheme for the urban energy budget in atmospheric models. *Boundary-layer meteorology*, 94(3):357–397, 2000.
- V. Masson, P. Le Moigne, E. Martin, S. Faroux, A. Alias, R. Alkama, S. Belamari, A. Barbu, A. Boone, F. Bouyssel, et al. The surfexv7. 2 land and ocean surface platform for coupled or offline simulation of earth surface variables and fluxes. *Geoscientific Model Development*, 6(4):929–960, 2013.
- V. Masson, J. Hidalgo, A. Amossé, F. Belaid, E. Bocher, M. Bonhomme, A. Bourgeois, G. Bretagne, S. Caillerez, E. Cordeau, et al. Urban climate, human behavior & energy consumption: from lcz mapping to simulation and urban planning (the mapuce project). In *9th International Conference on Urban Climate*, 2015.
- V. Masson, A. Lemonsu, J. Hidalgo, and J. Voogt. Urban climates and climate change. *Annual Review of Environment and Resources*, 45(1):411–444, 2020.
- E. P. Maurer, L. Brekke, T. Pruitt, and P. B. Duffy. Fine-resolution climate projections enhance regional climate change impact studies. *Eos, Transactions American Geophysical Union*, 88:504, 2007.
- J. Noilhan and S. Planton. A simple parameterization of land surface processes for meteorological models. *Monthly weather review*, 117(3):536–549, 1989.
- M. Nunez and T. R. Oke. The energy balance of an urban canyon. *Journal of Applied Meteorology and Climatology*, 16(1):11–19, 1977.
- T. R. Oke, G. Mills, A. Christen, and J. A. Voogt. *Urban Climates*. Cambridge University Press, 2017. doi: 10.1017/9781139016476.
- M. Pascal, S. Gorla, V. Wagner, M. Sabastia, A. Guillet, E. Cordeau, C. Mauclair, and S. Host. Greening is a promising but likely insufficient adaptation strategy to limit the health impacts of extreme heat. *Environment International*, 151:106441, 2021a.
- M. Pascal, R. Lagarrigue, A. Tabai, I. Bonmarin, S. Camail, K. Laaidi, A. Le Tertre, and S. Denys. Evolving heat waves characteristics challenge heat warning systems and prevention plans. *International journal of biometeorology*, 65:1683–1694, 2021b.

- E. Redon, A. Lemonsu, and V. Masson. An urban trees parameterization for modeling microclimatic variables and thermal comfort conditions at street level with the town energy balance model (teb-surfex v8. 0). *Geoscientific Model Development*, 13(2):385–399, 2020.
- E. C. Redon, A. Lemonsu, V. Masson, B. Morille, and M. Musy. Implementation of street trees within the solar radiative exchange parameterization of teb in surfex v8. 0. *Geoscientific Model Development*, 10(1):385–411, 2017.
- R. Salgado and P. Le Moigne. Coupling of the flake model to the surfex externalized surface model. *Boreal Environment Research*, 15:231–244, 2010. ISSN 1797-2469.
- R. Schoetter, V. Masson, A. Bourgeois, M. Pellegrino, and J.-P. Lévy. Parametrisation of the variety of human behaviour related to building energy consumption in the town energy balance (surfex-teb v. 8.2). *Geoscientific Model Development*, 10(7):2801–2831, 2017.
- I. D. Stewart and T. R. Oke. Local climate zones for urban temperature studies. *Bulletin of the American Meteorological Society*, 93(12):1879–1900, 2012.
- M. Suher-Carthy, T. Lagelouze, J. Hidalgo, R. Schoetter, N. Touati, R. Jouglu, and V. Masson. Urban heat island intensity maps and local weather types description for a 45 french urban agglomerations dataset obtained from atmospheric numerical simulations. *Data in Brief*, page 109437, 2023.
- R. Swart, L. Celliers, M. Collard, A. G. Prats, J.-T. Huang-Lachmann, F. L. Sempere, F. de Jong, M. Máñez Costa, G. Martinez, M. P. Velazquez, A. R. Martín, W. Segretier, E. Stattner, and W. Timmermans. Reframing climate services to support municipal and regional planning. *Climate Services*, 22:100227, 2021.
- J. Takakura, S. Fujimori, K. Takahashi, Y. Hijioka, T. Hasegawa, Y. Honda, and T. Masui. Cost of preventing workplace heat-related illness through worker breaks and the benefit of climate-change mitigation. *Environmental Research Letters*, 12(6):064010, 2017.
- N. Tornay, R. Schoetter, M. Bonhomme, S. Faraut, and V. Masson. Genius: A methodology to define a detailed description of buildings for urban climate and building energy consumption simulations. *Urban Climate*, 20:75–93, 2017.
- V. Vignié, A. Lemonsu, S. Hallegatte, A.-L. Beaulant, C. Marchadier, V. Masson, G. Pigeon, and J.-L. Salagnac. Early adaptation to heat waves and future reduction of air-conditioning energy use in paris. *Environmental Research Letters*, 15(7):075006, jul 2020.
- WCC3. World climate conference-3 conference statement 2009), available via <http://go.nature.com/beqma6>. 2009.
- L. Zhang and C. Yuan. Multi-scale climate-sensitive planning framework to mitigate urban heat island effect: A case study in singapore. *Urban Climate*, 49:101451, 2023. ISSN 2212-0955. doi: <https://doi.org/10.1016/j.uclim.2023.101451>. URL <https://www.sciencedirect.com/science/article/pii/S2212095523000457>.
- X. Zhang, L. Alexander, G. C. Hegerl, P. Jones, A. K. Tank, T. C. Peterson, B. Trewin, and F. W. Zwiers. Indices for monitoring changes in extremes based on daily temperature and precipitation data. *WIREs Climate Change*, 2(6):851–870, 2011. ISSN 1757-7799. doi: 10.1002/wcc.147.

A Appendix - Logical framework diagram for the interviews

The logical framework diagrams shown in fig. 10 and ?? highlight the chronology and the logical links between the questions that we asked during the interviews.

B Appendix - Climate simulations and impact indicators

The research work that motivated and fed the reflection on the information dissemination to potential actors and users comes from the PhD thesis of Le Roy [2021]. An original methodology has been developed to study the impacts of climate change in cities, taking into account the evolution of the regional climate and its interactions with the local urban climate generated by the city itself. This methodology was applied to the Paris region to produce a set of multi-sectoral indicators (described below) reflecting the evolution of the impacts of climate change at city-scale during the 21st century and according to two greenhouse gas emission scenarios. This required three major steps: (1) to configure an urban climate model, as well as associated descriptive databases, for the Paris region ; (2) to spatially downscale climate projections provided by regional climate models to run the urban model with atmospheric conditions tailored to city-scale ; (3) to define and calculate indicators to quantify some relevant impacts on urban climate, thermal comfort and energy consumption.

Urban climate model

Here, the future evolution of Paris urban climate is simulated using the modelling platform SURFEX (*Surface Externalisée*; Masson et al. [2013]) that describes and processes the surface with a regular square-mesh 2D grid. SURFEX combines three main land surface models devoted, respectively, to rivers and inland waters (FLake; Salgado and Le Moigne [2010]), natural soils and vegetation covers (Interaction Sol-Biosphere-Atmosphere (ISBA); Noilhan and Planton [1989]), and urban areas (Town Energy Balance (TEB); Masson [2000]).

TEB is a state-of-the-art urban canopy model for meteorological modelling applications, covering horizontal resolutions from few hundred meters to several kilometers. This is a parametrization that does not explicitly resolve each building but applies the average urban canyon assumption [Nunez and Oke, 1977] at the model mesh scale. This simple shaped canyon is defined by average parameters for geometry, land use and surface distribution, material properties, etc. This set of parameters is mapped according to the model grid to reflect to some extent the heterogeneity of the urban landscape. TEB incorporates urban vegetation in interaction with the built environment [Lemonsu et al., 2012], by separating the ground vegetation and the tree-foliage layer [Redon et al., 2017, 2020]. TEB also includes a building energy module (BEM; Bueno et al. [2012]) that resolves internal balance of buildings in interaction with outdoor climate conditions.

Data and hypotheses for simulation

The simulation domain is a 157 km \times 128 km rectangle covering the entire Île-de-France region with square meshes of 1 km sides. The descriptive characteristics of the study area that the land surface models need to run are derived from several databases. The land cover mapping of natural areas (crops, forests, grasslands, etc.) around the Paris urban area, is provided by the ECOCLIMAP-I database [Champeaux et al., 2005]), derived from the CORINE Land Cover European inventory [Bossard et al., 2000]) (and dating from the 1990s. For urban areas, the more recent and accurate data produced during the MApUCE project are used. They improve among other things the representation of land use, urban morphology [Bocher et al., 2018], materials of buildings and their physical properties [Tornay et al.,

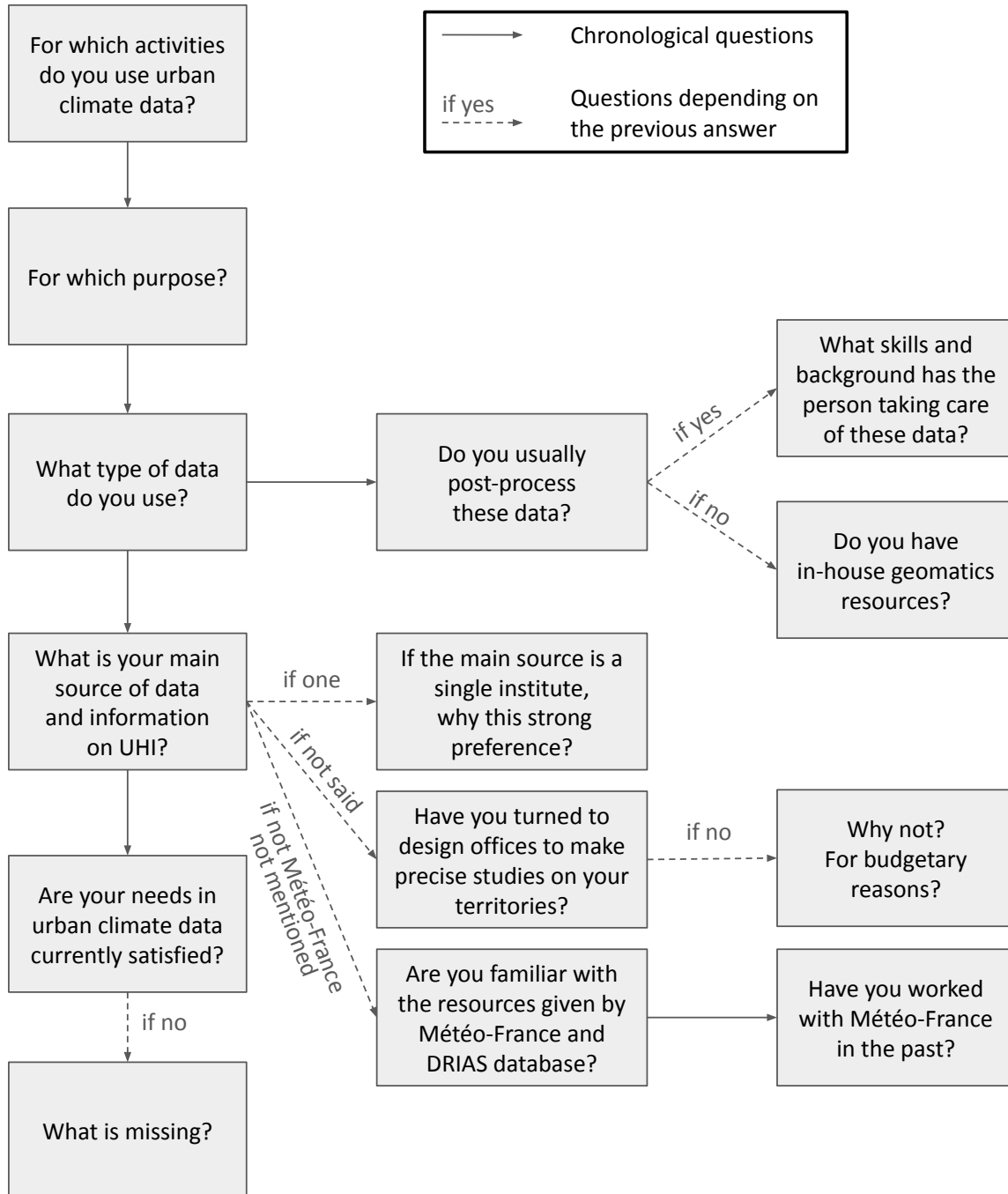


Figure 10: Logical framework diagram of the interview grid, Part 1: What are your current usage and need of urban climate data?

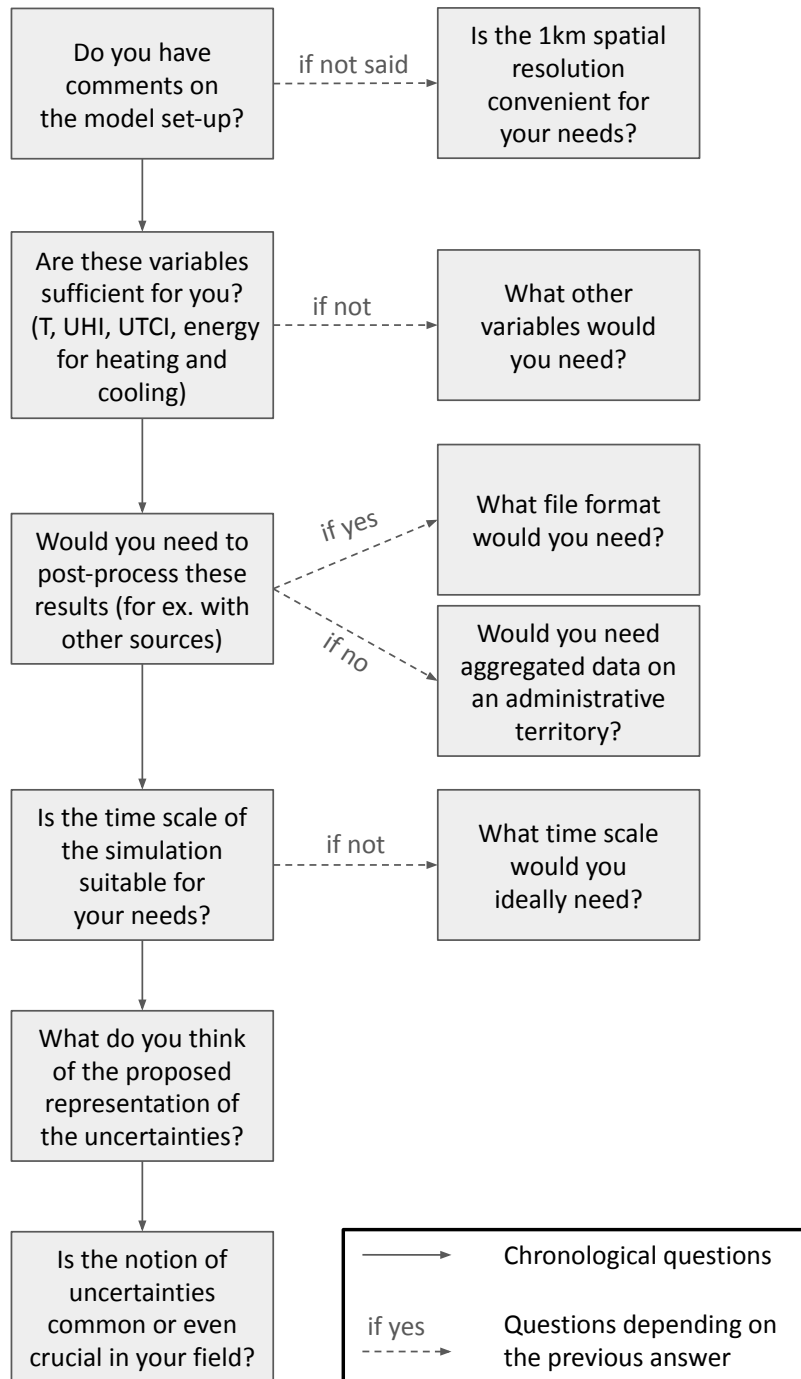


Figure 11: Logical framework diagram of the interview grid, Part 2: Feedbacks about current results on future urban climate?

2017], and building usage typologies (residential, tertiary, commercial and industrial). This data was combined with a more accurate description of urban vegetation, distinguishing between ground-based and tree-vegetation strata, provided by the region urban planning agency.

This description of the region and the urban area is prescribed as fixed data, i.e. it remains unchanged for the complete study time period.

Local climate conditions over the 21st century

To simulate the evolution of the urban climate with climate change, the surface modelling platform was fed by atmospheric conditions provided by regional climate projections, first adapted to local and urban scales. This so-called statistical-dynamical downscaling methodology is described in details by [Le Roy et al., 2021, 2024]. It corrects the regional atmospheric fields to incorporate the city’s air temperature footprint on the local atmosphere, which is not explicitly taken into account by the regional climate models [Daniel et al., 2019, Langendijk et al., 2019]).

A set of 55 climate projections has been processed from the EURO-CORDEX database [Jacob et al., 2014, 2020], using different pairs of general circulation and regional climate models, allowing the spread of climate models to be considered. The data cover the domain of interest with a horizontal resolution of 1 km, and the time period 1970–2099 continuously. They include 14 projections with the moderate emission scenario RCP4.5 and 41 projections with the high emission scenario RCP8.5. Before running the urban climate simulations, the regional climate projections used to drive the urban climate model were bias adjusted. This correction was carried out for the air temperature, as some of the impact indicators calculated can be very sensitive to thresholds being crossed (e.g. the activation of heating or air conditioning in buildings). A conservative adjustment of the average monthly temperature was chosen in order to maintain the representation of local climatic conditions simulated by the regional climate models. (see [Le Roy et al., 2024] for more details).

Impact indicators and main results

The use of the SURFEX platform including the TEB dedicated urban model makes it possible to compute meteorological variables and to derive more specific multi-sectoral indicators (summarized in table 1) that are of interest for public stakeholders or decision makers. One of the main question regarding the impact of climate change on the urban climate is related to the expected evolution of the UHI phenomenon. Prior studies have found conflicting results and are quite uncertain because of different methodologies [Doblas-Reyes et al., 2021]. The use of SURFEX and TEB makes it possible to analyze this evolution by comparing the urban and rural temperatures throughout the century. Le Roy et al. [2020] have proposed two indicators of the UHI, one focusing on its intensity and the other one on its extent (i.e. the area of the city where the temperature is a certain number of degrees higher than in the rural area).

To be able to quantify the outdoor thermal comfort of inhabitants inside the city beyond simply using the air temperature, a simplified version of Fiala et al. [2012]’s Universal Thermal Comfort Index (UTCI) has been implemented in TEB [Kwok et al., 2019, Redon et al., 2020]. The UTCI model computes a perceived temperature based on the thermal exchanges between an individual and the outdoor atmospheric conditions. It relies on the individual’s physical characteristics, its clothing, and level of activity, as well as the temperature, humidity, radiation and wind conditions in the street. The UTCI scale (in °C) is divided into 10 classes of thermal stress [Bröde et al., 2012] ranging from “Extreme Cold Stress” (UTCI < -40 °C) to “Extreme Heat Stress” (UTCI > +46 °C).

In TEB, the UTCI is computed at every dynamical step of the model for every urban grid point, which allows knowing how much time per hour was spent in each class. The results can then be aggregated in

time: average number of hours per day spent in some stress class, or in space: average conditions per type of building or land cover (fig. 9).

The last indicator that was studied is the energy consumption of buildings due to heating and cooling. It is simulated thanks to the BEM module. The amount of energy consumed depends on the air temperature outside the building as well as a setpoint temperature inside the building. Depending on the type of buildings and their usage, different setpoint temperatures and hours of occupancy are defined. Other behaviors are also taken into account, such as ventilation by opening the windows or the use of shading.

ENVIRONMENTAL RESEARCH
LETTERS

LETTER







Winter climate preconditioning of summer vegetation extremes in the Northern Hemisphere

OPEN ACCESS

RECEIVED
8 February 2024REVISED
4 July 2024ACCEPTED FOR PUBLICATION
12 July 2024PUBLISHED
14 August 2024

Original Content from this work may be used under the terms of the [Creative Commons Attribution 4.0 licence](#).

Any further distribution of this work must maintain attribution to the author(s) and the title of the work, journal citation and DOI.

Mohit Anand^{1,2,*} , Raed Hamed³ , Nora Linscheid⁴, Patrícia S Silva⁵ , Julie Andre^{6,7}, Jakob Zscheischler^{1,2,8} , Freya K Garry⁹  and Ana Bastos^{4,10} ¹ Department of Compound Environmental Risks, Helmholtz Centre for Environmental Research—UFZ, Leipzig, Germany² Technische Universität Dresden, Dresden, Germany³ Department of Water and Climate Risk, Institute for Environmental Studies (IVM), Vrije Universiteit Amsterdam, Amsterdam, The Netherlands⁴ Max Planck Institute for Biogeochemistry, Jena, Germany⁵ Universidade de Lisboa, Faculdade de Ciências, Instituto Dom Luiz, Lisboa, Portugal⁶ Laboratoire de Météorologie Dynamique / Institut Pierre Simon Laplace, ENS—PSL Université, Ecole Polytechnique—Institut Polytechnique de Paris, Sorbonne Université, CNRS, Palaiseau, France⁷ Ecole des Ponts, Champs-sur-Marne, France⁸ Center for Scalable Data Analytics and Artificial Intelligence (ScaDS.AI), Dresden-Leipzig, Germany⁹ Met Office, Fitzroy Road, Exeter EX1 3PB, United Kingdom¹⁰ Institute for Earth System Science and Remote Sensing, Leipzig University, Leipzig, Germany

* Author to whom any correspondence should be addressed.

E-mail: mohit.anand@ufz.de

Keywords: winter climate, leaf area index extremes, legacy effects, vegetation activity, compound events

Abstract

The impact of the spring climate on the Northern Hemisphere's summer vegetation activity and extremes has been extensively researched, but less attention has been devoted to whether and how the winter climate may additionally influence vegetation extremes in the summer. Here, we provide insights into the influence of winter temperature and precipitation on summer vegetation extremes in the Northern Hemisphere. To do this, we identify positive and negative extremes in the summer leaf area index (LAI, a proxy for vegetation activity) and assess winter effects on those extremes using logistic regression at the regional scale. Over a quarter of the regions in the Northern Hemisphere show strong winter climate preconditioning on summer LAI extremes, which is typically stronger for croplands than forests. In regions with strong winter preconditioning, the spring LAI mediates the link between winter climate and summer LAI extremes through the ecological memory in seasonal legacy effects. Our findings suggest that extremely low summer LAI in both croplands and forests is preconditioned by colder and drier winters, while extremely high summer LAI in forests is associated with warmer and wetter winters. For low summer LAI in croplands, warmer winters are associated with an increased likelihood of extremes in mid-latitude regions and a reduced likelihood in high-latitude regions. Consideration of winter preconditioning effects may improve our understanding of inter-annual variability of vegetation activity and support agricultural and land management practitioners in anticipating the detrimental effects of winter on crop yields and forest conditions.

1. Introduction

Global vegetation activity is strongly influenced by the variability in climatic conditions on sub-seasonal to decadal timescales, with the relative importance of temperature, radiation and water availability varying regionally (Ding *et al* 2020, Menzel *et al* 2020). Both the interannual climate variability (Nemani *et al*

2003, Bastos *et al* 2013, Gonsamo *et al* 2016, Zhu *et al* 2017) as well as climatic trends (Peng *et al* 2011, Piao *et al* 2011, 2014, Barichivich *et al* 2013, Fu *et al* 2015, Peñuelas *et al* 2017, Wang *et al* 2018a) directly influence the year-to-year differences in vegetation activity and carbon uptake. Understanding the seasonal predictability of future vegetation growth that emerges from climate variability may also assist agricultural

practitioners with planning and decision-making (e.g. Ogallo *et al* 2000, Bruno Soares 2017, An-Vo *et al* 2021).

Memory in land-surface properties—so-called preconditioning or legacy effects—can contribute to the lagged influence of seasonal climate anomalies. For example, winter precipitation and snowmelt can influence vegetation growth over the next growing season in water-limited regions (Peng *et al* 2010, Chen *et al* 2018). Vegetation activity itself can also mediate seasonal legacy effects, which can result in contrasting impacts throughout the growing season. Vegetation-mediated legacy effects arise, for example, in response to warmer spring temperatures than usual, resulting in increased springtime plant activity (Buermann *et al* 2018). This earlier onset of the growing season causes higher water use and faster water depletion until summer (Wolf *et al* 2016, Lian *et al* 2020, Bastos *et al* 2020a, Li *et al* 2022), with especially severe impacts during warm and dry summers (Bastos *et al* 2020a, Bevacqua *et al* 2021). The spring phenology may also influence autumn senescence timing, although the mechanisms of this relationship are not yet fully understood (Liu *et al* 2016).

While the preconditioning effects of spring warming have been widely studied, the influence of the winter climate on spring and summer vegetation activity is not so well understood. For example, warmer winter temperatures can lead to increased vegetation growth by increasing the water supply from glacial melting (Zhang *et al* 2016). However, warm winters can also have negative effects on plant growth due to the reduction in protective snow cover (Kreyling 2010) and fewer chilling days (Tominaga *et al* 2022). Warm winters that induce an earlier onset of the growing season may increase the risk of frost exposure in the leafing, budding and blossoming stages (Marino *et al* 2011, Bigler and Bugmann 2018), and such events could become more likely under climate change in some regions (Pfleiderer *et al* 2019, Vautard *et al* 2023). Short but extreme warming events have been shown to severely damage sub-Arctic landscapes, leading to considerably reduced summer growth (Bokhorst *et al* 2009).

There is mounting evidence of the influence of winter snow on the timing and productivity of the growing season across the Northern Hemisphere (Wang *et al* 2018b, Kelsey *et al* 2021) and the influence of winter precipitation on net primary productivity during the early growing season in forest–grassland ecosystems (Liu *et al* 2022). Chen *et al* (2018) investigated the preconditioning effects of winter temperature and precipitation on spring vegetation activity across Europe and North America and also found that reduced winter precipitation limited the spring vegetation activity over water-limited regions. In their study, the inclusion of climate information from the

previous season in regression models improved their capability to predict (the normalized difference vegetation index, a proxy for vegetation greenness). In Central Europe, winter teleconnections (including those associated with the North Atlantic Oscillation, the East Atlantic and the Scandinavian Patterns) significantly influence vegetation productivity during the growing season (Bastos *et al* 2016, Gonsamo *et al* 2016, Zhu *et al* 2017). Winter legacy effects may reach beyond the spring season, and compensatory effects across seasons also have to be considered (Buermann *et al* 2018, Bastos *et al* 2020a). To our knowledge, no studies have yet systematically addressed the impact of winter climate on vegetation activity extremes in subsequent summers.

Here, we assess the effect of interannual variability in the winter climate conditions on the vegetation activity extremes in the following summer across the Northern Hemisphere between 1982 and 2020. We use the leaf area index (LAI) as a proxy for vegetation activity and study the effect of winter temperature and precipitation on summer LAI extremes using logistic regression. Our study focuses on sub-continental regions and examines crops and forests separately, given the different controls on phenology, growth and stress responses between these two land cover types (Aspinwall *et al* 2015, Liu *et al* 2021, Miguez-Macho and Fan 2021).

2. Data and methods

2.1. Data

2.1.1. LAI

LAI data for the Northern Hemisphere were obtained from the GLOBMAP global LAI Version 3 product (Liu *et al* 2012). The GLOBMAP LAI combines data from the Moderate Resolution Imaging Spectroradiometer and the Advanced Very High Resolution Radiometer to provide a long-term LAI dataset from 1981 to 2020 at an 8 km spatial horizontal resolution. The LAI temporal resolution was fortnightly from 1981 to 2000 and at eight-day intervals from 2001 onwards. The LAI data were gridded to a spatial resolution of $0.25^\circ \times 0.25^\circ$ using area-weighted averages. In our analysis, we use data from 1982 to 2020.

2.1.2. Climate variables

Climate data were obtained from the European Centre for Medium-Range Weather Forecasts' ERA5 reanalysis (Hersbach *et al* 2020). We use monthly total precipitation (P), temperature at 2 m (T), total column volumetric soil water content and snow depth for the period 1982–2020 over the Northern Hemisphere (25° – 75° North). ERA5 data are provided on a regular lat/lon grid with $0.25^\circ \times 0.25^\circ$ spatial resolution.

2.1.3. Land cover

We use the European Space Agency Land Cover dataset (Santoro *et al* 2017) to quantify the fraction of forest and crop cover for each grid cell. The original land cover classification data are provided at 300 m spatial resolution for the period 1982–2019, and we regrid these data to a 0.25° lat/lon grid using the LC-CCI user tool. We use the lookup table from Poulter *et al* (2015), reproduced in table A1, to classify crop and forest grid cells. We aggregate the classes 10, 20 and 30 to represent cropland, and the classes 40–100 to represent forest. To minimise the influence of land cover changes in our analysis, only locations that are classified as forest or cropland for the entire 38 years are used for further analysis.

2.1.4. Reference regions

To explore the distinct regional dynamics over the Northern Hemisphere, we use the Intergovernmental Panel on Climate Change's (IPCC) Sixth Assessment Report Working Group I reference regions (Iturbide *et al* 2020). Of the 46 land regions, we only consider regions in the Northern Hemisphere and further remove regions if the crop cover or forest cover amounts to less than 100 grid cells. We analyse the vegetation activity of 19 regions in the Northern Hemisphere: 17 regions include both cropland and forest, the Russian Arctic (RAR) region contains only forests, and Eastern Central Asia contains only crops (figure A1). This leads to two different but largely overlapping sets of 18 regions (table A2).

2.2. Data preprocessing

We are interested in analysing how the climate affects the interannual variability of the summer LAI. To do this, we preprocess the data by taking the seasonal average precipitation, temperature, soil moisture, snow depth and LAI for boreal winter (December, January and February), spring (March, April and May) and summer (June, July and August). The seasonal averages are linearly detrended to remove potential long-term trends due to climate change since our interest is in the interannual variability. The detrended data are then standardised to unit variance. We identify high (LAI_{high}) and low (LAI_{low}) summer LAI extremes using the local (pixel-wise) 90th and 10th percentiles of the detrended and standardised seasonal LAI averages. To analyse the trends in the fraction of pixels with extreme LAI for each year, we use the Mann–Kendall non-parametric test (Mann 1945, Kendall 1975).

We separately consider croplands and forest areas in our results, referring to low and high summer LAI extremes for croplands as $\text{LAI}_{\text{low}}^{\text{crop}}$ and $\text{LAI}_{\text{high}}^{\text{crop}}$, and respectively for forest areas as $\text{LAI}_{\text{low}}^{\text{forest}}$ and $\text{LAI}_{\text{high}}^{\text{forest}}$.

2.3. Quantifying winter preconditioning effects

Logistic regression is a suitable method to analyse drivers of extreme impacts (Vogel *et al* 2021, Le Grix *et al* 2023) and specifically preconditioned compound events (Zscheischler *et al* 2020, Bevacqua *et al* 2021, Bastos *et al* 2023). Here, we extend the approach proposed by Bevacqua *et al* (2021) for the study of preconditioning effects of meteorological conditions on LAI extremes.

To quantify the importance of winter preconditioning, we train two separate logistic regression models to predict summer LAI extremes. The first model uses only spring and summer meteorological predictors (temperature and precipitation), while the second model additionally includes winter meteorological predictors. The first model is represented as

$$\mathbb{P}(\text{LAI}_{\text{extreme}} | \setminus w) = \frac{1}{1 + \exp(-X_{\text{extreme}}^{\setminus w})}$$

$$\text{with } X_{\text{extreme}}^{\setminus w} = \alpha_0 + \alpha_1 T_{\text{su}} + \alpha_2 P_{\text{su}} + \alpha_3 T_{\text{sp}} + \alpha_4 P_{\text{sp}}. \quad (1)$$

Here, T_{su} and T_{sp} correspond to the temperature in summer and spring, and P_{su} and P_{sp} correspond to the precipitation in summer and spring, respectively. Regression coefficients are given by $\alpha_0, \dots, \alpha_4$. Extreme summer LAI is abbreviated as $\text{LAI}_{\text{extreme}}$, where extremes can be low or high. The term $\setminus w$ indicates that winter climate was not included for this particular model. The model is used to predict how likely the occurrence of extreme summer LAI in summer is without considering the influence of winter climate, $\mathbb{P}(\text{LAI}_{\text{extreme}} | \setminus w)$.

The second model additionally includes the winter temperature (T_w) and winter precipitation (P_w) as well as their corresponding regression coefficients α_5 and α_6 :

$$\mathbb{P}(\text{LAI}_{\text{extreme}} | w) = \frac{1}{1 + \exp(-X_{\text{extreme}}^w)}$$

$$\text{with } X_{\text{extreme}}^w = \alpha_0 + \alpha_1 T_{\text{su}} + \alpha_2 P_{\text{su}} + \alpha_3 T_{\text{sp}} + \alpha_4 P_{\text{sp}} + \alpha_5 T_w + \alpha_6 P_w. \quad (2)$$

We train the logistic regression models based on pooled data for cropland and forest pixels separately and for each region. This increases the sample size, allowing us to analyse regional patterns but not sub-regional variability. We further consider LAI_{high} and LAI_{low} separately so that we consider 72 pairs of models for the Northern Hemisphere (two land-cover types, 18 regions, two types of extremes). The sample size N varies per region depending on the number of crop and forest pixels within that region ($N = n_{\text{years}} \times n_{\text{pixels}}$, table A2).

Rearranging the logistic regression equation, $X_{\text{extreme}} = \ln\left(\frac{\mathbb{P}(\text{LAI}_{\text{extreme}})}{1 - \mathbb{P}(\text{LAI}_{\text{extreme}})}\right)$, which are the log odds.

Hence, for interpretation of the fitted model, we take the exponential raised to the power of the coefficient of the logistic regression model as they provide a more direct interpretation with respect to the odds of experiencing an extreme over no extreme, $\frac{IP(LAI_{extreme})}{1-IP(LAI_{extreme})}$; for example, for a unit increase in T_w or P_w and keeping all the other variables fixed, the odds of experiencing an extreme relative to a non-extreme LAI change by e^{α_5} or e^{α_6} , respectively.

The model without winter climate (equation (1)) is a nested model with respect to the model with winter climate (equation (2)), as the latter contains all the parameters of the former as well as the parameters α_5 and α_6 . We therefore test whether including the winter climate significantly improves the prediction of summer LAI extremes using the likelihood ratio test with significance level $\alpha = 0.05$. The likelihood ratio test assesses the goodness of fit of two competing nested statistical models and provides a p -value associated with the null hypothesis that both models are equally good. A low p -value therefore means that the model with more parameters is better than the model with fewer parameters.

Given the very large sample size for each region (table A2), the likelihood ratio test might show significant differences even when the differences in predictability between the models are very small. To rank model differences across regions, we use the receiver operating characteristics curve, which is the plot of the true positive rate against the false positive rate for different threshold settings for a binary classifier. The area under the receiver operating characteristics curve (AUROC) is then a predictive performance metric ranging between 0 and 1, with a value of 0.5 representing prediction by random chance and a value of 1 representing perfect prediction. We quantify the strength of winter preconditioning based on the difference in AUROC between models with winter predictors (AUROC|w) and models without winter predictors (AUROC|\w).

For regions with strong winter preconditioning, we further analyse the standardised seasonal averages of anomalies in meteorological variables (i.e. composites) in the years with extreme LAI in summer to complement the interpretation of the results based on the logistic regression coefficients. We create composites from the predictors used in the logistic regression and also consider a few additional variables: winter, spring and summer precipitation, temperature, soil moisture, winter and spring snow depth, and spring LAI. As there is no snow in summer in many of the regions, we exclude summer snow from our analysis. We also exclude winter LAI from our analysis because of the very low vegetation activity in winter in the Northern Hemisphere.

3. Results

3.1. Occurrence of summer LAI extremes

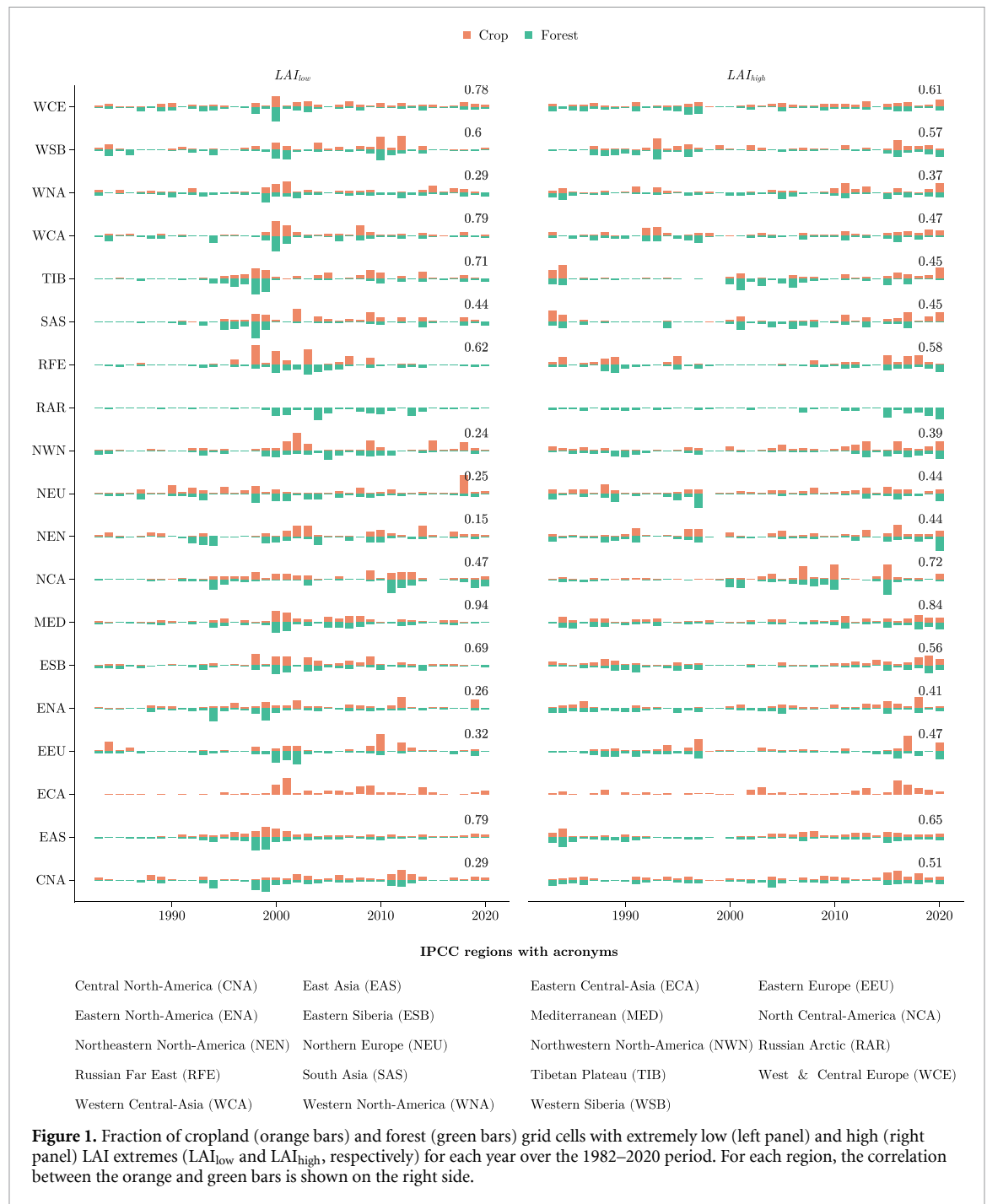
There is large interannual variability in the spatial extent of LAI extremes between 1982 and 2020 for each of the IPCC regions in the Northern Hemisphere (figure 1). Several regions show high temporal correlation between the cropland and forest extents experiencing LAI extremes (numbers in figure 1). The correlation of LAI_{low} between crops and forests tends to reach higher values (seven regions showing correlations above 0.6) than for LAI_{high} (four regions). The Mediterranean (MED) region shows the highest temporal correlation of all regions for both LAI_{low} and LAI_{high}.

Five regions show a significantly increasing trend in the extent of LAI_{low}^{crop}, and ten regions show significantly increasing extents of LAI_{high}^{crop} ($p < 0.05$, table A3). The only region showing a significantly increasing trend ($p < 0.05$) in the extent of LAI_{low}^{forest} is the RAR.

3.2. Preconditioning effect of winter climate on LAI extremes

In general, we find that extremes over cropland are better predicted compared to forests (tables A4 and A5). In all regions, the winter climate significantly improves the prediction of extreme LAI in summers, as determined by the likelihood ratio test of the logistic regression models in equations (1) and (2) ($p < 0.05$). However, despite the effect of the winter climate being significant, in many regions the preconditioning strength is small (overall, AUROC|w minus AUROC|\w ranges between 0 and 0.08; tables A4 and A5). For the subsequent analysis, we consider regions with preconditioning strength larger than 0.02 as winter 'preconditioned regions'. This threshold is fixed for all regions and the subjective choice is based on visual investigation of the strength of winter preconditioning for both LAI_{low} and LAI_{high} for crops and forests (figures 2(a), (c), (e) and (g)). This results in five preconditioned regions for both LAI_{low}^{crop} and LAI_{high}^{crop}, eight preconditioned regions for LAI_{low}^{forests}, and five for LAI_{high}^{forests} (figure 2). East Asia (EAS) is the only region where winter preconditioning effects are found for both LAI_{low}^{crop} and LAI_{high}^{crop}. Eastern Siberia (ESB) and RAR are the only regions with high winter preconditioning for both LAI_{low}^{forests} and LAI_{high}^{forests}.

For LAI_{low}, the change in odds ratios associated with P_w (e^{α_6}) is predominantly below 1 across most preconditioned regions for both cropland and forest (figure 3(a), y -axis). This indicates that positive P_w anomalies decrease the odds of LAI_{low} compared to non-extreme summer LAI in these regions. For instance, the decrease in odds of LAI_{low} is more than 40% for Western Central Asia (WCA) for a one



standard deviation increase in P_w over croplands. A notable exception is EAS, where no effect (forests) or the opposite effect (crops) of P_w is observed. In contrast, the effects of T_w (e^{α_5}) are more variable across regions (figure 3(a), x-axis) with the odds of LAI_{low} changing between -35% and $+40\%$ for a one standard deviation increase in T_w . Four regions show positive effects of T_w on LAI_{low} , either in croplands (MED), forests (Central North America (CNA)), or both croplands and forests (EAS, WCA). Two regions show negative T_w effects (Northeastern North America (NEN), Western Siberia (WSB)) for both croplands

and forests, and two regions show negative effects of T_w in forests (Russian Far East (RFE), ESB). These differences largely correspond to background climate conditions: warmer regions (below 40° N) consistently show that positive T_w anomalies increase the odds of LAI_{low} . Conversely, cooler regions (above 40° N) consistently show that positive T_w anomalies decrease the odds of LAI_{low} .

For LAI_{high} , we observe a symmetric effect of T_w , with positive T_w anomalies increasing the odds of LAI_{high} in the northern regions but decreasing them in southern regions (figure 3(b), x-axis). Positive P_w

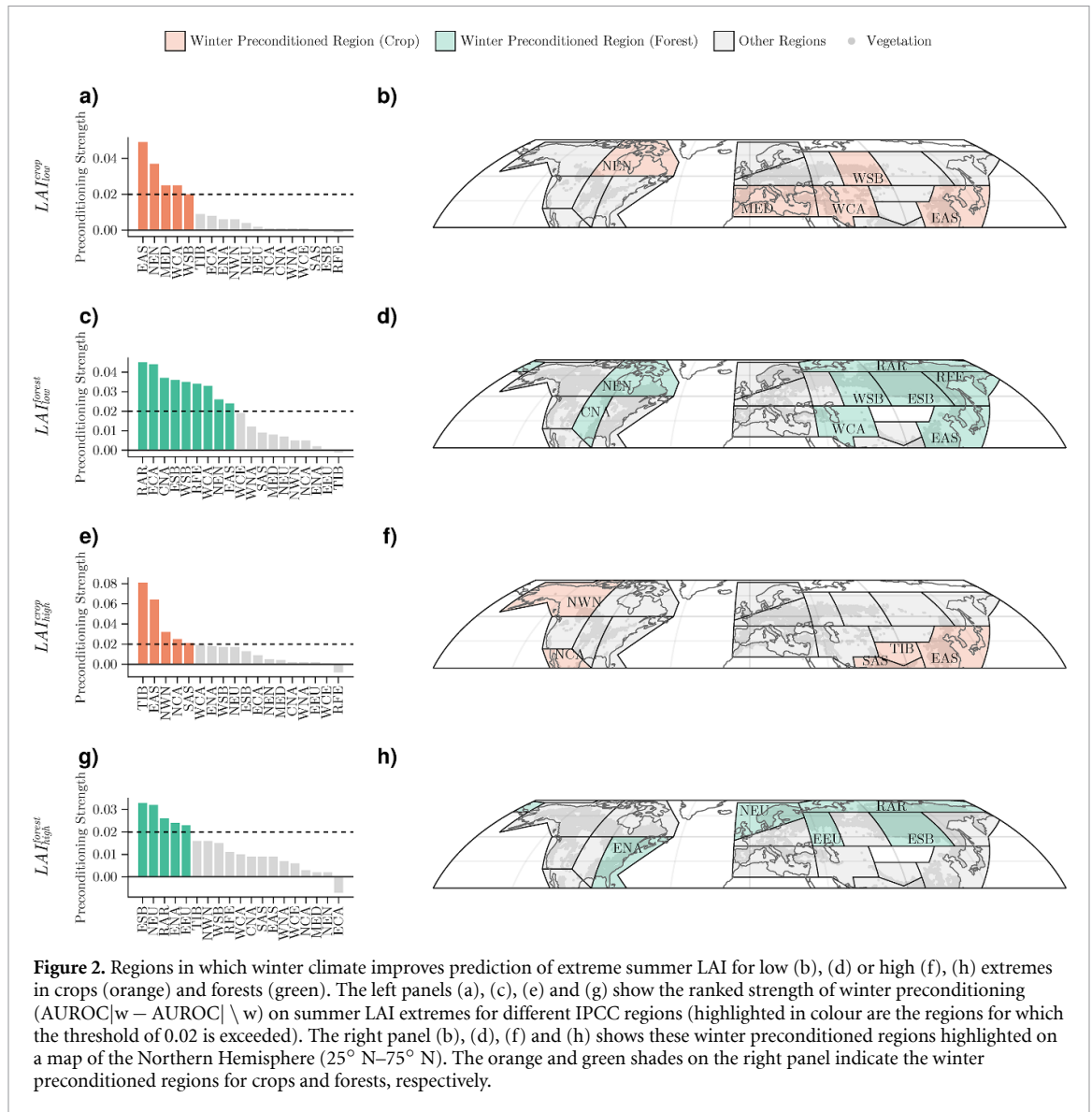
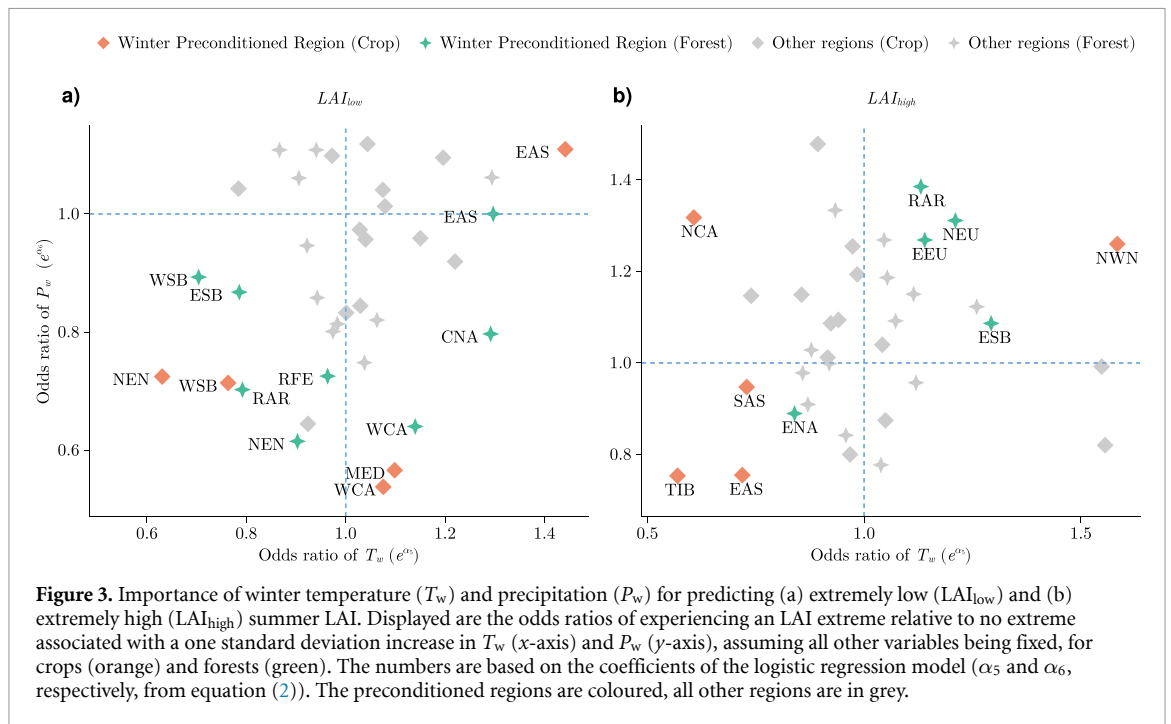


Figure 2. Regions in which winter climate improves prediction of extreme summer LAI for low (b), (d) or high (f), (h) extremes in crops (orange) and forests (green). The left panels (a), (c), (e) and (g) show the ranked strength of winter preconditioning ($AUROC_w - AUROC \setminus w$) on summer LAI extremes for different IPCC regions (highlighted in colour are the regions for which the threshold of 0.02 is exceeded). The right panel (b), (d), (f) and (h) shows these winter preconditioned regions highlighted on a map of the Northern Hemisphere ($25^\circ N-75^\circ N$). The orange and green shades on the right panel indicate the winter preconditioned regions for crops and forests, respectively.

anomalies increase the odds of LAI_{high} in northern regions and decrease them in southern regions, with the exception of crops in North Central America (NCA) that show positive P_w anomalies increase the odds of LAI_{high} (figure 3(b), y -axis). The effect of T_w on the odds ratios of LAI_{high} is stronger than that of P_w , with changes of -43% to 58% for one standard deviation change in T_w , compared to -25% to 38% for P_w .

To understand how relevant the effect of winter is, compared to spring and summer, we compute the odds ratios associated with all predictors for all seasons (tables A6–A9). In many winter preconditioned regions, the effect of a change in T_w is stronger than the effect of a change in the spring or summer climate. This holds for two cropland regions (EAS, NEN) and three forest regions (CNA, WSB, ESB) for LAI_{low} . Similarly, in three crop regions (Northwestern North America (NWN), South Asia (SAS), Tibetan

Plateau (TIB)) and one forest region (ESB), changing T_w leads to the largest change in the odds of LAI_{high} . P_w is affecting the odds of LAI_{low} the most in two regions (MED for croplands and WCA for forests). Even though in some regions neither T_w nor P_w lead to the strongest odds ratio, the effects of winter climate are often stronger than many predictors from spring or summer. For LAI_{low} , P_w is particularly relevant in forests, with seven out of eight regions showing a more strongly reduced odds ratio for P_w than those associated with precipitation in the spring and summer (CNA, ESB, NEN, RAR, RFE, WCA, WSB). Such a strong effect of P_w compared to spring or summer is only found in two out of the five LAI_{low}^{crop} regions (MED, NEN). For LAI_{high} regions, the effect of P_w can be stronger than that of spring (TIB for croplands and Eastern Europe (EEU) for forests), summer (ESB and Northern Europe (NEU) for forests), or spring and summer (EAS for croplands, Eastern North America



(ENA) and RAR for forests) precipitation. Even when T_w is not the most relevant predictor for LAI_{high} (see above), in many regions the effect is still stronger than that of spring (in NCA and EAS croplands and EEU and NEU forests), and stronger than or comparable to that of summer (in ENA forests and EAS croplands, respectively).

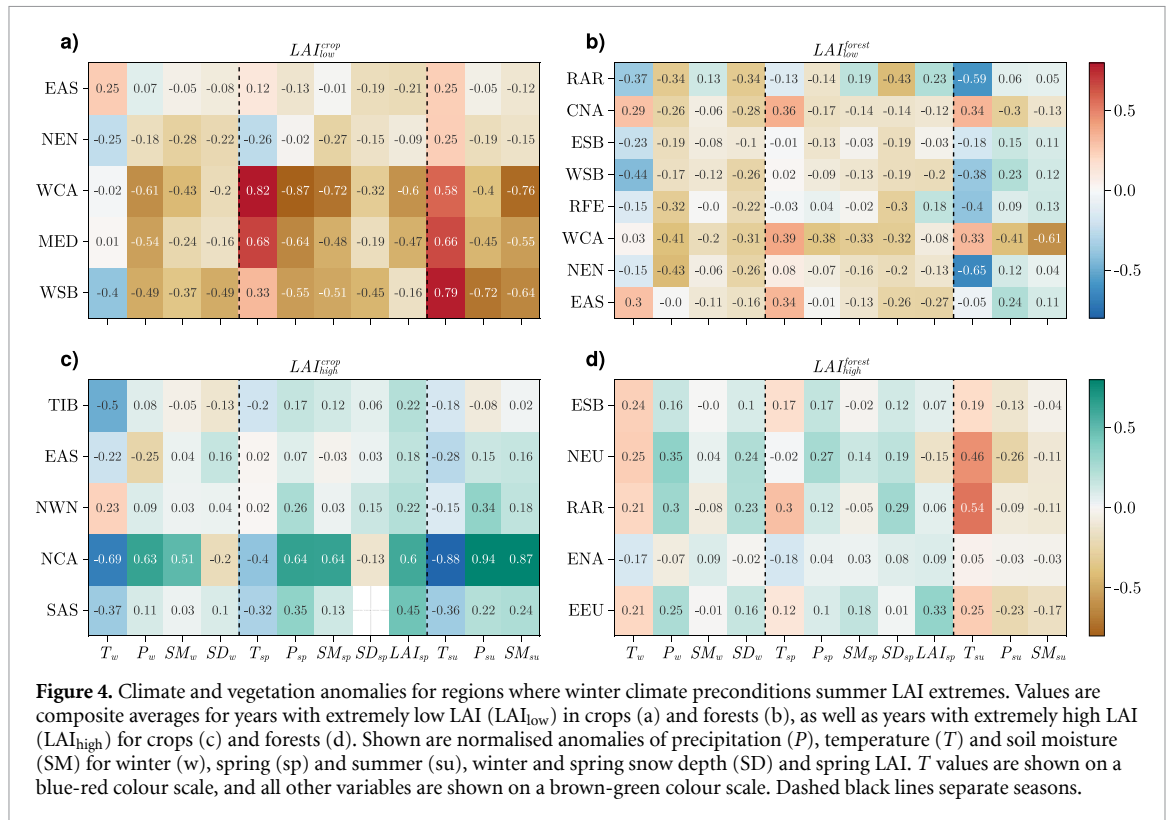
3.3. Direct and indirect climate contributions to summer extremes in winter preconditioned regions

Our analysis reveals that in many regions, winter climate conditions have substantial preconditioning effects on summer LAI extremes. The contribution of a given climatic driver in each season to summer LAI extremes depends not only on the sensitivity of vegetation to the driver but also on the magnitude of the anomalies experienced in those years. Furthermore, for those regions where winter preconditioning effects are relevant, the effects might be direct (e.g. with winter frost leading to vegetation damage) or indirect (e.g. through the winter climate's influence on spring LAI, which then impacts the summer LAI). To further understand the link between winter preconditioning and summer LAI extremes, we quantify the composites of anomalies in T , P and soil moisture in winter, spring and summer; snow depth in winter and spring; and LAI in spring.

Winters corresponding to LAI_{low} in croplands and forests (figures 4(a) and (b)) tend to be drier than average, with predominantly negative anomalies in P_w , SM_w and SD_w . Especially for forests, they also tend to be colder than average (negative T_w

anomalies). The strongest negative T_w anomalies are experienced by WSB (-0.44σ for forests and -0.4σ for croplands), while croplands in WCA, MED and WSB and forests in WCA and NEN show the strongest negative P_w anomalies (below -0.4σ). Exceptions to this pattern are EAS for croplands and forests and CNA for forests, where LAI_{low} is associated with warmer than average winters, and WCA and MED, where T_w anomalies are close to neutral.

In the spring and summer of LAI_{low} years, both croplands and forests show persisting negative anomalies in water-related variables in the spring (precipitation, soil moisture and snow depth), but show opposite anomalies in the summer: croplands are associated with drier and forests with wetter than average conditions for LAI_{low} years. Temperature anomalies are strongly positive in the spring and summer for croplands (except NEN), especially WCA, MED and WSB (with magnitudes $>0.5\sigma$). However, for forests, a switch from normal or warmer-than-average spring conditions to cold summers is found. CNA and WCA are exceptions to this pattern over forests, showing a pattern more consistent with croplands of persisting warmer and drier conditions over spring and summer. In some regions, spring is already associated with lower than average LAI, particularly WCA and MED over croplands and EAS for both croplands and forests. This indicates a potentially indirect effect of winter preconditioning through spring LAI for these regions. However, most regions do not show strongly negative spring LAI anomalies, and RAR even shows positive spring LAI (0.23σ), indicating that winter preconditioning effects on the



negative summer LAI extremes are unlikely to be only due to their effects on spring vegetation activity.

Preconditioned regions with LAI_{high} extremes tend to show opposite patterns for precipitation anomalies in years with LAI_{low} extremes for croplands and forests: most regions experience wetter than average winter and spring conditions, while summer precipitation is above average for croplands and below average for forests. The few exceptions, EAS and NCA for croplands and RAR and ENA for forests, show below-average anomalies in one water-related variable (e.g. SD_w in NCA croplands), but these anomalies are compensated by positive anomalies in the other water-related variables. T_w anomalies are predominantly strong and negative (-0.50σ to -0.22σ) across most preconditioned cropland regions. Unlike croplands, T_w over forest regions is predominantly positive for LAI_{high} extremes (0.21σ – 0.25σ) except ENA (-0.17σ).

The increased water availability during years with LAI_{high} extremes through winter and spring leads to a strong positive LAI anomaly already in the spring for all cropland (0.18σ – 0.60σ) and, less markedly, for most forest regions (0.06σ – 0.33σ) except NEU (-0.15σ). In the summer, as for LAI_{low} , croplands and forest regions show opposing climate anomaly patterns: cropland regions are associated with colder and wetter summers with the exception of TIB, with a small but negative summer precipitation anomaly (-0.08σ); in forest regions LAI_{high} extremes are

associated with drier and warmer conditions in all regions, although the anomalies are small for ENA.

4. Discussion

4.1. Patterns and trends in LAI extremes

Extremes for LAI_{low} tend to co-occur in croplands and forests more than LAI_{high} extremes, possibly because the drivers of LAI_{low} extremes (mostly water limitation) are more consistent between croplands and forests than those of LAI_{high} extremes (figures 3 and 4). However, this could also be due to the relatively coarse resolution of the LAI data ($0.25^\circ \times 0.25^\circ$), which does not allow for full separation of croplands and forests where the land cover heterogeneity is high.

Several regions in the Northern Hemisphere show significant positive trends in the spatial extent of extreme summer LAI over croplands (five regions for LAI_{low}^{crop} and ten for LAI_{high}^{crop}). The positive trends in LAI_{low}^{crop} could be associated with an increase in the spatial extent of compound hot-dry events, e.g. in China (Yang et al 2023), India (Chen et al 2016, Sharma and Mujumdar 2017, Mishra et al 2020), Europe (Manning et al 2019) and in central and western North America (Alizadeh et al 2020). The positive trends in the spatial extent of LAI_{high}^{crop} might be explained by the increased availability of nutrients (through fertilisers and deposition) that contribute to increased crop productivity and growth, especially

during favourable years (Zeng *et al* 2014). For forest regions, the spatial extent of LAI extremes is roughly stable over time (with only one region with a significant trend for LAI_{low}^{forest}). This might be due to the higher resistance of forests to heat and drought stress (Flach *et al* 2018, Xiao *et al* 2023), their longer development times (multi-annual) compared to many croplands (seasonal) as well as the higher diversity in traits influencing their stress responses (Martínez-Vilalta *et al* 2014, Aspinwall *et al* 2015, Anderegg *et al* 2016).

4.2. Winter climate is preconditioning LAI extremes

We show that the winter climate preconditions LAI_{low} and LAI_{high} extremes across large parts of the Northern Hemisphere. In many of the winter preconditioned regions, both high and low extreme summer LAI events are more strongly influenced by winter precipitation and temperature than by spring and summer conditions (tables A6–A9). Odds ratios range from 0.54 to 1.58, indicating an up to 58% change in the odds of occurrence of LAI extremes due to one standard deviation increase in the winter temperature or precipitation. This underscores the critical role of the winter climate in determining extreme summer LAI events, independent of spring and summer weather conditions. Some regions emerge as being particularly sensitive to winter climate conditions: EAS for LAI_{high}^{crop} , LAI_{low}^{crop} and LAI_{low}^{forest} , WCA, WSB and NEN for LAI_{high}^{crop} and LAI_{low}^{crop} , and RAR for LAI_{high}^{forest} and LAI_{low}^{forest} , showing strong winter preconditioning effects.

Similarities between forests and crops are found for low LAI extremes: drier winter conditions generally increase the odds of LAI_{low} (figure 3), and consistently, LAI_{low} extremes are generally preceded by dry winters (figure 4). Among the preconditioned regions, MED and WCA show the strongest sensitivity to winter precipitation and also the strongest negative anomalies in winter precipitation for extreme years. In these regions, summers are typically dry and the growing season starts earlier than in other regions, so drought extremes are more relevant when occurring in the winter and early spring (El-Madany *et al* 2020). Long droughts that span multiple months, including months before planting, have been shown to lead to lower-than-normal yields in various parts of the globe (Zampieri *et al* 2017, Webber *et al* 2018, Santini *et al* 2022). Droughts also have an adverse effect on forest productivity (Park Williams *et al* 2013, Anderegg *et al* 2015, Pohl *et al* 2023, van der Woude *et al* 2023).

Consistent with negative winter precipitation anomalies preceding LAI_{low} extremes, we observe negative snow cover anomalies in the winter, which are still prevalent in the spring in all of the preconditioned regions. Reduced snow cover in winter can lead

to a reduction of soil temperature due to decreased bulk thermal insulation (Henry *et al* 2018, Zhang *et al* 2018). Such conditions have been shown to significantly reduce winter crop productivity by increasing the sensitivity to freezing stress (Trnka *et al* 2014, Zhu *et al* 2019, 2022, Beillouin *et al* 2020). Additionally, the reduced snowpack coupled with below average precipitation in winter results in low soil water availability during the spring (figure 4), inhibiting the development of vegetation at the onset of the growing season (Buermann *et al* 2018, Heino *et al* 2023).

In contrast to the precipitation effects, the temperature effects are more complex, with large variability in the odds of LAI_{low} for both croplands and forests (figure 3), and opposite patterns for crops and forests for LAI_{high} ; in forests, warmer winters tend to increase the likelihood of LAI_{high} , and vice versa for croplands. Consistently, the years of LAI_{high}^{crop} are associated with colder than average temperatures, while LAI_{high}^{forest} years show warmer than average temperatures. This is supported by Zscheischler *et al* (2014), who found that low productivity extremes are associated with colder conditions in boreal forests in multiple vegetation models. Overall, higher winter temperatures reduce the risk of frost days, which impedes tree growth and regeneration (Girardin *et al* 2022).

In croplands, the sensitivity of LAI_{low} to winter temperature follows a latitudinal gradient: warmer winters are associated with a higher likelihood of LAI_{low} in mid-latitude regions and a reduced likelihood of LAI_{low} in high-latitude regions. This is supported by a regional study in Sweden, where increased temperatures favoured crop yields in the north but had a negative impact in the south over the period 1965–2020 (Sjulgård *et al* 2023). The relevance of warm winter temperatures for extremely low crop yields has also been highlighted for Europe in previous studies (Ben-Ari *et al* 2018, Beillouin *et al* 2020).

4.3. Winter preconditioning is modulated by spring LAI

In most preconditioned regions, the winter climate effect is already visible in the spring LAI, with similar directions in spring anomalies to those of summer (figure 4). This is consistent with the importance of memory effects in ecological processes (Ogle *et al* 2015, Cranko Page *et al* 2021) and seasonal legacy effects between spring and summer (Buermann *et al* 2018), including for extremes (Wolf *et al* 2016, Bastos *et al* 2020a, Bevacqua *et al* 2021). The climate and spring LAI anomalies in extreme years are generally stronger for crops than forests, reflecting the former's faster response times and also leading to better predictability of extreme years over croplands (tables A4 and A5). The higher predictability over cropland areas may thus be explained by the limited legacy effects of multi-year climate variations

on crops, which are typically annual plants, whereas forest growth and functioning are more likely to show multi-annual legacy effects (Bastos *et al* 2021, Yu *et al* 2022, Cranko Page *et al* 2023a, Anand *et al* 2024). For instance, droughts can have an effect on forest vegetation activity even two years after their occurrence (Yu *et al* 2022), which by far exceeds the nine-month time-span studied here, but could contribute to some variability in the results.

Interestingly, in three snow-dominated regions over forests, we see a reverse direction in the spring LAI anomalies compared to summer LAI anomalies. Specifically, for $LAI_{low}^{forests}$ in RAR and RFE, higher than usual spring LAI (>0.1) anomalies are observed, which might appear counter-intuitive. However, both regions are also associated with low spring snow cover anomalies, aiding in early greening in these years, but are followed by strongly negative summer temperature anomalies (< -0.4) and slightly wetter than average summer conditions. The cold anomalies in the summers, especially for those regions with short growing seasons, might result in damage to the newly budded leaves, leading to $LAI_{low}^{forests}$.

Over NEU for $LAI_{high}^{forests}$, we see a negative anomaly for spring LAI (-0.15σ), but these are followed by warmer and slightly drier summers. As the corresponding spring temperatures are not warmer, vegetation development may only catch up in summers but is favoured by the previous seasons' average moisture. Wang *et al* (2018b) also analysed the impact of snow water equivalent (SWE) in the Northern Hemisphere and found that higher SWE leads to a negative growth effect on vegetation by delaying the snowmelt and reducing the vegetative period, explaining the negative anomalies in the spring LAI. Furthermore, many of these high-latitude regions are typically energy-limited in summer, so colder than average and wetter (i.e. more cloudy) summers tend to be associated with low forest productivity and growth, and the opposite for warm and dry summers (Walther *et al* 2019, Bastos *et al* 2020b).

4.4. Compounding drivers and possible extensions

Large anomalies occur in different variables and seasons, highlighting the compounding nature of the drivers of extreme summer LAI events. For instance, a drier winter followed by a hotter and drier spring and summer typically leads to LAI_{low}^{crop} in WCA, MED and WSB. To fully understand the risks associated with such compound events, multivariate approaches are required that take into account the correlation structure across time and between variables (Ogle *et al* 2021, Cranko Page *et al* 2023a). For instance, Zscheischler *et al* (2017) found that bivariate return periods of precipitation and temperature can well explain crop yields in different European countries. Similarly, using a new index tailored to

bivariate variations in temperature and precipitation, Li *et al* (2022) found that compound warm-dry events increase vegetation productivity at high latitudes, consistent with the fact that these ecosystems are typically energy-limited in the summer. In contrast, such events reduce productivity in the mid-latitudes, and compound warm-dry springs can cause and amplify summer droughts, thereby reducing summer productivity.

Our study provides a first report on the large-scale winter preconditioning effects of summer LAI extremes. However, we note that we do not explore the effects of ecological and human factors in modulating the impacts on LAI (Bastos *et al* 2023). Such modulating factors include regional differences in phenology, the effects of landscape management, irrigation, topography, succession, as well as climate-driven disturbances such as fire or insects (Seidl *et al* 2017). However, we expect that these processes play minor roles at the coarse spatial and temporal resolution considered here. As such, our study lays the basis for more detailed, high-resolution regional analyses. Our approach is anchored in identifying linear relationships with no interactions, which eases the interpretation but with limited predictive skill. Nonlinear approaches based on machine learning can be combined with interpretation techniques to identify drivers of impact extremes (Jiang *et al* 2022, 2024) but require careful model calibration when working with spatiotemporal data (Sweet *et al* 2023). We also do not identify causal relationships between variables. As our results indicate multiple relevant climate anomalies across seasons, chains of weather patterns and their impacts (like droughts and heat waves) should be further studied to identify causal links and carry-over effects across seasons. Such causal links could be investigated using process-based models that simulate the climatic and non-climatic controls for vegetation functioning, structure and dynamics.

5. Conclusions

In this study, we analyse the influence of winter climate on summer LAI extremes for croplands and forests in the Northern Hemisphere. We define winter preconditioning strength based on the ability of the winter climate to improve the prediction of extremes in the summer LAI in comparison to using only spring and summer climate information. Winter preconditions the occurrence of summer LAI extremes for both crops and forests in more than a quarter of the IPCC Northern Hemisphere regions studied. We find that winter climate anomalies allow a better explanation of summer LAI extremes in many regions, but with importance differences between crops and forests and across regions. Low LAI extremes in summer are typically associated with

colder and drier winter conditions in most regions. More diverse responses are identified for high LAI extremes in summer, with the differences being particularly large between crops and forests. Generally, in forests, high summer LAI extremes are associated with warmer and wetter winters. For crops, we also find that the effect of winter climate on high LAI extremes in summer is dependent on latitude. In many regions, the influence of winter climate is already visible in the spring LAI, highlighting the importance of ecological memory in seasonal legacy effects. Moreover, the observed anomalies in different climate and state variables across different seasons illustrate the compound nature of the drivers of extreme LAI events. In particular, the winter temperature and precipitation precondition the summer LAI through multiple variables (soil moisture, snow depth and LAI) over winter and spring, highlighting the challenges associated with identifying drivers of summer LAI extremes and the importance of ecological memory for impact assessments. Overall, our study presents evidence for lagged climate and ecological effects spanning from winter to summer for many regions in the Northern Hemisphere, and provides a basis for more in-depth studies at the regional scale.

Data availability statement

All datasets that support the findings of this study are openly available. The GLOBMAP global leaf area index data is available on Zenodo at <https://doi.org/10.5281/zenodo.4700264>. ERA5 reanalysis datasets are freely available for download from the Copernicus website (<https://cds.climate.copernicus.eu/>). Landcover data can be downloaded from the ESA Landcover CCI website (<https://www.esa-landcover-cci.org/>).

No new data were created or analysed in this study.

Acknowledgments

The authors thank the DAMOCLES COST Action CA17109, which funded a Compound Events Training School where this work commenced. M A and J Z acknowledge funding from the Helmholtz Initiative and Networking Fund (Young Investigator Group COMPOUNDX, Grant Agreement VH-NG-1537). R H acknowledges funding from the European Union's Horizon 2020 Research and Innovation Programme under Grant Agreement 820712 (RECEIPT). N L, A B, R H and J Z acknowledge funding from the European Union's Horizon 2020 research and innovation programme under Grant Agreement No. 101003469 (XAIDA). P S S was supported by Fundação para a Ciência e a Tecnologia (FCT), Grant Number SFRH/BD/146646/2019. F K G was supported by the Strategic Priority Fund for UK Climate Resilience. The UK Climate Resilience programme was supported by the UK Research and Innovation Strategic Priorities Fund, and was co-delivered by the Met Office and NERC on behalf of UK Research and Innovation partners AHRC, EPSRC and ESRC. The contribution of F K G is subject to © Crown Copyright, Met Office. A B acknowledges funding by the European Union (ERC StG, ForExD, Grant Agreement No. 101039567).

Author contributions

M A, R H, N L, J Z and A B conceptualised the article and defined the methodology. M A wrote the original draft and did the formal analysis. P S S, J A and F K G contributed to the development of the article through discussion in the initial stage. All the authors contributed to the revision of the manuscript. R H and N L contributed equally.

Appendix. Additional figures and tables

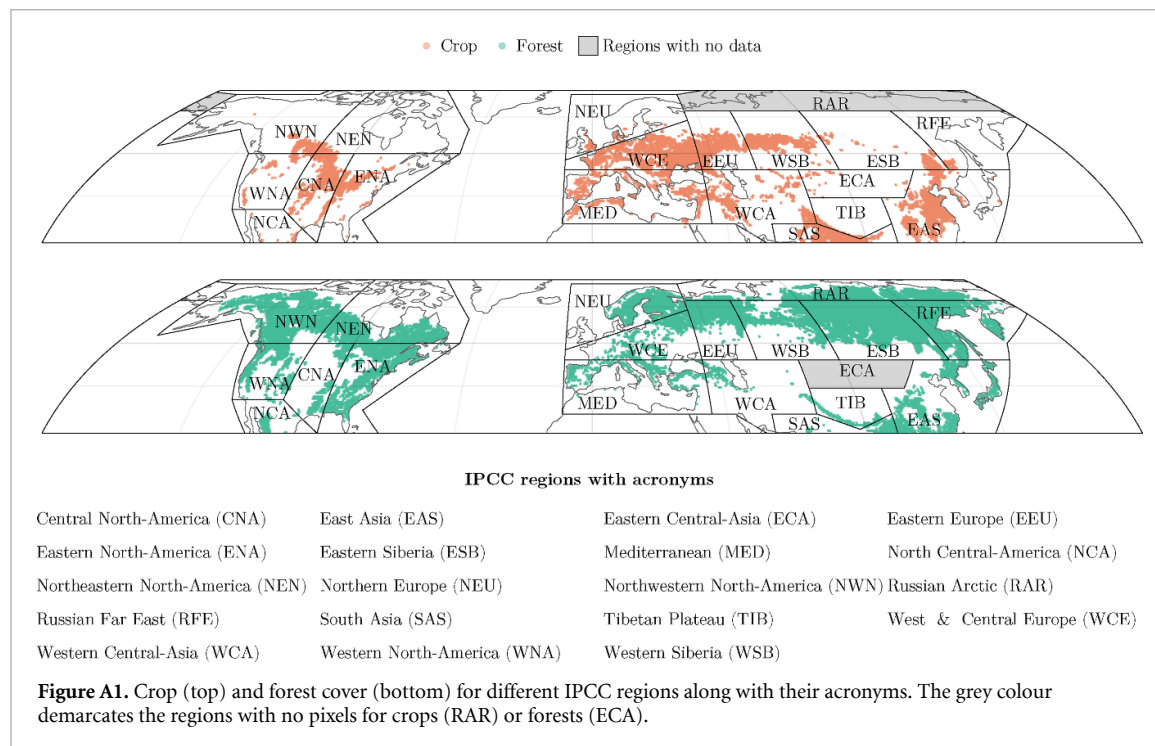


Table A1. Crop vs forest definition in this study.

Class	Description	Type
10	Cropland, rainfed	Crop
20	Cropland, irrigated or post-flooding	Crop
30	Mosaic cropland (>50 % nat. veg. (tree, shrub, herb.) (<50 %)	Crop
40	Mosaic nat. veg. (tree, shrub, herb.) (>50 %)/cropland (<50 %)	Forest
50	Tree cover, broadleaf, evergreen, closed to open (>15 %)	Forest
60	Tree cover, broadleaf, deciduous, closed to open (>15 %)	Forest
70	Tree cover, needleleaf, evergreen, closed to open (>15 %)	Forest
80	Tree cover, needleleaf, deciduous, closed to open (>15 %)	Forest
90	Tree cover, mixed leaf type (broadleaf and needleleaf)	Forest
100	Mosaic tree and shrub (>50 %)/herbaceous cover (<50 %)	Forest

Table A2. Total number of pixels and forest and crop fraction in the IPCC regions.

IPCC region (abbreviation)	Crop fraction (%)	Forest fraction (%)	Total pixels
Central North America (CNA)	33.80	16.95	4944
East Asia (EAS)	20.85	22.98	118 46
Eastern Central Asia (ECA)	3.92	0	4800
Eastern Europe (EEU)	27.92	44.67	6400
Eastern North America (ENA)	9.09	37.27	9638
Eastern Siberia (ESB)	4.60	72.09	128 00
Mediterranean (MED)	16.65	12.35	120 00
North Central America (NCA)	3.55	11.54	2876
Northeastern North America (NEN)	1.25	19.85	192 59
Northern Europe (NEU)	2.58	23.41	142 80
Northwestern North America (NWN)	2.98	32.54	206 72
Russian Arctic (RAR)	0	26.68	235 89
Russian Far East (RFE)	1.13	40.06	121 38
South Asia (SAS)	42.58	19.12	2400
Tibetan Plateau (TIB)	4.58	11.08	3600
Western Central Asia (WCA)	16.28	5.01	9010
Western North America (WNA)	6.63	30.91	5522
Western Siberia (WSB)	16.94	31.13	9600
West & Central Europe (WCE)	52.29	26.26	7720

Table A3. Levels of statistical significance for temporal trends in fractions of pixels with low and high LAI for crop and forest each year, indicated by asterisks and dots. Significance levels: $p < 0.001$ (***), $p < 0.01$ (**), $p < 0.05$ (*), and $p < 0.1$ (·). If trends are significant, they are always increasing.

IPCC region (abbreviation)	LAI _{low} ^{crop}	LAI _{high} ^{crop}	LAI _{low} ^{forest}	LAI _{high} ^{forest}
Central North America (CNA)	*	*		
East Asia (EAS)	·	*		
Eastern Central Asia (ECA)	**	*	NA	NA
Eastern Europe (EEU)				
Eastern North America (ENA)		*		·
Eastern Siberia (ESB)		·		
Mediterranean (MED)		*		
North Central America (NCA)	*	**		
Northeastern North America (NEN)				
Northern Europe (NEU)				
Northwestern North America (NWN)	·	·		
Russian Far East (RFE)				
Russian Arctic (RAR)	NA	NA	*	
South Asia (SAS)	**	**		
Tibetan Plateau (TIB)	*	*		
Western Central Asia (WCA)		*		
Western North America (WNA)				
Western Siberia (WSB)				
West & Central Europe (WCE)	·	*		

Table A4. AUROC curve for the prediction of LAI_{low}. Scores are bold for preconditioned regions.

IPCC region (abbreviation)	Crop ^{\w}	Crop ^w	Forest ^{\w}	Forest ^w
Central North America (CNA)	0.693	0.694	0.616	0.653
East Asia (EAS)	0.577	0.626	0.610	0.634
Eastern Central Asia (ECA)	0.713	0.721	—	—
Eastern Europe (EEU)	0.822	0.824	0.565	0.565
Eastern North America (ENA)	0.636	0.642	0.595	0.597
Eastern Siberia (ESB)	0.703	0.703	0.572	0.608
Mediterranean (MED)	0.793	0.818	0.765	0.773
North Central America (NCA)	0.815	0.816	0.715	0.720
Northeastern North America (NEN)	0.618	0.655	0.726	0.752
Northern Europe (NEU)	0.725	0.729	0.648	0.655
Northwestern North America (NWN)	0.818	0.824	0.704	0.709
Russian Arctic (RAR)	—	—	0.685	0.730
Russian Far East (RFE)	0.714	0.713	0.625	0.659
South Asia (SAS)	0.676	0.676	0.656	0.665
Tibetan Plateau (TIB)	0.623	0.632	0.653	0.652
Western Central Asia (WCA)	0.806	0.831	0.689	0.722
Western North America (WNA)	0.738	0.739	0.636	0.648
Western Siberia (WSB)	0.791	0.811	0.624	0.659
West & Central Europe (WCE)	0.745	0.746	0.608	0.627

Table A5. AUROC curves for the prediction of LAI_{high}. Scores are bold for preconditioned regions.

IPCC region (abbreviation)	Crop ^{\w}	Crop ^w	Forest ^{\w}	Forest ^w
Central North America (CNA)	0.623	0.625	0.583	0.592
East Asia (EAS)	0.587	0.651	0.558	0.567
Eastern Central Asia (ECA)	0.712	0.721	—	—
Eastern Europe (EEU)	0.754	0.756	0.615	0.638
Eastern North America (ENA)	0.648	0.666	0.561	0.585
Eastern Siberia (ESB)	0.664	0.677	0.591	0.624
Mediterranean (MED)	0.795	0.799	0.733	0.735
North Central America (NCA)	0.824	0.849	0.730	0.733
Northeastern North America (NEN)	0.595	0.600	0.681	0.683
Northern Europe (NEU)	0.680	0.697	0.669	0.701
Northwestern North America (NWN)	0.637	0.669	0.645	0.661
Russian Arctic (RAR)	—	—	0.697	0.723
Russian Far East (RFE)	0.566	0.558	0.627	0.638
South Asia (SAS)	0.639	0.660	0.586	0.595
Tibetan Plateau (TIB)	0.596	0.677	0.639	0.655
Western Central Asia (WCA)	0.735	0.754	0.653	0.663
Western North America (WNA)	0.700	0.702	0.633	0.640
Western Siberia (WSB)	0.717	0.734	0.626	0.641
West & Central Europe (WCE)	0.697	0.698	0.585	0.591

Table A6. Odds ratio of different regions for LAI_{low}^{crop}. Winter preconditioned regions are in bold.

IPCC region (abbreviation)	T_w	P_w	T_{sp}	P_{sp}	T_{su}	P_{su}
Central North America (CNA)	1.044	1.119	0.894	0.966	1.499	0.71
East Asia (EAS)	1.442	1.11	0.987	0.828	1.392	1.122
Eastern Central Asia (ECA)	1.196	1.095	1.077	0.45	1.124	0.685
Eastern Europe (EEU)	1.001	0.833	1.679	0.512	1.478	0.553
Eastern North America (ENA)	1.22	0.919	1.046	1.164	1.007	0.682
Eastern Siberia (ESB)	0.784	1.043	1.968	0.779	1.313	0.775
Mediterranean (MED)	1.099	0.566	1.721	0.603	1.448	0.644
North Central America (NCA)	1.079	1.013	1.018	0.472	1.292	0.257
Northeastern North America (NEN)	0.631	0.725	0.818	1.197	1.358	0.868
Northern Europe (NEU)	1.15	0.959	1.395	0.815	1.0	0.528
Northwestern North America (NWN)	0.924	0.645	0.723	0.416	0.975	0.45
Russian Far East (RFE)	0.972	1.099	1.87	0.615	1.738	0.76
South Asia (SAS)	1.04	0.957	1.373	1.097	1.891	1.154
Tibetan Plateau (TIB)	1.029	0.845	1.315	1.176	1.605	1.435
Western Central Asia (WCA)	1.076	0.538	1.336	0.474	1.314	0.71
Western North America (WNA)	1.028	0.973	1.203	0.53	0.971	0.643
Western Siberia (WSB)	0.763	0.714	1.697	0.669	1.401	0.532
West & Central Europe (WCE)	1.075	1.041	1.713	0.687	1.14	0.629

Table A7. Odds ratio of different regions for LAI_{low}^{forest}. Corresponding winter preconditioned regions are in bold.

IPCC region (abbreviation)	T_w	P_w	T_{sp}	P_{sp}	T_{su}	P_{su}
Central North America (CNA)	1.292	0.797	1.208	0.939	1.13	0.836
East Asia (EAS)	1.297	1.0	1.307	1.001	1.067	1.276
Eastern Europe (EEU)	0.941	1.108	1.017	0.946	0.813	0.99
Eastern North America (ENA)	0.906	1.061	1.257	0.813	0.86	1.069
Eastern Siberia (ESB)	0.786	0.868	1.107	0.912	0.801	1.078
Mediterranean (MED)	1.038	0.748	1.815	0.717	1.324	0.659
North Central America (NCA)	0.974	0.801	0.858	0.776	1.988	0.821
Northeastern North America (NEN)	0.903	0.615	1.476	0.862	0.434	0.928
Northern Europe (NEU)	1.063	0.82	0.962	0.808	0.625	0.985
Northwestern North America (NWN)	0.943	0.858	1.05	0.755	0.448	0.78
Russian Arctic (RAR)	0.792	0.703	1.073	0.824	0.475	0.897
Russian Far East (RFE)	0.964	0.725	0.975	1.007	0.599	0.911
South Asia (SAS)	0.867	1.108	1.575	1.085	1.186	1.611
Tibetan Plateau (TIB)	0.922	0.946	1.242	0.985	1.084	1.613
Western Central Asia (WCA)	1.14	0.64	1.261	0.705	1.129	0.702
Western North America (WNA)	0.983	0.814	1.006	0.62	0.889	1.069
Western Siberia (WSB)	0.704	0.893	1.146	0.905	0.725	1.08
West & Central Europe (WCE)	1.294	1.062	1.121	0.766	0.955	1.063

Table A8. Odds ratio of different regions for LAI_{high}^{crop}. Corresponding winter preconditioned regions are in bold.

IPCC region (abbreviation)	T_w	P_w	T_{sp}	P_{sp}	T_{su}	P_{su}
Central North America (CNA)	0.916	1.012	1.163	0.977	0.9	1.441
East Asia (EAS)	0.719	0.755	1.125	1.153	0.716	1.077
Eastern Central Asia (ECA)	0.856	1.149	1.053	1.706	0.914	1.557
Eastern Europe (EEU)	0.923	1.087	0.647	1.8	0.614	1.334
Eastern North America (ENA)	0.739	1.147	1.186	0.813	1.155	1.59
Eastern Siberia (ESB)	0.968	0.8	1.002	1.433	0.798	1.493
Mediterranean (MED)	0.973	1.255	0.601	1.704	0.618	1.37
North Central America (NCA)	0.607	1.318	1.293	1.667	0.461	1.707
Northeastern North America (NEN)	0.984	1.194	0.936	1.004	1.307	1.354
Northern Europe (NEU)	1.556	0.82	0.487	1.198	0.733	1.285
Northwestern North America (NWN)	1.584	1.26	0.783	1.283	0.819	1.39
Russian Far East (RFE)	1.049	0.875	1.09	0.961	1.201	0.983
South Asia (SAS)	0.729	0.947	0.938	1.223	0.736	1.071
Tibetan Plateau (TIB)	0.569	0.754	1.001	1.171	0.823	0.753
Western Central Asia (WCA)	0.893	1.478	0.864	1.642	0.784	1.231
Western North America (WNA)	1.042	1.04	0.81	1.545	0.996	1.464
Western Siberia (WSB)	1.548	0.992	0.671	1.05	0.788	1.817
West & Central Europe (WCE)	0.941	1.094	0.651	1.35	0.791	1.34

Table A9. Odds ratio of different regions for LAI_{high}^{forest}. Corresponding winter preconditioned regions are in bold.

IPCC region (abbreviation)	T_w	P_w	T_{sp}	P_{sp}	T_{su}	P_{su}
Central North America (CNA)	0.858	0.978	0.9	0.966	0.936	1.306
East Asia (EAS)	0.87	0.909	0.924	1.111	1.102	0.933
Eastern Europe (EEU)	1.14	1.269	1.022	1.061	1.269	0.768
Eastern North America (ENA)	0.839	0.89	0.805	1.011	1.115	0.984
Eastern Siberia (ESB)	1.293	1.087	1.117	1.198	1.25	0.962
Mediterranean (MED)	1.073	1.092	0.658	1.412	0.67	1.366
North Central America (NCA)	0.958	0.842	0.845	1.37	0.514	1.247
Northeastern North America (NEN)	0.878	1.028	0.676	1.245	1.95	1.247
Northern Europe (NEU)	1.21	1.311	0.862	1.323	1.782	0.993
Northwestern North America (NWN)	0.933	1.334	0.891	1.309	1.718	1.288
Russian Arctic (RAR)	1.131	1.385	1.307	1.124	2.05	1.058
Russian Far East (RFE)	1.053	1.186	1.215	0.978	1.476	0.95
South Asia (SAS)	1.12	0.957	1.02	1.228	0.888	0.742
Tibetan Plateau (TIB)	1.039	0.777	0.745	1.061	0.731	0.707
Western Central Asia (WCA)	1.046	1.269	0.94	1.175	0.715	1.244
Western North America (WNA)	1.114	1.15	0.81	1.369	0.998	1.111
Western Siberia (WSB)	1.26	1.123	1.091	0.94	1.473	0.962
West & Central Europe (WCE)	0.919	0.999	0.851	1.203	0.931	0.993

ORCID iDs

Mohit Anand  <https://orcid.org/0000-0002-1688-263X>

Raed Hamed  <https://orcid.org/0000-0003-2243-3109>

Patrícia S Silva  <https://orcid.org/0000-0003-0410-2971>

Freya K Garry  <https://orcid.org/0000-0002-9640-6675>

Ana Bastos  <https://orcid.org/0000-0002-7368-7806>

References

- Alizadeh M R, Adamowski J, Nikoo M R, AghaKouchak A, Dennison P and Sadegh M 2020 A century of observations reveals increasing likelihood of continental-scale compound dry-hot extremes *Sci. Adv.* **6** eaaz4571
- An-Vo D-A, Radanielson A M, Mushtaq S, Reardon-Smith K and Hewitt C 2021 A framework for assessing the value of seasonal climate forecasting in key agricultural decisions *Clim. Serv.* **22** 100234
- Anand M, Bohn F J, Camps-Valls G, Fischer R, Huth A, Sweet L-B and Zscheischler J 2024 Identifying compound weather drivers of forest biomass loss with generative deep learning *Environ. Data Sci.* **3** e4
- Anderegg W R L et al 2015 Pervasive drought legacies in forest ecosystems and their implications for carbon cycle models *Science* **349** 528–32
- Anderegg W R L, Klein T, Bartlett M, Sack L, Pellegrini A F A, Choat B and Jansen S 2016 Meta-analysis reveals that hydraulic traits explain cross-species patterns of drought-induced tree mortality across the globe *Proc. Natl Acad. Sci.* **113** 5024–9
- Aspinwall M J, Loik M E, Resco De Dios V, Tjoelker M G, Payton P R and Tissue D T 2015 Utilizing intraspecific variation in phenotypic plasticity to bolster agricultural and forest productivity under climate change *Plant Cell Environ.* **38** 1752–64
- Barichivich J, Briffa K R, Myneni R B, Osborn T J, Melvin T M, Ciais P, Piao S and Tucker C 2013 Large-scale variations in the vegetation growing season and annual cycle of atmospheric CO₂ at high northern latitudes from 1950 to 2011 *Glob. Change Biol.* **19** 3167–83
- Bastos A et al 2016 European land CO₂ sink influenced by NAO and East-Atlantic pattern coupling *Nat. Commun.* **7** 10315
- Bastos A et al 2020a Direct and seasonal legacy effects of the 2018 heat wave and drought on European ecosystem productivity *Sci. Adv.* **6** eaba2724
- Bastos A et al 2020b Impacts of extreme summers on European ecosystems: a comparative analysis of 2003, 2010 and 2018 *Phil. Trans. R. Soc. B* **375** 20190507
- Bastos A et al 2021 Increased vulnerability of European ecosystems to two compound dry and hot summers in 2018 and 2019 *Earth Syst. Dyn.* **12** 1015–35
- Bastos A, Running S W, Gouveia C and Trigo R M 2013 The global NPP dependence on ENSO: La Niña and the extraordinary year of 2011 *J. Geophys. Res. Biogeosci.* **118** 1247–55
- Bastos A, Sippel S, Frank D, Mahecha M D, Zaehle S, Zscheischler J and Reichstein M 2023 A joint framework for studying compound ecoclimatic events *Nat. Rev. Earth Environ.* **4** 333–50
- Beillouin D, Schauburger B, Bastos A, Ciais P and Makowski D 2020 Impact of extreme weather conditions on European crop production in 2018 *Phil. Trans. R. Soc. B* **375** 20190510
- Ben-Ari T, Boé J, Ciais P, Lecerf R, Van der Velde M and Makowski D 2018 Causes and implications of the unforeseen 2016 extreme yield loss in the breadbasket of France *Nat. Commun.* **9** 1627
- Bevacqua E et al 2021 Guidelines for studying diverse types of compound weather and climate events *Earth's Future* **9** e2021EF002340
- Bigler C and Bugmann H 2018 Climate-induced shifts in leaf unfolding and frost risk of European trees and shrubs *Sci. Rep.* **8** 9865
- Bokhorst S F, Bjerke J W, Tømmervik H, Callaghan T V and Phoenix G K 2009 Winter warming events damage sub-Arctic vegetation: consistent evidence from an experimental manipulation and a natural event *J. Ecol.* **97** 1408–15
- Bruno Soares M 2017 Assessing the usability and potential value of seasonal climate forecasts in land management decisions in the southwest UK: challenges and reflections *Adv. Sci. Res.* **14** 175–80
- Buermann W et al 2018 Widespread seasonal compensation effects of spring warming on northern plant productivity *Nature* **562** 110–4

- Chen C, He B, Guo L, Zhang Y, Xie X and Chen Z 2018 Identifying critical climate periods for vegetation growth in the northern hemisphere *J. Geophys. Res. Biogeosci.* **123** 2541–52
- Chen Y, Zhang Z, Wang P, Song X, Wei X and Tao F 2016 Identifying the impact of multi-hazards on crop yield—a case for heat stress and dry stress on winter wheat yield in northern China *Eur. J. Agron.* **73** 55–63
- Cranko Page J, De Kauwe M G, Abramowitz G, Cleverly J, Hinko-Najera N, Hovenden M J, Liu Y, Pitman A J and Ogle K 2021 Examining the role of environmental memory in the predictability of carbon and water fluxes across Australian ecosystems *Biogeosciences* **19** 1913–32
- Cranko Page J, De Kauwe M G, Abramowitz G and Pitman A J 2023a Non-stationary lags and legacies in ecosystem flux response to antecedent rainfall *J. Geophys. Res. Biogeosci.* **128** e2022JG007144
- Ding Y, Li Z and Peng S 2020 Global analysis of time-lag and-Accumulation effects of climate on vegetation growth *Int. J. Appl. Earth Obs. Geoinf.* **92** 102179
- El-Madany T S, Carrara A, Martín M P, Moreno G, Kolle O, Pacheco-Labrador J, Weber U, Wutzler T, Reichstein M and Migliavacca M 2020 Drought and heatwave impacts on semi-arid ecosystems' carbon fluxes along a precipitation gradient *Phil. Trans. R. Soc. B* **375** 20190519
- Flach M, Sippel S, Gans F, Bastos A, Brenning A, Reichstein M and Mahecha M D 2018 Contrasting biosphere responses to hydrometeorological extremes: revisiting the 2010 western Russian heatwave *Biogeosciences* **15** 6067–85
- Fu Y H et al 2015 Declining global warming effects on the phenology of spring leaf unfolding *Nature* **526** 104–7
- Girardin M P, Guo X J, Gervais D, Metsaranta J, Campbell E M, Arsenault A, Isaac-Renton M and Hogg E H 2022 Cold-season freeze frequency is a pervasive driver of subcontinental forest growth *Proc. Natl Acad. Sci.* **119** e2117464119
- Gonsamo A, Chen J M and Lombardozi D 2016 Global vegetation productivity response to climatic oscillations during the satellite era *Glob. Change Biol.* **22** 3414–26
- Heino M, Kinnunen P, Anderson W, Ray D K, Puma M J, Varis O, Siebert S and Kumm M 2023 Increased probability of hot and dry weather extremes during the growing season threatens global crop yields *Sci. Rep.* **13** 3583
- Henry H A L et al 2018 Increased soil frost versus summer drought as drivers of plant biomass responses to reduced precipitation: results from a globally coordinated field experiment *Ecosystems* **21** 1432–44
- Hersbach H et al 2020 The ERA5 global reanalysis *Q. J. R. Meteorol. Soc.* **146** 1999–2049
- Iturbide M et al 2020 An update of IPCC climate reference regions for subcontinental analysis of climate model data: definition and aggregated datasets *Earth Syst. Sci. Data* **12** 2959–70
- Jiang S, Bevacqua E and Zscheischler J 2022 River flooding mechanisms and their changes in Europe revealed by explainable machine learning *Hydrol. Earth Syst. Sci.* **26** 6339–59
- Jiang S, Tarasova L, Yu G and Zscheischler J 2024 Compounding effects in flood drivers challenge estimates of extreme river floods *Sci. Adv.* **10** ead14005
- Kelsey K C, Pedersen S H, Leffler A J, Sexton J O, Feng M and Welker J M 2021 Winter snow and spring temperature have differential effects on vegetation phenology and productivity across Arctic plant communities *Glob. Change Biol.* **27** 1572–86
- Kendall M G 1975 *Rank Correlation Methods* (Griffin)
- Kreyling J 2010 Winter climate change: a critical factor for temperate vegetation performance *Ecology* **91** 1939–48
- Le Grix N, Cheung W L, Reygondeau G, Zscheischler J and Frölicher T L 2023 Extreme and compound ocean events are key drivers of projected low pelagic fish biomass *Glob. Change Biol.* **29** 6478–92
- Li J, Bevacqua E, Chen C, Wang Z, Chen X, Myneni R B, Wu X, Xu C-Y, Zhang Z and Zscheischler J 2022 Regional asymmetry in the response of global vegetation growth to springtime compound climate events *Commun. Earth Environ.* **3** 123
- Lian X et al 2020 Summer soil drying exacerbated by earlier spring greening of northern vegetation *Sci. Adv.* **6** eaax0255
- Liu Q, Fu Y H, Zhu Z, Liu Y, Liu Z, Huang M, Janssens I A and Piao S 2016 Delayed autumn phenology in the northern hemisphere is related to change in both climate and spring phenology *Glob. Change Biol.* **22** 3702–11
- Liu X, Tian Y, Liu S, Jiang L, Mao J, Jia X, Zha T, Zhang K, Wu Y and Zhou J 2022 Time-lag effect of climate conditions on vegetation productivity in a temperate forest–grassland ecotone *Forests* **13** 1024
- Liu Y, Konings A G, Kennedy D and Gentile P 2021 Global coordination in plant physiological and rooting strategies in response to water stress *Glob. Biogeochem. Cycles* **35** e2020GB006758
- Liu Y, Liu R and Chen J M 2012 Retrospective retrieval of long-term consistent global leaf area index (1981–2011) from combined AVHRR and MODIS data *J. Geophys. Res. Biogeosci.* **117** G4
- Mann H B 1945 Nonparametric tests against trend *Econometrica* **13** 245–59
- Manning C, Widmann M, Bevacqua E, Van Loon A F, Maraun D and Vrac M 2019 Increased probability of compound long-duration dry and hot events in Europe during summer (1950–2013) *Environ. Res. Lett.* **14** 094006
- Marino G P, Kaiser D P, Gu L and Ricciuto D M 2011 Reconstruction of false spring occurrences over the southeastern United States, 1901–2007: an increasing risk of spring freeze damage? *Environ. Res. Lett.* **6** 024015
- Martínez-Vilalta J, Poyatos R, Aguadé D, Retana J and Mencuccini M 2014 A new look at water transport regulation in plants *New Phytol.* **204** 105–15
- Menzel A, Yuan Y, Matiu M, Sparks T, Scheffinger H, Gehrig R and Estrella N 2020 Climate change fingerprints in recent European plant phenology *Glob. Change Biol.* **26** 2599–612
- Miguez-Macho G and Fan Y 2021 Spatiotemporal origin of soil water taken up by vegetation *Nature* **598** 624–8
- Mishra V, Thirumalai K, Singh D and Aadhar S 2020 Future exacerbation of hot and dry summer monsoon extremes in India *npj Clim. Atmos. Sci.* **3** 10
- Nemani R R, Keeling C D, Hashimoto H, Jolly W M, Piper S C, Tucker C J, Myneni R B and Running S W 2003 Climate-driven increases in global terrestrial net primary production from 1982 to 1999 *Science* **300** 1560–3
- Ogallo L A, Boulahya M S and Keane T 2000 Applications of seasonal to interannual climate prediction in agricultural planning and operations *Agric. For. Meteorol.* **103** 159–66
- Ogle K, Barber J J, Barron-Gafford G A, Bentley L P, Young J M, Huxman T E, Loik M E, Tissue D T and Cleland E 2015 Quantifying ecological memory in plant and ecosystem processes *Ecol. Lett.* **18** 221–35
- Ogle K, Liu Y, Vicca S and Bahn M 2021 A hierarchical, multivariate meta-analysis approach to synthesising global change experiments *New Phytol.* **231** 2382–94
- Park Williams A et al 2013 Temperature as a potent driver of regional forest drought stress and tree mortality *Nat. Clim. Change* **3** 292–7
- Peng S, Chen A, Xu L, Cao C, Fang J, Myneni R B, Pinzon J E, Tucker C J and Piao S 2011 Recent change of vegetation growth trend in China *Environ. Res. Lett.* **6** 044027
- Peng S, Piao S, Ciais P, Fang J and Wang X 2010 Change in winter snow depth and its impacts on vegetation in China *Glob. Change Biol.* **16** 3004–13
- Peñuelas J, Ciais P, Canadell J G, Janssens I A, Fernández-Martínez M, Carnicer J, Obersteiner M, Piao S, Vautard R and Sardans J 2017 Shifting from a fertilization-dominated to a warming-dominated period *Nat. Ecol. Evol.* **1** 1438
- Pfleiderer P, Menke I and Schleussner C-F 2019 Increasing risks of apple tree frost damage under climate change *Clim. Change* **157** 515–25

- Piao S *et al* 2014 Evidence for a weakening relationship between interannual temperature variability and northern vegetation activity *Nat. Commun.* **5** 5018
- Piao S, Wang X, Ciais P, Zhu B, Wang T and Liu J 2011 Changes in satellite-derived vegetation growth trend in temperate and boreal Eurasia from 1982 to 2006 *Glob. Change Biol.* **17** 3228–39
- Pohl F, Werban U, Kumar R, Hildebrandt A and Rebmann C 2023 Observational evidence of legacy effects of the 2018 drought on a mixed deciduous forest in Germany *Sci. Rep.* **13** 10863
- Poulsen B *et al* 2015 Plant functional type classification for earth system models: results from the European space agency's land cover climate change initiative *Geosci. Model Dev.* **8** 2315–28
- Santini M, Noce S, Antonelli M and Caporaso L 2022 Complex drought patterns robustly explain global yield loss for major crops *Sci. Rep.* **12** 5792
- Santoro M, Kirches G, Wevers J, Boettcher M, Brockmann C, Lamarche C and Defourny P 2017 ESA. Land Cover CCI Product User Guide Version 2 *Tech. Rep.* (available at: maps.elie.ucl.ac.be/CCI/viewer/download/ESACCI-LC-Ph2-PUGv2_2.0.pdf)
- Seidl R *et al* 2017 Forest disturbances under climate change *Nat. Clim. Change* **7** 395–402
- Sharma S and Mujumdar P 2017 Increasing frequency and spatial extent of concurrent meteorological droughts and heatwaves in India *Sci. Rep.* **7** 15582
- Sjulgård H, Keller T, Garland G and Colombi T 2023 Relationships between weather and yield anomalies vary with crop type and latitude in Sweden *Agric. Syst.* **211** 103757
- Sweet L-B, Müller C, Anand M and Zscheischler J 2023 Cross-validation strategy impacts the performance and interpretation of machine learning models *Artif. Intell. Earth Syst.* **2** e230026
- Tominaga A, Ito A, Sugiura T and Yamane H 2022 How is global warming affecting fruit tree blooming? “Flowering (dormancy) disorder” in Japanese pear (*Pyrus pyrifolia*) as a case study *Front. Plant Sci.* **12** 787638
- Trnka M, Rötter R P, Ruiz-Ramos M, Kersebaum K C, Olesen J E, Žalud Z and Semenov M A 2014 Adverse weather conditions for European wheat production will become more frequent with climate change *Nat. Clim. Change* **4** 637–43
- van der Woude A M *et al* 2023 Temperature extremes of 2022 reduced carbon uptake by forests in Europe *Nat. Commun.* **14** 6218
- Vautard R *et al* 2023 Human influence on growing-period frosts like in early April 2021 in central France *Nat. Hazards Earth Syst. Sci.* **23** 1045–58
- Vogel J, Rivoire P, Deidda C, Rahimi L, Sauter C A, Tschumi E, van der Wiel K, Zhang T and Zscheischler J 2021 Identifying meteorological drivers of extreme impacts: an application to simulated crop yields *Earth Syst. Dyn.* **12** 151–72
- Walther S, Duveiller G, Jung M, Guanter L, Cescatti A and Camps-Valls G 2019 Satellite observations of the contrasting response of trees and grasses to variations in water availability *Geophys. Res. Lett.* **46** 1429–40
- Wang T *et al* 2018a Emerging negative impact of warming on summer carbon uptake in northern ecosystems *Nat. Commun.* **9** 5391
- Wang X, Wang T, Guo H, Liu D, Zhao Y, Zhang T, Liu Q and Piao S 2018b Disentangling the mechanisms behind winter snow impact on vegetation activity in northern ecosystems *Glob. Change Biol.* **24** 1651–62
- Webber H *et al* 2018 Diverging importance of drought stress for maize and winter wheat in Europe *Nat. Commun.* **9** 4249
- Wolf S *et al* 2016 Warm spring reduced carbon cycle impact of the 2012 US summer drought *Proc. Natl Acad. Sci.* **113** 5880–5
- Xiao C, Zaehle S, Yang H, Wigneron J-P, Schmulius C and Bastos A 2023 Land cover and management effects on ecosystem resistance to drought stress *Earth Syst. Dyn.* **14** 1211–37
- Yang Y, Maraun D, Ossó A and Tang J 2023 Increased spatial extent and likelihood of compound long-duration dry and hot events in China, 1961–2014 *Nat. Hazards Earth Syst. Sci.* **23** 693–709
- Yu X *et al* 2022 Contrasting drought legacy effects on gross primary productivity in a mixed versus pure beech forest *Biogeosciences* **19** 4315–29
- Zampieri M, Ceglar A, Dentener F and Toreti A 2017 Wheat yield loss attributable to heat waves, drought and water excess at the global, national and subnational scales *Environ. Res. Lett.* **12** 064008
- Zeng N, Zhao F, Collatz G J, Kalnay E, Salawitch R J, West T O and Guanter L 2014 Agricultural green revolution as a driver of increasing atmospheric CO₂ seasonal amplitude *Nature* **515** 394–7
- Zhang R, Ouyang Z-T, Xie X, Guo H-Q, Tan D-Y, Xiao X-M, Qi J-G and Zhao B 2016 Impact of climate change on vegetation growth in arid northwest of China from 1982 to 2011 *Remote Sens.* **8** 364
- Zhang Y, Sherstiukov A B, Qian B, Kokelj S V and Lantz T C 2018 Impacts of snow on soil temperature observed across the circumpolar north *Environ. Res. Lett.* **13** 044012
- Zhu L, Ives A R, Zhang C, Guo Y and Radeloff V C 2019 Climate change causes functionally colder winters for snow cover-dependent organisms *Nat. Clim. Change* **9** 886–93
- Zhu P *et al* 2022 The critical benefits of snowpack insulation and snowmelt for winter wheat productivity *Nat. Clim. Change* **12** 485–90
- Zhu Z, Piao S, Xu Y, Bastos A, Ciais P and Peng S 2017 The effects of teleconnections on carbon fluxes of global terrestrial ecosystems *Geophys. Res. Lett.* **44** 3209–18
- Zscheischler J *et al* 2014 Impact of large-scale climate extremes on biospheric carbon fluxes: an intercomparison based on MsTMIP data *Glob. Biogeochem. Cycles* **28** 585–600
- Zscheischler J *et al* 2020 A typology of compound weather and climate events *Nat. Rev. Earth Environ.* **1** 333–47
- Zscheischler J, Orth R and Seneviratne S I 2017 Bivariate return periods of temperature and precipitation explain a large fraction of European crop yields *Biogeosciences* **14** 3309–20



Titre : Caractérisation de l'évolution de la distribution de précipitations en région Méditerranée avec le changement climatique, dans le passé et le futur, en considérant à la fois les pluies extrêmes et les jours secs

Mots clés : précipitation, changement climatique, distribution, extrêmes, jours secs

Résumé : Le changement climatique a un impact significatif sur les régimes de précipitations, en particulier dans la région méditerranéenne, un point chaud du changement climatique. La littérature existante suggère un "paradoxe du cycle de l'eau" dans cette région (baisse des précipitations moyennes et hausse des extrêmes), en particulier au nord de la Méditerranée, mais cela n'est pas encore clair dans les observations.

Cette étude examine comment la distribution des précipitations en Méditerranée a évolué dans le passé et comment elle pourrait évoluer à l'avenir. En utilisant les données de la réanalyse ERA5 (1950-2020) et les simulations Euro-CORDEX (1950-2100), l'étude analyse les tendances temporelles des quantiles de précipitations. Nous étudions les distributions des jours de pluie (jours avec plus de 1 mm/jour) et de l'ensemble des jours, ainsi que la façon dont les changements dans la fréquence des jours secs influencent ces tendances. L'étude identifie quatre comportements distincts en matière de précipitations : les zones présentant une tendance en "U" (diminution

puis intensification des extrêmes), le schéma inverse (augmentation des quantiles faibles à moyens avec diminution des extrêmes) et les régions où tous les quantiles de jours de pluie augmentent ou diminuent de façon constante. À l'aide d'un modèle de distribution de Weibull, l'étude classe davantage ces tendances et met en évidence des différences régionales significatives. Dans la région méditerranéenne, les changements dans les précipitations sont en fait dominés par l'augmentation de la fréquence des jours secs.

Les projections futures sous le scénario RCP5.8 (fortes émissions) suggèrent des tendances robustes, avec une augmentation forte de la fréquence des jours secs dans toute la Méditerranée, contrastant avec la baisse du nombre de jours secs et l'intensification des jours de pluie en Europe du Nord. L'émergence de ces tendances est plus rapide en Europe du Nord qu'en Méditerranée. Cette étude souligne le rôle essentiel de la fréquence des jours secs dans l'évolution de la distribution des précipitations en Méditerranée.

Title : Characterisation of changes in the overall distribution of precipitation in the Mediterranean region with climate change, in the past and in the future, considering both extreme rainfall and dry-days frequency.

Keywords : precipitation, climate change, distribution, extremes, dry-days

Abstract : Climate change significantly impacts precipitation at global and regional scale, especially in the Mediterranean region, a climate change hotspot. Existing literature suggests a "water cycle paradox" in this region (decrease of mean precipitation but intensification of heavy precipitations) particularly in the Northern part of the Mediterranean, but this is not yet clear in observations.

This study investigates how the entire precipitation distribution in the Mediterranean has changed over the past and how it might evolve in the future. Using ERA5 reanalysis data (1950-2020) and Euro-CORDEX simulations (1950-2100), the study analyzes temporal trends in precipitation quantiles. We first study wet-days (days with more than 1 mm/day) in the past distributions, then look at how changes in dry-day frequency influence the all-days distribution. The study identifies four distinct precipitation regimes : a "U-shape" quantile trend curve (decreasing

low to medium quantiles but intensifying extremes), a reversed "U-shape", and two regimes where all quantiles either consistently increase or decrease. Using a Weibull model for the wet-days distribution, the study further determines these four regimes thanks to two parameters. We find regional differences, with a significant intensification in Europe, while in the Mediterranean, changes in precipitation are actually dominated by the increase of dry-days frequency.

Future projections under the RCP5.8 scenario (high emissions) suggest robust trends, with a sharp increase in the frequency of dry-days across the Mediterranean, contrasting with a decline in dry-days and an intensification of wet-days in Northern Europe. The time of emergence of these trends is faster in Northern Europe than in the Mediterranean. This study underlines the essential role of dry-day frequency in the evolution of the precipitation distribution in the Mediterranean.